Design and Synthesis of Bio-Inspired Functional Adhesive Polymer Coatings

MILLICAN, JONATHAN,MARTIN

Design and Synthesis of Bio-Inspired Functional Adhesive Polymer Coatings

A thesis submitted in fulfilment of the degree of

Doctor of Philosophy

By

Jonathan Millican

Department of Chemistry

Durham University

2019

Design and Synthesis of Bio-Inspired Functional Adhesive Polymer Coatings

Abstract

Inspired by the remarkable adhesive properties of mussels, the versatile chemistry of the catechol functional group is increasingly being utilised in a wide range of fields. In the work described in this thesis, copolymers were synthesised using the catechol-containing functional monomer dopamine methacrylamide (DMA) and its acetonide-protected analogue (ADMA) with the aim of producing a functional surface coating capable of immobilising biomolecules. The reactivity ratios for the free radical copolymerisation of ADMA with methyl methacrylate (MMA) or glycidyl methacrylate (GMA) were found to be $r_{MMA} = 2.21 \pm 0.26$ and $r_{ADMA} = 0.17 \pm 0.03$, and for the GMA/ADMA copolymerisation $r_{GMA} = 1.96 \pm 0.49$ and $r_{ADMA} = 0.18 \pm 0.08$. Accordingly, significant compositional drift was observed in polymerisations allowed to proceed to full conversion. Reversible addition-fragmentation chain-transfer (RAFT) polymerisation of ADMA with methacrylate comonomers was used to synthesise functional diblock copolymers and statistical copolymers with a gradient structure. Co- and terpolymers synthesised using hydroxyethyl methacrylate (HEMA), GMA and DMA were deposited onto silicon wafers by spin coating. Use of DMF as the spin-coating solvent enabled the deposition of homogenous films. Polymer films were also deposited directly from solution using immersion coating from a solution of dimethylformamide (DMF) containing 1% pyridine, taking advantage of the adhesive catechol functional group. The spin coated films were analysed by in-situ ellipsometry, captive bubble contact angle analysis and electrokinetic measurements. It was demonstrated that DMA had a large impact on chain mobility at the surface, ascribed to strong intermolecular H-bonding, however, the degree of swelling was largely influenced by the GMA content in the copolymers, ascribed to ring-opening induced crosslinking. Finally, it was demonstrated, using *in-situ* ellipsometry and quartz crystal microbalance, that a monolayer of IgG antibody was immobilised on a spin-coated copolymer film *via* covalent reaction with epoxide side chains.

Table of Contents

List of Figures i
List of Schemes v
List of Tables vi
List of Abbreviations viii
Statement of Copyright xi
Acknowledgements xii

Chapter 1 Introduction 1
1.1 Polymer definition and history 1
1.2 Polymer classification 1
1.3 Radical polymerisation and kinetics 1
1.3.1 The free radical mechanism 1
1.3.1.1 Initiation 2
1.3.1.2 Propagation and chain transfer 2
1.3.1.3 Termination 3
1.3.2 Kinetics of free radical polymerisation and reactivity ratios 3
1.3.2.1 Rate of propagation 3
1.3.2.2 Kinetics of copolymerisation 4
1.4 Living polymerisation 8
1.5 Reversible-deactivation radical polymerisation (RDRP) 9
1.5.1 RAFT polymerisation mechanism 10
1.5.2 Choice of RAFT agent 13
1.5.3 Synthesis of block copolymers using RAFT polymerisation 15
1.6 Mussel-inspired chemistry 15
1.6.1 The adhesion of mussels on rocks and other surfaces 15
1.6.2 The chemistry of catechol adhesion to surfaces 17
1.6.3 Surface coatings and functional polymers synthesised by mussel inspired chemistry 18
1.6.3.1 Surface coatings using catechol-containing monolayers, anchors or initiators. 19
1.6.3.2 Synthesis of surface coatings by the autopolymerisation of dopamine 20
1.6.3.3 Polypeptide mussel foot protein mimics 22
1.6.3.4 Synthesis of polymers with catechol end-groups 22
1.6.3.5 Post-polymerisation modification to introduce catechol side-chains 23
1.6.3.6 Synthesis of polymers containing catechol-functionalised monomers 24
1.6.3.6.1 Synthesis and protection of catechol-functionalised (meth)acrylamide monomers 25
1.7 Aims of the project 29
1.8 References 31
Chapter 2 Investigation of compositional drift in free radical (co)polymerisation of catechol containing methacrylamide monomers with methacrylate monomers. 36
2.1 Introduction 36
2.1.1 Radical reactions of monomers containing catechol functional groups 36
2.1.2 Reactivity ratios of catechol-containing monomers 37
2.1.3 The use of functional methacrylates as comonomers 39
2.2 Aims 40
2.3 Experimental 41
2.3.1 Materials 41

2.3.2 Synthesis of dopamine methacrylamide (DMA) 42
2.3.2.1 Synthesis of DMA, method 1 42
2.3.2.2 Synthesis of DMA, method 2 42
2.3.2.3 Synthesis of DMA, method 2 (scale-up) 43
2.3.2.4 Synthesis of DMA, method 3 43
2.3.3 Synthesis of acetonide protected dopamine methacrylamide (ADMA) 44
2.3.3.1 Synthesis of ADMA method 1 44
2.3.3.2 Synthesis of ADMA method 2 44
2.3.3.3 Synthesis of ADMA method 2 (larger scale) 44
2.3.4 Polymer Synthesis 45
2.3.4.1 Free radical homopolymerisation of DMA (FR-D-(DIOX)) 45
2.3.4.2 Free radical homopolymerisation of DMA (FR-D-(DMF)) 45
2.3.4.3 Free radical homopolymerisation of ADMA (FR-A) 45
2.3.4.4 Free radical copolymerisation for the estimation of reactivity ratios of MMA and ADMA 46
2.3.4.5 Free radical copolymerisation for the estimation of reactivity ratios of GMA and ADMA 46
2.3.4.6 Free radical copolymerisation of MMA and ADMA (FR-MA-90/10) 47
2.3.4.7 Free radical copolymerisation of MMA and ADMA (FR-MA-49/51) 47
2.3.4.8 Free radical copolymerisation of MMA and ADMA (FR-MA-24/76) 47
2.3.4.9 Free radical terpolymerisation of MMA, GMA and ADMA (FR-MGA-77/12/11) 47
2.3.4.10 Free radical terpolymerisation of MMA, GMA and ADMA (FR-MGA-52/26/22) 48
2.3.4.11 Free radical terpolymerisation of MMA, GMA and ADMA (FR-MGA-31/34/35) 48
2.3.4.12 Free radical terpolymerisation of HEMA, GMA and ADMA (FR-HGA-80/10/10-(DIOX)) 48
2.3.4.13 Free radical copolymerisation of SMA and ADMA (FR-SA-90/10) 49
2.3.4.14 Free radical copolymerisation of MMA and DMA (FR-MD-90/10-(DIOX)) 49
2.3.4.15 Free radical homopolymerisation of HEMA (FR-H) 50
2.3.4.16 Free radical copolymerisation of HEMA and DMA (FR-HD-90/10-(DMF)) 50
2.3.4.17 Free radical copolymerisation of HEMA and DMA (FR-HD-80/20-(DMF)) 50
2.3.4.18 Free radical copolymerisation of HEMA and DMA (FR-HD-70/30-(DMF)) 50
2.3.4.19 Free radical copolymerisation of HEMA and DMA (FR-HD-61/39-(DMF)) 51
2.3.4.20 Free radical copolymerisation of HEMA and DMA (FR-HD-50/50-(DMF)) 51
2.3.4.21 Free radical copolymerisation of PEGMEM and DMA (FR-PD-70/30-(DMF)) 51
2.3.4.22 Free radical terpolymerisation of MMA, GMA and DMA (FR-MGD-75/12/13-(DIOX)) 51
2.3.4.23 Free radical terpolymerisation of HEMA, GMA and DMA (FR-HGD-78/11/11-(DIOX)) 52
2.3.4.24 Free radical terpolymerisation of HEMA, GMA and DMA (FR-HGD-80/10/10) 52
2.3.4.25 Free radical terpolymerisation of HEMA, GMA and DMA (FR-HGD-58/9/33-(DMF)) 52
2.3.4.26 Free radical copolymerisation of MMA and GMA (FR-MG-50/50) 53
2.3.4.27 Free radical copolymerisation of HEMA and GMA (FR-HG-90/10) 53
2.3.5 Deprotection of ADMA and ADMA-containing copolymers 53
2.3.5.1 Deprotection of poly(MMA-co-ADMA) 53

2.3.5.2 Deprotection of ADMA 54
2.3.5.3 Deprotection of poly(SMA-co-ADMA)....54
2.3.6 Characterisation Methods 54
2.4 Results and Discussion....55
2.4.1 Synthesis of dopamine methacrylamide (DMA) 55
2.4.2 Acetonide protection of dopamine methacrylamide 59
2.4.3 Synthesis of homopolymers of DMA and ADMA by FR polymerisation....61
2.4.4 Estimation of reactivity ratios for the copolymerisation of ADMA with i) MMA and ii) GMA....65
2.4.5 Investigation of compositional drift during the synthesis of co/terpolymers containing ADMA 71
2.4.5.1 Investigation of compositional drift in ADMA/MMA copolymers 72
2.4.5.2 Investigation of compositional drift during the synthesis of terpolymers containing ADMA....79
2.4.6 Removal of the acetonide protecting group from ADMA and ADMA-containing copolymers....84
2.4.7 Investigation of compositional drift during the synthesis of co/terpolymers containing DMA 87
2.4.7.1 Investigation of compositional drift during the synthesis of copolymers containing DMA....88
2.4.7.2 Investigation of compositional drift during the synthesis of terpolymers containing DMA, GMA and a third monomer....94
2.4.8 Investigation of compositional drift during the synthesis of co/terpolymers containing no catechol-containing monomer....96
2.5 Conclusion....98
2.6 References 101
Chapter 3 Synthesis of statistical and block copolymers containing catechol functional groups using RAFT copolymerisation 104
3.1 Introduction 104
3.1.1 General requirements for a successful RAFT polymerisation 104
3.1.2 RAFT polymerisation of catechol-containing monomers....105
3.2 Aims 108
3.3 Experimental 109
3.3.1 Materials 109
3.3.2 Polymer Synthesis....109
3.3.2.1 Procedure for RAFT homopolymerisation of ADMA in DMF - RAFT-A-(DMF) 109
3.3.2.2 Procedure for RAFT polymerisation of ADMA in 1,4-dioxane, RAFT-A-(DIOX) 110
3.3.2.3 Procedure for RAFT homopolymerisation of MMA, RAFT-M-(DIOX/60C)110
3.3.2.4 Procedure for RAFT homopolymerisation of MMA, RAFT-M-(DIOX/70C)110
3.3.2.5 Procedure for RAFT homopolymerisation of MMA, RAFT-M-(DIOX)-2 111
3.3.2.6 Procedure for RAFT homopolymerisation of SMA, RAFT-S-(DIOX/60C) ..111
3.3.2.7 Procedure for RAFT homopolymerisation of GMA, RAFT-G-(DIOX/60C) .111
3.3.2.8 Procedure for RAFT homopolymerisation of GMA, RAFT-G-(DIOX/70C) .111
3.3.2.9 Procedure for RAFT statistical copolymerisation of MMA and ADMA, RAFT-MA-90/10....112
3.3.2.10 Procedure for RAFT statistical copolymerisation of MMA and ADMA, RAFT-MA-50/50....112

3.3.2.11 Procedure for RAFT statistical copolymerisation of GMA and ADMA, RAFT-GA-90/10 112
3.3.2.12 Procedure for RAFT statistical copolymerisation of SMA and ADMA, RAFT-SA-90/10 113
3.3.2.13 Procedure for RAFT statistical copolymerisation of SMA and ADMA, RAFT-SA-50/50 113
3.3.2.14 Procedure for RAFT statistical copolymerisation of HEMA and ADMA, RAFT-HA-90/10 113
3.3.2.15 Procedure for RAFT statistical terpolymerisation of HEMA, GMA and ADMA, RAFT-HGA-80/10/10 114
3.3.2.16 Procedure for RAFT statistical terpolymerisation of HEMA, GMA and DMA, RAFT-HGD-80/14/6 114
3.3.2.17 Procedure for RAFT statistical terpolymerisation of HEMA, GMA and DMA, RAFT-HGD-80/10/10 115
3.3.2.18 Procedure for RAFT statistical terpolymerisation of HEMA, GMA and DMA, RAFT-HGD-74/13/13 115
3.3.2.19 Procedure for RAFT block copolymerisation of ADMA with poly(MMA) macro-RAFT agent, RAFT-M-*b*-A-DIOX 115
3.3.2.20 Procedure for RAFT block copolymerisation of HEMA and GMA with poly(ADMA) macro-RAFT agent, RAFT-A-*b*-(HG-90/10) 115
3.3.3 Characterisation methods 116
3.3.3.1 Size exclusion chromatography (SEC) 116
3.3.3.2 Nuclear magnetic resonance (NMR) spectroscopy 116
3.4 Results and Discussion 116
3.4.1 Synthesis of homopolymers by RAFT polymerisation 117
3.4.1.1 Synthesis of poly(ADMA) using RAFT polymerisation 117
3.4.1.2 Synthesis of methacrylate homopolymers using RAFT polymerisation 123
3.4.2 Synthesis of statistical co/terpolymers containing ADMA by RAFT polymerisation 128
3.4.3 Synthesis of statistical terpolymers by RAFT polymerisation containing DMA, HEMA and GMA 134
3.4.4 Synthesis of diblock copolymers using RAFT polymerisation 137
3.5 Conclusion 142
3.6 References 145
Chapter 4 Optimisation of the deposition of catechol-containing polymer films on model substrates 147
4.1 Introduction 147
4.1.1 Coating methodologies 147
4.1.1.1 Spin-coating 147
4.1.1.2 Immersion-coating 148
4.1.2 Surface analysis techniques 149
4.1.2.1 Spectroscopic ellipsometry 149
4.1.2.2 Atomic force microscopy 149
4.2 Aims 150
4.3 Experimental 151
4.3.1 Investigation of (co)polymer solubility in various solvents 151
4.3.2 Substrate preparation method 151
4.3.3 Spin-coating experiments 152
4.3.4 Immersion-coating experiments 152

4.3.5 Ellipsometry measurements 152
4.3.6 AFM experiments 152
4.4 Results and Discussion 153
4.4.1 Investigation of (co)polymer solubility in various solvents 153
4.4.2 Cleaning and preparation of silicon wafer substrates 157
4.4.3 Details of (co)polymers used in the optimisation of film deposition 158
4.4.4 Optimisation of spin-coating methodology and thin film characterisation by AFM and ellipsometry 158
4.4.4.1 Characterisation of blank silicon wafer substrates by AFM and ellipsometry 161
4.4.4.2 Characterisation of copolymer films spin-coated from methanol 161
4.4.4.2.1 Analysis of spin-coated films of FR-HGD-80/10/10 using ellipsometry and AFM 162
4.4.4.2.1.1 Effect of spin-speed on film thickness of FR-HGD-80/10/10 coatings 163
4.4.4.2.1.2 Effect of spin-coating acceleration on film thickness of FR-HGD-80/10/10 coatings 165
4.4.4.2.1.3 Effect of terpolymer solution concentration on film thickness of FR-HGD-80/10/10 coatings 165
4.4.4.2.1.4 Analysis of spin-coated FR-HGD-80/10/10 films using AFM 167
4.4.4.2.2 Analysis of spin-coated films of copolymer FR-HD-90/10-(DMF) using ellipsometry and AFM 171
4.4.4.2.2.1 Effect of spin-speed on film thickness of FR-HD-90/10-(DMF) coatings 172
4.4.4.2.2.2 Effect of spin-coating acceleration on film thickness of FR-HD-90/10-(DMF) coatings 172
4.4.4.2.2.3 Effect of copolymer solution concentration on film thickness of FR-HD-90/10-(DMF) coatings 172
4.4.4.2.2.4 Analysis of spin-coated FR-HD-90/10-(DMF) films using AFM 174
4.4.4.2.3 Analysis of spin-coated films of copolymer FR-HG-89/11 using ellipsometry and AFM 175
4.4.4.2.3.1 Effect of spin-speed, acceleration and solution concentration on film thickness of FR-HG-89/11 coatings 175
4.4.4.2.3.2 Analysis of spin-coated FR-HG-89/11 films using AFM 176
4.4.4.2.4 Analysis of spin-coated films of terpolymer RAFT-HGD-74/13/13 using ellipsometry and AFM 177
4.4.4.2.4.1 Effect of spin-speed, acceleration and solution concentration on film thickness of RAFT-HGD-74/13/13 coatings 177
4.4.4.2.4.2 Analysis of spin-coated RAFT-HGD-74/13/13 films using AFM 177
4.4.4.2.5 Analysis of film thickness differences between the copolymer films 179
4.4.4.3 Characterisation of copolymer films spin-coated from DMF 181
4.4.4.3.1 Analysis of copolymer films spin-coated from DMF using ellipsometry and AFM 182
4.4.4.3.1.1 Effect of spin-speed, acceleration and solution concentration on films spin-coated from DMF 182
4.4.4.3.1.2 Analysis of films spin-coated from DMF using AFM 184
4.4.4.3.2 Investigation of the impact of solution viscosity on film roughness when spin-coating from DMF 185
4.4.5 Optimisation of immersion-coating and thin film characterisation with AFM and ellipsometry 187

4.4.5.1 Analysis of immersion-coating from copolymer solutions in DMF and pyridine 188
4.5 Conclusion 192
4.6 References 195
Chapter 5 Characterisation of the properties of functional, catechol-containing thin copolymer films 198
5.1 Introduction 198
5.1.1 Contact angle measurements 198
5.1.2 Electrokinetic streaming potential (zeta potential) measurements 199
5.1.3 In-situ spectroscopic ellipsometry 200
5.1.4 Quartz crystal microbalance measurements 201
5.2 Aims 201
5.3 Experimental 202
5.3.1 Materials 202
5.3.2 Testing of copolymer solubility upon storage 202
5.3.3 Ellipsometry measurements 202
5.3.4 Electrokinetic streaming potential measurements 203
5.3.5 Contact angle measurements 204
5.3.6 QCM analysis 204
5.4 Results and Discussion 205
5.4.1 Influence of temperature and storage time on the solubility of copolymers containing HEMA with GMA and/or DMA 205
5.4.2 Characterisation of surface properties of films on exposure to water 207
5.4.2.1 Contact angle analysis of copolymer films 208
5.4.2.2 Electrokinetic potential measurements of copolymer films 215
5.4.2.3 In-situ ellipsometry measurements of copolymer films immersed in buffer solution 219
5.4.3 Characterisation of the immobilisation of antibodies to a thin copolymer film using in-situ ellipsometry and QCM 228
5.4.3.1 Characterisation of antibody immobilisation using in-situ ellipsometry 229
5.4.3.2 Characterisation of antibody binding using QCM 231
5.5 Conclusion 233
5.6 References 236
Chapter 6 Conclusions and Future Work 239
6.1 Conclusions 239
6.2 Future work 243

List of Figures

Figure 1.1. Dithiobenzoate RAFT agents. A) 4-cyano-4-(phenylcarbonothioylthio)pentanoic acid (CTP), B) 2-cyano-2-propyl dithiobenzoate (CPDB), C) Cumyl dithiobenzoate (CDB). 14
Figure 1.2. The adhesion method of the marine mussel. A) Photograph of an adult mussel showing the byssal threads adhered to a mica surface B) Diagram of the mussel showing the organs responsible for the production and secretion of byssal threads containing mussel foot proteins. Image reproduced with permission [48]. Copyright © 2011 by Annual Reviews. 16
Figure 1.3. Binding modes of catechol functional group from the oxidised quinone form (above) and the catechol form (below). A) Covalent crosslinking, B) Schiff-base reaction, C) Coordination complex of a metal ion, D) Hydrogen bonding, E) Formation of borates, F) Bidentate bonding to metal oxide surfaces....18
Figure 1.4. Chemical structure of dopamine. 19
Figure 1.5. Examples of catechol functionalised small molecules used as surface coatings. 19
Figure 1.6. Examples of one-step immobilisation of molecules on substrate surfaces using PDA. Reproduced with permission.[83] Copyright © 2012 WILEY-VCH Verlag GmbH & Co. 21
Figure 1.7. Reaction of poly(pentafluorophenyl methacrylate) with dopamine. 24
Figure 1.8. Chemical structure of 3,4-dihydroxystyrene. 25
Figure 1.9. Chemical structures of catechol containing monomers. A) Catechol acetonide glycidyl ether, B) Silane-protected [3,4-dihydroxyphenyl)ethyl]-maleimide. 25
Figure 1.10. Chemical structures of A) DOPA methacrylamide (R = CH_3) and DOPA acrylamide (R = H). and B) dopamine methacrylamide (R = CH_3) and dopamine acrylamide (R = H). 26
Figure 1.11. Protecting groups used to modify DMA. A) Boronate B) Silane, where OSiR = tertbutyl dimethyl silyl ether or triethyl silyl ether C) Methyl D) Acetonide....27
Figure 1.12. Examples of polymers synthesised with DMA for various purposes. A) poly(DMA-co-HEMA) B) DMA and AAPBA cross-linked hydrogel C) poly(DMA-co-MPC-co-DMAEMA) D) poly(VDF-co-HFP)-graft-poly(DMA). 28
Figure 2.1. ^{1}H NMR spectrum of dopamine methacrylamide. Relative integrals are in blue text. 57
Figure 2.2. LC-MS spectrum of DMA with $[M+H]^+$ ion at *m/z* 222.2 g mol^{-1}. 57
Figure 2.3. ^{1}H NMR spectrum for DMA synthesised according to method 3. 58
Figure 2.4. LC-MS mass spectrum of ADMA with $[M+H]^+$ ion at *m/z* 262.2 g mol^{-1}. 60
Figure 2.5. ^{1}H NMR spectrum and relative integrals of ADMA. 61
Figure 2.6. NMR spectra of samples extracted from DMA polymerisation. Top = 24 h, bottom = 0 h. 63
Figure 2.7. ^{1}H NMR spectrum for FR-A. 65
Figure 2.8. Mayo-Lewis plot of mole fraction of monomer in feed vs mole fraction monomer in copolymer when copolymerised with ADMA. 67
Figure 2.9. Linearised plots allowing calculation of the reactivity ratios of MMA/ADMA and GMA/ADMA A) Fineman- Ross method B) Kelen-Tüdös method. 67
Figure 2.10. Monomers used as functional additional monomers in FR copolymerisations with ADMA. A) MMA, B) GMA, C) HEMA, D) SMA....72
Figure 2.11. Overlaid SEC RI chromatograms of MMA/ADMA and SMA/ADMA copolymers. 74
Figure 2.12. NMR spectrum of poly(MMA-co-ADMA), FR-MA-49/51. 74

Figure 2.13. Stacked ^{1}H NMR spectra ($CDCl_3$) of samples from the synthesis of FR-MA-49/51, polymerised in 1,4-dioxane at 70 °C. 75
Figure 2.14. Bar charts showing $F_{ADMA,t}$ (ADMA composition of copolymer, blue bars) and $F_{MMA,t}$ (orange bars), with predicted $F_{ADMA,i}$ (red circles). 77
Figure 2.15. SEC RI chromatograms. A) MMA/GMA/ADMA terpolymers, THF eluent. B) HEMA/GMA/ADMA terpolymer, DMF eluent. 82
Figure 2.16. Stacked ^{1}H NMR spectra ($CDCl_3$) of samples from the synthesis of FR-MGA-31/34/35, polymerised in 1,4-dioxane at 70 °C. 82
Figure 2.17. Terpolymer composition vs combined monomer conversion for ADMA-containing terpolymers. 84
Figure 2.18. NMR spectra of FR-MA-24/76. Top – Protected, Bottom – deprotected. 85
Figure 2.19. NMR spectrum for the removal of the acetonide protecting group of ADMA. 86
Figure 2.20. ^{1}H NMR spectra showing the progress of deprotection of FR-SA-90/10. Top (blue) - protected copolymer, Bottom (red) - 1 hr deprotection. Inset – expanded region 1.4 – 2.1 ppm. 87
Figure 2.21. SEC RI chromatograms. A) HEMA/DMA and PEGMEM/DMA copolymers, DMF eluent. B) MMA/DMA copolymer, THF eluent. 90
Figure 2.22. SEC RI chromatograms. A) HEMA/GMA/DMA terpolymers, DMF eluent. B) MMA/GMA/DMA terpolymer, THF eluent. 95
Figure 2.23. A) SEC RI chromatogram of FR-MG-50/50, eluent THF B) Evolution of copolymer composition for FR-MG-50/50. 97
Figure 2.24. SEC RI chromatogram of FR-HG-89/11, eluent DMF 98
Figure 3.1. ^{1}H NMR spectrum for RAFT-A-(DMF) with inset expanded region of the RAFT agent peaks. R = initiator or RAFT agent R-group. 121
Figure 3.2. Kinetic plot of the RAFT polymerisation of ADMA (RAFT-A-(DIOX)). 122
Figure 3.3. SEC chromatogram for statistical terpolymers RAFT-HGA-80/14/6, RAFT-HGA-80/10/10 and RAFT-HGA-74/13/13 136
Figure 3.4. A) Schematic representation of block copolymer RAFT-A-*b*-(HG-90/10). B) Schematic of hypothesised mode of adhesion of catechol-containing block copolymer. C) Schematic of hypothesised mode of adhesion of catechol-containing gradient copolymer. 138
Figure 3.5. SEC chromatogram of block copolymer of MMA and ADMA (RAFT-M-(DIOX)-2 and RAFT-M-*b*-A) 139
Figure 3.6. ^{1}H NMR spectrum of RAFT-M-*b*-A 140
Figure 3.7. ^{1}H NMR spectrum for RAFT-A-*b*-(HG-90/10) 142
Figure 3.8. RI SEC chromatogram of copolymer of HEMA and GMA and addition of ADMA block RAFT-A-(DMF) and RAFT-A-*b*-(HG-90/10) 142
Figure 4.1. Spin-coating process. A) Solution loading B) Acceleration of the substrate C) Thin film formation D) Evaporation-dominated drying. 148
Figure 4.2. Schematic of basic spectroscopic ellipsometer set-up. 149
Figure 4.3. Schematic of an AFM set up. 150
Figure 4.4. Ellipsometric data for the native oxide layer on a silicon wafer measured at four angles of incidence. A) Ψ *vs.* λ. B) Δ vs. λ. 161
Figure 4.5. Ellipsometry data for polymer films A) Coating 2, Ψ *vs.* λ, B) Coating 2, Δ *vs.* λ, C) Coating 4, Ψ *vs.* λ, B) Coating 4, Δ *vs.* λ. 163
Figure 4.6. Typical example of defects on a preliminary test for spin-coating of FR-HGD-80/10/10. Polymer-free spots on the film are due to solvent testing and not the spin-coating process. 166

Figure 4.7. Schematic of striations formed due to regions of high and low surface tension on a drying polymer film, where γ is surface tension. 167
Figure 4.8. 2D AFM images of films of FR-HGD-80/10/10, spin-coated from a solution in methanol. A) 37 nm film, coating 6 B) 61 nm film, coating 5 C) 61 nm film, coating 5 (enlarged section) D) 150 nm film, coating 7. AFM measurements carried out by Andreas Janke, IPF, Dresden. 168
Figure 4.9. A) 2D AFM image of films of FR-HD-90/10-(DMF), spin-coated from a 0.75% (w/v) solution in methanol, 4000 rpm, 600 rpm s^{-1}. B) AFM image of FR-HGD-80/10/10, film 6. Images obtained by Andreas Janke, IPF, Dresden. 175
Figure 4.10. 2D AFM image of films of FR-HG-89/11, spin-coated from a 0.75% (w/v) solution in methanol, 4000 rpm, 600 rpm s^{-1}. AFM measurements carried out by Andreas Janke, IPF, Dresden.....176
Figure 4.11. 2D AFM images of RAFT-HGD-74/13/13 terpolymer films, spin-coated from methanol solvent. A) 44 nm film, coating 33. B) 34 nm film, coating 29. 178
Figure 4.12. Average film thickness plotted against copolymer M_n for spin-coated copolymers at two concentrations. Crosses = 0.75% w/v, circles = 2% w/v.....180
Figure 4.13. Film thickness vs MSE for copolymer films coated at different spin-speeds and solution concentrations.....181
Figure 4.14. A) Photograph of coating 42, FR-HGD-80/10/10 spin-coated on silicon wafer from 0.75% (w/v) solution in DMF. B) 2D AFM image of coating 42. AFM image obtained by Andreas Janke, IPF, Dresden.....184
Figure 4.15. Scratched film of copolymer FR-HGD-58/9/33 spin-coated from DMF. A) Optical microscope image. B) 2D AFM image. C) Cross section height data for solid lines (red, orange and blue) on image B. D) Cross section height data for dashed line (purple) on image B.....186
Figure 4.16. A) AFM image of scratched blank wafer. The black dashed line indicates the boundary between the scratched and non-scratched regions B) Cross-sectional depth profile of the coloured lines on image A. 187
Figure 4.17. A) AFM image of scratched film of FR-HGD-58/9/33, immersion-coated from DMF with pyridine on silicon wafer. Blue squares indicate region of roughness measurement. B) Height profile corresponding to red arrow on image A. 189
Figure 4.18. A) AFM image of scratched film of FR-HD-70/30-(DMF), immersion-coated from DMF with pyridine on silicon wafer. Blue squares indicate region of roughness measurement. B) Height profile corresponding to red arrow on image A. 190
Figure 4.19. A) AFM image of scratched film of FR-HG-89/11, immersion-coated from DMF with pyridine on silicon wafer. Blue squares indicate region of roughness measurement. B) Height profile corresponding to red arrow on image A. 191
Figure 4.20. A) AFM image of scratched film of FR-H, immersion-coated from DMF with pyridine on silicon wafer. Blue squares indicate region of roughness measurement. B) Height profile corresponding to red arrow on image A. 192
Figure 5.1. Schematic representing four methods of ADSA-P. A) Pendant drop, B) Constrained sessile drop, C) Unconstrained sessile drop, D) Captive bubble.....199
Figure 5.2. Diagram of a captive bubble ADSA-P experimental set-up.....199
Figure 5.3. A) Schematic of a streaming potential electrokinetic measurement B) Schematic representation of the electrical double layer at a solid-liquid interface.....200
Figure 5.4. Schematic of the set-up for in-situ ellipsometry.....201

Figure 5.5. Schematic demonstrating the difference in measurement of advancing contact angle for: A) an expanding sessile drop and B) a retracting captive bubble (inverse contact angle). 208
Figure 5.6. Schematic representing reorganisation of the polymer surface region to allow hydrophobic chains to face the polymer-air interface. 210
Figure 5.7. Data for ADSA-P measurement of copolymers FR-HGD-80/10/10, FR-HD-90/10-(DMF), FR-HG-89/11 and RAFT-HGD-74/13/13. Top – Contact angle (θ) vs time / s. Middle – Radius of bubble (r) vs time / s. Bottom – Volume of bubble (V) vs time. Measurement carried out by Kathrin Pöschel, IPF Dresden. 211
Figure 5.8. ADSA-P captive bubble contact angle measurements. Advancing (blue) and receding (grey) angles in water. Measurement carried out by Kathrin Pöschel. 213
Figure 5.9. Zeta potential measurements of spin-coated films of FR-HGD-80/10/10, FR-HD-90/10-(DMF), FR-HG-89/11 and RAFT-HGD-74/13/13 on silicon wafer and a blank silicon wafer. Measurements carried out by Anja Caspari, IPF Dresden. 216
Figure 5.10. Examples of polymer swelling regimes, adapted from reference 52. A) Fickian diffusion B) Case II diffusion (dashed lines represent overshoot dynamics) C) Polymer dissolution. 220
Figure 5.11. Film thickness (h, blue) and normalised refractive index (n_{norm}, red) vs time for in-situ ellipsometry measurements of A) FR-HGD-80/10/10, B) FR-HD-90/10-(DMF), C) FR-HG-89/11 and D) RAFT-HGD-74/13/13. Blue dashed line indicated dry film thickness. 222
Figure 5.12. Schematic of an IgG antibody. 229
Figure 5.13. In-situ ellipsometry measurements of FR-HGD-80/10/10 for immobilisation of antibody in 0.001 mol dm^{-3} phosphate buffer solution. A) 0.08 mg mL^{-1} antibody concentration B) 0.04 mg mL^{-1} antibody concentration. n = refractive index. ...230
Figure 5.14. QCM data obtained during two immersion/rinse cycles. A) Frequency overtones (blue) and dissipation shift overtones (red/orange) and B) Film thickness calculated using the Sauerbrey equation. 232

List of Schemes

Scheme 1.1. Mechanism for termination reactions A) Chain combination B) Disproportionation. 3
Scheme 1.2. Mechanism of RAFT polymerisation with associated rate constants. 11
Scheme 1.3. Formation of DOPA from tyrosine. 16
Scheme 1.4. Reaction of dopamine with alkyl bromide compound and subsequent immobilisation on a silicon wafer surface, followed by grafting of polymer chains on the PDA surface by ATRP.[89] 22
Scheme 1.5. RAFT polymerisation of NIPAM using a catechol functionalised RAFT agent. 23
Scheme 2.1. A) Stabilisation of a catechol radical via intramolecular H-bonding. B) Reactions of catechol side chains to cause chain branching, termination or chain coupling. ... 36
Scheme 2.2. General reaction scheme for synthesis of dopamine methacrylamide from dopamine and methacrylic anhydride. 55
Scheme 2.3. Protection of dopamine methacrylamide with an acetonide group. 60
Scheme 2.4. Removal of protecting group from FR-MA-24/76. 85
Scheme 3.1. Reaction scheme for the RAFT polymerisation of ADMA using CTP 117
Scheme 5.1. Crosslinking reaction between epoxide and primary alcohol. R and R_1 = aromatic/aliphatic group 207

List of Tables

Table 2.1. Conditions used and conversion data for free radical homopolymerisations.....62
Table 2.2. Reactivity ratios for MMA/ADMA and GMA/ADMA calculated using the Fineman-Ross (FRM), Kelen-Tüdös (KTM) and non-linear least squares regression (NLLS) models.....68
Table 2.3. Polymerisation conditions and results for MMA/ADMA and SMA/ADMA statistical copolymers prepared by free radical polymerisation in 1,4-dioxane at 70 °C. 72
Table 2.4. Polymerisation conditions and results for ADMA and GMA containing statistical terpolymers prepared by free radical polymerisation in 1,4-dioxane at 70 °C.....80
Table 2.5. Polymerisation conditions and results for statistical copolymers containing DMA (except FR-H) prepared by free radical polymerisation in 1,4-dioxane or DMF at 70 °C.....88
Table 2.6. Polymerisation conditions and results for statistical terpolymers containing DMA and GMA prepared by free radical polymerisation in 1,4-dioxane or DMF at 70 °C.94
Table 2.7. Conditions for copolymers synthesised by free radical polymerisation using no catechol monomer. 96
Table 3.1. Summary of reaction conditions, monomer conversion and molecular weight data for poly(ADMA) synthesised using RAFT polymerisation.....119
Table 3.2. Summary of reaction conditions, monomer conversion and molecular weight data for poly(MMA), poly(SMA) and poly(GMA) synthesised using RAFT polymerisation.....124
Table 3.3. Data for a series of statistical RAFT copolymerisations. The molar feed ratios were [mon]:[CTA]:[I] = 75:1:0.75 and temperature was 60 °C in all cases. 129
Table 3.4. Statistical terpolymers containing HEMA, GMA and DMA by RAFT polymerisation in DMF. 134
Table 3.5. Data for diblock copolymers by RAFT polymerisation, synthesised at 60 °C, [CTA]:[I] = 1:0.75 139
Table 4.1. Results for (co)polymer solubility testing. Each (co)polymer immersed in solvent at concentration of 1 mg mL^{-1} and stirred overnight.....154
Table 4.2. Polymers used in spin-coating and immersion-coating. Constituent monomers and monomer molar feed ratios are indicated in the name of each polymer.....158
Table 4.3. Ellipsometry data for films of FR-HGD-80/10/10, spin-coated from methanol onto silicon wafer. 162
Table 4.4. Roughness data from the AFM images in Figure 4.8. Silicon wafers coated with FR-HGD-80/10/10 Film thickness was obtained by ellipsometry. 169
Table 4.5. Ellipsometry data for films of FR-HD-90/10-(DMF), spin-coated from methanol onto silicon wafer. 171
Table 4.6. Ellipsometry data for films of copolymer FR-HG-89/11, spin-coated from methanol onto silicon wafer. 175
Table 4.7. Ellipsometry data for films of RAFT-HGD-74/13/13, spin-coated from methanol onto silicon wafer. 177
Table 4.8. Ellipsometry data for dry copolymer films. Spin-coated from 0.75% (w/v) copolymer solution in DMF onto silicon wafer. 182
Table 4.9. Film thickness data, estimated using AFM, for polymer coatings, 2% (w/v) solution in DMF with 1% (v/v) pyridine.....189

Table 5.1. Solubility of selected copolymer samples after storage in bulk at a range of temperatures. Solubility tested in a 1 mg mL^{-1} solution in methanol after 1 h stirring. 205
Table 5.2. Copolymers used in spin-coating and immersion-coating reactions. Monomers and monomer feed molar ratios are indicated in the name of each copolymer. 208
Table 5.3. Film thickness, refractive index and swelling factor data for dry and swollen copolymer samples. 223
Table 5.4. Dissolution factor Ω for copolymer films at the end of in-situ ellipsometry measurements. 227

List of Abbreviations

AAPBA	3-acrylamido phenylboronic acid
ACHN	1,1′-azobis(cyclohexanecarbonitrile)
ADA	Acetonide-protected dopamine acrylamide
ADMA	Acetonide-protected dopamine methacrylamide
ADSA-P	Axisymmetric drop shape analysis-profile
AEMA	2-aminoethylmethacrylamide
AFM	Atomic force microscopy
AIBN	Azobisisobutyronitrile
AMBN	2,2'-Azodi(2-methylbutyronitrile)
ATRP	Atom transfer radical polymerisation
CDB	Cumyl dithiobenzoate
CPDB	2-cyano-2-propyl benzodithioate
CSIRO	Commonwealth Scientific and Industrial Research Organisation
CTA	Chain transfer agent
CTP	4-Cyano-4-(phenylcarbonothioylthio)pentanoic acid
Đ	Dispersity
DA	Dopamine acrylamide
DAA-p	Borax-protected dopamine acrylamide
DCM	Dichloromethane
DHI	5,6-dihydroxyindole
DHICA	5,6-dihydroxyindole-2-carboxylic acid
DHS	Dihydroxystyrene
DIOX	1,4-dioxane
DMA	Dopamine methacrylamide
DMAEMA	2-(dimethylamino)-ethyl methacrylate
DMF	Dimethylformamide
DMSO	Dimethylsulfoxide
DNB	Dinitrobenzene
DOPA	Dihydroxyphenylalanine
DP	Degree of polymerisation
DPE	Diphenylethylene
EGDMA	Ethylene glycol dimethacrylate
EGMEM	Ethylene glycol methyl ether methacrylate
EMA	Ethyl methacrylate
EVM	Errors-in-variables model
FR	Free radical
FRM	Fineman-Ross model
FTIR	Fourier Transfer Infrared
GMA	Glycidyl methacrylate
GPC	Gel permeation chromatography
HEMA	2-hydroxyethyl methacrylate
HFP	Hexafluoropropylene
HMPMA	N-(1-hydroxy-4-methyl-2-pentyl)methacrylamide
I	Initiator
IEP	Isoelectric point

IPA	Isopropyl alcohol
IPF	Institut für Polymerforschung
IR	Infrared
IUPAC	International Union of Pure and Applied Chemistry
KTM	Kelen-Tüdös model
LAM	Less active monomer
LbL	Layer-by-layer
LC-MS	Liquid chromatography - mass spectrometry
MAG	2-methacrylamido glucopyranose
MAM	More active monomer
MAP	Mussel adhesive protein
MEA	2-methyloxyethyl acrylate
MFP	Mussel foot protein
MHM	3-mercaptohexyl methacrylate
MMA	Methyl methacrylate
Mon.	Monomer
MPC	2-methacryloyloxyethyl phosphorylcholine
MSE	Mean square error
MWCO	Molecular weight cutoff
MWF	Molecular weight factor
N_A	Avagadro's number
NIPAM	N-isopropylacrylamide
NLLS	Non-linear least squares
NMP	Nitroxide-mediated polymerization
NMR	Nuclear Magnetic Resonance
PBS	Phosphate buffered saline
PDA	Polydopamine
PDMS	Poly(dimethyl siloxane)
PEG	Poly(ethylene glycol)
PEGMEM	Poly(ethylene glycol) methyl ether methacrylate
PMA	Phenyl methacrylate
PMAm	Phenyl methacrylamide
PTFE	Poly(tetrafluoroethylene)
QCM	Quartz crystal microbalance
QCM-D	Quartz crystal microbalance with dissipation monitoring
RAFT	Reversible addition-fragmentation chain-transfer
RDRP	Reversible-deactivation radical polymerisation
RI	Refractive index
ROMP	Ring-opening metathesis polymerisation
SEC	Size exclusion chromatography
SET	Single electron transfer
SF	Swelling factor
SI-ATRP	Surface-intiated atom transfer radical polymerisation
SMA	Stearyl methacrylate
TFA	Trifluoroacetic acid
THF	Tetrahydrofuran

TMA	Thiazoyl methacrylamide
UPLC	Ultra performance liquid chromatography
UV	Ultraviolet
VCA	Vinyl catechol acetonide
VDF	Vinylidene fluoride
XPS	X-ray photoelectron spectroscopy
ζ	Zeta Potential

Statement of Copyright

Acknowledgements

First and foremost, I would like to thank Lian Hutchings for his enthusiasm, ideas, tireless effort and patience throughout the project. I would like to thank all of the Hutchings group for their help and support over the last four years, particularly Natasha Boulding for the many productive discussions, Daniel Day, Antonella Pagliarulo, Lloyd Shaw, Utku Yolsal, Roberto Chincilla Pardos, Matthew Oti, Gabriele Benzi and Brunella Maranesi. I am grateful to the all of the Durham Chemistry Department students, academics and technical staff and lab attendants who have helped me along the way.

I would like to thank everyone involved with the SOFI CDT, all of the Cohort 1 students particularly, who made me feel part of a community from Day 1. Thanks to the dedication of Lian, Tom McLeish and Julie McLoughlin for creating the SOFI community, and also the contributions from those at the Universities of Durham, Leeds and Edinburgh. I acknowledge funding from the EPSRC gratefully.

Thanks also the members of the IPF institute in Dresden, Germany for their support and openness, particularly the hospitality and assistance from Doris Pospiech. Thanks also to Brigitte Voit, Eva Bittrich, Andreas Janke, Kathrin Pöschel, Anja Caspari, Uwe Freudenberg, Klaus-Jochen Eichorn, Kathrin Eckstein, Susanne Stehl and Frank Simon.

Thanks to Tim Ryan, for being a constant source of inspiration and curiosity, Niamh Kilcawley and all at Epigem.

Many thanks to my friends in and out of Durham; I wouldn't have been able to do it without your support. Thanks Aixa, Antonio, Celia, Cristiano, Juan, Nuria, Manu, Stina and every Son (and Grandson) of Durham. Thanks to Tessa, Meera and Charlie for being great housemates. Special thanks to Mareike Deuker for your love, support and patience.

Finally, thanks to my family, who have been encouraging me, making me laugh and providing me with strength and endless support for far longer than it takes to do a PhD. Mum, Dad and Abi, I owe you everything.

Chapter 1 Introduction

1.1 Polymer definition and history

Polymers are macromolecules consisting of small repeat units called monomers. Polymers were first described by Berzelius in the 1830s and had already been adopted by industry in the 1840s with the production of vulcanised rubber. Polymer synthesis on an industrial scale was transformed by the introduction of Bakelite in 1907, leading to rapid development of the field in industry in the 1930s and 1940s. Today, around 300 million tons of polymeric materials are produced annually and are an important aspect in almost every element of modern life. This thesis will focus on the synthesis of bio-inspired polymers and their deposition as surface coatings on model substrates.

1.2 Polymer classification

Historically, polymers have been classified by several means, however the International Union of Pure and Applied Chemistry (IUPAC) defined a general method to describe polymers by the type of reaction used in their synthesis, with further subdivision based on whether small molecules are formed in the reaction.[1]

Polymer synthesis mechanisms can be divided into step-growth and chain-growth reactions. Step-growth polymers are formed by the reaction between mutually reactive functional groups on growing polymer chains and a chain of any size may add to any other over the course of the reaction and remain active. Step-growth polymerisation can be subdivided into polycondensation reactions, where a small molecule, often water is produced as a by-product of the reaction, and polyaddition reactions.

In chain-growth polymerisation, the reaction between a monomer and an initiator forms an active species which propagates by the sequential addition of monomer units to the chain. Polymers formed using chain growth polymerisation may be terminated by several mechanisms depending on the reaction type. Common chain growth polymerisation mechanisms include radical, anionic, cationic and ring-opening polymerisation.

1.3 Radical polymerisation and kinetics

1.3.1 The free radical mechanism

The mechanism of free radical polymerisation can be broken down into three key mechanistic steps: initiation, propagation and termination.[2, 3] During propagation, the polymer can grow linearly or branching can occur due to chain transfer.

Free radical polymerisation is the most widely used industrial polymerisation method, accounting for about 45% of polymer production worldwide. It is a form of chain-growth polymerisation whereby initiation generates a propagating species comprising an unpaired electron.

1.3.1.1 Initiation

The initiation of a free radical polymerisation involves two steps (Equations 1.1 and 1.2). The first is the generation of a radical species, usually by homolytic cleavage of a relatively stable "initiator" molecule to generate two radical species, often by the action of heat (thermolysis) or of light (photolysis). The second step involves the addition of the radical species to a monomer, to generate the propagating species.

$$\mathbf{I} \xrightarrow{\mathbf{k_d}} \mathbf{2R}\cdot \qquad \mathbf{1.1}$$

$$\mathbf{R}\cdot + \mathbf{M} \xrightarrow{\mathbf{k_i}} \mathbf{M_1}\cdot \qquad \mathbf{1.2}$$

1.3.1.2 Propagation and chain transfer

During propagation, monomers are added sequentially to the chain-end (Equation 1.3). This process is rapid and, in a well-designed reaction, many hundreds or thousands of units can be added before termination occurs.

$$\mathbf{M_n}\cdot + \mathbf{M} \xrightarrow{\mathbf{k_p}} \mathbf{M_{n+1}}\cdot \qquad \mathbf{1.3}$$

Chain transfer is a process which can occur during polymer propagation, in which the propagating radical is transferred (usually) to another molecule e.g. solvent (Equation 1.4). Chain transfer can also be to another polymer chain, which causes chain branching. The rate of chain transfer is usually low, but it can be greatly enhanced if the polymer side chains contain labile bonds (*e.g.* halogens).

$$\mathbf{M_n}\cdot + \mathbf{CTA} \xrightarrow{\mathbf{k_{ct}}} \mathbf{M_n} + \mathbf{CTA}\cdot \qquad \mathbf{1.4}$$

Chain transfer agents (CTAs) with high rates of chain transfer (k_{ct}) can be added to a polymerisation. CTAs are commonly thiols, with a labile RS-H bond, which react with the propagating radical. The result of chain transfer is usually a decrease in polymer molecular weight. Careful design of chain transfer agent, such as in reversible addition-fragmentation

chain-transfer (RAFT) polymerisation, can be used to achieve specific mechanical or chemical polymer properties (see section 1.5.1).

1.3.1.3 Termination

Termination is the process by which a propagating chain is deactivated by the annihilation of the radical species. The two most common termination processes are combination and disproportionation. In combination, two growing chains combine to produce a single deactivated chain (Scheme 1.1A). In disproportionation, a β-hydrogen is abstracted from another propagation chain, resulting in a carbon-carbon double bond at the chain-end of one molecule and a carbon-carbon single bond at the end of the other molecule (Scheme 1.1B). The rate constants for the termination reactions are k_{tc} and k_{td} respectively.

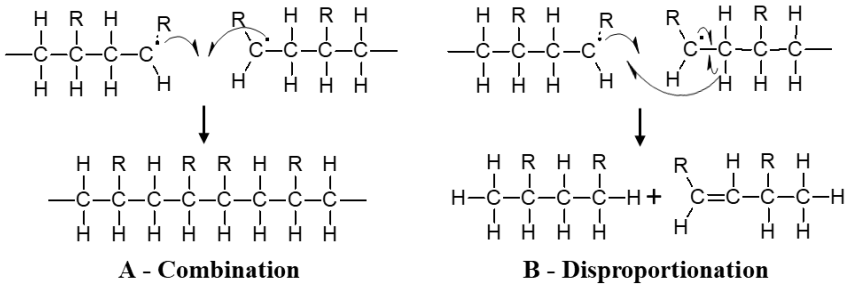

Scheme 1.1. Mechanism for termination reactions A) Chain combination B) Disproportionation.

1.3.2 Kinetics of free radical polymerisation and reactivity ratios

1.3.2.1 Rate of propagation

Kinetic studies of the propagation of a free radical polymerisation are important in understanding and predicting the outcome of polymer syntheses. The rate of propagation can be studied directly (by the growth of polymer chains) or indirectly (by the conversion of monomer). The rate of monomer conversion is given by Equation 1.5:

$$\frac{-\mathbf{d}[\mathbf{M}]}{\mathbf{dt}} = \mathbf{R_i} + \mathbf{R_p} \qquad \textbf{1.5}$$

where R_i and R_p are the rates of initiation and propagation respectively. As the total number of monomer molecules involved in initiation is much smaller than those involved in propagation throughout the polymerisation, R_i may be ignored. This means that the rate of propagation can be considered as simply the sum of all propagation steps, and expressed by the rate expression for propagation (Equation 1.6):

$$\mathbf{R_p} = \mathbf{k_p}[\mathbf{M}\cdot][\mathbf{M}] \qquad \textbf{1.6}$$

A steady-state approximation can be made, in which it is assumed that the radical concentration rapidly increases at the start of the reaction and then stays constant throughout most of the reaction, so the rate of polymerisation (R_{pol}) approximates to R_p (Equations 1.7 – 1.9). Under steady state conditions the rates of initiation and termination are therefore considered equal.

$$\mathbf{R_i = R_t = 2k_t[M\cdot]^2} \quad \textbf{1.7}$$

Rearrangement to:

$$\mathbf{[M\cdot] = \left(\frac{R_i}{2k_t}\right)^{\frac{1}{2}}} \quad \textbf{1.8}$$

And substitution into equation 1.6 gives:

$$\mathbf{R_{pol} = k_p[M]\left(\frac{R_i}{2k_t}\right)^{\frac{1}{2}}} \quad \textbf{1.9}$$

As such, the rate of polymerisation is proportional to the square root of the rate of initiation. The implications of this are that initiation and termination must be carefully considered in a free radical polymerisation to understand the overall rate of reaction.

1.3.2.2 Kinetics of copolymerisation

When more than one type of monomer is present in a free radical copolymerisation, each can be incorporated into a growing copolymer chain. In its simplest form, the chemical reactivity of a copolymer chain is considered to be dependent only on the identity of the final repeat unit at the propagating chain-end. This is known as the terminal model. As such, n^2 propagation reactions are possible (representing cross- and self-propagation between a propagating chain and a monomer) where n is the number of monomer types. For example, in a system with two monomers (M_1 and M_2), propagation can be described by four reactions, each with its own rate constant (k_{xy}) (Equations 1.10 – 1.13):

$$\mathbf{PM_1\cdot + M_1 \xrightarrow{k_{11}} PM_1\cdot} \quad \textbf{1.10}$$

$$\mathbf{PM_1\cdot + M_2 \xrightarrow{k_{12}} PM_2\cdot} \quad \textbf{1.11}$$

$$\mathbf{PM_2\cdot + M_1 \xrightarrow{k_{21}} PM_1\cdot} \quad \textbf{1.12}$$

$$\mathbf{PM_2\cdot + M_2 \xrightarrow{k_{22}} PM_2\cdot} \quad \textbf{1.13}$$

Using this model, two reactivity ratios can be defined (r_1 and r_2) which describe the individual monomer reactivity in the copolymerisation (Equation 1.14).

$$\mathbf{r_1 = \frac{k_{11}}{k_{12}}\ r_2 = \frac{k_{22}}{k_{21}}} \qquad \textbf{1.14}$$

The reactivity ratios represent the tendency of monomer 1 and monomer 2 to undergo self-propagation or cross-propagation. The monomer feed ratio and reactivity ratios determine the resulting monomer sequence distribution in the copolymer. Determination of reactivity ratios is therefore crucial to enable an understanding of the sequence and structure of a copolymer with a particular composition, and to enable copolymers to be designed with the desired properties.[4]

A reactivity ratio of 1.0 indicates an equal tendency for either monomer to add to the particular chain end. A reactivity ratio of >1.0 indicates a tendency for self-propagation, and a reactivity ratio of <1.0 indicates in a tendency for cross-polymerisation.

The product of the reactivity ratios is also considered to assess the randomness of the comonomer addition.[3] A polymerisation in which $r_1.r_2 = 1.0$ is termed "ideal" and the identity of the species on the end of the propagating radical does not affect the rate of addition of either monomer (i.e. the propagating radical species with either monomer on the chain-end show no preference towards either monomer). An ideal polymerisation has the following ratio of rate constants (Equation 1.15):

$$\mathbf{\frac{k_{22}}{k_{21}} = \frac{k_{12}}{k_{11}}} \qquad \textbf{1.15}$$

Note that in an ideal polymerisation one propagating radical chain-end can still be more reactive than the other, except in the special case in which $r_1 = r_2 = 1.0$, termed "random". In a random polymerisation, both monomers have equal chance of adding to the propagating radical, regardless of its identity.

When $r_1.r_2 = 0$, and neither r_1 nor r_2 are greater than 1, the polymerisation is described as alternating. When one of the reactivity ratios is greater than 0 but less than 1, the structure tends towards alternation. In a true alternating polymerisation, where $r_1 = r_2 = 0$, the monomers will add alternately and sequentially with no self-propagation possible. In real copolymerisation systems, the product of reactivity ratios lies somewhere between the alternating and ideal cases. Extreme differences in reactivity ratios lead to the formation

of homopolymers. Copolymer composition can be determined experimentally by several analytical methods including ^{1}H NMR, ^{13}C NMR, FTIR spectroscopy, UV-vis spectroscopy or gas chromatography.[5, 6] The copolymer composition is often analysed by monitoring the depletion of each monomer as a function of either time or total monomer conversion. This route offers information on average monomer sequence distribution and copolymerisation kinetics. NMR spectroscopy has been used to track monomer depletion, either by reaction sampling or using real-time NMR spectroscopy to monitor reaction kinetics.[7-13]

The chemical composition of copolymers is influenced by both the monomer feed ratio (f_1 : f_2) and reactivity ratios, which are the key variables in the Mayo-Lewis model, also known as the instantaneous copolymerisation equation, where F_1 is the mole fraction of monomer 1 in the copolymer (Equation 1.16).[14]

$$\mathbf{F_1 = \frac{r_1 f_1^{\,2} + f_1 f_2}{r_1 f_1^{\,2} + 2 f_1 f_2 + r_2 f_2^{\,2}}} \qquad \textbf{1.16}$$

Use of the Mayo-Lewis model allows for the estimation of reactivity ratios by linear and non-linear parameter estimation methods. This is achieved by obtaining the instantaneous copolymer composition – often by measuring the composition of a copolymer at very low conversion (<10 %), which diminishes the effect of drift in monomer feed composition.

Common linear models used to estimate reactivity ratios are the Fineman-Ross[15] and Kelen-Tüdös[16] methods. These methods were both derived from the Mayo-Lewis model (Equation 1.15), and reactivity ratios are estimated by linear least squares regression analysis.

The Fineman-Ross method (Equations 1.17 – 1.19) defines variables (G and H) which are assigned to equations based on measured values of the monomer mole fraction in the feed (f_{mon}) and the mole fraction of each monomer in the resulting copolymer (F_{mon}). G is plotted against H for each experiment, which yields a straight line of gradient r_1 and intercept r_2.

$$\mathbf{G = \frac{F_1}{F_2}\left(1 - \frac{f_2}{f_1}\right)} \qquad \textbf{1.17}$$

$$\mathbf{H = \left(\frac{F_1}{F_2}\right)^2 \left(\frac{f_2}{f_1}\right)} \qquad \textbf{1.18}$$

$$\mathbf{G = r_1 H - r_2} \qquad \textbf{1.19}$$

Kelen and Tüdös[16] refined the Fineman-Ross equation by the introduction of an arbitrary constant (α) to distribute the data more uniformly and eliminate bias from certain experimental data points (Equation 1.20):

$$\boldsymbol{\alpha = (H_{min}H_{max})^{\frac{1}{2}}} \qquad \textbf{1.20}$$

where H_{min} and H_{max} are the minimum and maximum values of H determined from the data.

This was based on the observation that reactions where there is a large difference in the monomer molar feed ratio lead to data points which bias the equation. The constant α can then be used to modify the values from the Fineman-Ross equation (G and H) giving values ξ and η (Equations 1.21 – 1.23). ξ is plotted against η for each experiment. Reactivity ratios can be obtained as the plotted line intercepts the lines ξ = 0 and ξ = 1 at values $-r_2 / \alpha$ and r_1 respectively.

$$\boldsymbol{\eta = \frac{G}{\alpha + H}} \qquad \textbf{1.21}$$

$$\boldsymbol{\xi = \frac{H}{\alpha + H}} \qquad \textbf{1.22}$$

and

$$\boldsymbol{\eta = \left(\frac{r_1 + r_2}{\alpha}\right)\xi - \frac{r_2}{\alpha}} \qquad \textbf{1.23}$$

Although the Kelen-Tüdös method has been widely used, it still relies on the assumption that there is no compositional drift at low conversion, which introduces error into the model. The same authors presented a more complex method to address this source of error, which is known as the extended Kelen-Tüdös method.[17] In this method, G and H are replaced (Equations 1.24 and 1.25):

$$\boldsymbol{G = \left(\frac{\log(1-\chi_2)}{\log(1-\chi_1)}\right)^2 \left(\frac{d[M_1]_0}{d[M_2]_0}\right)} \qquad \textbf{1.24}$$

$$\boldsymbol{H = \left(\frac{\log(1-\chi_2)}{\log(1-\chi_1)}\right)\left(\frac{d[M_1]_0}{d[M_1]_0} - 1\right)} \qquad \textbf{1.25}$$

where χ_1 and χ_2 are the partial molar conversions of the copolymer. The rest of the calculation is performed in the same way. This reduces the error from the low conversion assumption, but some systematic errors remain.

The greatest criticism of the preceding methods is that they impose linear analysis on what is fundamentally non-linear data. More statistically-correct non-linear methods of calculating reactivity ratios have been developed to reduce the systematic error in measurements. Tidwell and Mortimer used non-linear least squares analysis. Their method utilised a statistical approach to the design of experiment, allowing improved data to be obtained.[18] Meyer and Lowry developed a method which uses an integrated form of the instantaneous copolymerisation equation.[19] This method allowed multiple measurements to be used during each reaction, reducing experimental error and allowing in-situ reaction monitoring to be used to obtain data.[20]

Recent increases in computing power have also aided researchers in this field. Van den Brink *et al*.[21] and Kazemi *et al*.[22] introduced an errors-in-variables model (EVM) which uses non-linear regression to plot the data obtained from Meyer-Lowry equation. This increased the accessibility of the complex mathematical calculations required to calculate reactivity ratios using integrated non-linear methods whilst also including an estimate of experimental error in the calculations. EVM is becoming more user-friendly as further models are developed.[23] The EVM approach also allows users to calculate the reactivity ratios of ternary copolymerisations and higher, as these cannot be modelled accurately with traditional methods.[24] It can also be used to consider reactivity ratios using the penultimate model of free radical polymerisation (which considers that the penultimate repeat unit also contributes to the kinetics of the reaction) as it has been shown that the terminal model does not always describe the reaction kinetics with absolute accuracy.[25]

1.4 Living polymerisation

Living polymerisation is defined as a chain-growth polymerisation in which chain transfer and termination reactions are absent, such that the polymerisation may proceed indefinitely until no more monomer is present.[1] The rate of initiation is greater than or equal to the rate of propagation, unlike radical polymerisation, so all chains are initiated rapidly and grow at an equal rate to an (almost) equal chain length. Mechanisms which enable living polymerisation conditions include anionic, cationic and ring opening metathesis polymerisation reactions.

Living polymerisation allows the synthesis of very low dispersity polymers ($Đ < 1.1$). Dispersity, Đ, is defined by $Đ = M_w/M_n$, where M_w is the weight average molecular weight and M_n the number average molecular weight; living polymerisations often result in

polymers in which. The polymer chains remain active at the end of the polymerisation, so complex/advanced polymer architectures can be accessed, such as diblock, star and hyperbranched copolymers.[26] Anionic (co)polymerisation also allows for much greater control over the resulting copolymer structure, as the reactivity ratios of monomers are often more extreme compared to free radical polymerisation, due to the sensitivity of the propagating ion stability to both substituents and solvent.[4]

Despite having several advantages over free radical polymerisation, living polymerisations are usually very sensitive to impurities such as water, and reactive functional groups are often not tolerated, meaning there are a limited number of monomers which can be used in such reactions.

1.5 Reversible-deactivation radical polymerisation (RDRP)

Free radical polymerisation has many beneficial features such as high tolerance to many functional groups and solvent systems. However, there are also drawbacks – especially rapid and uncontrolled termination, which leads to high dispersity and means that controlling molecular weight and the synthesis of block copolymers and other complex polymer architectures are often not possible. Imparting the characteristics of a living polymerisation to a free radical system has been a target of synthetic polymer chemists and various methods have been developed towards the realisation of this aim. One of two general processes are generally utilised: i) reversible deactivation of the propagating chain; used in atom transfer radical polymerization (ATRP)[27, 28] and nitroxide-mediated polymerization (NMP)[29] or ii) degenerative chain transfer, used in reversible addition-fragmentation chain-transfer (RAFT) polymerisation.[30] Collectively the techniques are known as controlled radical polymerisations or RDRP.[3]

ATRP involves a redox equilibrium between an alkyl halide and a catalytic transition metal complex which acts as an activator. NMP relies upon the reversible decomposition of a nitroxide compound to form a reactive radical and a stable nitroxide radical. RAFT polymerisation uses a conventional initiator as a radical source and a chain transfer agent, often a dithioester compound, to supress termination by reversible degenerative chain transfer.

A generalised RDRP reaction involves an initiator or chain-transfer agent which undergoes reversible dissociation to form a dormant species and an active radical. The active radical reacts with a monomer to form a propagating radical, which can either revert to the dormant

species, another monomer to extend the polymer chain, or another radical species to terminate the chain. The ratio between these three processes is vital to maintaining control in RDRP. In ATRP and NMP, the equilibrium constant between the dormant species and propagating radical determines the rate of reaction. When the equilibrium between the dormant species and propagating radical lies towards the dormant species, the probability of bimolecular termination is reduced, however the equilibrium constant must be high enough to achieve a reasonable rate of polymerisation. In RAFT polymerisation, the rate of reaction is determined by the monomer concentration and the properties of the radical initiator.

Most chains continue to grow for the entire reaction which, combined with a low termination rate, reduces the dispersity of the polymer ($Đ \approx 1.1$ in a well-designed reaction) and allows specific molecular weights to be targeted. A further benefit of RDRP is that (most) active chain ends are retained, enabling further reaction to form more complex polymer architectures. These mechanisms cannot be described as living, as termination, although suppressed, still occurs. RAFT polymerisation is described in detail in section 1.5.1 as it is used in the current study, however ATRP and NMP will not be discussed further here.

1.5.1 RAFT polymerisation mechanism

RAFT polymerisation was first reported in 1998 by researchers at the Commonwealth Scientific and Industrial Research Organisation (CSIRO) in Melbourne, Australia.[30] Reversible chain transfer is achieved using a range of chain transfer agents known as RAFT agents.[31] They are most often dithioesters, but other forms of RAFT polymerisation use equivalent compounds such as xanthates or sulfur-free compounds.[32, 33]

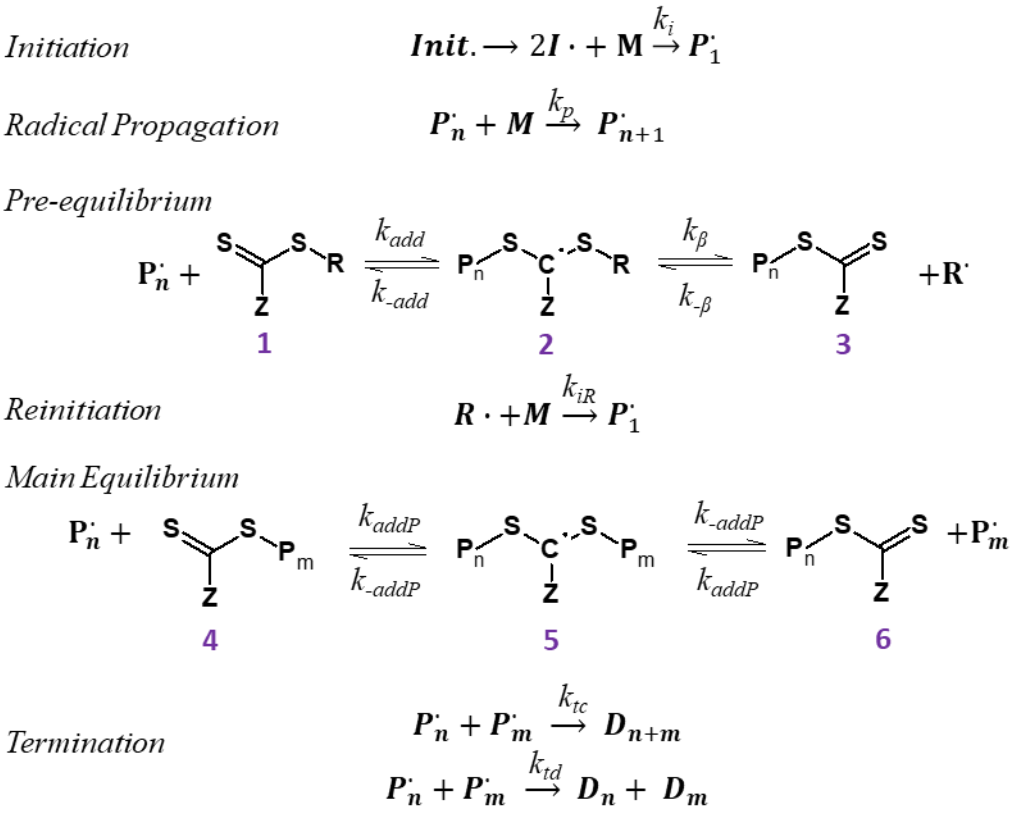

Scheme 1.2. Mechanism of RAFT polymerisation with associated rate constants.

The stages of a typical RAFT reaction are indicated in Scheme 1.2. A RAFT reaction begins with the use of a common radical initiator (e.g. azobisisobutyronitrile, AIBN), by which radicals are generated thermally or by using UV radiation. The initiating radical (I•) reacts with a monomer in solution to form an initial propagating radical (*initiation*). This may then react with another monomer to propagate the chain growth (*radical propagation*), or with a RAFT agent (**1**), setting up the RAFT *pre-equilibrium*. A carbon centred radical, the RAFT adduct, (**2**) is formed by the reaction of the propagating radical with the thiocarbonyl centre of the RAFT agent. This can then undergo reversible β-scission to form a leaving group (R•), and a dormant species (**3**). The R group should be chosen such that the pre-equilibrium equation lies to the right and the liberated R• radical can then (re)initiate a chain by reaction with monomer (*reinitiation*). The reinitiated chains can now set up the RAFT *main equilibrium* in which the RAFT end-group facilitates rapid chain transfer between growing polymer chains (**4** and **6**), in equilibrium with a second (dormant) RAFT adduct (**5**). This ensures that chain growth is statistically shared between growing chains, leading to polymers with low dispersity, and that termination is suppressed due to the low availability of radicals. As *termination* of propagating chains does still

occur, RAFT cannot be considered a true living polymerisation, but retains many advantages over traditional free radical polymerisation.

The control afforded by a RAFT agent can be considered in terms of two chain transfer coefficients, C_{tr} and C_{-tr}, which are defined by the following equations (1.26 – 1.29) which use the rate constants defined in Scheme 1.2:

$$\boldsymbol{C_{tr} = \frac{k_{tr}}{k_p}} \quad \textbf{1.26}$$

$$\boldsymbol{C_{-tr} = \frac{k_{-tr}}{k_{iR}}} \quad \textbf{1.27}$$

where

$$\boldsymbol{k_{tr} = k_{add}\phi = k_{add}\frac{k_\beta}{k_{-add} + k_\beta}} \quad \textbf{1.28}$$

and

$$\boldsymbol{k_{tr} = k_{-\beta}(1-\phi) = k_{add}\frac{k_{-add}}{k_{-add} + k_\beta}} \quad \textbf{1.29}$$

where ϕ is a partition coefficient that describes the preference for the pre-equilibrium to fragment to products or return to starting materials. For a controlled polymerisation, C_{tr} in the pre-equilibrium should be maximised (ideally >10) and C_{-tr} should be minimised.[34]

In an ideal RAFT polymerisation, the rate of propagation (R_p) is influenced by the radical concentration according to Equation 1.30:

$$\boldsymbol{R_p(t) = k_p[mon]\sqrt{\frac{fk_d[I]_0 e^{-k_d t}}{k_t}}} \quad \textbf{1.30}$$

Where k_p is the propagation coefficient, [*mon*] the monomer concentration, f the initiator efficiency, k_d the decomposition rate coefficient of the initiator, $[I]_0$ the initial initiator concentration, and k_t the termination rate coefficient.[31]

1.5.2 Choice of RAFT agent

Since its discovery in 1998, hundreds of RAFT agents have been developed.[35] The choice of an appropriate RAFT agent is of great importance as poor selection may lead to reduced control over dispersity and/or molecular weight. A successful RAFT reaction requires an acceptable rate of propagation to be maintained whilst ensuring the rate of termination by bimolecular chain coupling is insignificant. The R- and Z-groups of the RAFT agent (structure **1** in Scheme 1.2) are selected to maintain control of the polymerisation by determining the rates of addition and fragmentation.[34] The RAFT agent C=S bond must be more reactive than the monomer C=C bond.[31] The Z-group is responsible for the reactivity of the C=S bond towards radical addition, which must be considered in relation to the propagating chain. The R-group must be a good radical leaving group, yet rapidly reinitiate polymerisation to ensure all of the RAFT propagating radical species are generated in a short time period. The polarity of the R-group with respect to the solvent must be considered to ensure adequate stability of the free R· group.

The reactivity of the propagating radical P_n· depends on the monomer unit present at the chain end.[32] These are typically classified as more- or less-active monomers (MAMs and LAMs).[34] MAMs such as (meth)acrylates and (meth)acrylamides form relatively stable leaving groups due to conjugation of the vinyl double bond to an aromatic, carbonyl, or nitrile group, and therefore require a RAFT agent which is very reactive to radical addition to ensure the requirement for rapid chain transfer is met. Dithioesters and trithiocarbonates are often used to control these reactions.[36] LAMs such as vinyl acetate have unstable radicals, so are highly reactive to radical addition. Thus, the R and Z-group can be modified accordingly to ensure the RAFT adduct is less active. Xanthates are often selected for reactions involving LAMs. For selection of R-group, electron donating groups increase the RAFT agent transfer coefficient, so groups containing tertiary carbon centres are used often for MAMs.[34]

Switchable RAFT agents have also been developed. These are able to transfer between two states *via* an external stimulus, allowing them to control reactions involving both more and less active monomers.[37]

In this thesis, the selected monomers are all MAMs (methacrylate and methacrylamide). When considering the choice of RAFT agent for MAMs, dithiobenzoates (Z = Ph) have a very high chain transfer coefficient and are excellent at controlling the polymerisation of

methacrylates and methacrylamides. Three examples of commonly used dithiobenzoate RAFT agents are given in Figure 1.1.[38-40] Each uses tertiary alkyl R-groups to improve radical stability and partition rate. 4-Cyano-4-(phenylcarbonothioylthio)pentanoic acid (CTP, Figure 1.1A) and 2-cyano-2-propyl dithiobenzoate (CPDB, Figure 1.1B) both contain electron-withdrawing cyanoalkyl groups to increase C_{tr} by increasing the stability of the R˙ radical. CTP contains a pentanoic acid chain to improve compatibility in polar solvents compared to CPDB and cumyl dithiobenzoate (CDB, Figure 1.1C).[34] CDB forms a less polar and comparatively less stabilised R˙ radical.

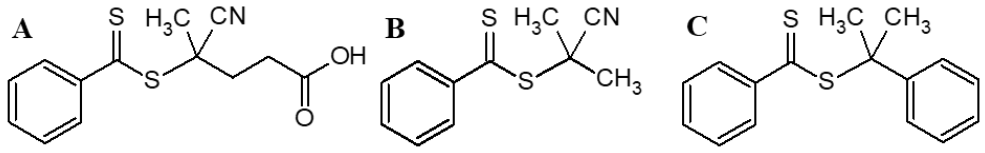

Figure 1.1. Dithiobenzoate RAFT agents. A) 4-cyano-4-(phenylcarbonothioylthio)pentanoic acid (CTP), B) 2-cyano-2-propyl dithiobenzoate (CPDB), C) Cumyl dithiobenzoate (CDB).

Despite the excellent control over reactions, dithiobenzoates suffer from poor stability in water, readily undergoing hydrolysis, and can cause rate retardation.[41] As shown in Equation 1.30, the rate of an ideal RAFT reaction is not dependent on the concentration of RAFT agent; however, high dithiobenzoate concentrations often lead to reduction of polymerisation rate. The precise cause of the rate retardation is complex and has been debated in the literature.[41] However, in general, retardation is due to excessive stabilisation of the RAFT adducts, which reduces the rate of fragmentation. The extra stabilisation is due to resonance forms of the RAFT adduct arising from the phenyl Z-group. The stable adducts either allow the formation of cross-termination products (*i.e.* side reactions whereby the adduct reacts with a propagating radical to form a 3-arm star) or slow fragmentation of the RAFT adduct (**2** and **5**) prevents the accumulation of propagating radicals necessary to achieve the rate of reaction predicted by the radical concentration.[41] The retardation could be due to either, or possibly both of these effects.[42] A further phenomenon observed with dithiobenzoate RAFT agents is an inhibition period at the beginning of the reaction, where monomer consumption is very slow for an extended period, before increasing to a steady rate.[41] This can be caused by inappropriate selection of the R-group, whereby either the R˙ radical is unable to reinitiate new chains or is too reactive with the RAFT group (*i.e.* does not fragment).[43] These effects cause very slow chain growth at the start of the reaction. This effect can lead to incomplete utilisation of the RAFT agent in the RAFT mechanism, which may lead to side reactions, or some RAFT

agent may remain unconsumed at the end of the reaction. This leads to higher-than-predicated molecular weights, as molecular weight predictions assume complete usage of RAFT agent.[35]

1.5.3 Synthesis of block copolymers using RAFT polymerisation

Many examples of block copolymer synthesis using RAFT polymerisation have been reported.[44] Initially, a homopolymer block is synthesised, which is subsequently used as a macro-RAFT agent to add a further monomer type.[32, 45] The monomer used in the first block must be a good homolytic leaving group with respect to the propagating radical of the second block to enable the macro-RAFT agent to reinitiate the polymerisation. In practice, this requires the "more active" monomer to be polymerised first, *e.g.* methacrylate must be prepared before acrylate and methacrylamide before acrylamide.[32, 46]

1.6 Mussel-inspired chemistry

An increasing number of scientists of all disciplines are turning to nature for inspiration. The hydrophobicity of the lotus leaf, the physical adhesion of the feet of geckos and the structural colour of some insects and birds are classic examples of physical phenomena which have been mimicked by researchers.[47]

Mussels are remarkable because of their ability to adhere strongly to rocks under challenging conditions: under water, with high ionic strength and under constant physical stresses from wave action. The ability of the marine mussel (of the family *Mytilidae*) to stick to an astonishing variety of substrates has been extensively studied and inspired a field of innovative chemistry.[48]

1.6.1 The adhesion of mussels on rocks and other surfaces

Mussels can bind to virtually any surface by the secretion of proteins from an organ known as the foot, which forms anchors called byssal threads (Figure 1.2).[49] These threads demonstrate remarkable hardness and stiffness but at the same time extensibility and resistance to damage.[50] It has been shown that the proteins found in the foot and byssal threads (mussel foot proteins [MFP], or mussel adhesive proteins [MAP]) contain the amino acid dihydroxyphenylalanine (DOPA) which is an oxidation product of tyrosine (Scheme 1.3). Many of the MFPs contain a significant amount of DOPA (20 – 30 mol%), which is thought to be the main component responsible for their excellent adhesion. Several different MFPs are known, which perform different roles in the adhesion process, some of which are still not completely understood. It has been observed however, that

MFPs with higher concentrations of DOPA are found nearest to the binding sites of the threads. The bonding prowess of DOPA has been attributed to the catechol functional group which is found in many naturally occurring molecules that adhere to a variety of substrates, through varied reaction processes.[51]

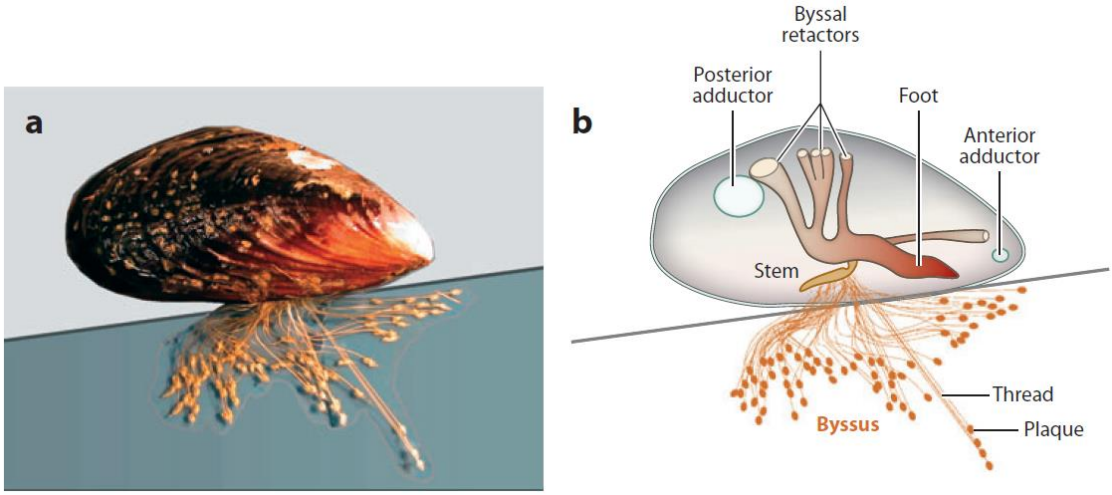

Figure 1.2. The adhesion method of the marine mussel. A) Photograph of an adult mussel showing the byssal threads adhered to a mica surface B) Diagram of the mussel showing the organs responsible for the production and secretion of byssal threads containing mussel foot proteins. Image reproduced with permission [48]. Copyright © 2011 by Annual Reviews.

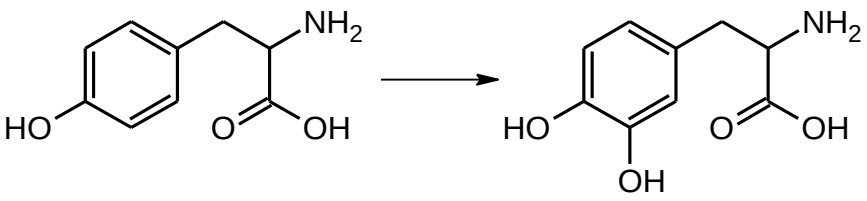

Scheme 1.3. Formation of DOPA from tyrosine.

The presence of DOPA in MFPs was discovered in 1981,[52] but it took another 18 years for it to be experimentally demonstrated that DOPA was responsible for the majority of the MFP's adhesive properties, and that DOPA itself could form an adhesive plaque.[53] However, the binding activity of mussels and the process is remarkably complex and has been shown to rely on more factors than simply the presence of DOPA in the MFPs.[54]

The presence of catechol oxidase enzyme in the mussel foot is thought to contribute to a crosslinking process *via* the oxidation of DOPA to a quinone.[52] It has been shown, however, that although the intermolecular crosslinking caused by the oxidation of DOPA was necessary to form a plaque, the oxidative process actually diminished the adhesion between a poly(DOPA) film and a mica substrate.[54] The lack of adhesion was caused by uncontrolled oxidative crosslinking of DOPA, however, oxidation is mediated in mussels

by the use of a protein rich in antioxidant thiols.[55] The crosslinking rate could be controlled under lab conditions by preparing a coating under acidic conditions (pH 3), and it was suggested that tautomerism of the proteins played a role in the crosslinking.[54] As the pH is raised, adhesion strength diminishes as oxidation occurs, but increases again at pH 7.5, similar to the pH of seawater.[56] This phenomenon was attributed to the binding modes of the catechol group; it adhered to metal oxide surfaces *via* hydrogen bonding at low pH, but the (oxidised) quinone formed strong bidentate coordination bonds at higher pH. Underwater adhesion is made possible by displacement of the surrounding water molecules when the catechol groups bind to the surface.[57]

Remarkably, the mussel also appears to be able to form the robust byssal threads using a different type of catechol chemistry; coordination complexes between MFP and Fe^{3+} contribute to the excellent combination of tensile strength and hardness.[58] Such variation and complex design suggests that there is still much to learn from the adhesion of animals such as mussels and confirms that the binding mechanism of the catechol functional group is impossible to consider in isolation.

1.6.2 The chemistry of catechol adhesion to surfaces

The adjacent hydroxyl groups in the catechol functionality have been observed to bind strongly to many surfaces. An advantage of using a catechol functionality is that it may bind by several different methods, which vary depending on the substrate and chemical environment (Figure 1.3).[47]

The catechol group may be attracted to a surface by non-covalent bonds. Due to the two hydroxyl groups, it it can bind strongly to a surface *via* hydrogen bonds, particularly organic coatings that contain hydrogen bonding functional groups, which are often found on biological surfaces.[59, 60] Additionally, the conjugated phenyl ring of catechol can form π-π stacking interactions and π-cation bonds.[61]

As discussed in section 1.6.1, catechols strongly chelate metal ions *via* bidentate interactions from the hydroxyl groups. This has been demonstrated for a variety of metal ions in solution.[62, 63] An alternative method of binding catechols in solution is with boronic acids, which form strong, reversible bonds, resulting in the formation of hydrogels when catechol-containing polymers were used.[64]

Catechols can form strong coordination bonds to metal oxides.[65, 66] Atomic force microscopy (AFM) studies of single molecules containing catechol attached to probes,

suggested that even a single catechol group could form strong bonds to a metal oxide surface. Oxidation of the catechol was shown to reduce the adhesion to metal oxides, but promote covalent bonding to organic surfaces.[67] It has also been proposed that as well as bidentate bonding, monodentate bonding can be supplemented by hydrogen bonding from the second hydroxyl group on the catechol.[68] This report also suggested a strongly chelating buffer such as citric acid buffer can compete with the catechol, leading to supressed binding to metal ions.

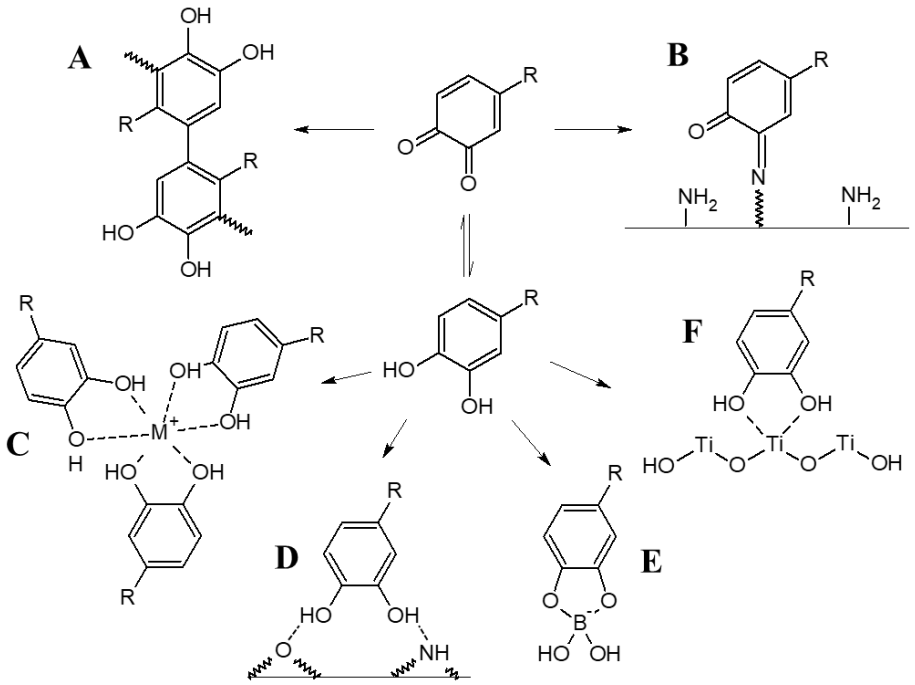

Figure 1.3. Binding modes of catechol functional group from the oxidised quinone form (above) and the catechol form (below). A) Covalent crosslinking, B) Schiff-base reaction, C) Coordination complex of a metal ion, D) Hydrogen bonding, E) Formation of borates, F) Bidentate bonding to metal oxide surfaces.

Catechols have also been shown to bind to surfaces *via* covalent bonds. These can be oxidation-induced bonding of the quinone form to amine, thiol or imidazole groups on a surface.[67] The oxidative state of catechol is important to consider, as depending on the substrate, it could enhance or diminish the strength of the binding.

1.6.3 Surface coatings and functional polymers synthesised by mussel inspired chemistry

It has been demonstrated that MFPs bind strongly to many surfaces in aqueous conditions. This makes them excellent candidates to be utilised as adhesives in situations which are inaccessible or challenging for traditional synthetic materials, such as wound dressings, antifouling coatings and underwater adhesives.[69] Although one mussel foot protein

(MFP1) is now available commercially, the price and practicality at industrial scale are prohibitive for all but the most specialist applications. For this reason, coatings have been developed using DOPA and similar catechol-containing molecules.[70] The most prominent of these catechol-containing molecules is dopamine (Figure 1.4), a chemical which notably occurs naturally as a neurotransmitter (amongst other functions) in the human body, but is widely available as a synthetic form.[71]

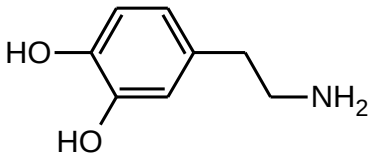

Figure 1.4. Chemical structure of dopamine.

A vast number of catechol-containing coatings and adhesives have been reported, which can be categorised into small molecule-based surface layers and polymeric coatings. The polymeric coatings can be further divided into auto-polymerised coatings of DOPA or dopamine, polymers with catechol side chains, and polymers with catechol end groups, each of which is discussed briefly herein.

1.6.3.1 Surface coatings using catechol-containing monolayers, anchors or initiators

Small molecules containing catechol groups are useful for functionalising surfaces *via* the formation of self-assembled monolayers. Such coatings can be used to change the physical properties of the substrate or can be further functionalised *via* layer-by-layer coating, polymer brush formation or chemical reaction *e.g.* click chemistry, and have been reviewed.[47] Three demonstrative examples are given in Figure 1.5 and discussed below.

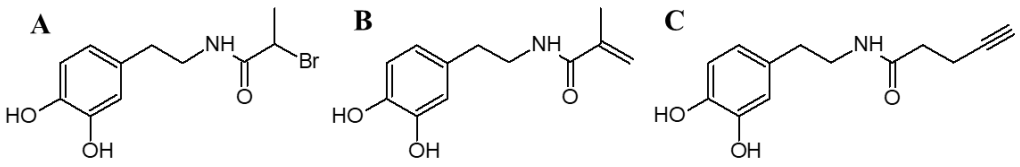

Figure 1.5. Examples of catechol functionalised small molecules used as surface coatings.

A facile method for producing catechol-containing compounds from dopamine was originally developed in 2005 by Messersmith *et al.*[65] who modified dopamine by reaction with a 2-bromopropionyl bromide (Figure 1.5A). The reaction product was subsequently used as an ATRP initiator, allowing the synthesis of polymer brushes from the surface by the "graft-from" method. This approach has been adopted and adapted by several authors

to synthesise catechol-functionalised initiators for the grafting-from method, using ring-opening metathesis polymerisation (ROMP) and RAFT polymerisation, and catechol functionalised polymer chains based on poly(ethylene glycol) (PEG) have been used to create polymer brushes by the "grafting-to" method, in which pre-formed polymer chains are attached to a surface.[72-74]

Dopamine methacrylamide (DMA) has also been used as an anchor point for graft copolymers (Figure 1.5B). It was deposited as a monolayer and the methacrylamide group was subsequently either initiated using AIBN to grow a polymer chain from the surface,[75] or a pre-formed polymer was grafted to the DMA using click-chemistry.[76] Surface coatings which enable subsequent functionalisation using click-chemistry have been reported. Dopamine was modified with an alkyne (Figure 1.5C) and immobilised on an iron oxide nanoparticle.[77] The anchored catechol-alkyne molecules were subsequently reacted with an N_3-capped PEG chains or N_3-functionalised rhodamine to prepare nanoparticles which were either water soluble or fluorescent.

1.6.3.2 Synthesis of surface coatings by the autopolymerisation of dopamine

In 2007, Messersmith *et al.* showed that dopamine can be autopolymerised in an aqueous alkaline solution at room temperature, and found it to be an effective surface coating for almost any material, including metals, organic surfaces, glass and even Teflon.[78] This discovery led to a significant body of research dedicated to investigating the properties of polydopamine coatings and how they can be utilised.

The chemical structure of the film, known as polydopamine (PDA), has come under some scrutiny and is not discussed in detail here, but is the subject of a number of informative review articles.[79, 80] However, it is currently thought to be an extended network of catecholamine-based oligomers connected with non-covalent bonds.[81] Due to the opportunity for modification before, during or after deposition, potential applications for polydopamine are wide ranging and subject to many recent publications.[79, 82]

To create functional surface coatings, PDA has been used to directly immobilise a variety of chemicals to a substrate surface by simply co-dissolving with dopamine during PDA deposition. Due to the wide range of possible binding interactions of the catechol, quinone, indole and amine groups found in PDA, many additional molecules can be incorporated within the PDA film as it forms, and the functional groups of the added molecules can become available at the film surface. This technique was exploited to facilitate a range of

secondary reactions on substrate surfaces, such as silicification and graft polymerisation by ATRP (Figure 1.6).[83]

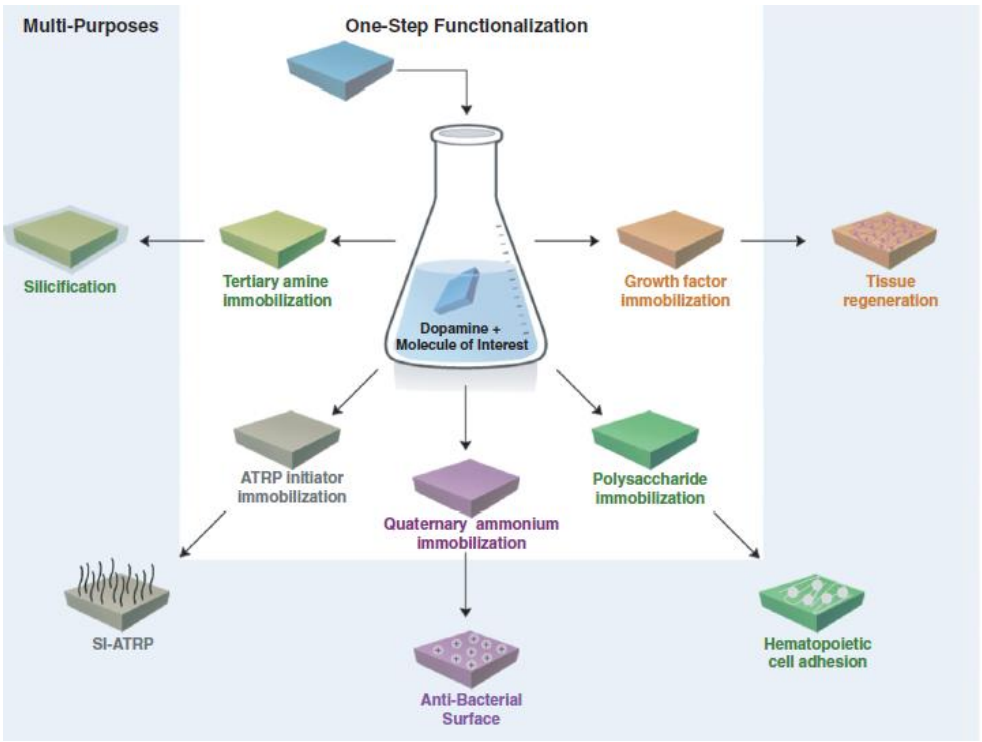

Figure 1.6. Examples of one-step immobilisation of molecules on substrate surfaces using PDA. Reproduced with permission.[83] Copyright © 2012 WILEY-VCH Verlag GmbH & Co.

The synthesis of PDA results in reactive catechol groups on the surface of the film and thus reaction between primary amines or thiols and catechol groups on the surface, often *via* Schiff base or Michael reactions (see Figure 1.3).[84-88] For example, PDA has been used to immobilise fluorescently labelled antibodies to a surface by reaction of the antibody thiol and primary amine groups with the catechols, simply by stirring in solution at pH 7.4 at 4 °C for 12 h.[85] The antibodies were subsequently used to immobilise a cancer biomarker, and the composite surfaces were used to test the efficacy of a diagnostic nanoparticle.

Films with the desirable adhesive properties of PDA can be formed using chemically modified dopamine-type precursors to add additional functionality to the coatings.[79] An example of this is the incorporation of an alkyl bromide group on dopamine (Scheme 1.4). The alkyl bromide was reacted with dopamine under oxygen-free basic conditions to form an uncharacterised intermediate, which was subsequently exposed to normal PDA reaction conditions. This formed a coating modified with the alkyl bromide, which could

subsequently be used to grow (methacrylate) polymer chains from the surface using ATRP to form potentially antifouling polymer brushes.[89]

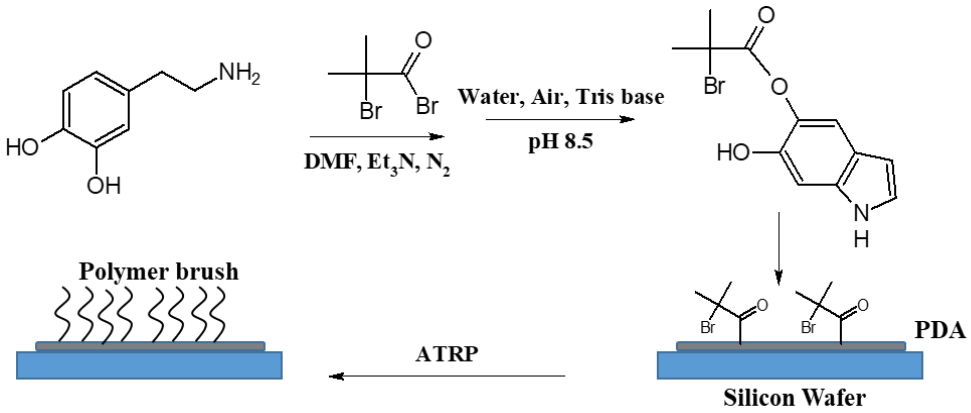

Scheme 1.4. Reaction of dopamine with alkyl bromide compound and subsequent immobilisation on a silicon wafer surface, followed by grafting of polymer chains on the PDA surface by ATRP.[89]

1.6.3.3 Polypeptide mussel foot protein mimics

To mimic mussel foot proteins, polypeptides of varying complexity have been synthesised by combining DOPA with further amino acids and assessed to establish whether these simplified systems could successfully replicate the adhesive properties of the MFPs.[90-93] In a recent example, a 25 amino acid peptide was prepared, with structural features mimicking those of a real MFP. It was shown that DOPA was necessary for underwater adhesion of the polypeptide to mineral surfaces, as the DOPA displaces water molecules from the substrate surface.[92]

The advantage of these polypeptides was that once the structure-property relationships have been investigated, the polypeptide can be specifically tailored by altering the amino acid sequence to improve adhesion and to shorten the chain length for easier processing. However, as yet they are not straightforward or cost-effective to produce at a large scale.

1.6.3.4 Synthesis of polymers with catechol end-groups

The reactivity and strongly adhesive nature of the catechol functional group has been exploited via the synthesis of end-capped polymers for various purposes. A single catechol group at the end of a polymer chain can be used to graft polymers to a substrate. Techniques such as ionic polymerisation or RDRP allow facile functionalisation of polymer chain ends. The catechol group can either be established at the chain end directly using a functionalised initiator or chain-transfer agent, or indirectly by modifying a polymer already terminated with a reactive end-group.[71]

In a reported procedure, N-hydroxysuccinimidyl propionate-activated PEG was coupled with five catechol derivatives.[68] This facile modification of a commercially available polymer allowed the preparation of anti-fouling coatings on metal oxide surfaces. It was shown that nitrodopamine-PEG formed a particularly effective end group, as the electron withdrawing nitro group increased the acidity of the hydroxyl protons, encouraging strong coordination bonding to metal oxide surfaces and resistance to oxidation in solution. The solution pH was important in determining the binding mode and film coverage, depending on the pK_a of the catechol derivative.

Alternatively, catechol-modified RAFT agents have been used to introduce catechol-functionalised end groups during the polymerisation, so further modification is not necessary. An example is the RAFT polymerisation of N-isopropylacrylamide (NIPAM) using a catechol-containing RAFT agent (Scheme 1.5).[94] The functionalised poly(NIPAM) showed switchable solubility in water determined by the presence of Fe^{3+} ions. This was due to the ability of the catechol groups to chelate ions to form insoluble clusters of 3 chains per Fe^{3+} ion. As Fe^{3+} is found in the body and is associated with neurodegenerative conditions, this approach could have therapeutic applications in future.

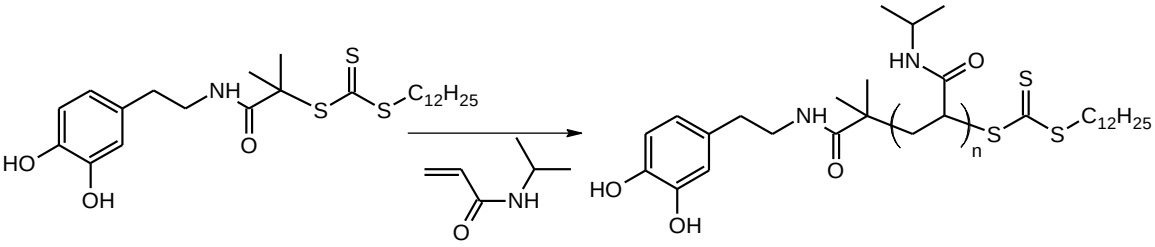

Scheme 1.5. RAFT polymerisation of NIPAM using a catechol functionalised RAFT agent.

1.6.3.5 Post-polymerisation modification to introduce catechol side-chains

As well as functionalising polymer chain ends with catechol groups, it is possible to functionalise the side chains of existing polymers with catechols to increase the density of the active groups in the chain.

One approach to grafting catechol side-chains to polymers is the synthesis of polymers containing pentafluorophenyl (meth)acrylate. Catechol side chains can be grafted on to the resulting polymer by nucleophilic substitution of the labile pentafluorophenyl group using dopamine (Figure 1.7).[95-98]

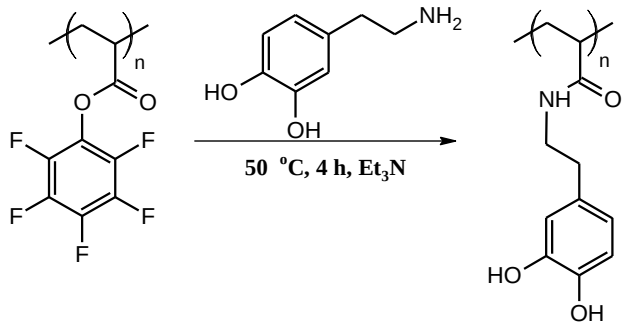

Figure 1.7. Reaction of poly(pentafluorophenyl methacrylate) with dopamine.

Catechol groups have also been grafted onto natural polymers. The first report of the use of dopamine as an adhesive involved crosslinking dopamine in the presence of chitosan and a tyrosinase enzyme. This oxidised the dopamine, causing it to graft onto the chitosan, subsequently allowing the adhesion of two glass slides underwater.[99]

1.6.3.6 Synthesis of polymers containing catechol-functionalised monomers

Compared to the functionalisation of pre-formed polymers, it is usually more straightforward to directly polymerise catechol-containing monomers. The direct incorporation of catechol side chains enables the synthesis of materials combining the versatile adhesive properties of the catechol with various other functionalities. This can be achieved by copolymerisation of catechol containing monomers with a wide range of functional monomers; an approach which has recently been reviewed by Detrembleur *et al.*[70] The approaches reviewed included the use of styrene derivatives, ring-opening polymerisation, and (meth)acrylamide monomers, examples of which are provided below.

Catechols are radical scavengers and in some cases have been used as polymerisation inhibitors *e.g.* 4-*tert*-butylcatechol or 3,5-di-*tert*-butylcatechol.[100] It may thus seem surprising that unprotected catechols can be used as monomers in polymerisations, but a number of reports confirm that this is possible. The polymerisation of unprotected catechol-containing monomers has been known to cause chain branching and insoluble deposits during polymerisation. Moreover such monomers also may inhibit reactions in which radical concentration is suppressed, such as RDRP reactions.[71] Therefore in many of the examples discussed, protection of the hydroxyl groups in the catechol was necessary.

The simplest approach to the incorporation of a catechol side chain is the polymerisation of 3,4-dihydroxystyrene (DHS) (Figure 1.8), which has been used in free radical polymerisation[101, 102], anionic polymerisation (in protected form),[20, 103] and RAFT polymerisation[104, 105] to synthesise homo- or copolymers with catechol functionalities.

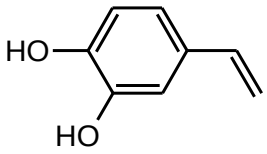

Figure 1.8. Chemical structure of 3,4-dihydroxystyrene.

Strategies to protect the catechol group of DHS include converting the catechol to its methyl ether, the use of silyl protecting groups or protection as an acetonide.[70] It is possible to remove the protecting group from the catechols post-polymerisation to reactivate the adhesive properties of the catechol functional group. In one example, the protecting groups were used proactively to influence polymer structure.[9] Frey *et al.* took advantage of modified protecting groups to influence monomer reactivity ratios in copolymerisations of 2,3-DHS or 3,4-DHS with styrene.

As well as the use of styrene derivatives, catechol-functionalised monomers have been synthesised using other common polymerisable functional groups. Ring-opening polymerisation has been used to synthesise catechol-containing polymers using a specially designed monomer containing an epoxide ring (catechol-acetonide glycidyl ether, Figure 1.9A).[106] The monomer was copolymerised with ethylene oxide and glycidol to obtain catechol functionalised linear and hyperbranched poly(ethylene glycol) and poly(glycidol) polymers respectively. These polymers were used to form biocompatible, adhesive, hydrogen-bonded networks which could be reversibly swollen by controlling the pH.

Dopamine maleimide has also been synthesised (Figure 1.9B).[107] The copolymerisation of this monomer with alkyl acrylate comonomers took advantage of the strong preference for maleimides to cross-propagate, leading to catechol functionalised alternating copolymers.

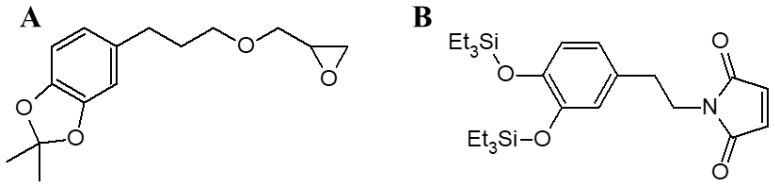

Figure 1.9. Chemical structures of catechol containing monomers. A) Catechol acetonide glycidyl ether, B) Silane-protected [3,4-dihydroxyphenyl)ethyl]-maleimide.

1.6.3.6.1 Synthesis and protection of catechol-functionalised (meth)acrylamide monomers

A common method of producing catechol-functionalised monomers is *via* the synthesis and polymerisation of catechol-containing (meth)acrylamide monomers. This class of

monomer has been studied in the current work, and various previously reported examples are discussed here.

Two of the most commonly investigated (meth)acrylamide monomers are DOPA (meth)acrylamide and dopamine (meth)acrylamide (Figure 1.10). The synthesis and polymerisation of DOPA (meth)acrylamide (Figure 1.10A) has been reported by several groups[108, 109] and has obvious similarities to the DOPA residues in MFPs, however the carboxylic acid group may provide unwanted reactivity in some applications.

Dopamine (meth)acrylamide (Figure 1.10B) has been more widely reported due to its relatively facile synthesis and compatibility with multiple polymerisation mechanisms, if suitably protected. [98, 110-112] The synthesis of dopamine methacrylamide (DMA) by the reaction of dopamine with methacrylic anhydride was first reported by Messersmith *et al.* in 2007.[110] DMA and its acrylamide variant (DA) have also been synthesised by the reaction between dopamine and (meth)acryloyl chloride, however this is far less commonly used due to the toxicity of the (meth)acryloyl chloride.[113]

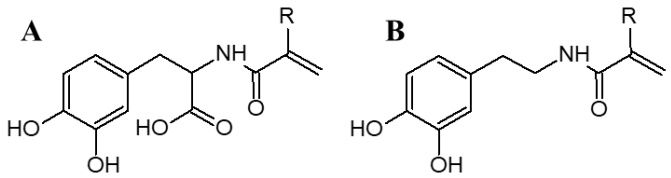

Figure 1.10. Chemical structures of A) DOPA methacrylamide (R = CH_3) and DOPA acrylamide (R = H). and B) dopamine methacrylamide (R = CH_3) and dopamine acrylamide (R = H).

Free radical copolymerisation of unprotected DMA and DA has been reported.[114] The apparent freedom to leave the functional group unprotected is surprising due to the potential for both crosslinking and radical scavenging by the catechol. The unprotected monomers do not inhibit their polymerisation, but there is some evidence that branched copolymers are formed through chain transfer via radical scavenging by the catechol group towards the propagating radical.[71]

Protecting group chemistry is usually necessary for the RDRP and ionic polymerisation of catechol containing monomers, as the influence of the hydroxyl groups is more pronounced (due to low radical concentrations or functional group-sensitive initiators), although RAFT copolymerisation of unprotected DMA with MMA has been reported.[115]

In an example of free radical polymerisation, Kamperman *et al*. protected DMA as a methyl ether and subsequently successfully deprotected the polymeric catechol with

BBr_3.[116] However, Detrembleur *et al*.[117], reported that BBr_3 is too acidic and can promote the hydrolysis of amides or oxidation of catechols. In contrast, they polymerised acetonide-protected DA and DMA (ADA/ADMA) using RAFT to synthesise block copolymers of ADMA and poly(ethylene glycol) methyl ether methacrylate. In this case the ADMA was deprotected post-polymerisation with trifluoroacetic acid.[117] Many other strategies have successfully been utilised to protect the catechol groups of monomers, including the use of a boronate and silanes (Figure 1.11).[70]

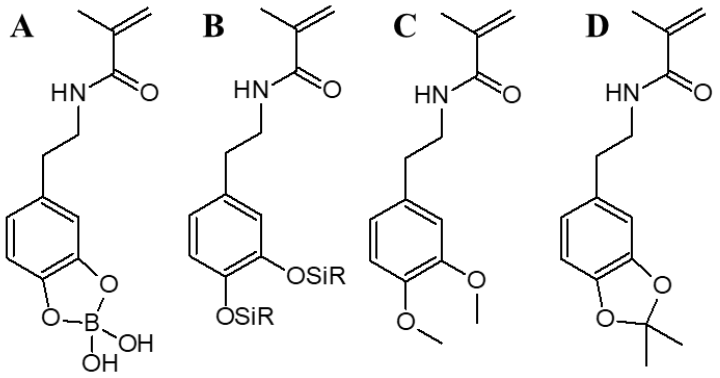

Figure 1.11. Protecting groups used to modify DMA. A) Boronate B) Silane, where OSiR = tertbutyl dimethyl silyl ether or triethyl silyl ether C) Methyl D) Acetonide.

The synthesis and application of a variety of adhesive copolymers containing DMA have been reported, and a few typical examples are discussed in more detail here, to highlight the versatility of DMA based polymers (see Figure 1.12). Copolymers comprising DMA have been used as functional adhesives[111, 116, 118-128] and for other diverse functions including filtration membranes and energy storage.[129, 130] The tendency of catechol containing compounds to chelate Fe^{3+} to form a cross-linked structure has also been utilised to form reversible hydrogels using DMA copolymers. [131-134]

A recent report described a pH switchable adhesive, based on copolymers of 3-acrylamido phenylboronic acid (AAPBA) and DMA.[135] Under basic conditions the boronate and catechol groups formed a complex which prevented the catechol from oxidising to the quinone form and subsequently crosslinking. When the solution was acidified, the complex disassociated and strong binding to a surface was observed.

The polymerisation of DMA with 2-hydroxytheyl methacrylate gave a system that could adhere to superparamagnetic iron oxide nanoparticles.[125] The versatility of the catechol was exploited as part of a dual-attack smart therapeutic system in which the unbound catechol groups in the polymer could conjugate to bortezomib, a borate-containing cancer

drug, which was subsequently released in the low pH environment of a tumour, whilst in parallel, a hyperthermic treatment was used to kill cancer cells by heating the nanoparticles using a magnetic field.

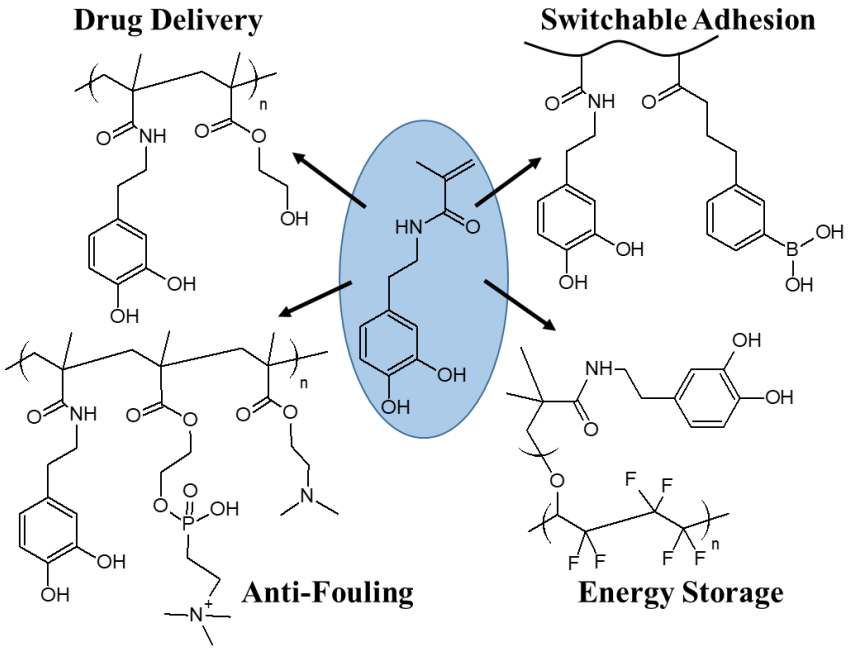

Figure 1.12. Examples of polymers synthesised with DMA for various purposes. A) poly(DMA-co-HEMA) B) DMA and AAPBA cross-linked hydrogel C) poly(DMA-co-MPC-co-DMAEMA) D) poly(VDF-co-HFP)-graft-poly(DMA).

Antifouling is another common application of DMA containing polymers. [109, 117, 123, 127, 136, 137] One approach is to combine cationic or zwitterionic monomers with DMA to produce antibacterial adhesive coatings. In one example, DMA was subjected to free radical polymerisation with 2-(dimethylamino)-ethyl methacrylate (DMAEMA) and 2-methacryloyloxyethyl phosphorylcholine (MPC).[136] This zwitterionic copolymer was subsequently immobilised on surfaces and quaternised and showed strong bactericidal properties and resisted biofilm formation.

Due to the redox potential of catechols, PDA and DMA have been used for energy storage applications. A poly(vinylidene fluoride-co-hexafluoropropylene) (VDF-co-HFP) was synthesised, treated with oxygen plasma, and p(DMA) was subsequently grafted onto the side chains.[130] This approach took advantage of the stability of the fluoropolymer, coupled with the polarisable hydroxyl groups, leading to a high energy density of 33 J cm^{-3}. The adhesive catechol groups also endowed the polymer with a very large dielectric breakdown strength, due to strong adhesion to a metal electrode.

In summary, the preceding discussion illustrates the wide variety of approaches that can be used to incorporate catechol functional groups into surface coatings and the diverse applications of such films.

1.7 Aims of the project

The primary objective of the work described in this thesis was to design a copolymer coating capable of adhering strongly to a wide variety of substrates and subsequently immobilising biomolecules for use in analytical devices. This was approached *via* the synthesis of a library of catechol-containing copolymers with various additional functional comonomers. The project aimed to address an industrial challenge to develop a low-cost, reliable device to detect aflatoxin M1, a potent human carcinogen which can be found in dairy products, particularly in the developing world.[138-140] Thus, antibody for aflatoxin M1 was chosen as the model biomolecule for the current work. However, due to the versatile adhesive properties of the catechol functional group and the epoxide functionality used to provide reactivity, the coatings could hypothetically be used on a variety of substrates to immobilise biomolecules for a wide variety of potential applications, especially in biomedical devices. The following paragraphs describe how the aims of the project were targeted *via* synthesis of copolymers using free radical and RAFT polymerisation, deposition of those coatings on silicon wafer substrates, and analysis of the physical properties of the polymer coatings.

Chapter 2: The synthesis of dopamine methacrylamide (DMA) and its protection using an acetonide group (acetonide-protected DMA, ADMA) was investigated to determine the most effective synthetic route. Free radical homopolymerisation of both monomers was investigated. A library of largely novel co- and terpolymers comprising either DMA or ADMA were synthesised, using a range of methacrylate comonomers, providing several candidates for coating investigations. The kinetics of copolymerisation of ADMA with i) MMA and ii) GMA in 1,4-dioxane were investigated to determine the reactivity ratios of the monomers. The compositional drift in several co- and terpolymer syntheses was monitored by NMR and compared to the reactivity ratio data to gain a greater understanding of the monomer sequence distributions obtained.

Chapter 3: RAFT polymerisations were carried out to determine appropriate conditions for the homopolymerisation of ADMA. Similar conditions were used homopolymerise several methacrylate monomers. Narrow dispersities and controlled molecular weights were

targeted. Potential factors affecting control, including solvent, temperature and the molar ratios of monomer, RAFT agent and initiator were considered. Novel gradient co- and terpolymers containing ADMA or DMA with methacrylate comonomers were synthesised for subsequent studies into coating performance in comparison with statistical copolymers prepared using free radical polymerisation. Block copolymers were also synthesised to provide a wider range of polymer architectures to explore.

Chapter 4: Selected co- and terpolymers were deposited onto model silicon wafer substrates. The polymers had a range of monomer compositions, comprising HEMA, DMA and/or GMA. The aim was to determine if smooth, repeatable and controllable coatings could be deposited using spin-coating. Methanol and DMF were used as solvents for the spin-coating experiments. Furthermore, deposition of the same copolymers was investigated *via* immersion coating with the aim of assessing the ability of the catechol functional group to promote adhesion to a silicon wafer directly from solution. The film thickness and topography was studied using spectroscopic ellipsometry and AFM.

Chapter 5: The physical properties of DMA-containing copolymers and their films, coated on silicon wafer, were investigated, using a variety of techniques, to determine their behaviour in water, and their suitability for immobilisation of biomolecules. Contact angle analysis was used to determine the wettability of the films. The surface charge in aqueous solutions of various pH was determined using electrokinetic streaming potential measurements. The swelling, dissolution or relaxation of the films in water was monitored in-situ using spectroscopic ellipsometry. Finally, the immobilisation of the antibody for aflatoxin on a terpolymer of HEMA, GMA and DMA was monitored using both in-situ ellipsometry and quartz crystal microbalance.

1.8 References

1. R. G. Jones, J. Kahovec, R. Stepto, E. S. Wilks, M. Hess, T. Kitayama and W. V. Metanomski, *Compendium of Polymer Terminology and Nomenclature -IUPAC Recommendations*, RSC Publishing, Cambridge, UK, 2008.
2. P. J. Flory, *J. Am. Chem. Soc.*, 1937, **59**, 241-253.
3. G. Odian, *Principles of Polymerization*, Wiley, 4th edn., 2004.
4. L. R. Hutchings, P. P. Brooks, D. Parker, J. A. Mosely and S. Sevinc, *Macromolecules*, 2015, **48**, 610-628.
5. S. V. Arehart and K. Matyjaszewski, *Macromolecules*, 1999, **32**, 2221-2231.
6. E. Baeten, J. Haven and T. Junkers, *Polym. Chem.*, 2017, **8**, 3815-3824.
7. A. Natalello, M. Werre, A. Alkan and H. Frey, *Macromolecules*, 2013, **46**, 8467-8471.
8. B. Obermeier, F. Wurm and H. Frey, *Macromolecules*, 2010, **43**, 2244-2251.
9. D. Leibig, A.-K. Lange, A. Birke and H. Frey, *Macromol. Chem. Phys.*, 2017, **218**, 1600553.
10. M. M. Alam, H. Peng, K. S. Jack, D. J. T. Hill and A. K. Whittaker, *J. Polym. Sci., Part A: Polym. Chem.*, 2017, **55**, 919-927.
11. N. S. Pujari, M. Wang and K. E. Gonsalves, *Polymer*, 2017, **118**, 201-214.
12. J. de la Fuente, M. Fernandez-Garcia, M. Fernandez-Sanz and E. Madruga, *Macromolecules*, 2001, **34**, 5833-5837.
13. A. S. Brar, A. K. Goyal, S. Hooda and R. Shankar, *J. Polym. Sci., Part A: Polym. Chem.*, 2009, **47**, 25-37.
14. F. R. Mayo and F. M. Lewis, *J. Am. Chem. Soc.*, 1944, **66**, 1594-1601.
15. M. Fineman and S. D. Ross, *J. Polym. Sci.*, 1949, **5**, 259-265.
16. T. Kelen and F. Tudos, *J. Macromol. Sci.: Part A - Chem.*, 1975, **9**, 1-27.
17. F. Tüdos, T. Kelen, T. Földes-Berezsnich and B. Turcsányi, *J. Macromol. Sci.: Part A - Chem.*, 1976, **10**, 1513-1540.
18. P. W. Tidwell and G. A. Mortimer, *J. Polym Sci: Part A*, 1965, **3**, 369-387.
19. V. E. Meyer and G. G. Lowry, *J. Polym Sci: Part A*, 1965, **3**, 2843-2851.
20. D. Leibig, A. H. E. Müller and H. Frey, *Macromolecules*, 2016, **49**, 4792-4801.
21. M. van den Brink, W. Smulders, A. M. van Herk and A. L. German, *J. Polym. Sci., Part A: Polym. Chem.*, 1999, **37**, 3804-3816.
22. N. Kazemi, T. A. Duever and A. Penlidis, *Macromol. React. Eng.*, 2011, **5**, 385-403.
23. A. Scott and A. Penlidis, *Processes*, 2018, **6**, 8.
24. A. J. Scott and A. Penlidis, *Eur. Polym. J.*, 2018, **105**, 442-450.
25. M. L. Coote and T. P. Davis, *Prog. Polym. Sci.*, 1999, **24**, 1217-1251.
26. L. R. Hutchings, S. Agostini, I. W. Hamley and D. Hermida-Merino, *Macromolecules*, 2015, **48**, 8806-8822.
27. J.-S. Wang and K. Matyjaszewski, *J. Am. Chem. Soc.*, 1995, **117**, 5614-5615.
28. M. Kato, M. Kamigaito, M. Sawamoto and T. Higashimura, *Macromolecules*, 1995, **28**, 1721-1723.
29. E. Rizzardo and D. H. Solomon, *Polym. Bull. (Berlin)*, 1979, **1**, 529-534.
30. J. Chiefari, Y. K. B. Chong, F. Ercole, J. Krstina, J. Jeffery, T. P. T. Le, R. T. A. Mayadunne, G. F. Meijs, C. L. Moad, G. Moad, E. Rizzardo and S. H. Thang, *Macromolecules*, 1998, **31**, 5559-5562.
31. S. Perrier, *Macromolecules*, 2017, **50**, 7433-7447.
32. C. Barner-Kowollik, *Handbook of RAFT Polymerization*, Wiley-VCH, 2008.

33. N. G. Engelis, A. Anastasaki, G. Nurumbetov, N. P. Truong, V. Nikolaou, A. Shegiwal, M. R. Whittaker, T. P. Davis and D. M. Haddleton, *Nature Chem.*, 2017, **9**, 171-178.
34. D. J. Keddie, G. Moad, E. Rizzardo and S. H. Thang, *Macromolecules*, 2012, **45**, 5321-5342.
35. G. Moad, E. Rizzardo and S. H. Thang, *Aust. J. Chem*, 2005, **58**, 379-410.
36. G. Moad, E. Rizzardo and S. H. Thang, *Polymer*, 2008, **49**, 1079-1131.
37. M. Benaglia, J. Chiefari, Y. K. Chong, G. Moad, E. Rizzardo and S. H. Thang, *J. Am. Chem. Soc.*, 2009, **131**, 6914-6915.
38. D. Fan, J. He, J. Xu, W. Tang, Y. Liu and Y. Yang, *J. Polym. Sci., Part A: Polym. Chem.*, 2006, **44**, 2260-2269.
39. C. S. Gudipati, M. B. H. Tan, H. Hussain, Y. Liu, C. He and T. P. Davis, *Macromol. Rapid Commun.*, 2008, **29**, 1902-1907.
40. Y. K. B. Chong, T. P. T. Le, G. Moad, E. Rizzardo and S. H. Thang, *Macromolecules*, 1999, **32**, 2071-2074.
41. C. Barner-Kowollik, M. Buback, B. Charleux, M. L. Coote, M. Drache, T. Fukuda, A. Goto, B. Klumperman, A. B. Lowe, J. B. McLeary, G. Moad, M. J. Monteiro, R. D. Sanderson, M. P. Tonge and P. Vana, *J. Polym. Sci., Part A: Polym. Chem.*, 2006, **44**, 5809-5831.
42. D. Konkolewicz, B. S. Hawkett, A. Gray-Weale and S. Perrier, *Macromolecules*, 2008, **41**, 6400-6412.
43. G. Moad, J. Chiefari, Y. K. Chong, J. Krstina, R. T. Mayadunne, A. Postma, E. Rizzardo and S. H. Thang, *Polym. Int.*, 2000, **49**, 993-1001.
44. D. J. Keddie, *Chem. Soc. Rev.*, 2014, **43**, 496-505.
45. M. Eberhardt and P. Théato, *Macromol. Rapid Commun.*, 2005, **26**, 1488-1493.
46. Y. A. Vasilieva, C. W. Scales, D. B. Thomas, R. G. Ezell, A. B. Lowe, N. Ayres and C. L. McCormick, *J. Polym. Sci., Part A: Polym. Chem.*, 2005, **43**, 3141-3152.
47. Q. Ye, F. Zhou and W. Liu, *Chem. Soc. Rev.*, 2011, **40**, 4244-4258.
48. B. P. Lee, P. B. Messersmith, J. N. Israelachvili and J. H. Waite, *Annu. Rev. Mater. Res.*, 2011, **41**, 99-132.
49. J. H. Waite, *Int. J. Adhes. Adhes.*, 1987, **7**, 9-14.
50. N. Holten-Andersen, G. E. Fantner, S. Hohlbauch, J. H. Waite and F. W. Zok, *Nat. Mater.*, 2007, **6**, 669-672.
51. B. A. Borgais, S. R. Cooper, Y. B. Koh and K. N. Raymond, *Inorg. Chem.*, 1984, **23**, 1009-1016.
52. J. H. T. Waite, M. L., *Science*, 1981, **212**, 1038-1040.
53. M. Yu, J. Hwang and T. J. Deming, *J. Am. Chem. Soc.*, 1999, **121**, 5825-2826.
54. J. Yu, W. Wei, E. Danner, J. N. Israelachvili and J. H. Waite, *Adv Mater*, 2011, **23**, 2362-2366.
55. J. Yu, W. Wei, E. Danner, R. K. Ashley, J. N. Israelachvili and J. H. Waite, *Nat. Chem. Biol.*, 2011, **7**, 588-590.
56. J. Yu, W. Wei, M. S. Menyo, A. Masic, J. H. Waite and J. N. Israelachvili, *Biomacromolecules*, 2013, **14**, 1072-1077.
57. J. Wang, M. N. Tahir, M. Kappl, W. Tremel, N. Metz, M. Barz, P. Theato and H.-J. Butt, *Adv. Mater.*, 2008, **20**, 3872-3876.
58. M. J. Harrington, A. Masic, N. Holten-Andersen, J. H. Waite and P. Fratzl, *Science*, 2010, **328**, 216-220.
59. P. K. Forooshani and B. P. Lee, *J. Polym. Sci., Part A: Polym. Chem.*, 2016, **55**, 9-33.

60. T. H. Anderson, J. Yu, A. Estrada, M. U. Hammer, J. H. Waite and J. N. Israelachvili, *Adv. Funct. Mater.*, 2010, **20**, 4196-4205.
61. W. Wei, J. Yu, M. A. Gebbie, Y. Tan, N. R. Martinez Rodriguez, J. N. Israelachvili and J. H. Waite, *Langmuir*, 2015, **31**, 1105-1112.
62. M. J. Sever and J. J. Wilker, *Dalton Trans.*, 2006, **6**, 813-822.
63. B. P. Lee, C.-Y. Chao, F. N. Nunalee, E. Motan, K. R. Shull and P. B. Messersmith, *Macromolecules*, 2006, **39**, 1740-1748.
64. L. He, D. E. Fullenkamp, J. G. Rivera and P. B. Messersmith, *Chem Commun (Camb)*, 2011, **47**, 7497-7499.
65. X. W. Fan, L. J. Lin, J. L. Dalsin and P. B. Messersmith, *J. Am. Chem. Soc.*, 2005, **127**, 15843-15847.
66. J. L. Dalsin, L. Lin, S. Tosatti, J. Vörös, M. Textor and P. B. Messersmith, *Langmuir*, 2005, **21**, 640-646.
67. H. Lee, N. F. Scherer and P. B. Messersmith, *Proc. Natl. Acad. Sci. U. S. A.*, 2006, **103**, 12999-13003.
68. B. Malisova, S. Tosatti, M. Textor, K. Gademann and S. Zurcher, *Langmuir*, 2010, **26**, 4018-4026.
69. A. M. Baty, P. A. Suci, B. J. Tyler and G. G. Geesey, *J. Coll. Int. Sci.*, 1995, **177**, 307-315.
70. N. Patil, C. Jérôme and C. Detrembleur, *Prog. Polym. Sci.*, 2018, **82**, 34-91.
71. E. Faure, C. Falentin-Daudré, C. Jérôme, J. Lyskawa, D. Fournier, P. Woisel and C. Detrembleur, *Prog. Polym. Sci.*, 2013, **38**, 236-270.
72. Q. Ye, X. Wang, S. Li and F. Zhou, *Macromolecules*, 2010, **43**, 5554-5560.
73. Z. Shafiq, J. Cui, L. Pastor-Perez, V. San Miguel, R. A. Gropeanu, C. Serrano and A. del Campo, *Angew. Chem., Int. Ed. Engl.*, 2012, **51**, 4332-4335.
74. Y. Oz, M. Arslan, T. N. Gevrek, R. Sanyal and A. Sanyal, *ACS Appl. Mater. Interfaces*, 2016, **8**, 19813-19826.
75. A. Muñoz-Bonilla, G. Marcelo, C. Casado, F. J. Teran and M. Fernández-García, *J. Polym. Sci., Part A: Polym. Chem.*, 2012, **50**, 5087-5096.
76. X. Li, M. Bao, Y. Weng, K. Yang, W. Zhang and G. Chen, *J. Mater. Chem. B*, 2014, **2**, 5569.
77. A. S. Goldmann, C. Schodel, A. Walther, J. Yuan, K. Loos and A. H. Muller, *Macromol Rapid Commun*, 2010, **31**, 1608-1615.
78. H. Lee, S. M. Dellatore, W. M. Miller and P. B. Messersmith, *Science*, 2007, **318**, 426-430.
79. J. H. Ryu, P. B. Messersmith and H. Lee, *ACS Appl. Mater. Interfaces*, 2018, **10**, 7523-7540.
80. J. Liebscher, R. Mrowczynski, H. A. Scheidt, C. Filip, N. D. Hadade, R. Turcu, A. Bende and S. Beck, *Langmuir*, 2013, **29**, 10539-10548.
81. M. d'Ischia, A. Napolitano, V. Ball, C. T. Chen and M. J. Buehler, *Acc. Chem. Res.*, 2014, **47**, 3541-3550.
82. Y. Liu, K. Ai and L. Lu, *Chem Rev*, 2014, **114**, 5057-5115.
83. S. M. Kang, N. S. Hwang, J. Yeom, S. Y. Park, P. B. Messersmith, I. S. Choi, R. Langer, D. G. Anderson and H. Lee, *Adv. Funct. Mater.*, 2012, **22**, 2949-2955.
84. H. Lee, J. Rho and P. B. Messersmith, *Adv Mater*, 2009, **21**, 431-434.
85. J. Peng, L. N. Feng, K. Zhang, J. J. Li, L. P. Jiang and J. J. Zhu, *Chemistry*, 2011, **17**, 10916-10923.
86. J. Zhang, W. Zhang, N. Zhou, Y. Weng and Z. Hu, *RSC Advances*, 2014, **4**, 24973.
87. W. J. Yang, K.-G. Neoh, E.-T. Kang, S. Lay-Ming Teo and D. Rittschof, *Polym. Chem.*, 2013, **4**, 3105.

88. W. Sheng, B. Li, X. Wang, B. Dai, B. Yu, X. Jia and F. Zhou, *Chem. Sci.*, 2015, **6**, 2068-2073.
89. B. Zhu and S. Edmondson, *Polymer*, 2011, **52**, 2141-2149.
90. M. Yu and T. J. Deming, *Macromolecules*, 1998, **31**, 4739-4745.
91. M. J. Sever and J. J. Wilker, *Tetrahedron*, 2001, **57**, 6139-6146.
92. W. Wei, L. Petrone, Y. Tan, H. Cai, J. N. Israelachvili, A. Miserez and J. H. Waite, *Adv. Funct. Mater.*, 2016, **26**, 3496-3507.
93. A. R. Statz, R. J. Meagher, A. E. Barron and P. B. Messersmith, *J. Am. Chem. Soc.*, 2005, **127**, 7972-7973.
94. D. J. Phillips, I. Prokes, G. L. Davies and M. I. Gibson, *Acs Macro Letters*, 2014, **3**, 1225-1229.
95. L. Q. Xu, D. Pranantyo, J. B. Liu, K.-G. Neoh, E.-T. Kang, Y. X. Ng, S. Lay-Ming Teo and G. D. Fu, *RSC Advances*, 2014, **4**, 32335.
96. M. Eberhardt, R. Mruk, R. Zentel and P. Théato, *Eur. Polym. J.*, 2005, **41**, 1569-1575.
97. B. Oschmann, D. Bresser, M. N. Tahir, K. Fischer, W. Tremel, S. Passerini and R. Zentel, *Macromol. Rapid Commun.*, 2013, **34**, 1693-1700.
98. L. Q. Xu, H. Jiang, K.-G. Neoh, E.-T. Kang and G. D. Fu, *Polym. Chem.*, 2012, **3**, 920.
99. K. Yamada, T. Chen, G. Kumar, O. Vesnovsky, L. D. T. Topoleski and G. F. Payne, *Biomacromolecules*, 2000, **1**, 252-258.
100. L. R. C. Barclay, C. E. Edwards and M. R. Vinqvist, *J. Am. Chem. Soc.*, 1999, **121**, 6226-6231.
101. Z. Yang and R. Pelton, *Macromol. Rapid Commun.*, 1998, **19**, 241-246.
102. J. D. White and J. J. Wilker, *Macromolecules*, 2011, **44**, 5085-5088.
103. G. Westwood, T. N. Horton and J. J. Wilker, *Macromolecules*, 2007, **40**, 3960-3964.
104. A. Isakova, P. D. Topham and A. J. Sutherland, *Macromolecules*, 2014, **47**, 2561-2568.
105. Y. Saito and H. Yabu, *Chem Commun (Camb)*, 2015, **51**, 3743-3746.
106. K. Niederer, C. Schüll, D. Leibig, T. Johann and H. Frey, *Macromolecules*, 2016, **49**, 1655-1665.
107. M. A. Bartucci, E. Napadensky, J. L. Lenhart and J. A. Orlicki, *RSC Adv.*, 2017, **7**, 49114-49118.
108. B. P. Lee, K. Huang, F. N. Nunalee, K. R. Shull and P. B. Messersmith, *J. Biomater. Sci., Polym. Ed.*, 2004, **15**, 449-464.
109. E. Faure, P. Lecomte, S. Lenoir, C. Vreuls, C. Van De Weerdt, C. Archambeau, J. Martial, C. Jérôme, A.-S. Duwez and C. Detrembleur, *J. Mater. Chem.*, 2011, **21**, 7901.
110. H. Lee, B. P. Lee and P. B. Messersmith, *Nature*, 2007, **448**, 338-341.
111. P. Glass, H. Chung, N. R. Washburn and M. Sitti, *Langmuir*, 2009, **25**, 6607-6612.
112. F. Zhang, S. Liu, Y. Zhang, J. Xu and Z. Chi, *Int. J. Adhes. Adhes.*, 2011, **31**, 583-586.
113. J. Yang, I. Bos, W. Pranger, A. Stuiver, A. H. Velders, M. A. Cohen Stuart and M. Kamperman, *J. Mater. Chem. A*, 2016, **4**, 6868-6877.
114. C. R. Matos-Perez, J. D. White and J. J. Wilker, *J. Am. Chem. Soc.*, 2012, **134**, 9498-9505.
115. A. GhavamiNejad, A. R. K. Sasikala, A. R. Unnithan, R. G. Thomas, Y. Y. Jeong, M. Vatankhah-Varnoosfaderani, F. J. Stadler, C. H. Park and C. S. Kim, *Adv. Funct. Mater.*, 2015, **25**, 2867-2875.

116. J. Yang, J. Keijsers, M. van Heek, A. Stuiver, M. A. Cohen Stuart and M. Kamperman, *Polym. Chem.*, 2015, **6**, 3121-3130.
117. N. Patil, C. Falentin-Daudré, C. Jérôme and C. Detrembleur, *Polym. Chem.*, 2015, **6**, 2919-2933.
118. H. Chung, P. Glass, J. M. Pothen, M. Sitti and N. R. Washburn, *Biomacromolecules*, 2011, **12**, 342-347.
119. J. K. Park, K. S. Kim, J. Yeom, H. S. Jung and S. K. Hahn, *Macromol. Chem. Phys.*, 2012, **213**, 2130-2135.
120. S. Skelton, M. Bostwick, K. O'Connor, S. Konst, S. Casey and B. P. Lee, *Soft Matter*, 2013, **9**, 3825.
121. J. Xue, T. Wang, J. Nie and D. Yang, *J. Appl. Polym. Sci.*, 2013, **127**, 5051-5058.
122. H. J. Meredith and J. J. Wilker, *Adv. Funct. Mater.*, 2015, **25**, 5057-5065.
123. *World Patent Pat.*, WO 2015/175665 A1, 2015.
124. X. Wang, Q. Ye, J. Liu, X. Liu and F. Zhou, *J. Colloid Interface Sci.*, 2010, **351**, 261-266.
125. A. R. Sasikala, A. GhavamiNejad, A. R. Unnithan, R. G. Thomas, M. Moon, Y. Y. Jeong, C. H. Park and C. S. Kim, *Nanoscale*, 2015, **7**, 18119-18128.
126. H. N. Nguyen, E. T. Nadres, B. G. Alamani and D. F. Rodrigues, *J. Mater. Chem. B*, 2017, **5**, 6616-6628.
127. A. GhavamiNejad, C. H. Park and C. S. Kim, *Biomacromolecules*, 2016, **17**, 1213-1223.
128. S. Yamamoto, S. Uchiyama, T. Miyashita and M. Mitsuishi, *Nanoscale*, 2016, **8**, 5912-5919.
129. Y. S. Choi, H. Kang, D. G. Kim, S. H. Cha and J. C. Lee, *ACS Appl. Mater. Interfaces*, 2014, **6**, 21297-21307.
130. M. Rahimabady, L. Qun Xu, S. Arabnejad, K. Yao, L. Lu, V. P. W. Shim, K. Gee Neoh and E.-T. Kang, *Appl. Phys. Lett.*, 2013, **103**, 262904.
131. E. M. White, J. E. Seppala, P. M. Rushworth, B. W. Ritchie, S. Sharma and J. Locklin, *Macromolecules*, 2013, **46**, 8882-8887.
132. H. Shao and R. J. Stewart, *Adv Mater*, 2010, **22**, 729-733.
133. G. Marcelo, E. Kaplan, M. P. Tarazona and F. Mendicuti, *Colloids Surf., B*, 2015, **128**, 237-244.
134. H. O. Ham, Z. Liu, K. H. Lau, H. Lee and P. B. Messersmith, *Angew. Chem., Int. Ed. Engl.*, 2011, **50**, 732-736.
135. A. R. Narkar, B. Barker, M. Clisch, J. Jiang and B. P. Lee, *Chem. Mater.*, 2016, **28**, 5432-5439.
136. B. L. Wang, T. W. Jin, Y. M. Han, C. H. Shen, Q. Li, Q. K. Lin and H. Chen, *J. Mater. Chem. B*, 2015, **3**, 5501-5510.
137. H. Wu, V. Sariola, C. Zhu, J. Zhao, M. Sitti and C. J. Bettinger, *Adv Mater*, 2015, **27**, 3398-3404.
138. A. Karczmarczyk, M. Dubiak-Szepietowska, M. Vorobii, C. Rodriguez-Emmenegger, J. Dostalek and K. H. Feller, *Biosens. Bioelectron.*, 2016, **81**, 159-165.
139. W. Hu, X. Li, G. He, Z. Zhang, X. Zheng, P. Li and C. M. Li, *Biosens. Bioelectron.*, 2013, **50**, 338-344.
140. L. K. Sorensen and T. H. Elbaek, *J. Chromatogr., B: Anal. Technol. Biomed. Life Sci.*, 2005, **820**, 183-196.

Chapter 2 Investigation of compositional drift in free radical (co)polymerisation of catechol containing methacrylamide monomers with methacrylate monomers

2.1 Introduction

2.1.1 Radical reactions of monomers containing catechol functional groups

It has been well established in the literature that the catechol functional group is able to scavenge radicals by the donation of a hydrogen atom to a free radical.[1] Indeed, certain catechol-containing species with electron donating substituents are used as polymerisation inhibitors. Relative to the dihydroxybenzene isomers with the hydroxyl groups in the *meta* and *para* positions (resorcinol and hydroquinone respectively), the proximity of the two hydroxyl groups in catechol has been shown to increase its radical scavenging ability due to H-bonding (Scheme 2.1A).[2] However, in the absence of oxygen the ability of the catechol group to scavenge radicals is reduced such that free radical copolymerisation using catechol-containing monomers is possible with mole fractions of up to 50%.[3, 4]

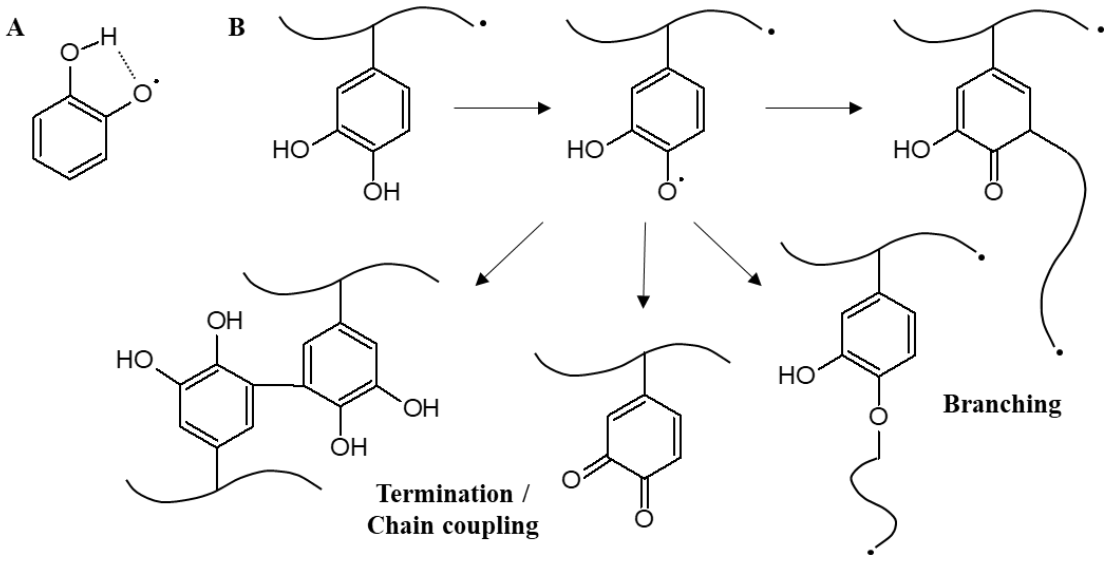

Scheme 2.1. A) Stabilisation of a catechol radical via intramolecular H-bonding. B) Reactions of catechol side chains to cause chain branching, termination or chain coupling.

In copolymerisations comprising unprotected catechol-containing monomers, the radical scavenging effect of catechols on polymerisation is largely ignored as the by-products do not significantly affect the desired functions of the polymer and are difficult to identify. Furthermore, there is some confusion arising from use of the term "radical scavenging", which is generally used to refer to any reaction between a free radical and the hydroxyl group on the catechol. However, the potential side-reactions of a catechol group in a free radical polymerisation are numerous and varied. A catechol side chain on a polymer or a

catechol-containing monomer could react with: i) an initiator-derived radical, ii) the propagating radical of another chain (branching) or of the same chain (backbiting).[5-7] Once formed, catechol radicals may couple with propagating radicals from other chains or catechol side chains, potentially forming cross-linked networks or reaction with monomers may form branched chains (Scheme 2.1B). Catechol-containing monomers can also participate in reactions i) and ii). If initiator radicals are removed from the polymerisation by reaction i), the rate of reaction may be retarded and fewer polymer chains initiated. On the other hand, reaction ii) leads to chain transfer. Both reactions result in the formation of a side-chain radical on the catechol, which can either terminate by hydrogen abstraction or react further. Furthermore, potential chain transfer to monomer could lead to copolymers with reduced molecular weight. To avoid ambiguity, in this chapter, the term "radical scavenging" will only be used to describe the reaction between catechol species and initiator-derived radicals. The reactions of catechol side chains to generate coupled or branched polymers will be considered separately.

2.1.2 Reactivity ratios of catechol-containing monomers

Compositional drift (the change in composition of copolymer chains synthesised over the course of a reaction) is often an unavoidable feature of free radical (FR) polymerisations. When using functional monomers, understanding the compositional drift can be vital, as the structure of the resulting copolymers may change throughout the course of the reaction, potentially leading to unintended copolymer properties and behaviour. Compositional drift is thus often unwelcome and avoided if possible but, with greater understanding of the distribution of monomers in the copolymers, it can be advantageous.[8] For example, in one report, compositional drift in the synthesis of poly(d-styrene-*ran*-2-vinylpyridine) was found to improve the interfacial strength of an adhesive by providing a gradient of bulk copolymer composition over an interface.[9] Use of deuterated styrene allowed analysis of the composition gradient of the adhesive coatings using ion beam analysis. In contrast, no improved adhesion was detected when copolymers synthesised with low monomer conversion – to reduce the compositional drift – were tested. Compositional drift has been observed in polymerisations of dopamine methacrylamide (DMA) with alkyl methacrylates.[10] An increasing feed mole fraction of DMA was required to achieve the targeted 10 % DMA polymer composition as the comonomer alkyl side chain length increased. However, the effect was not investigated further by the authors.

A useful way to predict and understand compositional drift is to calculate the reactivity ratios of the system of interest. Reactivity ratios are important parameters which are used to understand and predict the outcome of copolymerisations. Various mathematical models have been developed to estimate reactivity ratios and are described in Chapter 1.

Despite a significant number of previous reports on the copolymerisation of catechol containing monomers, no reactivity ratio data for the FR copolymerisation of DMA, or other catechol-containing (meth)acrylamide monomers, with methacrylate monomers has been previously published. Herein, for the first time to the best of our knowledge, we report reactivity ratios for the copolymerisation of acetonide-protected DMA (ADMA) with i) methyl methacrylate (MMA) and ii) glycidyl methacrylate (GMA).

Reactivity ratios for the polymerisation of methacrylamide monomers with various methacrylate comonomers have been widely reported in the literature and values for many common systems are available in textbooks.[11-14] In general, the reported data indicate that self-propagation of the methacrylate monomer and cross-propagation of the methacrylamide monomer is favoured. Thus, the reactivity ratio for the methacrylate monomer is >1 and for the methacrylamide is <1.[13, 15] This will lead to compositional drift in FR polymerisations.

Even within the family of methacrylate/methacrylamide copolymers, the specific copolymerisation kinetics can vary significantly from system to system and one should be cautious about making assumptions about the behaviour of any particular comonomer system. For instance, a change in solvent can have a dramatic effect in the rate of propagation or copolymerisation reactivity:[16] the homopolymerisation propagation rate of methacrylic acid increases by an order of magnitude when carried out in water compared to in bulk, due to interactions between the solvent and propagating radical in the propagation transition state.[17]

There are, however, a very limited number of reports of the copolymerisation kinetics of catechol containing monomers, especially those using FR polymerisation. Reactivity ratios have been previously reported for the FR copolymerisation of borax-protected dopamine acrylamide (DAA-p) with 2-aminoethylmethacrylamide (AEMA), using water as the solvent.[18] The calculated ratios were $r_{DAA\text{-}p} = 0.00$ and $r_{AEMA} = 0.46$. As both reactivity ratios are less than 1.0 and with r_{DA} being equal to zero, it would be expected that this polymerisation would lead to a copolymer with a close to alternating monomer sequence.

However, the authors incorrectly state that as $r_{AEMA} = 0.46$, "*AEMA propagating radicals add to DAA-p in about half of the case*s" when in fact cross-propagation (addition of DAA-p to a propagating radical with a terminal AEMA group) would be strongly favoured. Although the kinetics of the DAA-p and AEMA system are of interest due to the catechol functionalised monomer, the data cannot be used to directly inform the copolymerisation kinetics of the systems of interest in the current work because of the different nature of the comonomers and solvent.

2.1.3 The use of functional methacrylates as comonomers

MMA has been studied extensively in the wider literature and exploited by industry due to its versatile properties, wide solubility range and chemical resistance.[19] It is often copolymerised with a range of functional monomers to achieve desired properties.[20] Investigating the copolymerisation kinetics of MMA with functional monomers is vital to improve understanding of the monomer composition in the resulting copolymers.[21] Such data is becoming more widely available for the reaction of MMA with a selection of functional monomers.[22, 23]

Numerous functional derivatives of MMA have been investigated for various applications and are often used to modify monomer hydrophobicity or solubility. A commonly utilised hydrophilic methacrylate monomer is 2-hydroxyethyl methacrylate (HEMA) which is often copolymerised with cross-linkable monomers to yield hydrogels, and often used in biomedical fields.[24-26] Poly(ethylene glycol) methyl ether methacrylate (PEGMEM) has also been widely investigated, as the hydrophilicity of copolymers can be tuned according to the length of the poly(ethylene glycol) (PEG) side chain and the mole fraction of PEGMEM.[27] Copolymers containing PEG methacrylates are popular in industry and academia due to their biocompatibility, antifouling properties and solubility in water.[28]

Epoxide-containing monomers such as glycidyl methacrylate (GMA) have been utilised to introduce reactive functionality into (co)polymers synthesised by radical polymerisation.[29] The reactivity of the epoxide functional group is well known and has been widely exploited.[30] The most common use of epoxides is condensation polymerisation to form epoxy-resins. A particular advantage of GMA is that the epoxide-containing side chain does not undergo ring-opening reactions during FR polymerisation, so it can be subsequently modified post-polymerisation.[31] Many other functional groups react with epoxides, notably amines and thiols, making the inclusion of epoxide functionalities in

copolymers a useful method for the immobilisation of proteins such as enzymes or antibodies.[32, 33]

As GMA is utilised in this project with the aim of synthesising copolymers capable of binding biomolecules to a surface, two previously reported examples of GMA-containing polymerisations of particular relevance are discussed here. A terpolymer of MMA, GMA and a crosslinkable monomer (ethylene glycol dimethacrylate) was synthesised by suspension polymerisation to form polymer beads.[34] The epoxy groups were subsequently modified with ammonia or 1,6-diaminohexane, followed by covalent attachment of the amino acid L-arginine. Antibodies were immobilised onto the surface of the beads by a reversible interaction with the L-arginine. Introduction of the spacer group (1,6-diaminohexane) increased protein binding due to reduced steric hindrance. In another example, HEMA was copolymerised with GMA by surface-initiated atom transfer radical polymerization (SI-ATRP) to form surface-bound copolymer brushes which were able to immobilise antibodies directly under mild conditions (phosphate buffered saline, 0.15 M, 37 °C, 1 h).[35] The binding occurred due to a covalent reaction of the epoxide group of the GMA with the antibody primary amine groups. In neither of the two previous examples were the reactivity ratios or polymerisation kinetics considered or reported, which could assist in understanding the behaviour of the copolymers.

2.2 Aims

The aims of the work reported in this chapter were:

1. To compare the effectiveness of previously reported methods to synthesize DMA.[3, 6] The synthesis of DMA were optimised to obtain the most effective reaction conditions. The conditions required for protection of the catechol functional group of DMA as an acetonide were also investigated, with a view to supressing the radical scavenging ability of the catechol group.

2. To compare the homopolymerisation of DMA and ADMA to gain an insight into the effect of protecting the catechol group on the FR polymerisation of DMA, and to explore conditions for the free radical polymerisation of ADMA which has not previously been reported.

3. To investigate the copolymerisation kinetics of i) ADMA and MMA and ii) ADMA and GMA in 1,4-dioxane to determine the reactivity ratios of each pair of monomers using the

Fineman-Ross and Kelen-Tüdös models and non-linear least squared regression analysis (NLLS). The reactivity ratios were determined to improve our understanding of the compositional drift expected in each case and inform the design of future polymerisations.

4. To synthesise a library of novel copolymers containing DMA or ADMA and methacrylate comonomers, including GMA, which is incorporated to allow the surface-bound copolymers to immobilise antibodies. Further methacrylate monomers investigated were HEMA, PEGMEM and stearyl methacrylate (SMA). Key reactions were monitored by NMR to determine the relative rate of monomer conversion, which in turn allowed compositional drift in the resulting copolymers to be studied. In some cases, a third functional methacrylate monomer was incorporated to modify the solubility of the resulting copolymers to promote their deposition from solvents of varying polarity.

5. To explore the conditions required to deprotect ADMA post polymerisation to allow the catechol side chains to act as adhesive functional groups.

2.3 Experimental

2.3.1 Materials

Dopamine hydrochloride (99%), sodium carbonate monohydrate (99.5%), sodium tetraborate (99.5%, borax), *p*-toluenesulfonic acid (98%), 2,2-dimethoxypropane (98%), anhydrous magnesium sulfate (99.5%) and trifluoroacetic acid (99%, TFA) were supplied by Sigma-Aldrich, UK and used as received. Azobisisobutyronitrile (98%, AIBN) was supplied by Sigma-Aldrich, UK and recrystallised from methanol before use. 1,4-dioxane (99.8%), methacrylic anhydride (94%), glycidyl methacrylate (97%, GMA), 2-hydroxyethyl methacrylate (97%, HEMA), poly(ethylene glycol) methyl ether methacrylate (97%, average M_n = 500 g mol^{-1}, PEGMEM) and methyl methacrylate (99%, MMA) were supplied by Sigma-Aldrich, UK and passed through a column of activated alumina before use to purify and to remove inhibitor. Hydrochloric acid (36.5% w/v solution) and *N*,*N*-dimethylformamide (anhydrous, 99.8%, DMF) were supplied by Fisher Scientific, UK and used as received. Stearyl methacrylate (97%, SMA) was supplied by TCI UK and used as received. Dimethyl sulfoxide-d_6 (99.9% D atom, DMSO-d6) was supplied by Sigma-Aldrich, UK and used as received, deuterated chloroform (99.8% D atom, $CDCl_3$) was supplied by Apollo Scientific, UK and used as received.

2.3.2 Synthesis of dopamine methacrylamide (DMA)

2.3.2.1 Synthesis of DMA, method 1

DMA was synthesised using the method of Detrembleur[28] (building on the work of Messersmith and coworkers[36]).

A two-necked round bottomed flask was charged with borax ($Na_2B_4O_7.10\ H_2O$, 3.84 g, 10 mmol), Na_2CO_3 (2.00 g, 16 mmol) and 100 mL of deionised water. The solution was deoxygenated by bubbling with N_2 for 60 min before the addition of dopamine.HCl (0.95 g, 6 mmol). The solution was stirred for a further 15 minutes with nitrogen bubbling. The resulting solution was then cooled to 0 °C in an ice bath, and methacrylic anhydride (1.6 mL, 10 mmol) was added dropwise. The reaction mixture was allowed to return to room temperature and was stirred for 24h under N_2. The pH of the solution was maintained at pH 9–10 by the addition of a further 2.00 g of Na_2CO_3 during the reaction. The reaction solution was then acidified to pH 2 with aqueous conc. HCl and extracted five times with ethyl acetate (40mL). The combined organic layers were washed twice with 0.1 M HCl, dried over $MgSO_4$ and the drying agent was removed by gravity filtration. The solvent was evaporated under reduced pressure to give a dark brown powder. The crude product was purified by column chromatography (dichloromethane (DCM) : methanol, 9:1) to give a light brown powder. Yield 0.17 g, 12.4%. ^{1}H NMR (400 MHz, DMSO-d6): δ (ppm) = 8.76, 8.65 (br s, -OH, 2H), 7.93 (t, -NH-, 1H), 6.64–6.44 (m, Ph, 3H), 5.62, 5.31 (s, 1H, C**H$_2$**=C-CH$_3$), 3.22 (q, 2H, -CH$_2$-C**H$_2$**-NH-), 2.55 (t, 2H, -C**H$_2$**-CH$_2$-NH-), 1.84 (s, 3H, CH$_2$=C-C**H$_3$**). ^{13}C NMR (400 MHz, DMSO-d6): δ (ppm) = 167.8 (1C, -NH-C=O), 145.5 (1C, Ph-OH), 143.9 (1C, Ph-OH), 140.5 (1C, CH$_2$=**C**-CH$_3$), 130.7 (CH$_2$-**Ph**), 119.6 (1C, **C**H$_2$=C-CH$_3$), 119.2 (1C, Ph), 116.4 (1C, Ph), 115.9 (1C, Ph), 41.4 (-CH$_2$-NH-), 35.1 (Ph-**C**H$_2$-CH$_2$-), 19.1 (1C, CH$_2$=C-**C**H$_3$).

2.3.2.2 Synthesis of DMA, method 2

The synthesis of DMA was carried out according to the procedure described above in Section 2.3.2.1 using the following reagents: borax ($Na_2B_4O_7.10\ H_2O$, 40.4 g, 105 mmol), Na_2CO_3 (21.1 g, 168 mmol), deionised water (1000 mL), dopamine.HCl (10.0 g, 105 mmol) and methacrylic anhydride (16.8 mL, 105 mmol). The reaction was carried out in a 2 litre round bottomed flask. The following minor adjustments were made to the described procedure: 1) The solution was deoxygenated by bubbling with N_2 for 180 min. 2) The pH of the solution was maintained at pH 9–10 by the addition of 20 g of Na_2CO_3 during the reaction.

The workup was carried out as described in section 2.3.2.1, except the light brown crude DMA was washed with chloroform immediately prior to purification by column chromatography. After column chromatography (DCM : methanol 94:6 raised to 9:1), a white powder was obtained. Yield, white powder, 6.51 g, 55.5%. ^{1}H NMR (400 MHz, DMSO-d6) as 2.3.2.1.

2.3.2.3 Synthesis of DMA, method 2 (scale-up)

The synthesis of DMA by method 2 was repeated on a larger scale using the following quantities of reagents: borax ($Na_2B_4O_7.10\ H_2O$, 80.84 g, 211 mmol), Na_2CO_3 (42.11 g, 336 mmol), deionised water (2000 mL), dopamine.HCl (20.0 g, 105 mmol), methacrylic anhydride (33.6mL, 210 mmol) and a further 20 g of Na_2CO_3 added during the reaction. The reaction was carried out in a 5 litre round bottomed flask. Yield, white powder, 15.25 g, 65.7%. ^{1}H NMR (400 MHz, DMSO-d6) as 2.3.2.1.

2.3.2.4 Synthesis of DMA, method 3

The synthesis of DMA was carried out according to the procedure described above in Section 2.3.2.2 using the following reagents: borax ($Na_2B_4O_7.10\ H_2O$, 3.84 g, 10 mmol), Na_2CO_3 (2.00 g, 16 mmol), 100 mL water, dopamine.HCl (0.95 g, 5mmol), methacrylic anhydride (1.6 mL, 10 mmol). The pH of the solution was maintained at pH 9–10 by the addition of a further 2.00 g of Na_2CO_3 during the reaction. After 24 h, ~1 g of undissolved Na_2CO_3 remained in the flask. The undissolved Na_2CO_3 was removed by vacuum filtration and the aqueous filtrate washed twice with ethyl acetate. The aqueous layer was then acidified to pH 2 with 1M HCl and extracted three times with ethyl acetate. The combined organic fractions were dried over $MgSO_4$ and the drying agent was removed by gravity filtration. The volume of the filtrate was reduced by 2/3 under reduced pressure and the remaining product precipitated into 400 mL hexane. The flask containing the crude DMA precipitate and hexane was stored overnight in the refrigerator to allow crystals to form, which were subsequently collected by vacuum filtration, re-dissolved in ethyl acetate, and precipitated once more into hexane. The crystals formed by the second precipitation were collected by vacuum filtration and dried to give a light-yellow powder. Yield 1.20 g, 54.1%; LC-MS *m/z*: 222.2 g mol^{-1} $[M+H]^+$ ion. ^{1}H NMR (400 MHz, DMSO-d6) as 2.3.2.1.

2.3.3 Synthesis of acetonide protected dopamine methacrylamide (ADMA)

2.3.3.1 Synthesis of ADMA method 1

300 mL of anhydrous toluene was transferred to a 500 mL round-bottomed flask and bubbled with nitrogen for 120 minutes. DMA (1.40 g, 6.3 mmol) and *p*-toluene sulfonic acid (64 mg, 0.37 mmol) were added, and the mixture was refluxed for 3 hours with Dean-Stark apparatus attached. The resulting solution was cooled to 0 °C in an ice bath and 2,2-dimethoxypropane (7.50 mL, 61 mmol) was added. A Soxhlet extractor whose thimble was filled with 40.0 g of $CaCl_2$, was fitted and the solution was refluxed for 4 hours in the dark with vigorous stirring. The reaction mixture was washed twice with water and brine. The organic extract was dried over $MgSO_4$ and the drying agent was removed by gravity filtration. The remaining solvent was removed under reduced pressure and the yellow solid product was purified by column chromatography (hexane/ethyl acetate 5:1). The final product was a light-brown solid (acetonide protected dopamine methacrylamide – ADMA). Yield 1.13 g, 68.5%. LC-MS *m/z*: 262.8 g mol^{-1} $[M+H]^+$ ion. ^{1}H NMR (400 MHz, $CDCl_3$): δ (ppm) = 6.69–6.60 (m, **Ph**, 3H), 5.64, 5.32 (s, 1H, C**H$_2$**=C-CH_3), 3.53 (q, 2H, -CH_2-C**H$_2$**-NH-), 2.77 (t, 2H, -C**H$_2$**-CH_2-NH-), 1.94 (s, 3H, CH_2=C-C**H$_3$**), 1.69 (s, 6H, O-C-C**H$_3$**).

2.3.3.2 Synthesis of ADMA method 2

DMA was protected using the procedure described in section 2.3.3.1, using the following reagents: anhydrous toluene (250 mL), DMA (6.29 g, 28.4 mmol), *p*-toluene sulfonic acid (270 mg, 1.42 mmol) and 2,2-dimethoxypropane (33.33 mL, 272.9 mmol). The yellow crude product was purified by column chromatography (hexane/ethyl acetate 3:1) to remove a bright yellow by-product, before the product was eluted using hexane/ethyl acetate 1:1. The product was a white solid, yield 5.63 g, 75.8%. ^{1}H NMR (400 MHz, $CDCl_3$) as 2.3.3.1.

2.3.3.3 Synthesis of ADMA method 2 (larger scale)

DMA was protected using the procedure described in section 2.3.3.1 using the following reagents: anhydrous toluene (300 mL), DMA (10.00 g, 45.2 mmol), *p*-toluene sulfonic acid (430 mg, 2.26 mmol) and 2,2-dimethoxypropane (53.0 mL, 432.5 mmol). The crude product was purified by column chromatography (hexane/ethyl acetate 3:1) to remove a bright yellow by-product, before the product was eluted using hexane/ethyl acetate 1:1. The product was a white solid, yield 9.60 g, 81.3%. ^{1}H NMR (400 MHz, $CDCl_3$) as 2.3.3.1.

2.3.4 Polymer Synthesis

2.3.4.1 Free radical homopolymerisation of DMA (FR-D-(DIOX))

DMA (0.25 g, 1.13 mmol) was added to 1,4-dioxane (2.3 mL) in a 50 mL two-necked, round-bottomed flask fitted with a condenser; the other neck was sealed with a rubber septum. The solution was sparged with nitrogen for 60 minutes whilst stirring using a magnetic stirrer bar, then heated to 70 °C in an oil bath under a nitrogen blanket. An initial sample was collected in a vial for analysis using a syringe and rapidly cooled by submersion into liquid N_2. AIBN (2 mg, 0.01 mmol) was dissolved in 0.1 mL 1,4-dioxane and injected into the reaction. The reaction was allowed to proceed for 7 hours before a final sample was collected. The solution was poured into diethyl ether, yielding a white solid, which turned brown and became insoluble on exposure to air. Yield = 0.07 g, 28%.

2.3.4.2 Free radical homopolymerisation of DMA (FR-D-(DMF))

The homopolymerisation of DMA (1.00 g, 4.52 mmol) was repeated in DMF (9.5 mL) using the procedure described above (2.3.4.1). AIBN (7 mg, 0.05 mmol) was dissolved in 0.1 mL DMF and injected into the reaction. The reaction was allowed to proceed for 24 hours before a final sample was collected. The homopolymer was precipitated in diethyl ether, yielding a white solid, which was collected and dried overnight under vacuum. Yield = 0.61 g, 61% M_n = 95300 g mol^{-1}, Đ = 1.24. ^{1}H NMR (DMSO-d6, 400 MHz) δ (ppm) = 8.60 (s, 2H, Ph-O**H**), 7.38 (s, 1H, N**H**-CH_2), 6.59–6.38 (m, 3H, Ph-**H**), 3.42 (s, 2H, NH-C**H**$_2$), 3.05 (s, 2H, C**H**$_2$-Ph), 1.63 (s, 2H, C**H**$_2$-C-CH_3), 1.05–0.95 (m, 3H, CH_2-C-C**H**$_3$,).

2.3.4.3 Free radical homopolymerisation of ADMA (FR-A)

The homopolymerisation of ADMA (0.60 g, 2.30 mmol) was carried out in DMF (5.2 mL) using the procedure described above (2.3.4.1). AIBN (4 mg, 0.02 mmol) was dissolved in 0.1 mL DMF and injected into the reaction. The reaction was allowed to proceed for 16 hours before a final sample was collected. The homopolymer was precipitated in diethyl ether, yielding a white solid, which was collected and dried overnight under vacuum. Yield = 0.09 g, 15%, M_n = 24300 g mol^{-1}, Đ = 1.17. ^{1}H NMR (DMSO-d6, 400 MHz) δ (ppm) = 6.59 – 6.49 (m, 3H, Ph-**H**), 3.60 (s, 1H, N**H**-CH_2), 3.11 (s, 2H, NH-C**H**$_2$), 2.56 (s, 2H, C**H**$_2$-Ph), 1.56 (br m, 8H, O-C-C**H**$_3$, C**H**$_2$-C-CH_3), 0.97–0.86 (br m, 3H, CH_2-C-C**H**$_3$).

2.3.4.4 Free radical copolymerisation for the estimation of reactivity ratios of MMA and ADMA

A typical procedure is given for the synthesis of poly(MMA-co-ADMA) to determine reactivity ratios. MMA (0.10 g, 1.00 mmol) and ADMA (0.26 g, 1.00 mmol) were added to 1,4-dioxane (3 mL) in a 50 mL two-necked, round-bottomed flask fitted with a condenser; the other neck was sealed with a rubber septum. The solution was sparged with nitrogen for 60 minutes with magnetic stirring. It was then heated to 70 °C in an oil bath under a nitrogen blanket. A sample was collected using a syringe at time t = 0 and rapidly cooled by submersion into liquid nitrogen. AIBN (3.20 mg, 0.02 mmol) was dissolved in 0.1 mL 1,4-dioxane and injected into the reaction. After 10 minutes, the reaction was quenched with hydroquinone (0.05 g, 0.45 mmol). A sample was collected, and the reaction allowed to cool. The reaction mixture was dialysed (benzoylated dialysis tubing, 2000 MWCO) in methanol for three days. The methanol was removed under reduced pressure, yielding a white solid. In subsequent reactions monomer feed ratios were adjusted as required. Yield 0.01 g, 1%. ^{1}H NMR ($CDCl_3$, 400 MHz) δ (ppm) = 6.86–6.65 (m, 3H, Ph-**H**), 5.75 (s, 1H, N**H**-CH_2), 3.65 (m, 3H, C-O-C**H₃** *MMA*), 3.41 (s, 2H, NH-C**H₂**-CH_2), 2.75 (s, 2H, CH_2-C**H₂**-Ph), 1.89 (m, 8H, C**H₂**-C-CH_3 *polymer main chain protons*, O-C-C**H₃** *acetonide group*),1.08-0.90 (m, 3H, CH_2-C-C**H₃**, *methacrylamide / methacrylate methyl groups*).

2.3.4.5 Free radical copolymerisation for the estimation of reactivity ratios of GMA and ADMA

A general procedure is given for the synthesis of poly(GMA-co-ADMA) for experiments to determine reactivity ratios. In a typical example, GMA (0.13 g, 0.91 mmol) and ADMA (0.24 g, 0.91 mmol) were added to 1,4-dioxane (3 mL). The synthesis was carried out according to the procedure described above (2.3.4.4) and initiated using AIBN (3.0 mg, 0.02 mmol) dissolved in 0.1 mL 1,4-dioxane. Yield 0.02 g, 5%. ^{1}H NMR ($CDCl_3$, 400 MHz) δ (ppm) = 6.67–6.59 (m, 3H, Ph-**H**), 5.85 (s, 1H, N**H**-CH_2), 4.31, 3.83 (2s, 1H, O-C**H₂**-CH), 3.35 (s, 2H, NH-C**H₂**), 3.25 (s, 1H, O-C**H**-CH_2 *epoxide ring*), 2.85 (s, 1H, O-CH-C**H₂** *epoxide ring*), 2.67 (s, 2H, C**H₂**-Ph), 1.93 (m, 8H, C**H₂**-C-CH_3 *polymer main chain protons*, O-C-C**H₃** *acetonide* group), 1.10-0.90 (m, 3H, CH_2-C-C**H₃**, *methacrylamide methyl group*).

2.3.4.6 Free radical copolymerisation of MMA and ADMA (FR-MA-90/10)

MMA (0.50 g, 5.00 mmol), ADMA (0.15 g, 0.55 mmol) and AIBN (9.1 mg, 0.06 mmol) were added to 10 mL of 1,4-dioxane in a 50 mL two-necked round-bottomed flask, fitted with a condenser and the other neck sealed with a rubber septum. The solution was sparged with nitrogen for 60 minutes and magnetically stirred. An initial sample was removed for analysis with a syringe. The flask was then heated to 70 °C in an oil bath under a nitrogen blanket. Further samples were collected after 20 min and 60 min and quenched by rapid cooling in liquid N_2. The reaction was allowed to proceed for 24 hours before a final sample was taken. The reaction solution was poured into methanol, causing precipitation of white solid which was collected and dried overnight under vacuum. Yield = 0.52 g, 80%, M_n = 24300 g mol^{-1}, Đ = 1.50. ^{1}H NMR ($CDCl_3$, 400 MHz) δ (ppm) as 2.3.4.4.

2.3.4.7 Free radical copolymerisation of MMA and ADMA (FR-MA-49/51)

The copolymerisation of MMA (0.10 g, 1.00 mmol) and ADMA (0.26 g, 1.00 mmol) was initiated using AIBN (3.3 mg, 0.02 mmol) in 3 mL of 1,4-dioxane according to the procedure described above (2.3.4.6) except for the following modifications. Samples were collected for NMR analysis after 0, 20, 40, 60, 90, 120, 180, 240, 300, 360 and 420 min and quenched by rapid cooling in liquid N_2. The reaction was allowed to proceed for 22.5 hours before a final sample was taken. Yield = 0.02 g, 6%. M_n = 142700 g mol^{-1}, Đ = 2.30. ^{1}H NMR ($CDCl_3$, 400 MHz) δ (ppm) as 2.3.4.4.

2.3.4.8 Free radical copolymerisation of MMA and ADMA (FR-MA-24/76)

The copolymerisation of MMA (0.10 g, 1.00 mmol) and ADMA (0.78 g, 3.00 mmol), was initiated using AIBN (6.6 mg, 0.04 mmol) in 8 mL of 1,4-dioxane according to the procedure described above (2.3.4.6) except for the following modifications. Samples were collected for NMR analysis after 0, 30, 40, 60, 90, 120, 210 and 300 min and quenched by rapid cooling in liquid N_2. The reaction was allowed to proceed for 22 hours before a final sample was taken. Yield = 0.05 g, 6%, M_n = 138200 g mol^{-1}, Đ = 1.11. ^{1}H NMR ($CDCl_3$, 400 MHz) δ (ppm) as 2.3.4.4.

2.3.4.9 Free radical terpolymerisation of MMA, GMA and ADMA (FR-MGA-77/12/11)

The copolymerisation of MMA (0.80 g, 8.00 mmol), GMA (0.14 g, 1.00 mmol) and ADMA (0.26 g, 1.00 mmol) was initiated using AIBN (16 mg, 0.10 mmol) in 30 mL of 1,4-dioxane according to the procedure described above (2.3.4.6) except for the following modifications. Samples were collected for NMR analysis after 0, 30, 60, 120, 180, 300,

1260 and 1560 min and quenched by rapid cooling in liquid N_2. The reaction was allowed to proceed for 45 hours before a final sample was taken. Yield = 0.06 g, 5%, M_n = 30800 g mol^{-1}, Đ = 1.54. ^{1}H NMR ($CDCl_3$, 400 MHz) δ (ppm) = 6.69 – 6.60 (m, 3H, Ph-**H**), 5.70 (s, 1H, N**H**-CH_2), 4.33, 3.81 (2s, 1H, O-C**H$_2$**-CH), 3.61 (m, 3H, C-O-C**H$_3$** *MMA side chain*), 3.37 (s, 2H, NH-C**H$_2$**), 3.24 (s, 1H, O-C**H**-CH_2 *epoxide ring*), 2.88 (s, 1H, O-CH-C**H$_2$** *epoxide ring*), 2.67 (s, 2H, C**H$_2$**-Ph), 2.01-1.82 (m, 2H, C**H$_2$**-C-CH_3 *polymer main chain protons*), 1.68 (s, 6H, O-C-CH_3 *acetonide* group), 1.03 – 0.86 (m, 3H, CH_2-C-C**H$_3$**).

2.3.4.10 Free radical terpolymerisation of MMA, GMA and ADMA (FR-MGA-52/26/22)

The copolymerisation of MMA (0.30 g, 3.00 mmol), GMA (0.14 g, 1.00 mmol) and ADMA (0.26 g, 1.00 mmol) was initiated using AIBN (8 mg, 0.05 mmol) in 30 mL of 1,4-dioxane according to the procedure described above (2.3.4.6) except for the following modifications. Samples were collected for NMR analysis after 0, 30, 60, 120, 190, 255, 300, and 1530 min and quenched by rapid cooling in liquid N_2. The reaction was allowed to proceed for 71 hours before a final sample was taken. Yield = 0.03 g, 4%, M_n = 42700 g mol^{-1}, Đ = 1.67. ^{1}H NMR ($CDCl_3$, 400 MHz) δ (ppm) as 2.3.4.9.

2.3.4.11 Free radical terpolymerisation of MMA, GMA and ADMA (FR-MGA-31/34/35)

The copolymerisation of MMA (0.08 g, 0.80 mmol), GMA (0.11 g, 0.80 mmol) and ADMA (0.21 g, 0.80 mmol) was initiated using AIBN (4 mg, 0.02 mmol) in 10 mL of 1,4-dioxane according to the procedure described above (2.3.4.6) except for the following modifications. Samples were collected for NMR analysis after 0, 20, 40, 60, 90, 120, 150, 180, 240, 300, 360 and 420 min and quenched by rapid cooling in liquid N_2. The reaction was allowed to proceed for 25.5 hours before a final sample was taken. Yield = 0.02 g, 5%, M_n = 85400 g mol^{-1}, Đ = 1.47. ^{1}H NMR ($CDCl_3$, 400 MHz) δ (ppm) as 2.3.4.9.

2.3.4.12 Free radical terpolymerisation of HEMA, GMA and ADMA (FR-HGA-80/10/10-(DIOX))

The copolymerisation of HEMA (0.78 g, 6.00 mmol), GMA (0.11 g, 0.75 mmol), ADMA (0.20 g, 0.75 mmol) was initiated using AIBN (12 mg, 0.08 mmol) in 9 mL of 1,4-dioxane in a 50 mL two-necked round-bottomed flask, fitted with a condenser and the other neck sealed with a rubber septum. The solution was sparged with nitrogen for 60 minutes and magnetically stirred. An initial sample was removed for analysis with a syringe. The flask

was then heated to 70 °C in an oil bath under a nitrogen blanket. Samples were collected for NMR analysis after 0, 20, 60 and 300 min and quenched by rapid cooling in liquid N_2. The reaction was allowed to proceed for 24 hours before a final sample was taken. The reaction solution was poured into diethyl ether, causing precipitation of white solid which was collected and dried overnight under vacuum. Yield = 0.09 g, 8%, M_n = 12800 g mol^{-1}, Đ = 2.53. ^{1}H NMR (DMSO-d6, 400 MHz) δ (ppm) = 6.73 – 6.58 (m, 3H, Ph-**H**), 4.81 (s, 1H, CH_2-O**H**), 4.24 (s, 1H, O-C**H$_2$**-CH *GMA*), 3.90 (s, 2H, O-C**H$_2$**-CH_2 *HEMA*), 3.72 (s, 1H, O-C**H$_2$**-CH *GMA*), 3.59 (s, 2H, O-CH_2-C**H$_2$** *HEMA*), 3.20, 2.79 (2s, 1H, O-CH-C**H$_2$** *epoxide ring*), 2.65 (s, 2H, C**H$_2$**-Ph), 2.57 (s, 1H, O-CH-C**H$_2$** *epoxide ring*) 2.03-1.72 (s, 2H, C**H$_2$**-C-CH_3 *polymer main chain protons*), 1.63 (br m, 6H, C-CH_3 *acetonide group*), 0.96 – 0.76 (br m, 3H, CH_2-C-C**H$_3$**, *methacrylamide / methacrylate methyl groups*).

2.3.4.13 Free radical copolymerisation of SMA and ADMA (FR-SA-90/10)

The copolymerisation of SMA (3.05 g, 9.00 mmol) and ADMA (0.26 g, 1.00 mmol) was initiated using AIBN (16 mg, 0.10 mmol) in 12 mL of 1,4-dioxane according to the procedure described above (2.3.4.6) except for the following modifications. The reaction was allowed to proceed for 7 hours before a final sample was taken. The reaction solution was poured into methanol, causing precipitation of yellow solid which was collected and dried overnight under vacuum. Yield = 3.01 g, 91%. M_n = 93300 g mol^{-1}, Đ = 3.34. ^{1}H NMR ($CDCl_3$, 400 MHz) δ (ppm) = 6.65 – 6.60 (m, 3H, Ph-**H**), 5.67 (s, 1H, N**H**-CH_2), 3.92 (s, 2H, O-C**H$_2$**-CH_2, *SMA*), 3.37 (s, 2H, NH-C**H$_2$**), 2.68 (s, 2H, C**H$_2$**-Ph), 1.92 – 1.82 (s, 2H, C**H$_2$**-C-CH_3 *polymer main chain protons*), 1.69 (br m, 6H, C-CH_3 *acetonide group*), 1.59 (s, 2H, O-CH_2-C**H$_2$**-), 1.28 (m, 30H, O-CH_2-CH_2-(C**H$_2$**)$_{15}$), 1.12 – 0.90 (m, 6H, CH_2-C-C**H$_3$**, *methacrylate / methacrylamide methyl group* and $(CH_2)_{15}$-C**H$_3$**).

2.3.4.14 Free radical copolymerisation of MMA and DMA (FR-MD-90/10-(DIOX))

The copolymerisation of MMA (0.45 g, 4.49 mmol) and DMA (0.11 g, 0.50 mmol) was initiated using AIBN (8 mg, 0.05 mmol) in 5 mL of 1,4-dioxane according to the procedure described above (2.3.4.6) except for the following modifications. The reaction was allowed to proceed for 20 hours before a final sample was taken. Yield = 0.02 g, 4%. M_n = 1100 g mol^{-1}, Đ = 1.78. ^{1}H NMR ($CDCl_3$, 400 MHz) δ (ppm) = 6.83 – 6.59 (m, 3H, Ph-**H**), 5.96 (s, 1H, N**H**-CH_2), 3.61 (m, 3H, C-O-C**H$_3$** *MMA*), 2.68 (s, 2H, CH_2-C**H$_2$**-Ph), 2.03-1.78 (m, 2H, C**H$_2$**-C-CH_3 *polymer main chain protons*), 1.02, 0.84 (m, 3H, CH_2-C-C**H$_3$**, *methacrylamide / methacrylate methyl groups*).

2.3.4.15 Free radical homopolymerisation of HEMA (FR-H)

The polymerisation of HEMA (2.08 g, 16.0 mmol) was initiated using AIBN (26 mg, 0.16 mmol) in 19 mL of DMF according to the procedure described above (2.3.4.12) except for the following modifications. The reaction was allowed to proceed for 21 hours before a final sample was taken. Yield = 1.86 g, 89%, M_n = 17250, Đ = 2.67. ^{1}H NMR (DMSO-d6, 400 MHz) δ (ppm) = 4.82 (s, 1H, CH_2-O**H**), 3.90 (s, 2H, O-C**H$_2$**-CH_2), 3.33 (s, 2H, O-CH_2-C**H$_2$**), 2.90 (s), 2.73 (s), 2.00-1.69 (s, 2H, C**H$_2$**-C-CH_3 *polymer main chain protons*), 1.48 (s) 1.17 (s), 0.95, 0.76 (br m, 3H, CH_2-C-C**H$_3$**, *methacrylate methyl group*).

2.3.4.16 Free radical copolymerisation of HEMA and DMA (FR-HD-90/10-(DMF))

The copolymerisation of HEMA (1.04 g, 8.00 mmol) and DMA (0.20 g, 0.89 mmol) was initiated using AIBN (15 mg, 0.09 mmol) in 12 mL of DMF according to the procedure described above (2.3.4.12) except for the following modifications. The reaction was allowed to proceed for 21 hours before a final sample was taken. Yield = 1.16 g, 94%. M_n = 36200 g mol^{-1}, Đ = 3.17. ^{1}H NMR (DMSO-d6, 400 MHz) δ (ppm) = 8.70 (s, 2H, Ph-O**H**), 6.61 – 6.41 (m, 3H, Ph-**H**), 4.80 (s, 1H, CH_2-O**H**), 4.11 (s, 1H, N**H**-CH_2), 3.88 (s, 2H, O-C**H$_2$**-CH_2), 3.55 (s, 2H, O-CH_2-C**H$_2$**), 3.33 (s, 2H, NH-C**H$_2$**), 3.15 (s), 2.90 (s), 2.77 (s), 1.80 (br m, 6H, C-CH_3 *acetonide group*), 0.96, 0.77 (br m, 3H, CH_2-C-C**H$_3$**, *methacrylamide methyl group*).

2.3.4.17 Free radical copolymerisation of HEMA and DMA (FR-HD-80/20-(DMF))

The copolymerisation of HEMA (0.78 g, 6.00 mmol) and DMA (0.33 g, 1.50 mmol) was initiated using AIBN (12 mg, 0.08 mmol) in 11 mL of DMF according to the procedure described above (2.3.4.12) except for the following modifications. The reaction was allowed to proceed for 21 hours before a final sample was taken. Yield = 1.01 g, 91%. M_n = 13650 g mol^{-1}, Đ = 3.13. ^{1}H NMR (DMSO-d6, 400 MHz) δ (ppm) as 2.3.4.16.

2.3.4.18 Free radical copolymerisation of HEMA and DMA (FR-HD-70/30-(DMF))

The copolymerisation of HEMA (0.65 g, 5.00 mmol) and DMA (0.47 g, 2.14 mmol) was initiated using AIBN (11 mg, 0.07 mmol) in 11 mL of DMF according to the procedure described above (2.3.4.12) except for the following modifications. The reaction was allowed to proceed for 21 hours before a final sample was taken. Yield = 1.08 g, 96%. M_n = 10000 g mol^{-1}, Đ = 4.43. ^{1}H NMR (DMSO-d6, 400 MHz) δ (ppm) as 2.3.4.16.

2.3.4.19 Free radical copolymerisation of HEMA and DMA (FR-HD-61/39-(DMF))

The copolymerisation of HEMA (0.39 g, 3.00 mmol) and DMA (0.44 g, 2.00 mmol) was initiated using AIBN (8 mg, 0.05 mmol) in 8 mL of DMF according to the procedure described above (2.3.4.12) except for the following modifications. The reaction was allowed to proceed for 21 hours before a final sample was taken. Yield = 0.69 g, 83%. M_n = 3050 g mol^{-1}, Đ = 14.27. ^{1}H NMR (DMSO-d6, 400 MHz) δ (ppm) as 2.3.4.16.

2.3.4.20 Free radical copolymerisation of HEMA and DMA (FR-HD-50/50-(DMF))

The copolymerisation of HEMA (0.33 g, 2.50 mmol) and DMA (0.55 g, 2.50 mmol) was initiated using AIBN (8 mg, 0.05 mmol) in 8 mL of DMF according to the procedure described above (2.3.4.12) except for the following modifications. The reaction was allowed to proceed for 21 hours before a final sample was taken. Yield = 0.71 g, 81%. M_n = 3500 g mol^{-1}, Đ = 11.84. ^{1}H NMR (DMSO-d6, 400 MHz) δ (ppm) = as 2.3.4.16.

2.3.4.21 Free radical copolymerisation of PEGMEM and DMA (FR-PD-70/30-(DMF))

The copolymerisation of PEGMEM (1.75 g, 3.50 mmol) and DMA (0.33 g, 1.50 mmol) was initiated using AIBN (8 mg, 0.05 mmol) in 20 mL of DMF according to the procedure described above (2.3.4.12) except for the following modifications. The reaction was allowed to proceed for 16 hours before a final sample was taken. The reaction solution was poured into diethyl ether with stirring, and the viscous, colourless liquid product could be decanted. The viscous liquid was dried overnight under vacuum. Yield = 0.41 g, 21%. M_n = 17750 g mol^{-1}, Đ = 3.38. ^{1}H NMR (DMSO-d6, 400 MHz) δ (ppm) = 8.69 (d), 7.51 (m), 6.64 – 6.41 (m), 4.01 (br s), 3.61 (s), 3.51 (s) 3.43 (s), 3.34 (s), 3.34 (s), 3.24 (s), 3.06 (s), 2.89 (s), 2.56 (s), 1.88 (s), 1.84 (s) 0.95 (br s), 0.81 (br s).

2.3.4.22 Free radical terpolymerisation of MMA, GMA and DMA (FR-MGD-75/12/13-(DIOX))

The copolymerisation of MMA (0.40 g, 4.00 mmol), GMA (0.07 g, 0.50 mmol) and DMA (0.11 g, 0.50 mmol) was initiated using AIBN (8 mg, 0.05 mmol) in 5 mL of 1,4-dioxane according to the procedure described above (2.3.4.6) except for the following modifications. The reaction was allowed to proceed for 20 hours before a final sample was taken. Yield = 0.45 g, 78%, M_n = 8250 g mol^{-1}, Đ = 2.65. ^{1}H NMR ($CDCl_3$, 400 MHz) δ (ppm) = 8.69 (s, 2H, Ph-O**H**), 6.63 – 6.41 (m, 3H, Ph-**H**), 4.31 (s, 1H, O-C**H**$_2$-CH), 4.12 (m), 3.72 (s, 1H, O-C**H**$_2$-CH), 3.61 (m, 3H, C-O-C**H**$_3$ *MMA side chain*), 3.55 (br s), 3.37 (s, 2H, NH-C**H**$_2$), 3.18 (s, 1H, O-C**H**-CH_2 *epoxide ring*), 2.82 (s, 1H, O-CH-C**H**$_2$ *epoxide*

ring), 2.67 (s, 2H, C**H**$_2$-Ph), 2.32 – 1.82 (m, 2H, C**H**$_2$-C-CH$_3$ *polymer main chain protons*), 0.91 – 0.74 (m, 3H, CH$_2$-C-C**H**$_3$)

2.3.4.23 Free radical terpolymerisation of HEMA, GMA and DMA (FR-HGD-78/11/11-(DIOX))

The terpolymerisation of HEMA (1.04 g, 8.00 mmol), GMA (0.14 g, 1.00 mmol) and DMA (0.22 g, 1.00 mmol) was initiated using AIBN (16 mg, 0.10 mmol) in 12 mL of 1,4-dioxane according to the procedure described above (2.3.4.12) except for the following modifications. The reaction was allowed to proceed for 21 hours before a final sample was taken. Yield = 1.21 g, 86%. M_n = 39100 g mol^{-1}, Đ = 16.65. ^{1}H NMR (DMSO-d6, 400 MHz) δ (ppm) = 8.69 (2s, 2H, Ph-O**H**), 6.65 – 6.44 (m, 3H, Ph-**H**), 4.81 (s, 1H, CH$_2$-O**H**), 4.62 (s, 1H, N**H**-CH$_2$), 4.26 (s, 1H, O-C**H**$_2$-CH *GMA*), 3.89 (s, 2H, O-C**H**$_2$-CH$_2$ *HEMA*), 3.73 (s, 1H, O-C**H**$_2$-CH *GMA*), 3.59 (s, 2H, O-CH$_2$-C**H**$_2$ *HEMA*), 3.34 (s, 2H, NH-C**H**$_2$), 3.20, 2.90 (2s, 1H, O-CH-C**H**$_2$ *epoxide ring*), 2.66 (s, 2H, C**H**$_2$-Ph), 2.57 (s, 1H, O-CH-C**H**$_2$ *epoxide ring*), 2.12-1.75 (s, 2H, C**H**$_2$-C-CH$_3$ *polymer main chain protons*), 0.96, 0.76 (br m, 3H, CH$_2$-C-C**H**$_3$, *methacrylamide / methacrylate methyl groups*).

2.3.4.24 Free radical terpolymerisation of HEMA, GMA and DMA (FR-HGD-80/10/10)

The terpolymerisation of HEMA (1.04 g, 8.00 mmol), GMA (0.14 g, 1.00 mmol) and DMA (0.22 g, 1.00 mmol) was initiated using AIBN (16 mg, 0.10 mmol) in 13 mL of DMF according to the procedure described above (2.3.4.12) except for the following modifications. The reaction was allowed to proceed for 15 hours before a final sample was taken. Yield = 0.97 g, 69%. M_n = 43400 g mol^{-1}, Đ = 3.23. ^{1}H NMR (DMSO-d6, 400 MHz) δ (ppm) as 2.3.4.23.

2.3.4.25 Free radical terpolymerisation of HEMA, GMA and DMA (FR-HGD-58/9/33-(DMF))

The terpolymerisation of HEMA (0.39 g, 3.00 mmol), GMA (0.07 g, 0.50 mmol) and DMA (0.33 g, 1.50 mmol) was initiated using AIBN (8 mg, 0.05 mmol) in 7 mL of DMF according to the procedure described above (2.3.4.12) except for the following modifications. The reaction was allowed to proceed for 21 hours before a final sample was taken. Yield = 0.38 g, 48%. M_n = 110650 g mol^{-1}, Đ = 3.48. ^{1}H NMR (DMSO-d6, 400 MHz) δ (ppm) as 2.3.4.23.

2.3.4.26 Free radical copolymerisation of MMA and GMA (FR-MG-50/50)

The copolymerisation of MMA (0.50 g, 5.00 mmol) and GMA (0.71 g, 5.00 mmol) was initiated using AIBN (16 mg, 0.10 mmol) in 11 mL of DMF according to the procedure described above (2.3.4.6) except for the following modifications. Samples were collected for NMR analysis after 0, 5, 10, 20, 30, 40, 50, 60, 90, 120, 150, 180, 250, 300 and 360 min and quenched by rapid cooling in liquid N_2. The reaction was allowed to proceed for 24 h before a final sample was taken. Yield = 0.03 g, 2%. M_n = 35500 g mol^{-1}, Đ = 2.22. ^{1}H NMR ($CDCl_3$, 400 MHz) δ (ppm) = 4.31 (s, 1H, O-C**H**$_2$-CH), 3.82, 3.72 (s, 1H, O-C**H**$_2$-CH), 3.61 (m, 3H, C-O-C**H**$_3$ *MMA side chain*), 3.45 (s), 3.26 (s, 1H, O-C**H**-CH_2 *epoxide ring*), 2.87 (s, 1H, O-CH-C**H**$_2$ *epoxide ring*), 2.66 (s, 2H, C**H**$_2$-Ph), 1.98 – 1.87 (m, 2H, C**H**$_2$-C-CH_3 *polymer main chain protons*), 1.08, 0.91 (m, 3H, CH_2-C-C**H**$_3$).

2.3.4.27 Free radical copolymerisation of HEMA and GMA (FR-HG-90/10)

The copolymerisation of HEMA (1.56 g, 12.0 mmol) and GMA (0.19 g, 1.33 mmol) was initiated using AIBN (21 mg, 0.13 mmol) in 11 mL of DMF according to the procedure described above (2.3.4.12) except for the following modifications. The reaction was allowed to proceed for 18.5 hours before a final sample was taken. Yield = 1.32 g, 75%. M_n = 133500 g mol^{-1}, Đ = 4.26. ^{1}H NMR (DMSO-d6, 400 MHz) δ (ppm) = 4.83 (s, 1H, CH_2-O**H**), 4.28 (s, 1H, O-C**H**$_2$-CH *GMA*), 3.91 (s, 2H, O-C**H**$_2$-CH_2 *HEMA*), 3.72 (s, 1H, O-C**H**$_2$-CH *GMA*), 3.61 (s, 2H, O-CH_2-C**H**$_2$ *HEMA*), 3.45 (s), 3.35 (s), 3.20, 2.87 (2s, 1H, O-CH-C**H**$_2$ *epoxide ring*), 2.73 – 1.80 (s, 2H, C**H**$_2$-C-CH_3 *polymer main chain protons*), 0.96, 0.76 (br m, 3H, CH_2-C-C**H**$_3$).

2.3.5 Deprotection of ADMA and ADMA-containing copolymers

2.3.5.1 Deprotection of poly(MMA-co-ADMA)

FR-MA-24/76 (0.02 g, 0.8 µmol), chloroform (0.74 mL, 9.2 mmol), water (0.01 mL, 0.55 mmol) and trifluoroacetic acid (0.25 mL, 3.26 mmol) were added to a 50 mL round bottomed flask, open to the air, and stirred at 35 °C for 12 hours with regular collection of samples for analysis. After the reaction, the solvent was removed by rotary evaporation to yield a light brown solid. Yield 0.011 g, 55%. ^{1}H NMR (DMSO-d6, 400 MHz) δ (ppm) = 7.44 (br s), 6.58 (br s), 6.39 (br s), 3.49 (s), 3.08 (s), 2.46 (s), 1.57 (br s), 0.86 (br s).

2.3.5.2 Deprotection of ADMA

The acetonide protecting group from ADMA (0.02 g, 7.6 μmol) was removed according to the procedure in section 2.3.5.1 with chloroform (0.74 mL, 9.2 mmol), water (0.01 mL, 0.55 mmol) and trifluoroacetic acid (0.25 mL, 3.26 mmol). After the reaction, the solvent was removed by rotary evaporation to yield a light brown solid. Yield 0.015 g, 75%. ^{1}H NMR (DMSO-d6, 400 MHz) δ (ppm) = 8.64 (br s), 6.64–6.42 (m, 3H), 5.62(s, 1H,), 5.31 (s, 1H), 3.23 (dd, 2H), 2.54 (t, 2H), 1.84 (s, 3H).

2.3.5.3 Deprotection of poly(SMA-co-ADMA)

The acetonide protecting group from FR-SA-90/10 (0.20 g, 0.002 mmol) was removed according to the procedure in section 2.3.5.1 with chloroform (7.4 mL, 92.3 mmol), water (0.1 mL, 5.5 mmol) and trifluoroacetic acid (2.5 mL, 32.6 mmol). After the reaction, the solvent was removed by rotary evaporation to yield a light brown solid. Yield 0.14 g, 70%. ^{1}H NMR ($CDCl_3$, 400 MHz) δ (ppm) = 6.68-6.58 (m), 3.93 (s), 3.73 (m), 3.56 (s), 3.15 (m), 1.68 (s), 1.63 (br s), 1.28 (m), 0.90 (m).

2.3.6 Characterisation Methods

Molecular weights were obtained by size exclusion chromatography (SEC) using a Viscotek TDA 302 with refractive index, viscosity, and light scattering detectors. 2 × 300 mm PLgel 5 μm mixed C-columns (with a linear range of molecular weight from 200 to 2,000,000 g mol^{-1}) were used. In some cases, THF was used as the eluent with a flow rate of 1.0 mL min^{-1} at a temperature of 35 °C and in other cases DMF with 0.1 wt.% of lithium bromide was used as the eluent with a flow rate of 1.0 mL^{-1} at a temperature of 70 °C. Unless otherwise indicated the molecular weights were obtained using data obtained by triple detection SEC with light scattering, using a *dn/dc* value of 0.085 mL g^{-1} for MMA in THF, 0.084 mL g^{-1} for GMA in THF, 0.075 mL g^{-1} for SMA in THF and 0.076 mL g^{-1} for HEMA in DMF.[13] The *dn/dc* for ADMA in THF was measured as 0.125 mL g^{-1}. The *dn/dc* value of the most prevalent monomer was used for the analysis of copolymers. Where indicated, the molecular weights were obtained from the RI detector and a conventional calibration curve constructed using nine reference polystyrene standards (Polymer Laboratories, M_n between 580-1112000 g mol^{-1}, $Đ \leq 1.11$).

^{1}H NMR spectra were recorded on a Bruker-400 MHz spectrometer using $CDCl_3$ or DMSO-d6 as a solvent. Spectra were referenced to the trace proton peaks present in $CDCl_3$ (7.26 ppm) or DMSO-d6 (2.50 ppm). NMR spectra were analysed using MestReNova

(Mestrelab Research, Spain). Dinitrobenzene (DNB) or DMF were used as internal standards to calculate monomer conversion.

Mass spectrometry was carried out using a triple quadruple mass spectrometer (Waters Ltd.) with an Acquity UPLC and an electrospray ion source in positive ion mode.

2.4 Results and Discussion

2.4.1 Synthesis of dopamine methacrylamide (DMA)

DMA, a catechol-containing methacrylamide monomer, can be used to synthesise (co)polymers bearing catechol side chains. The synthesis of DMA was investigated to identify optimal conditions for laboratory synthesis and scale-up for potential industrial use. Three synthetic methods are compared herein. A general reaction scheme for DMA synthesis is provided in Scheme 2.2.

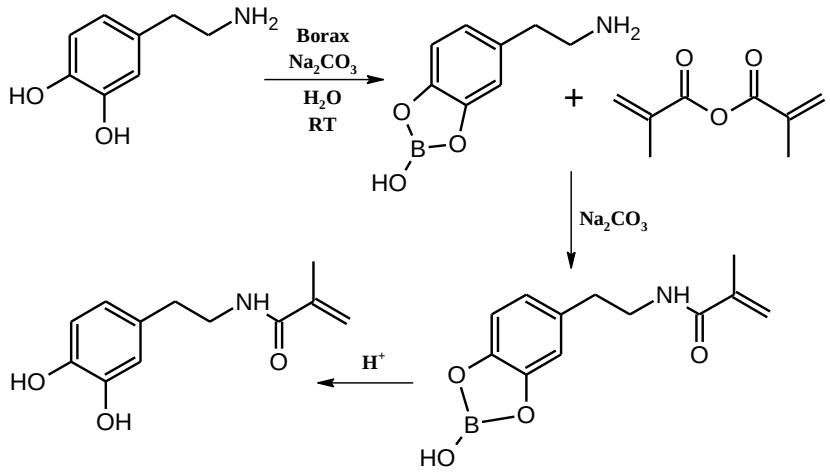

Scheme 2.2. General reaction scheme for synthesis of dopamine methacrylamide from dopamine and methacrylic anhydride.

The synthesis of DMA was carried out in aqueous conditions according to the procedure originally reported by Messersmith *et al.*,[37] referred to herein as method 1. The catechol group of dopamine was protected using borax to prevent side reactions, *e.g.* oxidation of the catechol to a quinone, which would enable the autopolymerisation of dopamine. Reaction of the borate-protected dopamine with methacrylic anhydride at pH 9 gave borate-protected DMA, which was subsequently deprotected by adjusting the solution to pH 2 using 2M HCl. Dark brown crystals of crude, unprotected DMA were recovered by extraction using ethyl acetate. It was hypothesised that the brown colour was due to the formation of cross-linked by-products which form *via ortho*-quinones arising from the oxidation of the dopamine starting material.[7] The cause of the oxidation was suspected to

be insufficient deoxygenation of the solvent (water) indicated by a colour change from colourless to light brown upon addition of dopamine to water (before addition of methacrylic anhydride). Purification of the crude DMA was attempted using column chromatography (DCM : methanol, 9:1) but a poor yield (12.4%) of light brown crystals was obtained, suggesting that a significant quantity of by-product was generated, which was not completely removed by column chromatography.

In method 2, the procedure of method 1 was repeated, with modifications described herein. Based on the hypothesis that oxidation of dopamine was the primary cause for the poor yield obtained in method 1, the procedure was modified to improve solvent deoxygenation. The duration of the nitrogen sparge before addition of dopamine was increased from 60 to 180 minutes. Moreover, nitrogen bubbling was continued throughout the reaction. A colourless to light pink colour change upon addition of dopamine to suggested significantly reduced oxidation of dopamine compared to method 1. Furthermore, a noticeable colour difference was observed between the crude DMA crystals (before column chromatography) from method 1 (dark brown) and method 2 (light brown). This implied that oxidation still occurred in method 2, but to a lesser extent. In an additional modification to method 1, organic impurities were removed by rinsing the DMA crystals with chloroform, evidenced by a colour change of the crystals from light brown to light yellow. In the column chromatography, an eluent of DCM : methanol (96:4) was used to effect more efficient separation of less-polar impurities, before using DCM : methanol (9:1) to ensure complete elution of DMA. White crystals were obtained, indicating successful purification of DMA. The identity of the pure DMA was confirmed using ^{1}H NMR spectroscopy (see Figure 2.1).

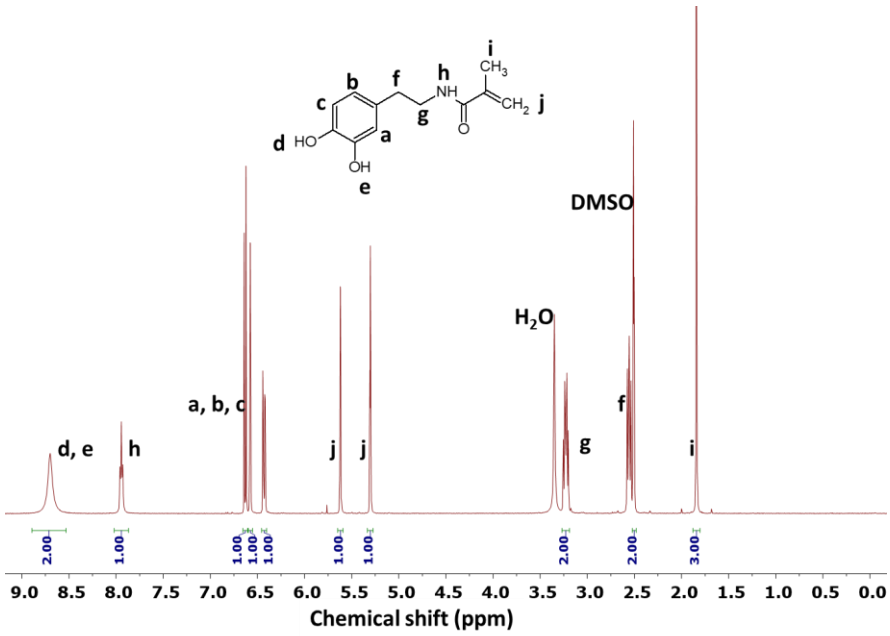

Figure 2.1. ^{1}H NMR spectrum of dopamine methacrylamide. Relative integrals are in blue text.

The yields for method 2 (55.3% using 10 g dopamine and 63.7% using 20 g dopamine) were vastly improved compared to method 1. The purity of DMA was confirmed using mass spectrometry; the mass peak ($[M+H]^+$) was observed at *m/z* 222.2 g mol^{-1} (Figure 2.2). Peaks attributed to $[2M+H]^+$ and $[2M+Na]^+$ can be observed at *m/z* 443.3 and 465.3 g mol^{-1} respectively.

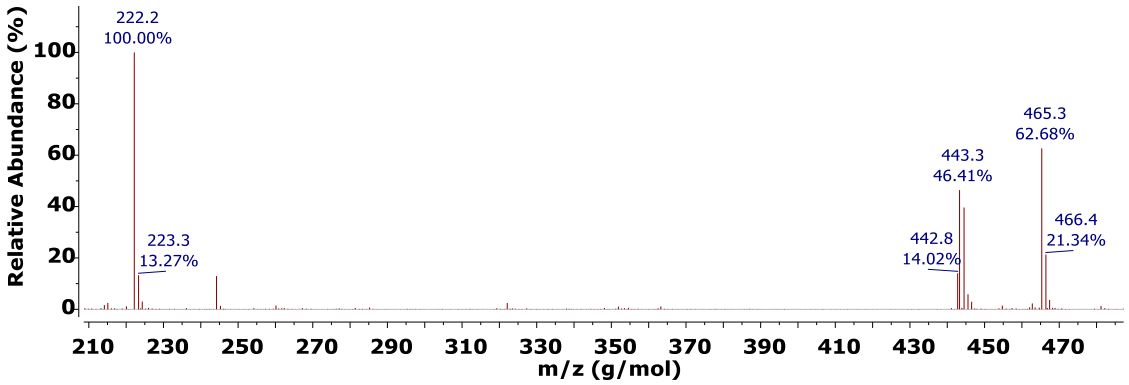

Figure 2.2. LC-MS spectrum of DMA with $[M+H]^+$ ion at *m/z* 222.2 g mol^{-1}.

The DMA synthesis was then modified according to the procedure reported by Kamperman *et al.*[6], referred to herein as method 3. The synthetic procedure was similar to method 2 except for the following modifications: i) undissolved Na_2CO_3 was removed at the end of the reaction by vacuum filtration, ii) the aqueous filtrate recovered after said filtration was washed with ethyl acetate and iii) after deprotection and extraction with ethyl acetate, the crude product was purified by twice precipitating in hexane (in preference to

column chromatography). Modification i) reduced the amount of acid required to remove the borate protecting group and facilitated the ethyl acetate wash in modification ii). Modification ii) removed organic impurities such as unreacted methacrylic anhydride. Modification iii) – precipitation in hexane – was much simpler than the column chromatography used in methods 1 and 2 and could have potentially increased the reaction yield.

A yield of 54% was obtained using method 3 which was comparable to method 2 despite the much smaller scale (0.95 g dopamine was used for method 3). However, despite the comparable yields, it was observed that column chromatography (method 2) usually resulted in the isolation of white crystals, whilst the precipitation workup (method 3), resulted in light brown (less pure) crystals. The presence of impurities in the product of method 3 was confirmed by ^{1}H NMR, evidenced by additional peaks in the phenyl proton region between 6.2 and 6.4 ppm (Figure 2.3). These peaks suggest the presence of oxidised dopamine by-products.

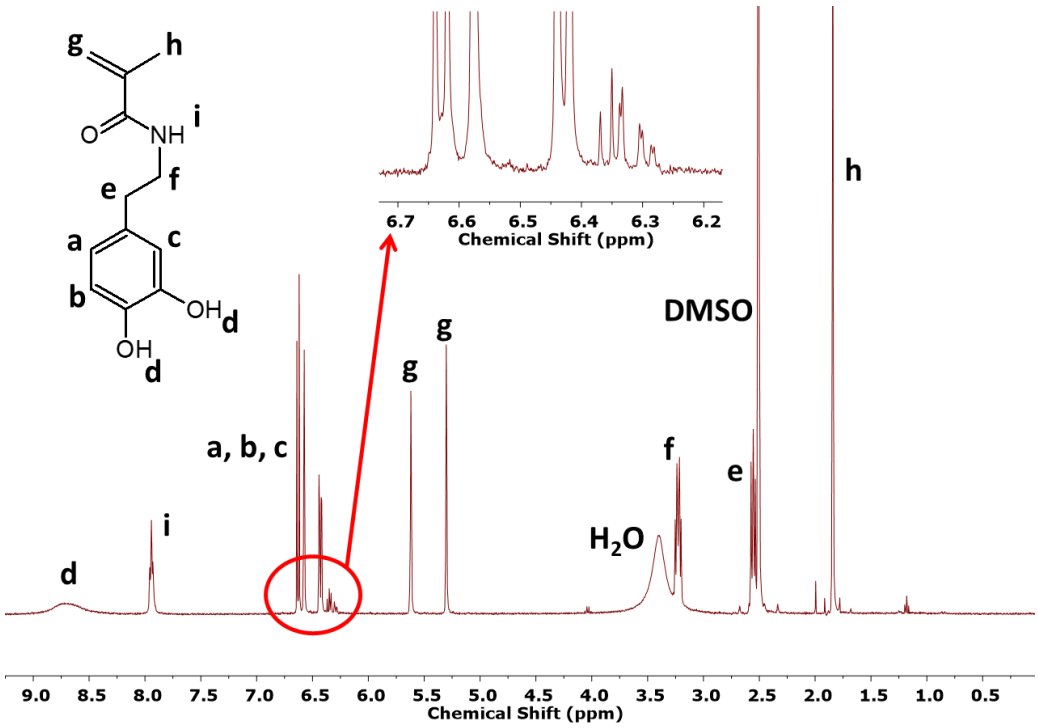

Figure 2.3. ^{1}H NMR spectrum for DMA synthesised according to method 3.

Method 2 was therefore adopted as the preferred synthesis and purification procedure due to the superior yield and purity of the resulting product.

2.4.2 Acetonide protection of dopamine methacrylamide

The ability of the catechol functional group in DMA to act as a radical scavenger is widely acknowledged.[3, 4] In practice, in FR copolymerisation, the impact of a small degree of radical deactivation is limited due to the high concentration of radicals generated by the initiator. However, there is potential for chain branching or chain transfer to affect the polymer chain skeletal structure.[6, 38] Moreover, in reversible-deactivation radical polymerisation (RDRP) reactions, where the radical concentration is supressed, any radical scavenging by the catechol is likely to be significant. It was therefore considered necessary to protect the catechol group in DMA, in order to achieve linear polymers and a low dispersity in subsequent reversible activation-fragmentation chain transfer (RAFT) polymerisations.[28] A further benefit of protecting the catechol group was prevention of unwanted side reactions of the catechol during storage, such as oxidative crosslinking.[7]

Several protection strategies for catechols have been described in the literature, including conversion of the hydroxyl groups to silyl, methyl or ethyl ethers, to a borate or to an acetonide.[3, 39-43] Protection of the catechol functional group of DMA as a borate (as used in DMA synthesis above, Scheme 2.2) was deemed inappropriate for the polymerisations discussed in this thesis as the borate-protected DMA is insoluble in polar aprotic solvents such as 1,4-dioxane and DMF. Kamperman *et al*. used DMA, with the hydroxyl groups protected as methyl ethers, to synthesise copolymers and subsequently successfully deprotected the catechol using BBr_3.[6] However, Detrembleur *et al*.,[28] argued that BBr_3 is too strongly acidic and can promote the hydrolysis of amides or other ethers present (such as the PEGMEM comonomers used in their reported investigation). Consequently, they used an acetonide-protected DMA monomer (ADMA) to synthesise block copolymers with poly(ethylene glycol) methyl ether (PEGMEM) using RAFT polymerisation, which were deprotected post-polymerisation with trifluoroacetic acid.

Acetonide protection was chosen in the current study due to the milder deprotection conditions required compared to methyl or ethyl esters. A general procedure is outlined in Scheme 2.3. The acetonide protection of DMA was initially carried out according to the method of Detrembleur *et al*,[28] referred to as protection method 1, wherein DMA was heated under reflux with *p*-toluene sulfonic acid in toluene for 3 hours, before the reaction was cooled to 0 °C and 2,2-dimethoxypropane was added dropwise. The reaction mixture was again heated under reflux for 4 hours. After removal of the toluene by rotary evaporation, purification of the crude yellow ADMA crystals was attempted using column

chromatography which resulted in light brown crystals of ADMA in 68.5% yield. The light brown colour suggested the presence of impurities, which may have been caused by catechol oxidation prior to successful protection.

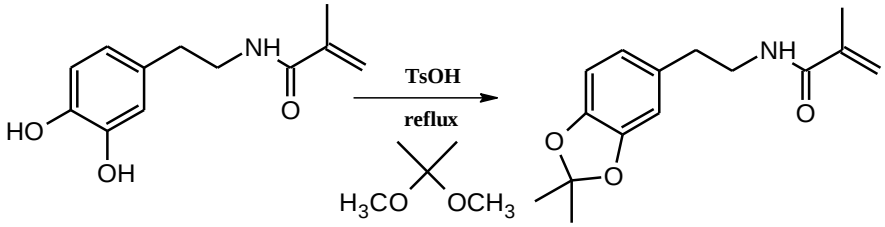

Scheme 2.3. Protection of dopamine methacrylamide with an acetonide group.

An NMR spectrum indicated the presence of ADMA, although additional signals were observed between 1.0 and 1.8 ppm, and at 7.8 ppm, suggesting significant impurities were present. The peaks at 7.8 ppm correspond to catechol (unprotected) hydroxyl protons. Recrystallisation of the crude crystals was difficult due to the low melting point of the product (~60 °C), and a viscous oil was often produced, however, small quantities of white crystals could be obtained in low yield from petroleum ether (40 – 60 °C). Evidence of the identity of the ADMA was obtained using mass spectrometry (Figure 2.4). The partial spectrum shows the mass peak ($[M+H]^+$) at *m/z* 262.2 g mol^{-1}. A significant peak at *m/z* 523.4 g mol^{-1} is assigned to the $[2M+H]^+$ adduct. The peaks with lower relative abundance at *m/z* 303.3 and 325.2 g mol^{-1} are due to impurities; they have been assigned previously to complexes of dihydroxyindole (DHI) and dopamine, which both contain the unprotected catechol functional group.[44]

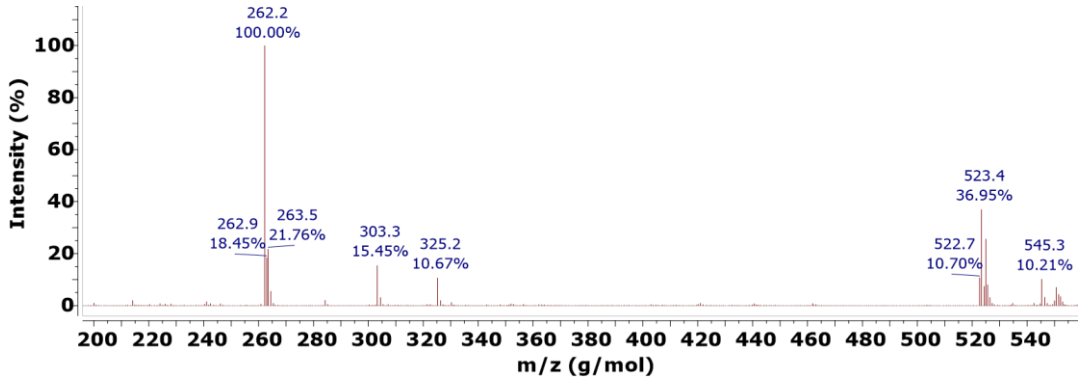

Figure 2.4. LC-MS mass spectrum of ADMA with $[M+H]^+$ ion at *m/z* 262.2 g mol^{-1}.

The approach was modified slightly to improve the yield and prevent catechol oxidation (protection method 2). The concentration of DMA in toluene was increased from 0.5% (w/v) (protection method 1) to 2.5% (w/v) to increase the rate of reaction. The column chromatography procedure was also modified by increasing the proportion of hexane :

ethyl acetate from 5:1 to 3:1 to reduce tailing and ensure efficient separation of any unprotected starting material. Protection method 2 resulted in improved yields of 75.8% (6.29 g DMA starting material) and 81.3% (10.00 g DMA starting material). The improved yields compared to protection method 1 could have been due to the larger scale, but the crystalline product obtained by method 2 was noticeably whiter. ^{1}H NMR was used to confirm the identity of the crystals and assess purity. Figure 2.5 shows the ^{1}H NMR spectrum of purified ADMA synthesised using protection method 2. Successful acetonide protection is evidenced by a peak at δ = 1.69 ppm, which was ascribed to the CH_3 protons on the acetonide protecting group. Moreover, no peaks were observed in the region attributed to the catechol hydroxyl protons (from 7.5 – 8.5 ppm). Protection method 2 was therefore preferred due to the improved purity and yield of ADMA.

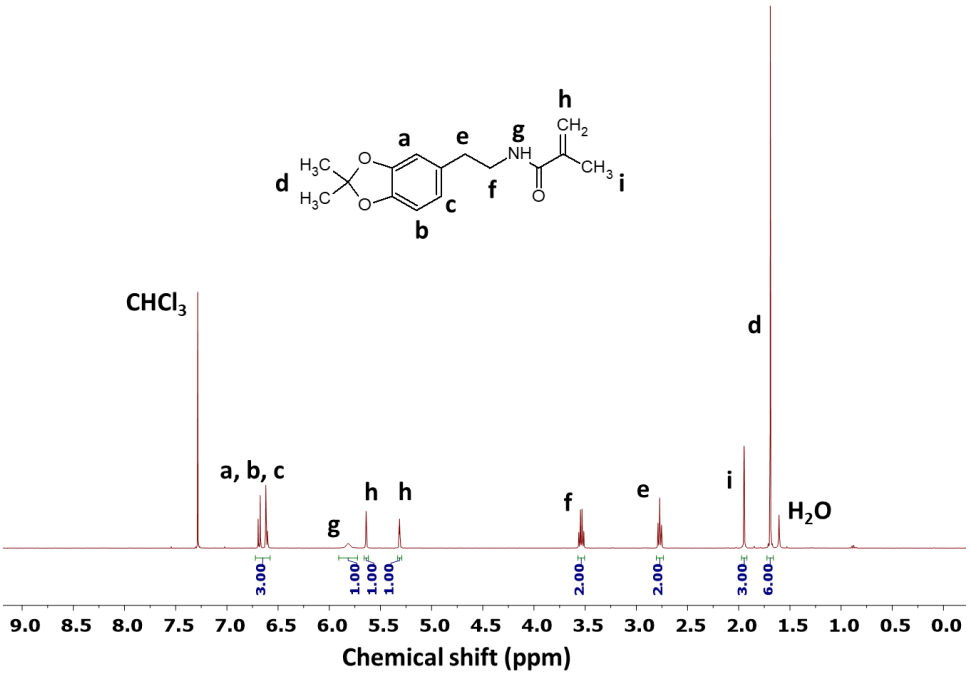

Figure 2.5. ^{1}H NMR spectrum and relative integrals of ADMA.

2.4.3 Synthesis of homopolymers of DMA and ADMA by FR polymerisation

Homopolymers of DMA and ADMA were synthesised to establish suitable reaction conditions and to inform future copolymerisation reactions. The conditions, monomer conversion, ρ, number average molecular weight, M_n, and dispersity, Đ, for the homopolymerisation reactions are summarised in Table 2.1. Polymers in this thesis are referred to individually using a code where the first element describes the type of polymerisation, FR or RAFT, and the second denotes the monomers used where A = ADMA, D = DMA, G = GMA, H = HEMA, M = MMA, P = PEGMEM and

S = SMA. Further information is then included for the avoidance of ambiguity between samples *e.g.* monomer feed mole fraction, solvent or reaction temperature. For example, FR-D-(DIOX) is a DMA homopolymer synthesised by FR polymerisation in 1,4-dioxane, and FR-MGA-77/12/11 is a terpolymer with a monomer feed consisting of MMA (71 mol%), GMA (12 mol%) and ADMA (11 mol%).

Table 2.1. Conditions used and conversion data for free radical homopolymerisations.

Polymer	Solvent	Time / h	ρ / %	M_n / g mol^{-1}	Đ
FR-D-(DIOX)	1,4-dioxane	7	28[a]	-	-
FR-D-(DMF)	DMF	24	46	95300	1.24
FR-A	1,4-dioxane	24	20	24300	1.17

a) Conversion estimated from yield of polymer collected.

FR homopolymerisation of DMA has been reported by a limited number of other groups, but has been overlooked by many due to potential for crosslinking[6, 45, 46] which may occur *via* coupling reactions between side chains containing the catechol functional group. The rate of reaction may also be retarded due to radical scavenging by the catechol. It has been reported that during synthesis of copolymers containing DMA, both of these effects can be mitigated somewhat by the use of a polar aprotic solvent, as they can act as hydrogen bond acceptors, thus reducing the chance of interaction between catechol groups and propagating radicals.[6] For example, a reported homopolymerisation of DMA in DMF resulted in an M_n of ~7550 g mol^{-1} after polymerisation for 16 h at 60 °C ([mon]:[I] = 10:1).[47] The reasonably high yield (72%) illustrates the potential for DMA polymerisation in a polar aprotic solvent.

In the current work, the effect of solvent on the homopolymerisation of DMA was investigated at 70 °C using 1,4-dioxane (FR-D-(DIOX)) and DMF (FR-D-(DMF)) (Table 2.1). All polymers described in this chapter were synthesised using the same molar ratio of monomer to initiator – 100:1 ([mon]:[I]).

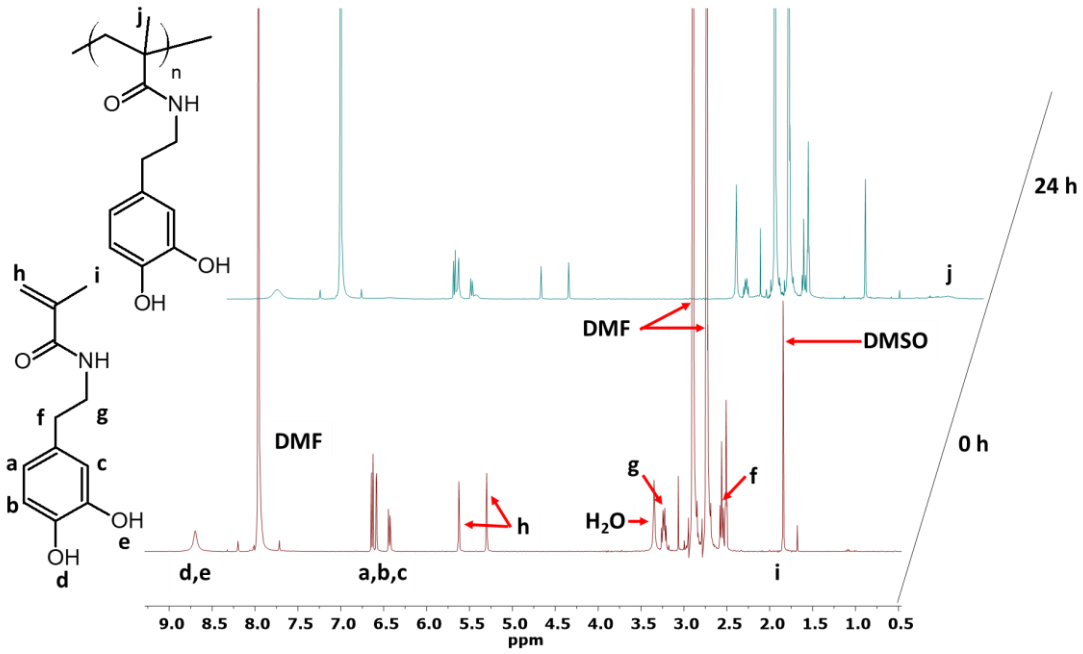

Figure 2.6. NMR spectra of samples extracted from DMA polymerisation. Top = 24 h, bottom = 0 h.

The homopolymerisation of DMA in 1,4-dioxane (FR-D-(DIOX)) resulted in a 28% yield. A white solid was recovered upon precipitation into diethyl ether, however upon exposure to air (oxygen) after drying, the polymer turned brown and became insoluble in any solvent, suggesting that the catechol groups were oxidised to form quinones, which subsequently formed crosslinks.[7] The lack of solubility prevented measurement of the molecular mass of FR-D-(DIOX) by SEC.

NMR spectroscopy was used to monitor monomer conversion during the polymerisation of DMA in DMF (FR-D-(DMF)), however data could not be obtained for FR-D-(DIOX). The NMR spectra of the initial sample and the sample at 24 h are shown in Figure 2.6. The conversion of the monomer to polymer is indicated by the emergence of a peak at 1.0 ppm from the protons labelled **j** on the polymer backbone. The integrals of the peaks arising from the vinyl protons of the residual monomer (**h**: 5.30, 5.62 ppm) were normalised by dividing the integral of each peak by the integral of the DMF solvent peak at 7.97 ppm (acting as an internal standard). Normalisation allowed the monomer conversion to be calculated according to Equation 2.1 (with the assumption that all monomer consumed was incorporated into the polymer):

$$\textit{Monomer conversion}\ (\%) = \frac{[mon]_0 - [mon]_t}{[mon]_0} \times 100 \qquad 2.1$$

where $[mon]_0$ is the normalised integral of the peaks assigned to the monomer vinyl protons at the start of the reaction and $[mon]_t$ is the normalised integral of the peaks assigned to the vinyl protons at the time of the reaction sample. Equation 2.1 can be used to calculate the conversion of individual monomers by only considering the vinyl proton peaks arising from that particular monomer. The signal arising from DMF was used as an internal standard to normalise the integrals.

The synthesis of FR-D-(DMF) only reached 46% monomer conversion after 24 h. This could be due to radical scavenging by the catechol. Despite this, SEC showed the homopolymer had a reasonably high M_n of 95300 g mol^{-1}, which was much higher than the literature reference (7550 g mol^{-1}) probably due to the increased [mon]:[I] molar ratio used in the current investigation.[47] The dispersity was 1.24; lower than generally expected for a free radical polymerisation. However, the light scattering signal was weak, and dispersity calculated using only the RI signal was 1.46, which although still low is more realistic for a free radical polymerisation. The product of the reaction was a white solid, and browning occurred on exposure to air. Excessive contact with oxygen was avoided by drying under vacuum and storage at -18 °C under nitrogen.

FR polymerisation of ADMA has not previously been reported in the literature. It was hypothesised that homopolymerisation of ADMA would proceed with fewer side reactions, to a higher monomer conversion and yield a more stable homopolymer product with respect to DMA. This principle was demonstrated previously by the synthesis of poly(DMA) after the protection of the catechol functionality as methoxyl groups, which yielded a linear polymer.[6] ADMA was more soluble in 1,4-dioxane than DMF, hence 1,4-dioxane was chosen as the reaction solvent. Multiple preliminary attempts at polymerisation of ADMA were unsuccessful. It was hypothesised that the reaction was very sensitive to impurities in the reaction solvent and the monomer. Successful homopolymer synthesis required careful purification of 1,4-dioxane to remove reactive peroxide autoxidation products which accumulate upon storage.[48]

The most successful polymerisation (FR-A, Table 2.1) was monitored by NMR and only reached 20% conversion after 24 hours at 70 °C. When analysed by SEC, M_n was 24300 g mol^{-1} indicating many low molecular weight species were present compared to FR-D-(DMF). The dispersity was 1.17, again surprisingly low. When calculated from the RI signal only, a dispersity of 1.88 was obtained. This indicated the original dispersity was

an artefact of the weak light scattering signal. The low conversion compared to FR-D-(DMF) could indicate a low rate of propagation and potentially rapid termination of polymer chains by reaction of the propagating radical with catechol or quinone-containing impurities. This could have arisen due to impurities arising from traces of dopamine or DHI species which may not have been completely removed from the monomer; evidence for the presence of these species in the monomer prior to purification by column chromatography is presented in the monomer mass spectrum (Figure 2.4). The recovered homopolymer was a white powder which did not brown upon exposure to air. This indicated that the acetonide protecting group successfully supressed the oxidation reactions which occurred during the synthesis of DMA homopolymers. An NMR spectrum showed unambiguously that poly(ADMA) was recovered, due to the peak from the methyl protons at 0.9 ppm, the broadening of the signal from the phenyl protons at 6.7 ppm compared to the monomer and the lack of vinyl proton signals (Figure 2.7).

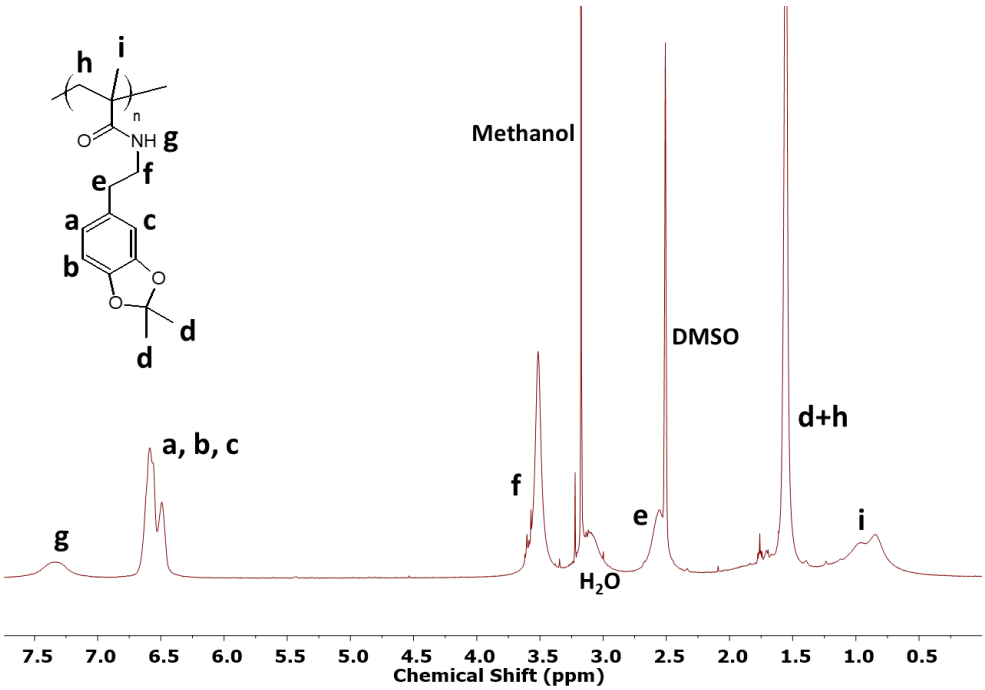

Figure 2.7. ^{1}H NMR spectrum for FR-A.

2.4.4 Estimation of reactivity ratios for the copolymerisation of ADMA with i) MMA and ii) GMA

The synthesis of functional copolymers containing DMA has been reported by several groups, however to the best of the author's knowledge the FR copolymerisation of ADMA and the resulting reactivity ratios are reported here for the first time. They are the subject of a recently published manuscript from our research group.[49]

A kinetic study of the copolymerisation of ADMA with i) MMA and ii) GMA was carried out to estimate the reactivity ratios. The reactivity ratios could be used to predict and therefore influence copolymer monomer sequence in future polymerisations and understand the properties of each monomer. Copolymers of ADMA with i) MMA and ii) GMA were selected according to the stated aims of the project *i.e.* to investigate, in detail, the synthesis of multifunctional catechol-containing copolymers.

Reactivity ratios were estimated using three models derived from the Mayo-Lewis method – the Fineman-Ross model (FRM), the Kelen-Tüdös model (KTM) and non-linear least squares regression analysis (NLLS).[50] All three models require the synthesis of copolymers with a range of monomer feed ratios. Thus, a series of copolymerisation reactions were carried out in 1,4-dioxane with mole fractions of ADMA in the feed ranging from 10 to 90 mol%. The reactions were quenched after 10 minutes to obtain copolymers with low conversion, ideally <10%, to minimise the potential impact of compositional drift. As the mass of monomer used in each reaction was very low, it was necessary to use dialysis to recover sufficient copolymer for analysis by NMR spectroscopy. Due to the small amount of recovered copolymer, no further analysis was carried out on the copolymer samples used for reactivity ratio determination.

The molar composition of a monomer feed consisting of 2 monomers, monomer 1 and monomer 2, was calculated using NMR according to Equation 2.2:

$$\boldsymbol{f_1 = \frac{x_0}{x_0 + y_0} \times 100} \qquad \textbf{2.2}$$

where f_1 is the mol% of monomer 1 in the feed and x_0 and y_0 are the integrals arising from the vinyl peaks of monomer 1 and monomer 2 respectively from a sample taken when time = 0. The mol% of monomer 2, f_2, is equal to $1 - f_1$.

NMR analysis of the recovered polymers was used to determine the copolymer composition as described in Equation 2.3:

$$\boldsymbol{F_1 = \frac{[mon]_a/x}{[mon]_b/3} \times 100} \qquad \textbf{2.3}$$

where F_1 is the mole fraction of monomer 1 in the copolymer; $[mon]_a$ is the integral of the signal arising from the monomer side chain; x is the number of protons attributed to that

signal and $[mon]_b$ is the integral of the methyl group in the copolymer backbone. The mol% of monomer 2, F_2, is equal to $1 - F_1$.

Initially, reactivity ratios were estimated using linear least squares regression analysis. Values for $f_{1,2}$ and $F_{1,2}$ were calculated using Equations 2.2 and 2.3 and are plotted in Figure 2.8. The Fineman-Ross (FRM) and Kelen-Tüdös (KTM) methods, as described in Chapter 1 (Equations 1.17 – 1.23), were used to analyse the data and obtain values for G, H, ξ and η. A linear fit was generated to estimate reactivity ratios according to each method (Figure 2.9).

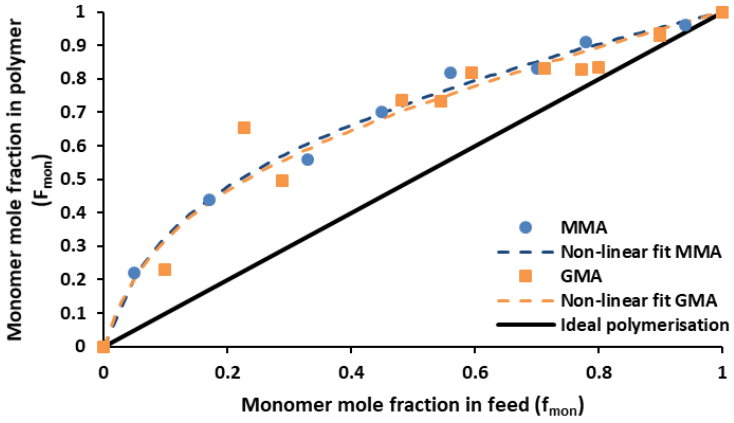

Figure 2.8. Mayo-Lewis plot of mole fraction of monomer in feed vs mole fraction monomer in copolymer when copolymerised with ADMA.

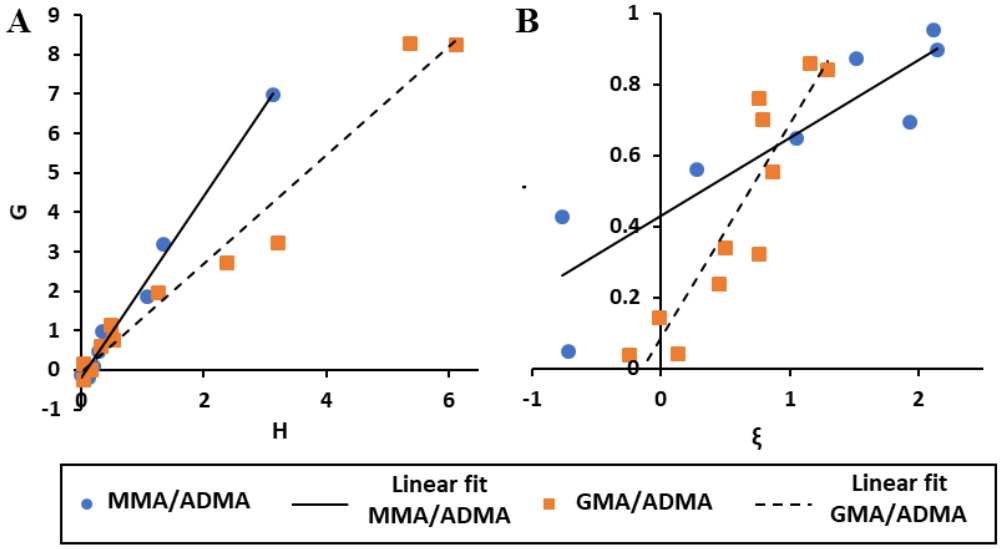

Figure 2.9. Linearised plots allowing calculation of the reactivity ratios of MMA/ADMA and GMA/ADMA A) Fineman- Ross method B) Kelen-Tüdös method.

Table 2.2. Reactivity ratios for MMA/ADMA and GMA/ADMA calculated using the Fineman-Ross (FRM), Kelen-Tüdös (KTM) and non-linear least squares regression (NLLS) models.

	MMA/ADMA		GMA/ADMA	
	r_{MMA}	r_{ADMA}	r_{GMA}	r_{ADMA}
FRM	2.30 ± 0.11	0.22 ± 0.14	1.38 ± 0.08	0.06 ± 0.23
KTM	2.26 ± 0.73	0.21 ± 0.17	1.36 ± 0.34	0.01 ± 0.15
NLLS	2.21 ± 0.26	0.17 ± 0.03	1.96 ± 0.49	0.18 ± 0.08

The estimated reactivity ratios (FRM and KTM) for the MMA/ADMA and GMA/ADMA systems are presented in Table 2.2. These initial estimates show that there is a large disparity between the reactivity ratios of the methacrylamide and methacrylate monomers, which will result in a high degree of compositional drift. 95% confidence intervals for the FRM were calculated using linear least squares regression of the data in Figure 2.9A. KTM 95% confidence intervals were calculated according to the method of Kelen, Tüdös and Turcsanyi.[51]

Despite being widely reported and a useful estimation technique for reactivity ratios, linear methods have been shown not to be a statistically sound method for calculation of reactivity ratio data.[52, 53] This is due to the incorrect statistical treatment of errors upon the linearisation of fundamentally non-linear data, which can result in inaccurate reactivity ratio estimates.[54] To obtain a more accurate estimate of the reactivity ratios, the mole fraction of the methacrylate monomer in the monomer feed (f_{mon}) was plotted against the mole fraction of the methacrylate monomer in copolymer (F_{mon}) (Figure 2.8) for both the MMA/ADMA and GMA/ADMA systems and a non-linear least squares regression was carried out using the Mayo-Lewis equation (Equation 1.16) to estimate the reactivity ratios. The estimated reactivity ratios are reported in Table 2.2. A line with the equation $x = y$ is included in Figure 2.8 to represent an ideal polymerisation (where $r_1.r_2 = 1.0$). All the data points fall above the line of $x = y$ which indicates that MMA will be consumed preferentially at all monomer feed ratios.[55] The dashed best fit lines for both MMA/ADMA and GMA/ADMA almost overlap, which suggests the copolymerisation kinetics of the two systems is very similar. NLLS 95% confidence intervals were obtained from the regression data.

When considering the MMA/ADMA system, it is clear from the reactivity ratios (r_{MMA} = 2.21 ± 0.26 and r_{ADMA} = 0.17 ± 0.03 (NLLS)) in Table 2.2 that MMA shows a

strong preference for self-propagation, and ADMA shows a strong preference to undergo cross-propagation. There is relatively little difference in the values obtained by the three methods, which increases confidence in the estimated reactivity ratios. Due to the more correct statistical treatment of the data, the value obtained by NLLS will be used in further discussion of the data.

The product of the reactivity ratios ($r_1.r_2 = 0.38$) indicates that the rate of monomer addition is far from random and both types of propagating radical (MMA and ADMA terminated) show a preference to react with MMA. Polymer chains formed throughout the reaction would comprise higher proportions of MMA in the copolymer than in the feed. Thus, little ADMA would be incorporated in chains formed in the early stages of polymerisation but as the reaction progresses, the mole fraction of ADMA in the monomer feed would increase and the fraction of ADMA incorporated into the polymer chains would rise accordingly. As such, over the course of a reaction poly(MMA-*co*-ADMA) with significant compositional drift will be synthesised.

A survey of the literature for other methacrylate/methacrylamide copolymerisation systems reveals a general agreement with the reported observations from the current work, whereby the methacrylate monomer is consumed in preference to the methacrylamide monomer. For the copolymerisation of MMA with methacrylamide (MAm), the range of reported reactivity ratios was $r_{MMA} = 1.39 – 1.73$ and $r_{MAm} = 0.43 – 1.27$.[13] However, such reports describe copolymerisation reactions carried out in a variety of solvents, which should not be ignored, as it has been shown that solvation can strongly affect reactivity ratios, and could be a source for the wide range of reported values.[27, 56] The reactivity of methacrylates is intrinsically greater than methacrylamides as the propagating radical is destabilised more by the methacrylate ester linkage then the methacrylamide amide linkage.[57]

The copolymerisation of MMA and N-(1-hydroxy-4-methyl-2-pentyl)methacrylamide (HMPMA) in methanol had reported reactivity ratios of $r_{MMA} = 2.38$ and $r_{HMPMA} = 0.50$[58] and the polymerisation of MMA and thiazoyl methacrylamide (TMA) in DMF had reactivity ratios of $r_{MMA} = 2.72$ and $r_{TMA} = 0.59$.[59] Both of these systems support the general trend that MMA is consumed in strong preference to methacrylamide monomers with bulky side chains. However, variations in published reactivity ratios highlight the risk in simply making assumptions about copolymerisation kinetics and demonstrate the value

of carrying out rigorous experimental studies to obtain accurate reactivity ratio data for each specific system. Indeed, in the MMA/ADMA system discussed in this work, the reactivity ratio of ADMA with MMA (0.17 ± 0.03) is much lower than the examples cited above.

When considering the GMA/ADMA system, the data in Table 2.2 illustrates a clear difference between the linear and non-linear estimation methods, with $r_{GMA} = 1.36 \pm 0.34$ and $r_{ADMA} = 0.01 \pm 0.15$ by the Kelen-Tüdös method, but $r_{GMA} = 1.96 \pm 0.49$ and $r_{ADMA} = 0.18 \pm 0.08$ by NLLS regression analysis. When the confidence intervals are considered, the estimates generated could converge between the lower bounds of the NLLS regression and the upper bounds of the KTM. The uncertainty associated with these measurements is rather high, which is probably due to experimental error *e.g.* measurement of reagents, polymer recovery and determination of polymer composition using NMR. As such, the data should be considered with some caution. As a method of reducing the uncertainty, the errors in variables method (EVM) takes account of experimental error, so would improve the confidence in the data,[60] but the mathematical complexity of the approach was beyond the scope of this study.

As with the MMA/ADMA system, only the NLLS data will be considered for further discussion of the GMA/ADMA system. A reactivity ratio of $r_{GMA} = 1.96 \pm 0.49$ (NLLS) indicated that whilst GMA still shows a preference for self-propagation, the tendency to self-propagate is slightly less pronounced than that of MMA when copolymerised with ADMA. In copolymerisation with GMA, $r_{ADMA} = 0.18 \pm 0.08$, suggesting an extremely high tendency for ADMA to undergo cross-propagation. Although it appears that in a copolymerisation with ADMA, MMA shows a slightly stronger tendency for self-propagation than GMA, both reactivity ratios fall within error of each other, indicating the epoxide ring in the side chain of GMA does not have a significant effect on the reactivity ratios in this case.

It was unclear if the steric bulk of the catechol side chain was responsible for the unexpectedly low reactivity ratio of ADMA in both systems (compared to the usual range of reactivity ratios in methacrylate-methacrylamide copolymerisations). The effect of steric bulk on copolymerisation is a pertinent discussion. Indeed, it has been shown that methacrylate macromonomers with flexible side chains, such as methacrylate-functionalised poly(caprolactone)s can be polymerised with MMA with reactivity ratios

close to unity, in which solvation appears to play a greater role than macromonomer size in determining reactivity ratio.[61] The reactivity of the monomers depended on the solvent, especially when the macromonomer side chain contained groups capable of H-bonding.[16, 61] For the polymerisation of phenyl methacrylamide (PMAm) and MMA in DMF, reactivity ratios of $r_{PMAm} = 0.17$, $r_{MMA} = 0.79$ were obtained.[12] For the polymerisation of PMAm with GMA, the same authors reported reactivity ratios of $r_{PMA} = 0.09$, $r_{GMA} = 2.47$.[62] Discussion of the reason for the contrasting methacrylate reactivity ratios is unfortunately lacking. In contrast, the polymerisation of phenyl methacrylate (PMA) with MMA resulted in reactivity ratios of $r_{PMAm} = 1.04$, $r_{MMA} = 0.81$.[63] These examples demonstrate the importance of the polymerisable group in determining reactivity ratios.

Steric bulk of monomers can play a significant role in copolymerisations as demonstrated by previous work on the steric (and electronic) impact on the anionic copolymerisation and terpolymerisation of diphenylethylene (and derivatives) with styrene and butadiene.[64, 65] In these cases the steric bulk of DPE renders it unable to homopolymerise. However, these earlier reports suggest that for bulky substituents to impact upon copolymerisation kinetics, the steric bulk must be in direct proximity to the propagating species. It could therefore be suggested that the flexible linking segment between the protected catechol functionality and the reactive methacrylamide group in ADMA diminishes much of the steric effect of the side chain on the monomer reactivity. It is therefore proposed that the extent of spatial separation in between the bulky side chain and propagating group is crucial when considering the impact on reactivity. Consequently, for the observed reactivity ratios in the current work involving ADMA, electronic and solvation effects may be dominant. Thus, reduced solvation of the ADMA in comparison to the methacrylate monomers could be responsible for lower than expected reactivity, and further studies of these monomer systems in various solvents would be informative. Having obtained the reactivity ratios discussed here, one can confidently predict that at any monomer feed ratio, MMA or GMA will be polymerised in preference to ADMA.

2.4.5 Investigation of compositional drift during the synthesis of co/terpolymers containing ADMA

To obtain a quantitative understanding of the full impact of compositional drift on the heterogeneity of MMA/ADMA and GMA/ADMA copolymers, statistical copolymers with a range of monomer feed ratios were synthesised and allowed to run to full conversion. It was expected that the disparate reactivity ratios between ADMA and MMA or GMA,

would result in considerable compositional drift. Likewise, significant compositional drift would be predicted in the copolymerisation of ADMA with alternative methacrylate comonomers such as HEMA.

A library of co and terpolymers was prepared comprising ADMA with one or more methacrylate comonomers (MMA, GMA, HEMA and SMA, see Figure 2.10). The methacrylate monomers in Figure 2.10 vary significantly in polarity, so were used with the intention of tuning the solubility of the resulting copolymers, in line with the aim of developing copolymers with a range of solubilities for deposition on various substrates. The residual (unreacted) comonomer composition was calculated by collecting samples at intermediate reaction times and using ^{1}H NMR to analyse the residual monomer in the feed. This could be used to infer the compositional drift during the polymerisation.

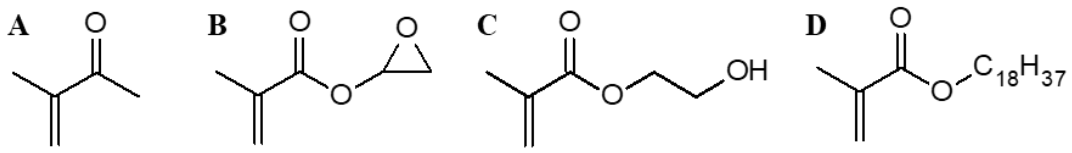

Figure 2.10. Monomers used as functional additional monomers in FR copolymerisations with ADMA. A) MMA, B) GMA, C) HEMA, D) SMA.

2.4.5.1 Investigation of compositional drift in ADMA/MMA copolymers

Copolymers of MMA/ADMA were prepared in 1,4-dioxane, using ADMA mole fractions of 10%, 51% and 76% in the monomer feed. A summary of monomer conversion (inferred from unreacted monomer at the time of the final sample), the composition of the residual feed monomer, final copolymer composition and SEC data is provided in Table 2.3. The composition of the final copolymer was calculated according to Equation 2.3 in Section 2.4.4.

Table 2.3. Polymerisation conditions and results for MMA/ADMA and SMA/ADMA statistical copolymers prepared by free radical polymerisation in 1,4-dioxane at 70 °C.

Polymer	Time / h	Comp.[a]	RM[b]	ρ / %	M_n / g mol^{-1}	Đ
FR-MA-90/10	24	92/8	66/34	93	37300	1.50
FR-MA-49/51	22.5	55/45	20/80	81	142700	2.30
FR-MA-24/76	22	29/71	7/93	81	138200	1.11
FR-SA-90/10	7	92/8	-	91[c]	93300	3.34

a) Composition, given with respect to the order of monomers in the polymer name. b) Residual monomer composition. c) Conversion estimated from yield of copolymer collected.

Initially, a molar feed ratio of 90/10 (FR-MA-90/10) was selected as a previous report suggested that good adhesion between a DMA/2-methoxyethyl methacrylate (MEA) copolymer and glass substrates could be achieved with as little as 5 mol% catechol groups in the copolymer chain.[6] Furthermore, a reported AFM study which compared the adhesion of a series of poly(DMA-co-butylamine methacrylamide) copolymers and a DMA homopolymer on a titanium substrate indicated that when the copolymer contained more than 10 mol% DMA, the force of adhesion plateaued and become independent of the mole fraction of catechol.[45] This indicated that strong adhesion could be achieved with a low mole fraction of catechol groups.

All three MMA/ADMA reactions reached high conversion (81 – 93 %). The polymerisations were quenched before reaching full conversion, although slow consumption of monomer at the time of termination could indicate radical scavenging by impurities in the ADMA monomer. Furthermore, the lower rate of propagation for the acrylamide monomer compared to the methacrylate may have reduced the overall conversion. However, given the shorter reaction times of FR-MA-49/51 and FR-MA-24/76, the effect was not thought to be significant. Additionally, the slow rate of propagation for the methacrylamide monomer could be partially responsible for the slower conversion. A high mole fraction of ADMA appeared to correlate with increased M_n, although there is no clear trend. The dispersity of 1.11 is clearly anomalous for FR-MA-24/76 and is ascribed to the weak light scattering signal at high mole fractions of ADMA. A dispersity of 1.68 was obtained using only the RI signal. The SEC chromatograms (Figure 2.11) show broad unimodal molecular weight distributions. The chromatograms were normalised for peak height and by the characteristic solvent peaks, so the position of the peaks should be considered representative rather than absolute.

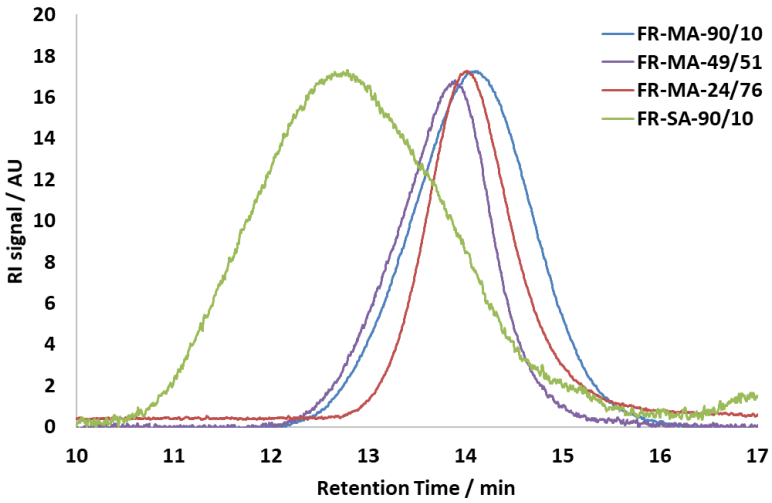

Figure 2.11. Overlaid SEC RI chromatograms of MMA/ADMA and SMA/ADMA copolymers.

Copolymer composition was calculated by ^{1}H NMR, using Equation 2.3. The NMR spectrum of FR-MA-49/51 is given as an example (Figure 2.12). Peaks for the aromatic protons on the ADMA side chain can be unambiguously observed at 6.7 ppm (**g, h, i**), and for the methyl group in the backbone at 0.9 ppm (**b**).

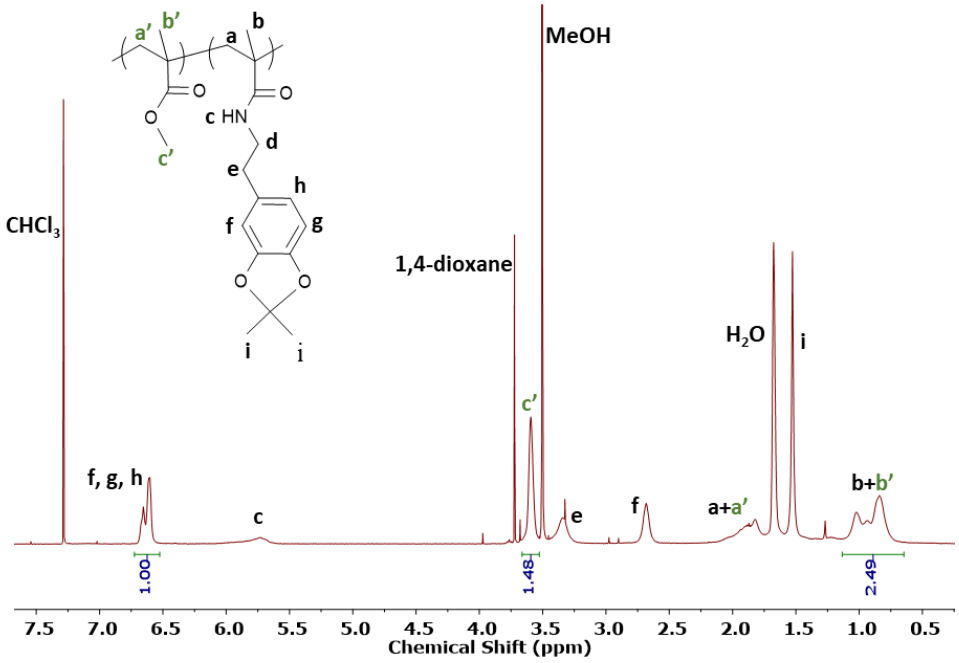

Figure 2.12. NMR spectrum of poly(MMA-co-ADMA), FR-MA-49/51.

Considering the reactivity ratios for the copolymerisation of ADMA and MMA (r_{MMA} = 2.21 and r_{ADMA} = 0.17 (NLLS)), significant compositional drift is expected over the course of a polymerisation allowed to proceed to high monomer conversion. From the data in Table 2.3, it is clear that ADMA is incorporated in the final copolymers. In each

case the mole fraction of MMA is greater in the final copolymer than the monomer feed *e.g.* the composition of FR-MA-49/51 is 55/45 (MMA/ADMA mol%). The difference between feed and copolymer composition indicates some compositional drift in the polymerisation. Furthermore, in each case the residual monomer feed at the end of the reaction comprised a larger proportion of ADMA compared to the initial feed *e.g.* the residual monomer composition for FR-MA-49/51 is 20/80 (MMA/ADMA mol%). This indicated chains formed at the end of the reaction were composed of a larger proportion of ADMA than at the start of the reaction.

Samples were obtained during the reaction and analysed using NMR spectroscopy. The evolution of the residual monomer composition can be observed qualitatively from the stacked NMR spectra of samples taken throughout the reaction, enlarged in the region of the peaks arising from the vinyl protons of each monomer (Figure 2.13). The peaks from MMA vinyl protons (δ 5.52 and 6.06 ppm) reduced in intensity much faster than those arising from the equivalent protons on ADMA (δ 5.25 and 5.57 ppm), indicating the formation of MMA-rich chains early in the reaction (Figure 2.13). The consistent intensity of the multiplet arising from the protons in the ADMA aromatic ring (δ 6.63 ppm) emphasizes the reduction in intensity of the vinyl peaks. Moreover, the gradual broadening of the aromatic proton signal is characteristic of the conversion of monomer to polymer.

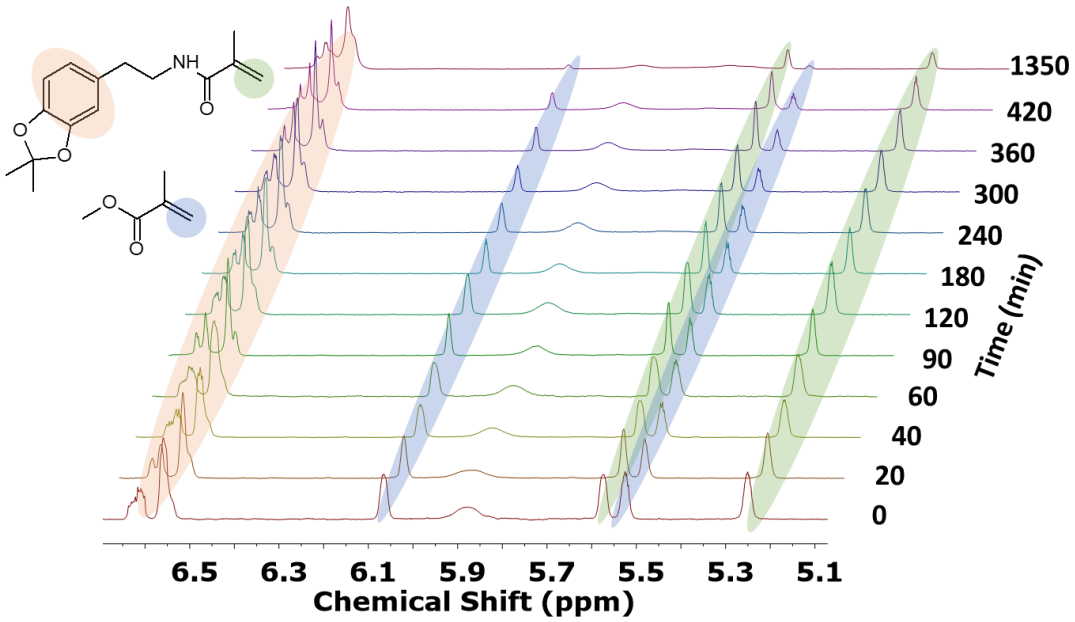

Figure 2.13. Stacked ^{1}H NMR spectra ($CDCl_3$) of samples from the synthesis of FR-MA-49/51, polymerised in 1,4-dioxane at 70 °C.

Compositional drift in a copolymer can be inferred from the mol% of a particular monomer in the copolymer, F_{mon}, at the time of each sample using Equation 2.4:

$$\boldsymbol{F_{mon1,t} = \frac{\rho_{mon1,t} \cdot f_{mon1}}{(\rho_{mon1,t} \cdot f_{mon1}) + (\rho_{mon2,t} \cdot f_{mon2})}} \qquad \textbf{2.4}$$

where the two monomers are referred to as *mon1* and *mon2*, ρ refers to the conversion of a particular monomer at a given time, *t*, and f_{mon1} and f_{mon2} are the initial monomer feed ratios. $F_{mon2,t}$ can be calculated by inverting the monomers in Equation 2.4 (which in a copolymer = 1 - $F_{mon1,t}$).

For the copolymerisations of MMA and ADMA, bar charts were generated in order to demonstrate the evolution of F_{ADMA} at various points during the reaction, *i.e.* the compositional drift (Figure 2.14). The width of each bar represents the instantaneous combined monomer conversion ($\rho_{MMA+ADMA,i}$), *i.e.* $\rho_{ADMA+MMA}$ in the period between samples. The height of the blue bars represents $F_{ADMA,t}$: the average (cumulative) ADMA content of the copolymer at the time of each sample. Consequently, the orange bars represent $F_{MMA,t}$. Additionally, the reactivity ratios calculated above were used to predict values for $F_{ADMA,i}$ using the Mayo-Lewis equation (Equation 1.16) using experimentally observed values of f_{MMA} and f_{ADMA}. The red points on Figure 2.14 indicate the predicted content of ADMA in a chain formed. The nature of the reactivity ratios is such that they are instantaneous predictions, so do not take into account compositional drift. Additionally, they predict the chains formed at each time point, so do not consider the cumulative nature of the copolymer composition. Thus, the red circles are not predictions of the cumulative ADMA composition indicated by the blue bars, but of the ADMA content of copolymer chains formed at the time of each sample and are presented to aid the reader's estimation of the expected chain composition.

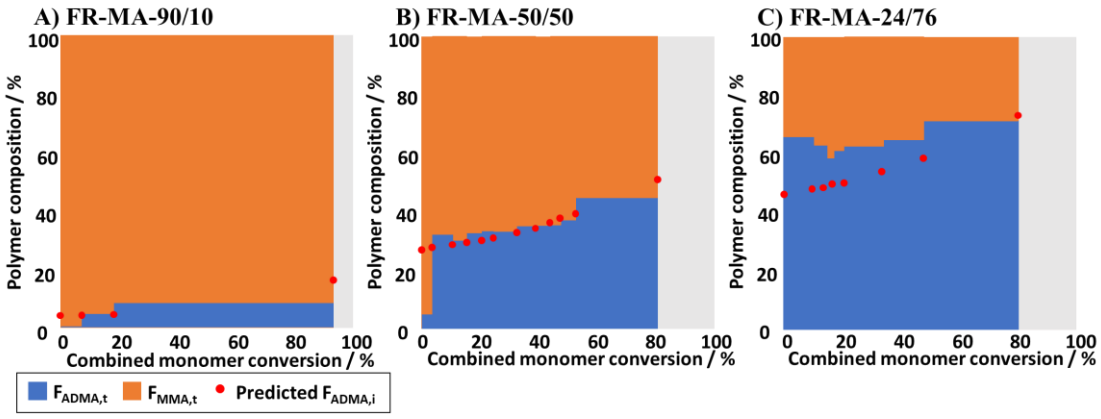

Figure 2.14. Bar charts showing $F_{ADMA,t}$ (ADMA composition of copolymer, blue bars) and $F_{MMA,t}$ (orange bars), with predicted $F_{ADMA,i}$ (red circles).

FR-MA-90/10 reached 93% conversion (Table 2.3). Figure 2.14A indicates that the chains formed from the first 7% of monomer consumed were almost entirely composed of MMA. At 18% conversion, the average copolymer chain contained 5% ADMA. ADMA composition increased to 8% between 18% – 93% conversion, although significant compositional drift is likely within this period, thus it is very likely that some chains formed towards the end of the reaction comprised >10% ADMA. The trend observed agrees with the reactivity ratios for ADMA and MMA; that MMA is preferentially consumed at the beginning of the reaction. The predicted ADMA composition data (red circles) indicated the chains formed at the early stages of the reaction would be expected to comprise a higher proportion of ADMA compared to the experimentally determined values (predicted value ~5%). Towards higher combined conversion, higher ADMA incorporation as predicted by the reactivity ratios increases the average ADMA composition. This indicates the reactivity ratios predicted the copolymer composition fairly accurately at this monomer feed composition. The data in Figure 2.14A clearly indicates variation in the ADMA content of the copolymer chains, which could have consequences for coatings applications.

FR-MA-50/50 reached 81% conversion, and the copolymer composition showed a similar trend to FR-MA-90/10. A gradual increase in the proportion of ADMA incorporated in the copolymer chains can be observed in Figure 2.14B. The large variation between the average compositions of the first two samples indicate large potential experimental error at low conversion, probably due to the statistical nature of the copolymer chains formed. Despite this, in general the average copolymer ADMA content increased gradually as predicted by the reactivity ratios. The average copolymer ADMA content remained <35%

up to ~60% combined monomer conversion, whereas later in the reaction, the average chain was composed of >45% ADMA, indicating ADMA-rich chains were formed. The compositional drift of the copolymer again appeared to agree with the predictions made using the reactivity ratios.

FR-MA-24/76 also reached 81% conversion and showed the predicted increase in ADMA incorporation over the course of the polymerisation. At 10% monomer conversion, the ADMA composition of the copolymer chains was 61%, which was a larger incorporation of ADMA than predicted, highlighting the less repeatable nature of the chains at low conversion. Subsequently, the F_{ADMA} value dropped to around the expected value before increasing in line with predictions.

The charts in Figure 2.14 clearly show the implications of a copolymerisation between two monomers with widely divergent reactivity ratios, with significant compositional drift observed. The experiments also highlight the risks of relying on one data set for prediction of statistical copolymer composition, particularly at low conversion.

A copolymer of SMA and ADMA (FR-SA-90/10) was synthesised in 1,4-dioxane for 7 h. SMA was selected as a monomer to investigate the incorporation of ADMA in copolymerisation with a non-polar methacrylate monomer. A white solid was recovered with an M_n of 93300 g mol^{-1} in a 91% yield (recovered copolymer). The SEC peak shown in Figure 2.11 is at a significantly higher molecular weight than the poly(MMA-co-ADMA) equivalent, which is almost certainly due to the higher molar mass of the SMA monomer. The composition calculation could not be carried out according to Equation 2.3 as the proton peaks for the backbone methyl group and the final CH_3 in the SMA side chain overlapped, so the integrals of the proton peaks for the copolymer side chains were compared according to Equation 2.5:

$$\boldsymbol{F_1 = \frac{[mon]_a/x}{([mon]_c/y) + ([mon]_a/x)} \times 100} \qquad \textbf{2.5}$$

where $[mon]_a$ is the integral of the ADMA side chain, x is the number of protons attributed to $[mon]_a$, $[mon]_b$ is the integral of the first CH_2 group in the SMA side chain and y is the number of protons attributed to $[mon]_b$. ^{1}H NMR of the copolymer confirmed that ADMA was incorporated, with a resulting copolymer composition of 92/8. The final composition of FR-SA-90/10 was the same as the equivalent polymerisation of MMA and ADMA, indicating the compositional drift probably followed a similar trend.

2.4.5.2 Investigation of compositional drift during the synthesis of terpolymers containing ADMA

Terpolymers are important from an academic and industrial perspective due to the potential for multifunctionality. Each monomer can contribute a particular function to the overall performance of the terpolymer, depending on the desired application. For example, in a reported polymeric adhesive consisting of DMA, MMA and PEGMEM, the mole fractions of MMA and PEGMEM were altered while the mole fraction of DMA was kept constant. The adhesive modulus and yield strength varied strongly with terpolymer composition, with the best adhesion observed in a copolymer with 45 mol% PEGMEM and 27 mol% MMA.[46] The variation in adhesive properties was attributed to the increase in ductility afforded by moderate mole fractions of PEGMEM, whilst the MMA was necessary to maintain the mechanical strength of the terpolymer. This example illustrates the potential mechanical and chemical impact of each comonomer on adhesive performance.

Three terpolymers were synthesised using different mole ratios of MMA, GMA and ADMA. Additionally, a terpolymer was synthesised consisting of ADMA, GMA and HEMA to expand the range of polarity of the copolymer library. The solubility of the resulting copolymers is discussed in Chapter 4.

Considering the calculated estimates for the reactivity ratios of ADMA with i) MMA ($r_{MMA} = 2.21 \pm 0.26$ and $r_{ADMA} = 0.17 \pm 0.03$ (NLLS)) and ii) GMA ($r_{GMA} = 1.96 \pm 0.49$ and $r_{ADMA} = 0.18 \pm 0.08$ (NLLS)), and given that the reported reactivity ratios for the copolymerisation of MMA and GMA are both close to 1;[66, 67] it could be predicted that the ADMA containing terpolymerisations discussed here would lead to significant compositional drift. It was predicted that the methacrylate monomers would be consumed at a relatively similar rate, and both in preference to ADMA which would be consumed much more slowly.

It has been reported that the reactivity ratios of three binary pairs of monomers cannot be used to accurately predict ternary reactivity ratios (although there are many examples of such predictions reported in the literature).[68, 69] Given the scope of this study, a semi-quantitative set of full conversion experiments was deemed sufficient in this case rather than a full set of experiments to accurately calculate ternary reactivity ratios for the ADMA systems. Thus, samples were withdrawn from each terpolymerisation reaction for analysis by NMR spectroscopy, to study the dependence of rate of reaction and compositional drift

on i) molar feed ratio of ADMA and ii) identity of the two methacrylate co-monomers. The monomer feed ratios and terpolymer characteristics are summarised in Table 2.4.

Table 2.4. Polymerisation conditions and results for ADMA and GMA containing statistical terpolymers prepared by free radical polymerisation in 1,4-dioxane at 70 °C.

Terpolymer	t / h	Comp	RM[a]	ρ / %	M_n / g mol^{-1}	Đ
FR-MGA-77/12/11	21	78/12/9	56/0/44	84	30800	1.54
FR-MGA-52/26/22	25	58/28/15	39/23/28	71	42700	1.67
FR-MGA-31/34/35	25.5	33/41/25	23/16/61	73	85400	1.47
FR-HGA-80/10/10-(DIOX)	24	83/10/7	57/10/33	86	12800[b]	2.53

a) Residual monomer composition. b) M_n calculated using conventional calibration (PS standard).

A terpolymer was synthesised comprising MMA, GMA and ADMA (FR-MGA-77/12/11). The combined monomer conversion was 84% after 21 hours. The composition of the resulting terpolymer - 78/12/9 (mol% MMA/GMA/ADMA) - indicated a relatively uniform incorporation of all three monomers, however the residual monomer feed composition of 56/0/44 mol% clearly showed the methacrylate monomers had been incorporated preferentially. Consequently, chains that would have been formed in the final stages of the reaction would be ADMA-rich and could contain little or no GMA. This finding is useful to consider for functional coating applications, as some terpolymer chains may not contain any of the reactive epoxide monomer. The M_n, 30800 g mol^{-1}, was similar to FR-MA-90/10, indicating the GMA did not have a significant impact on the molecular weight.

A second terpolymer synthesis, with a different feed composition (FR-MGA-52/26/22) only reached 71% conversion after 25 hours under the same reaction conditions. It has previously been shown that an increase in ADMA composition in the MMA/ADMA copolymers resulted in lower combined conversion, and therefore it seems reasonable to conclude that the lower conversion in this terpolymer can be attributed to the increased mole fraction of ADMA in the feed. The methacrylamide monomer has a lower rate of propagation than the methacrylates and further inhibition could arise due to possible radical scavenging from impurities present in ADMA. The composition of the resulting terpolymer - 58/28/15 (mol% MMA/GMA/ADMA) - again indicated preferential incorporation of the methacrylate monomers, with MMA and GMA consumed relatively evenly. In this case 28% of the residual (unreacted) monomer was ADMA. The M_n was

42700 g mol^{-1} and the increase in molecular weight can be attributed to the increasing weight fraction of ADMA, which has a relative molecular mass which is more than double that of MMA.

The synthesis of FR-MGA-31/34/35 reached a moderate conversion, 73%, after 25.5 h. The terpolymer composition, 33/41/25 (mol% MMA/GMA/ADMA), and residual monomer composition again demonstrated the preferential incorporation of methacrylate monomers over ADMA. It also appeared that GMA was consumed in slight preference to MMA. The M_n of 85400 g mol^{-1} continued the trend of molecular weight increasing according to monomer weight fraction. In this case the DP of the polymer increased, suggesting that the concentration of the initiator radicals may have been reduced by impurities in the ADMA.

A HEMA, GMA and ADMA copolymer (FR-HGA-80/10/10-(DIOX)) reached a total monomer conversion after 24 h of 86%. Similar total monomer conversions were observed for FR-MA-90/10 (93 %, 24 h) and FR-MGA-77/12/11 (84%, 21 h) which had very similar molar feed ratios, indicating that the change in methacrylate monomer, from MMA to HEMA, had little effect on the overall monomer conversion. This is slightly surprising given the twofold increase in k_p reported for GMA with respect to MMA, and a further twofold increase for HEMA with respect to GMA,[16] however, k_p of the current reactions have not been measured, and the monomer conversion could be affected by many other variables such as impurities in the monomer, solvent and the presence of the ADMA comonomer.

The SEC chromatograms for the poly(MMA-*co*-GMA-*co*-ADMA) terpolymers show broad unimodal molecular weight distributions (Figure 2.15A). The peak shapes of FR-MGA-77/12/11 and FR-MGA-52/26/22 are almost identical and the M_n values are accordingly close. FR-MGA-31/34/35 shows significant tailing towards low molecular weight. FR-HGA-80/10/10-(DIOX), eluted with DMF, showed a very broad monomodal peak, and a large dispersity was calculated (2.53).

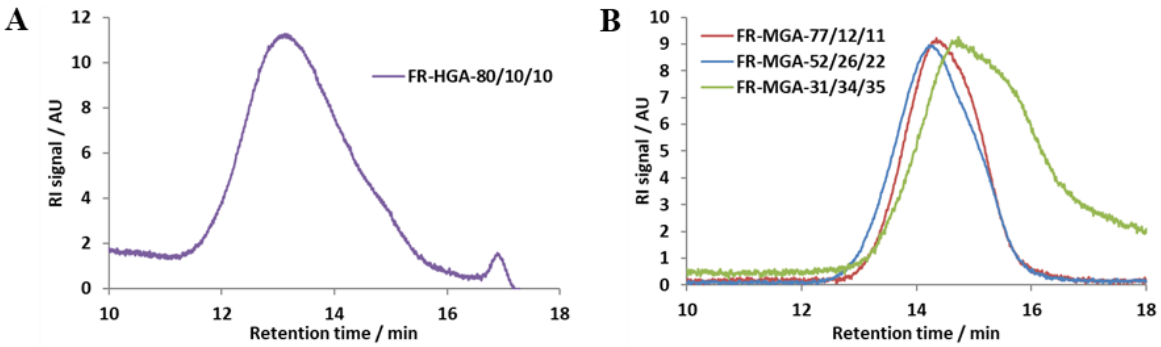

Figure 2.15. SEC RI chromatograms. A) MMA/GMA/ADMA terpolymers, THF eluent. B) HEMA/GMA/ADMA terpolymer, DMF eluent.

The reaction samples withdrawn from each polymerisation were analysed to gain a better understanding of the compositional drift. The stacked NMR spectra of samples withdrawn throughout the polymerisation of FR-MGA-31/34/35 demonstrate the preferential consumption of the methacrylate monomers (Figure 2.16).

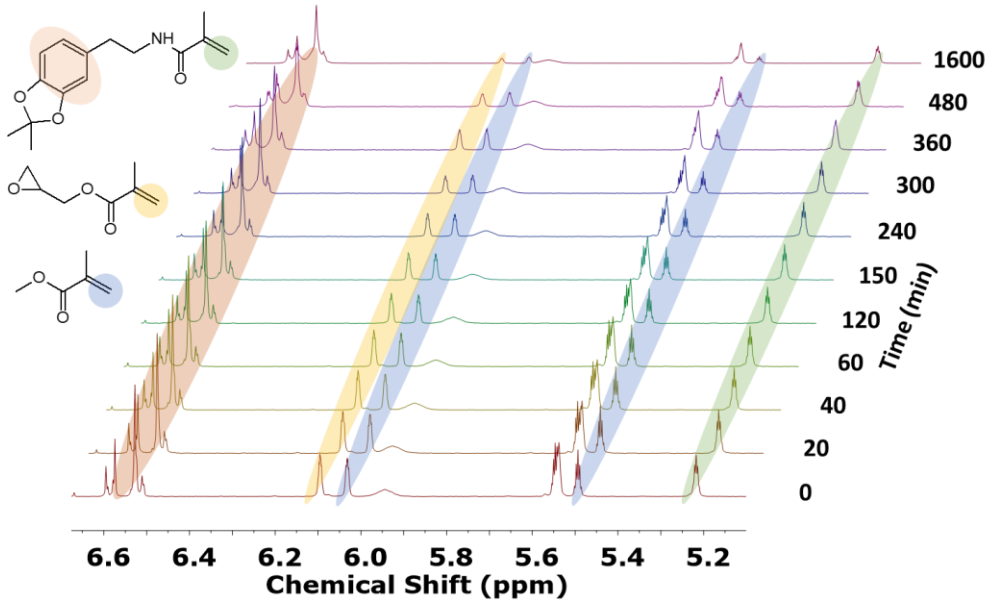

Figure 2.16. Stacked ^{1}H NMR spectra ($CDCl_3$) of samples from the synthesis of FR-MGA-31/34/35, polymerised in 1,4-dioxane at 70 °C.

The peak at 5.57 ppm (Figure 2.16) is assigned to overlapped vinyl signals from GMA and ADMA and the peak at 5.98 ppm is due to the ADMA acrylamide proton (-CH_2-**N**H-). The intensity of the MMA peaks (6.06 ppm and 5.52 ppm, highlighted blue), and the GMA peaks, (6.10 ppm, yellow) clearly decrease much faster than those of ADMA (5.25 ppm, green); a clear illustration of compositional drift. The broadening of the multiplet arising from the aromatic ADMA protons at ~6.6 ppm is also characteristic of conversion of monomer to polymer.

The evolution of the terpolymer composition throughout the reaction was plotted against combined monomer conversion (Figure 2.17). FR-MGA-77/12/11 and FR-MGA-52/26/22 show an unexpected effect at low conversion, where the incorporation of ADMA into the chains at the early part of the reaction is similar to the molar feed ratio. A lower incorporation of ADMA would be expected in these cases. As previously discussed, the error at low conversion appears to be significant and could be the cause of the observed composition. The relative proportions of the methacrylate monomers incorporated remained relatively constant. However, for FR-MGA-77/12/11 the mole fraction of residual ADMA in the feed (f_{ADMA}) steadily increased from 11% to 14% and 44% when ρ = 0%, 51% and 92% respectively. This provides indirect evidence that the methacrylate monomers are preferentially incorporated, aside from the unusually high incorporation of ADMA early in the reaction. Similarly, f_{ADMA} for FR-MGA-52/26/22 increased from 21% to 29% and 38% when ρ = 0%, 50% and 73% respectively.

For FR-MGA-31/34/35, the first sample again had a higher-than-expected incorporation of ADMA. However, from around 20% conversion onwards, the expected trend was observed; the DMA composition slowly increased to ~25%. However, f_{ADMA} for FR-MGA-31/34/35 supported the expected trend, increasing from 35% to 48% and 61% when ρ = 0%, 51% and 73% respectively. There was little compositional drift between the methacrylate monomers.

For FR-HGA-80/10/10-(DIOX), the first measurement had a higher F_{ADMA} than expected, however it dropped before slowly increasing at higher total monomer conversion. f_{ADMA} increased from 11% to 21% and 33% when ρ = 0%, 58% and 89% respectively. When compared to FR-MGA-77/12/11, the trends are very similar, with observed compositional drift of ADMA, indicating the effect of switching from MMA to a more polar methacrylate monomer is not significant under the conditions used here. In the case of FR-HGA-80/10/10-(DIOX), F_{GMA} also increased throughout the reaction, from 5% up to 10%. This indicates that there is also compositional drift between the GMA and the HEMA, with HEMA consumed slightly faster initially.

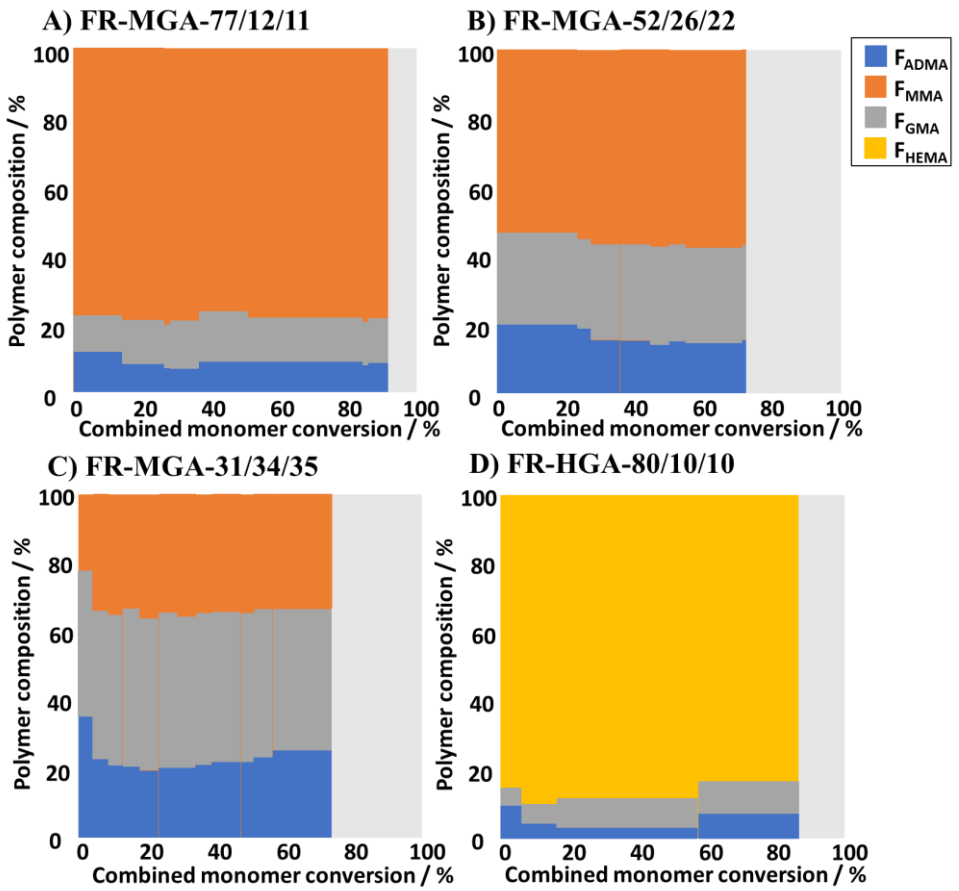

Figure 2.17. Terpolymer composition vs combined monomer conversion for ADMA-containing terpolymers.

2.4.6 Removal of the acetonide protecting group from ADMA and ADMA-containing copolymers

For the catechol group to become effective in promoting adhesion, the acetonide protecting group must be removed from ADMA by acid-catalysed hydrolysis of the cyclic acetal.[42] Detrembleur *et al.* previously reported the deprotection of poly(ADMA-*block*-PEGMEM), which had been synthesised using RAFT polymerisation,[28] using trifluoroacetic acid (TFA) as the deprotection agent in a mixture of TFA, methanol, water and DMSO (28:44:14:14 volume respectively) at 35 °C. The reaction was carried out in an open vessel to allow evaporation of the generated acetone, driving the reaction to completion. In the current work, an optimisation procedure was carried out to modify the reported procedure for use with less polar copolymers.

FR-MA-24/76 was subjected to deprotection using a modified version of the previously reported approach (Scheme 2.4).[28] However, FR-MA-24/76 was insoluble in the reported (highly polar) solvent mixture (methanol/water/DMSO), so the deprotection was carried out using chloroform (74% v/v), TFA (25% v/v) and water (1 % v/v) at 35 °C. A small

quantity of water was required to react with the acetonide leaving group to reform acetone. After deprotection, the solubility of the copolymer changed such that it was no longer soluble in chloroform and precipitated out of the reaction solution.

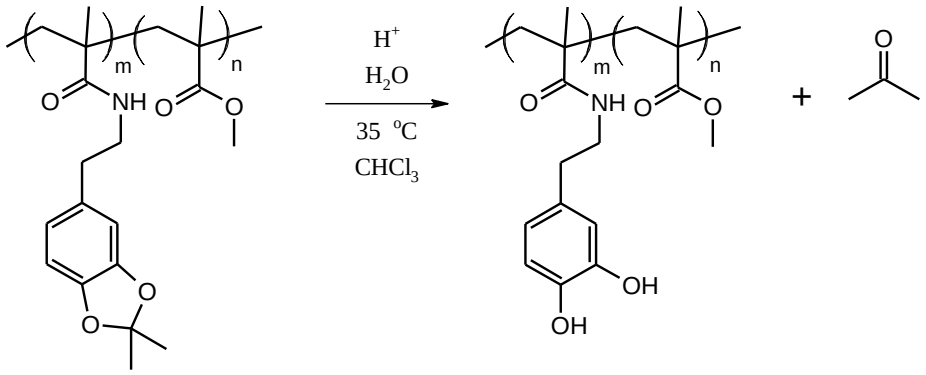

Scheme 2.4. Removal of protecting group from FR-MA-24/76.

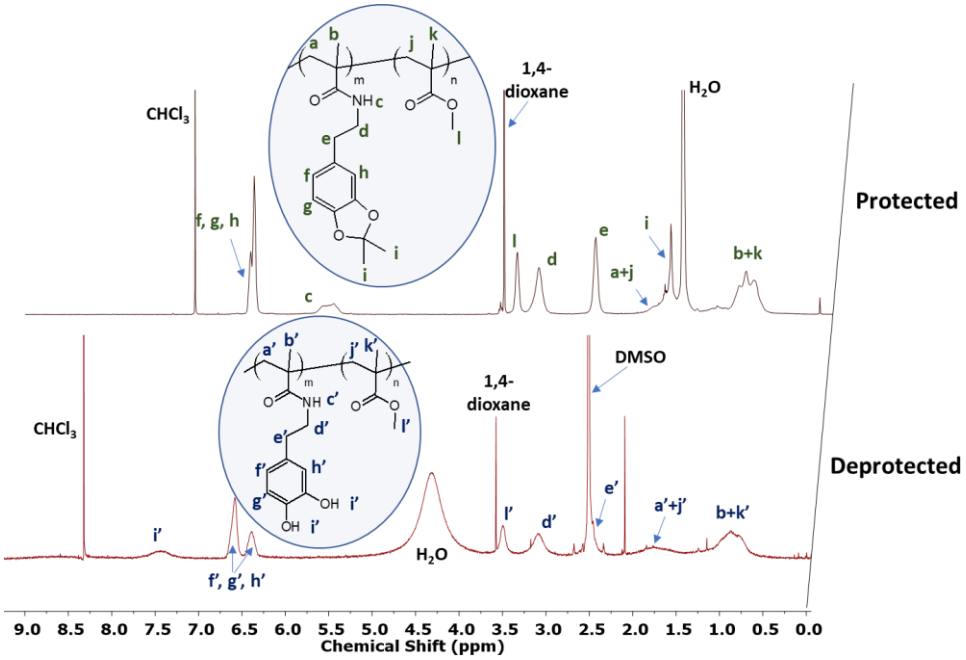

Figure 2.18. NMR spectra of FR-MA-24/76. Top – Protected, Bottom – deprotected.

After 12 h, the reaction solvent was removed by rotary evaporation and the copolymer was analysed using NMR using deuterated DMSO as the solvent. The spectrum was compared with that of FR-MA-24/76 to analyse the extent of deprotection (Figure 2.18). Successful deprotection was evidenced by the disappearance of the peak assigned to the acetonide protons (1.80 ppm, peak **i**) after 12 hours.[28] A broad peak also can be observed in the spectrum of the deprotected copolymer at ~7.5 ppm which is assigned to the hydroxyl protons on the catechol functional group (**i'**).

To confirm the method described above had successfully removed the acetonide group from the copolymer, the test was repeated using ADMA monomer. The same solvent and reagents were used, and the monomer sample was analysed using NMR before and after the reaction (Figure 2.19). The disappearance of the peak at 1.69 ppm from the ADMA spectrum, and appearance of a very broad peak at ~8.7 ppm clearly indicated the removal of the acetonide group.

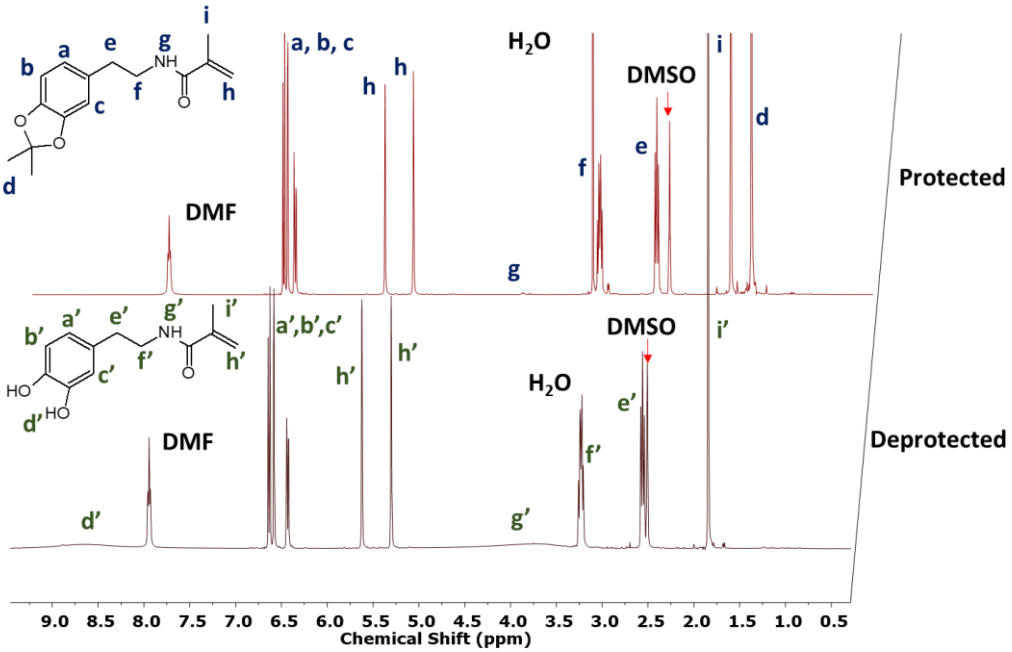

Figure 2.19. NMR spectrum for the removal of the acetonide protecting group of ADMA.

The ADMA side chains in FR-SA-90/10 were also deprotected to test the reaction conditions for a copolymer synthesised with a less polar comonomer. The extent of deprotection was monitored by the withdrawal of a sample at t = 0 h and a further sample at t = 1 h, which were analysed using ^{1}H NMR (see Figure 2.20). Successful deprotection was evidenced by the disappearance of the peak assigned to the acetonide protons (1.69 ppm, peak **i**) after 1 hour, which can be observed more clearly in the inset region.[28] The peak at 1.59 ppm is due to water, which was removed upon drying of the deprotected samples, and the peak at 1.64 ppm, **d'**, is due to protons on the aliphatic SMA side chain. In this case, the broad peak arising from the (labile) catechol hydroxyl groups was not observed, probably due to the low mole fraction of ADMA in the copolymer.

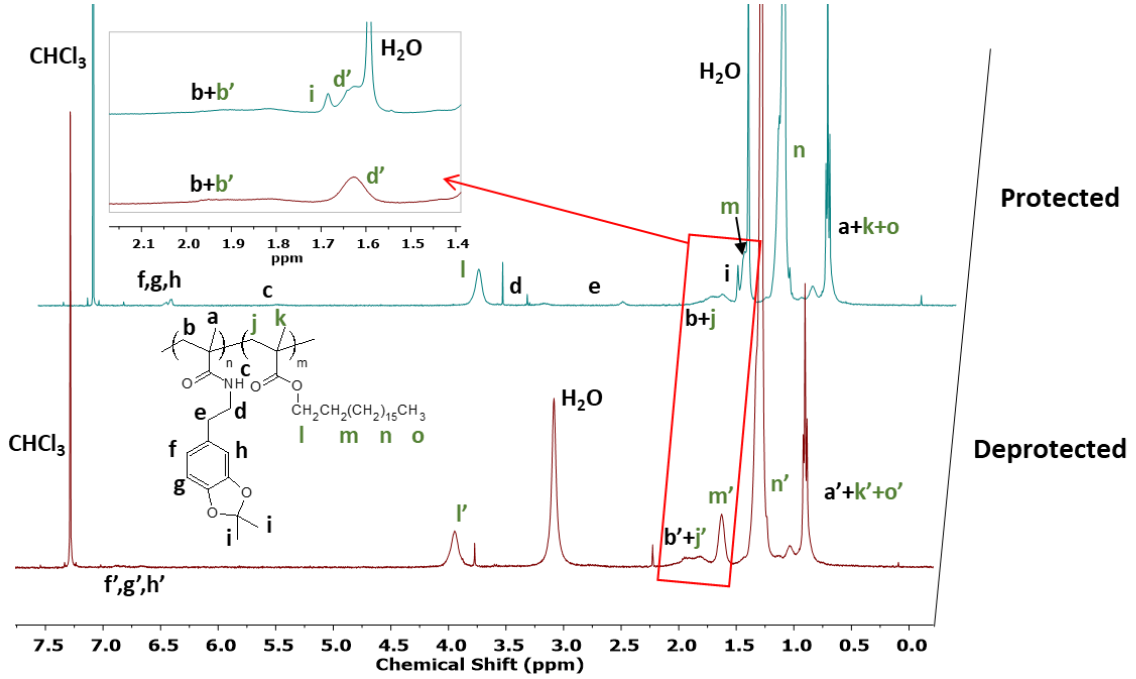

Figure 2.20. ^{1}H NMR spectra showing the progress of deprotection of FR-SA-90/10. Top (blue) - protected copolymer, Bottom (red) - 1 hr deprotection. Inset – expanded region 1.4 – 2.1 ppm.

Although the deprotection procedure described above was successful, a potential problem with the deprotection of ADMA in copolymers which also contain GMA is the reactivity of the epoxide group; epoxide ring-opening can occur in the presence of acid/base and water.[70] In the current study, the stated aim was to enable covalent binding of biomolecules to the surface *via* reaction with the epoxide group, thus requiring the reactive rings to remain intact during and after deprotection. A terpolymer containing GMA (FR-MGA-31/34/35) was exposed to the deprotection conditions described above, but an insoluble gel was quickly formed, thought to be due to the ring-opening of the epoxide groups and subsequent formation of a cross-linked network. As such, the resulting product could not be analysed. Successful deprotection of copolymers containing both ADMA and GMA without epoxide ring-opening remains an area requiring further research but was not investigated further as copolymerisations involving unprotected DMA were prioritised; as described herein.

2.4.7 Investigation of compositional drift during the synthesis of co/terpolymers containing DMA

The FR copolymerisation of ADMA has been discussed in this chapter, however the majority of previous reports of DMA-containing copolymers used the unprotected monomer.[3] A small amount of chain coupling has been reported in copolymers using unprotected DMA, but in coatings applications a small amount of chain coupling often

does not significantly reduce the effectiveness of the copolymer.[6] Furthermore, the use of unprotected DMA confers a significant time-saving advantage over the use of protected monomers and provides a simple method to avoid the ring-opening of epoxide rings in the GMA during deprotection of ADMA.

In this section of work, the primary aim was to synthesise co- and terpolymers suitable for coatings tests. As such, regular sampling to enable a full assessment of the compositional drift in the DMA-containing copolymers described herein was not carried out. The copolymer composition and residual monomer composition was compared with similar reactions containing ADMA.

2.4.7.1 Investigation of compositional drift during the synthesis of copolymers containing DMA

Several copolymers were synthesised, consisting of DMA with i) MMA, ii) HEMA and iii) PEGMEM to enhance the range of copolymers available for testing as surface coatings and to compare with similar ADMA-containing copolymers. A summary of the molar feed ratios, solvents and associated data for DMA containing copolymers is given in Table 2.5. A HEMA homopolymer (FR-H) was also synthesised for comparison with the copolymers.

Table 2.5. Polymerisation conditions and results for statistical copolymers containing DMA (except FR-H) prepared by free radical polymerisation in 1,4-dioxane or DMF at 70 °C.

Polymer	t / h	Comp	RM[a]	ρ / %	M_n / g mol^{-1}	Đ
FR-MD-90/10-(DIOX)	20	92/8	78/22	91	1100[b]	1.78
FR-H	21	-	-	94	17250	2.67
FR-HD-90/10-(DMF)	21	92/8	45/55	95	13650	3.18
FR-HD-80/20-(DMF)	21	84/16	24/76	93	10000	4.43
FR-HD-70/30-(DMF)	21	75/25	34/66	84	3050	14.27
FR-HD-61/39-(DMF)	21	71/29	16/84	81	3500	11.84
FR-HD-50/50-(DMF)	21	59/41	5/95	83	17750	3.33
FR-PD-71/29-(DMF)	22	74/26	34/66	80	9700	5.35

a) Residual monomer composition. b) M_n calculated using conventional calibration (PS standards).

A copolymer comprising MMA and DMA was synthesised in 1,4-dioxane (FR-MD-90/10-(DIOX)). After 20 h reaction time, the M_n was surprisingly low. No SEC light scattering signal could be obtained, but a value for M_n of 1100 g mol^{-1} was obtained using conventional calibration (PS standards) – a point which will be discussed below. Monomer conversion was 91%, confirming that the polymerisation could reach high

conversion with low mole fractions of unprotected DMA. In comparison to the previously discussed ADMA-containing analogue, FR-MD-90/10-(DIOX) reached a very similar overall monomer conversion (FR-MA-90/10 = 93%, 24 h). This suggested that, in contrast to DMA homopolymerisation, the rate of DMA copolymerisation with methacrylates at low DMA mole fractions was not strongly affected by the unprotected catechol monomer; scavenging of initiator radicals was not significant. At the time of the final sample, the residual monomer for FR-MD-90/10-(DIOX) comprised 22 mol% DMA compared to 33 mol% ADMA for FR-MA-90/10, suggesting compositional drift occurred in both reactions. Additionally, the composition of FR-MD-90/10-(DIOX), calculated according to Equation 2.3, was 92/8 (MMA/DMA mol%); the same average composition as FR-MA-90/10. This suggests that replacing ADMA with DMA has little effect on the overall copolymer composition. A reaction in which regular sampling was carried out would be required to reveal the extent of the compositional drift. The synthesis of FR-MD-90/10-(DIOX) yielded a white solid product which slowly turned brown on exposure to air, probably due to slow oxidation of the catechol side chains.

The very low molecular weight of FR-MD-90/10-(DIOX), evidenced by SEC (Figure 2.21B), was somewhat surprising given the high conversion. Poly(MMA-co-DMA) synthesised using FR polymerisation has been reported several times in the literature, using DMF or toluene as a solvent.[10, 46, 71, 72] Low M_n was consistently reported (<10000 g mol^{-1}). In one case, polymerisation of MMA and DMA in toluene with a monomer to initiator molar ratio of 66:1 yielded a copolymer with an M_n of 1200 g mol^{-1}.[71] The authors claim this molecular weight is “as expected from the high initiator concentration”, but provide no additional explanation. No other authors attempted to explain the low M_n. In a similar report in which copolymers of DMA and MEA were synthesised, Kamperman *et al.* observed a trend of decreasing M_n with increasing DMA mole fraction.[6] They speculated that the reduction in molecular mass was due to an increased rate of termination from reactions between the catechol side chains and propagating radicals.

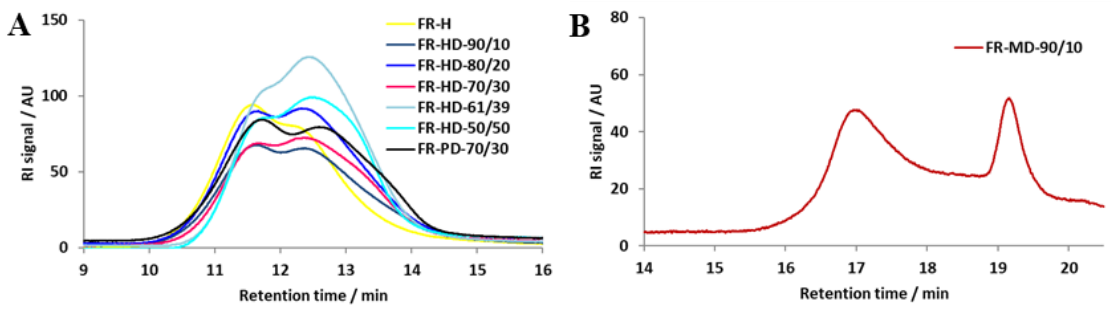

Figure 2.21. SEC RI chromatograms. A) HEMA/DMA and PEGMEM/DMA copolymers, DMF eluent. B) MMA/DMA copolymer, THF eluent.

In the work described in this chapter, comparison of FR-MD-90/10-(DIOX) with the copolymers of MMA and ADMA (Table 2.3) showed M_n was lower by a factor of at least 10 in the former, suggesting the unprotected catechol affected the M_n. A possible explanation for the low M_n, despite the high conversion, could be *via* chain transfer to the catechol monomer, although there is currently not enough evidence to confirm this hypothesis. A chain transfer mechanism for catechol-containing monomers has been previously proposed, owing to the high reactivity of the radical species.[38]

A series of HEMA/DMA copolymers were synthesised using mole fractions of DMA from 10 mol% to 50 mol% (see Table 2.5). The purpose was to determine the effect of increasing DMA composition in the monomer feed on the copolymer composition and monomer conversion and take forward selected copolymers for testing as functional adhesive coatings. Each of the reactions were terminated after 21 h. A copolymer was also synthesised using PEGMEM (macromonomer M_n = 500 g mol^{-1}) with DMA in DMF (FR-PD-71/29-(DMF)).

Two examples of poly(HEMA-co-DMA) synthesised by FR polymerisation have been previously reported in the literature. In the first example, a DMA mole fraction of 17% was used and the reaction was carried out at 70 °C in DMF.[73] The [mon]:[AIBN] molar ratio was 66:1. The resulting copolymer had surprisingly low molecular weight of only 2800 g mol^{-1} after reaction overnight, but a relatively high yield (62%). No dispersity was reported. Again, the low M_n could be indicative of chain transfer to the catechol monomer, coupled with a high concentration of radicals from the relatively low ratio of initiator to monomer. In the second example, poly(HEMA-co-DMA) was synthesised using a mole fraction of 15% DMA. The resulting copolymer had a reported M_n of 29500 g mol^{-1} in an 84% yield after reaction for 16 h at 60 °C in DMF.[47] The [mon]:[AIBN] molar ratio was 100 : 1. The increased M_n compared to the first example is due to the lower radical

concentration arising from reduced temperature and higher monomer to initiator molar ratio. This is plausible as the decomposition rate of AIBN is reduced by an order of magnitude per ~20 °C reduction in temperature,[74] therefore the 10 °C reduction in this case is significant.

The M_n for the HEMA/DMA copolymers and the PEGMEM/DMA copolymer produced in this study ranged from 3050 – 17750 g mol^{-1}. Synthesis of the HEMA homopolymer (FR-H) as a control, yielded a homopolymer with M_n = 17250 g mol^{-1} and Đ = 2.67. For the HEMA/DMA copolymers, M_n generally decreased, and dispersity increased with increasing DMA mole fraction, whilst the M_w remained relatively constant between 40000 and 44000 g mol^{-1}. The obvious exception was FR-HD-50/50-(DMF), which had a high M_n, and was identified as a possible anomalous result. This could be due to experimental error, the cause of which is not clear. The dispersity trend indicated that the rate and mechanism of termination stayed relatively constant with the increasing DMA mole fraction, but a competing chain transfer mechanism emerged. This is evidenced by tailing to low molecular weight in the SEC chromatograms, generally with increasing mole fraction of DMA, which suggested the synthesis of low molecular weight chains (Figure 2.21A). This supports the chain transfer to catechol monomer mechanism suggested above, with branching also possible *via* a chain transfer to polymer mechanism.

The trend for chain branching to increase relative to the DMA comonomer mole fraction of DMA has been reported, and attributed to chain transfer *via* the catechol side chain.[5, 6, 72] Kamperman *et al.* measured the branching density in poly(MEA-co-DMA) and found that it increased according to the mole fraction of DMA from 0.12 for a copolymer with 5 mol% DMA to 0.31 for 25% DMA (*i.e.* ~1 branch per every 3 chains).[6] This was attributed to chain branching *via* radical reactions of the catechol side chains with other catechol groups (Scheme 2.1). Furthermore, the reported copolymerisation of styrene and 3-mercaptohexyl methacrylate (MHM), a monomer capable of chain transfer, indicated that increased mole fraction of MHM resulted in increased dispersity and reduced M_n due to the formation of hyperbranched polymers.[75]

The M_n of FR-HD-90/10-(DMF) was significantly higher than FR-MD-90/10-(DIOX), suggesting termination was decreased in the former. A similar observation was made by Rodrigues *et al*., who reported the M_n of poly(HEMA-co-DMA) was higher by a factor of ~4 compared to poly(ethyl methacrylate-co-DMA). The authors did not attempt to explain

the differences in M_n. It has been suggested that the interaction between catechols and propagating radicals is reduced in the presence of hydrogen bond donors such as methanol,[6] due to the stronger intermolecular interactions altering the mechanism of catechol hydroxyl proton abstraction by the radical species.[76] Furthermore, the lack of backbiting in the homopolymerisation of hydroxyethyl acrylate has been attributed to the stabilising effect of intermolecular H-bonding (although an increase in backbiting was observed upon introduction of DMF as a solvent).[77] Moreover, it has been shown that the introduction of a monomer with an H-bonding side chain could inhibit bimolecular termination and promote inter-chain coupling in the copolymerisation of dimethacrylate monomers.[78] Thus, it could be speculated that the reduction in termination could be due to intermolecular H-bonding between the catechol and the HEMA side chains, which may disrupt the ability of the catechol side chains to react with the propagating radical and promote chain transfer. Accordingly, we propose that the propagating radicals in MMA/DMA copolymer are strongly affected by chain transfer due to the lack of radical stabilisation *via* H-bonding or steric hindrance provided by the MMA side chains. Given the high relative molecular mass of the PEGMEM monomer compared to HEMA, the M_n of FR-PD-71/29-(DMF) was unexpectedly low, and the dispersity was very high. This indicated similar behaviour of the PEGMEM to HEMA side chains, which could be due to the ability of PEGMEM to accept H-bonds and reduced interaction between catechol and the propagating radical due to steric factors.

The overlaid SEC RI chromatograms revealed similar bimodal molecular weight distributions for the HEMA/DMA copolymers (Figure 2.21A). FR-PD-71/29-(DMF) and FR-H also had bimodal distributions – the latter indicating the effect in that case was not due to catechol. The termination mechanism of a growing polymer chain can lead to bimodal SEC distribution. In radical polymerisation the usual modes of termination are *via* disproportionation and combination. The identity of the monomer species often influences the termination mechanism. Methacrylate monomers often undergo termination predominantly *via* disproportionation as the propagating radical is less accessible compared to *e.g.* acrylates and styrene, which terminate primarily by combination.[79, 80] However, the bimodal peaks suggest that the polar, hydrophilic polymer species (HEMA, PEGMEM) have a significant proportion of termination by combination. The bimodal peaks in all of the chromatograms in Figure 2.21A suggests that despite the proposed variation in chain branching observed in the HEMA/DMA copolymers, termination

occurred with similar contributions from both combination and disproportionation regardless of the DMA mole fraction.

Factors impacting the ratio between combination and disproportionation in the radical polymerisation of methacrylates are currently poorly understood. Solvent viscosity has been shown to affect the ratio of combination to disproportionation, with more viscous solvents leading to a greater proportion of disproportionation due to slower diffusion of polymer chains.[81, 82] This could potentially explain the difference observed between the monomodal peaks observed for the MMA/ADMA(/GMA) copolymers synthesised in 1,4-dioxane (viscosity = 1.19 mPa s^{-1} at 298 K) compared to the bimodal peaks for the copolymers synthesised in DMF (viscosity = 0.92 mPa s^{-1} at 298 K), attributed to an increased proportion of termination by combination. The monomodal peak observed for FR-HGA-80/10/10-(DIOX) could also be due to the viscosity of the reaction solvent (Figure 2.21B). Alternatively, the intermolecular hydrogen bonding which may affect the chain transfer may also reduce termination by disproportionation, and lead to an increase in combination. However, this argument is contradicted by the monomodal peak for FR-HGA-80/10/10-(DIOX). It appears that there is insufficient data to make a confident assertion as to the cause of the bimodal SEC peaks, and further investigation is required.

In the work reported in this chapter, when the combined monomer conversion for each reaction was analysed by NMR, a general trend of decreasing monomer conversion with increasing mole fraction of DMA in the feed was observed e.g. FR-HD-90/10-(DMF) reached 95% conversion (very similar to FR-H), whereas FR-HD-61/39-(DMF) reached only 81% conversion. It would seem reasonable to assume that this was due to the slower rate of consumption of DMA relative to HEMA; the conversion of HEMA was >92% in all cases. Reaction FR-HD-50/50-(DMF) appeared to be an outlier as the conversion was slightly higher than FR-HD-61/39-(DMF). After 22 h, the overall monomer conversion was 80%, very similar to the equivalent copolymerisation with HEMA and DMA (FR-HD-70/30-(DMF), $\rho = 84\%$, $t = 21$ h). The final copolymer composition of FR-PD-71/29-(DMF) was 76/24 (mol% PEGMEM/DMA). When compared to FR-HD-70/30-(DMF), the copolymer composition was virtually identical (76/24), indicating the incorporation of DMA was very similar in copolymerisation of HEMA and PEGMEM.

It is clear that compositional drift occurs, as each copolymer contained a smaller mol% of DMA than in the initial monomer feed (Table 2.5). The ratio of DMA mol% in monomer feed to DMA mol% in copolymer of 0.75 – 0.81 in all cases indicating a similar degree of compositional drift in each case. Furthermore, the residual monomer detected in the final sample of each reaction contained a greater proportion of DMA than the feed – strongly indicating the preferential incorporation of HEMA.

2.4.7.2 Investigation of compositional drift during the synthesis of terpolymers containing DMA, GMA and a third monomer

In section 2.4.5.2, the synthesis of several terpolymers consisting of ADMA, GMA and a further methacrylate monomer was discussed. Deprotection of ADMA without causing ring-opening of GMA was problematic. The copolymerisation of HEMA with DMA (section 2.4.7.1) yielded hydrophilic copolymers which did not require deprotection. Unprotected DMA was therefore used in the synthesis of terpolymers with GMA and a further methacrylate monomer (MMA or HEMA). The reaction conditions and terpolymer properties are summarised in Table 2.6.

Table 2.6. Polymerisation conditions and results for statistical terpolymers containing DMA and GMA prepared by free radical polymerisation in 1,4-dioxane or DMF at 70 °C.

Terpolymer	t / h	Comp.	RM[a]	ρ / %	M_n / g mol^{-1}	Đ
FR-MGD-75/12/13-(DIOX)	20	76/12/12	66/12/22	89	8250[b]	2.65
FR-HGD-78/11/11-(DIOX)	21	78/11/10	65/6/29	94	39100	16.65
FR-HGD-80/10/10-(DMF)	15	83/12/6	71/7/22	75	43400	3.23
FR-HGD-58/9/33-(DMF)	21	73/12/15	45/6/49	50	110650	3.48

a) Residual monomer composition. b) M_n calculated using conventional calibration (PS standard).

A terpolymer was synthesised comprising MMA, GMA and DMA in 1,4-dioxane at 70 °C (FR-MGD-75/12/13-(DIOX)). NMR analysis of the resulting terpolymer indicated that combined monomer conversion was 89% after 20 h; very similar to the analogous reaction using ADMA (FR-MGA-77/12/11, 84% after 21 h). The final composition of FR-MGD-75/12/13-(DIOX) was 12 mol% DMA, which represented a marginally higher catechol monomer composition with respect to FR-MGA-77/12/11 (9 mol% ADMA). For FR-MGD-75/12/13-(DIOX), a residual feed composition of 22 mol% DMA indicated compositional drift still occurred and the overall rate of (A)DMA incorporation is very similar for both terpolymers. The M_n of FR-MGD-75/12/13-(DIOX) was low

(8250 g mol^{-1}), similar to FR-MD-90/10-(DIOX). This supported the suggestion that the rate of chain transfer is increased by the presence of unprotected DMA in MMA-containing copolymers. Surprisingly, the SEC RI chromatogram showed a bimodal distribution, indicating combination was a significant mode of termination (Figure 2.22B). This was not the case in other copolymers containing MMA in this work, and the reason for this is not clear, as discussed above.

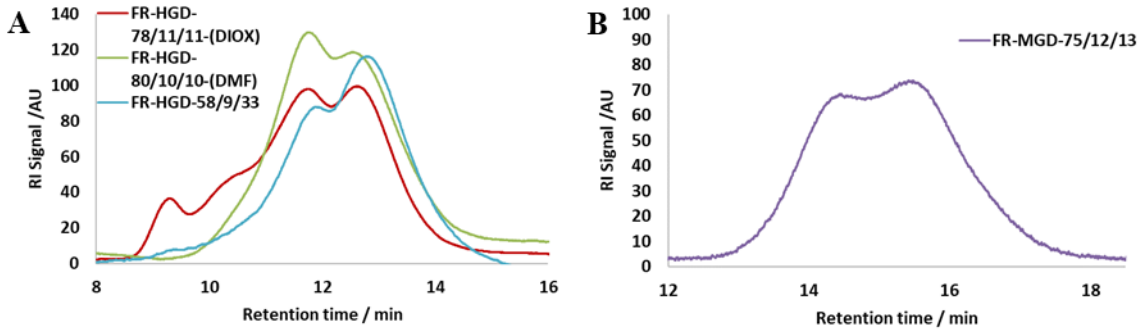

Figure 2.22. SEC RI chromatograms. A) HEMA/GMA/DMA terpolymers, DMF eluent. B) MMA/GMA/DMA terpolymer, THF eluent.

A terpolymer comprising HEMA, GMA and DMA was synthesised in 1,4-dioxane at 70 °C (FR-HGD-78/11/11-(DIOX)). The combined monomer conversion was 94% after 21 h; slightly higher than FR-MGD-75/12/13-(DIOX), indicating fast consumption of HEMA. The polymerisation mixture turned cloudy towards the end of the reaction and upon cooling the terpolymer precipitated due to poor solubility in the reaction solvent. The final terpolymer composition was 78/11/10 (M/G/D), showing the monomers had all been incorporated into the terpolymer. Compositional drift is likely to have occurred, evidenced by the 29% DMA in the residual monomer feed. The M_n was relatively high and dispersity very high (M_n = 39100 g mol^{-1}, Đ = 16.65) compared to the HEMA/DMA copolymers. The SEC chromatogram of FR-HGD-78/11/11-(DIOX) was multimodal (Figure 2.22A). The high dispersity could indicate significant chain branching, as suggested previously. The two lower molecular weight peaks were similar to those observed for the HEMA/DMA copolymers, indicating significant termination *via* combination in both cases; however, two higher molecular weight shoulders were also observed. This could indicate coupling *via* the DMA side chains could have occurred. It could be speculated that this effect occurred towards the end of the polymerisation when polymer solubility became poor and polymer chains were in close proximity.

Two subsequent terpolymers (FR-HGD-80/10/10-(DMF) and FR-HGD-58/9/33-(DMF)) were synthesised in DMF at 70 °C to avoid precipitation, The monomer conversion of FR-HGD-58/9/33-(DMF) was low (50% after 21 h). This was surprising, as larger mole fractions of DMA did not appear to inhibit polymerisation in the HEMA/DMA copolymers and could therefore be an anomalous result. The final composition of FR-HGD-80/10/10-(DMF) and FR-HGD-58/9/33-(DMF) indicated in each case the expected preferential incorporation of methacrylate monomers, with final DMA content of 6% and 15% respectively. The low incorporation of DMA in FR-HGD-58/9/33-(DMF) is due to the low combined monomer conversion – reflecting the compositional drift in the polymerisations. The SEC RI chromatograms were bimodal, similar to the observation for the HEMA/DMA copolymers. The dispersity of 3.48 for FR-HGD-58/9/33-(DMF) indicated a similar amount of chain transfer to FR-HD-90/10, however the M_n was significantly higher. The reason for this was unclear, although a hint of a high molecular weight peak for FR-HGD-58/9/33-(DMF) indicated some chain coupling could have occurred.

2.4.8 Investigation of compositional drift during the synthesis of co/terpolymers containing no catechol-containing monomer

A key aim of the work discussed in this thesis was to synthesise a series of copolymers to allow correlation of the properties, including adhesion, of a variety of catechol containing copolymers with copolymer composition. As such, it was necessary to synthesise copolymers without catechol side chains as controls. Two copolymers were synthesised, and the polymerisation conditions and copolymer properties are summarised in Table 2.7.

Table 2.7. Conditions for copolymers synthesised by free radical polymerisation using no catechol monomer.

Copolymer	Time / h	Composition	RM[a]	ρ / %	M_n / g mol^{-1}	Đ
FR-MG-50/50	24	45/55	46/54	95	35500	2.22
FR-HG-89/11	18.5	78/22	89/11	83	133500	4.26

a) Residual monomer composition.

A copolymer comprising MMA and GMA was synthesised (FR-MG-50/50). The reaction was carried out in 1,4-dioxane. Samples were collected at regular intervals for NMR analysis of monomer conversion. The reaction reached a combined monomer conversion of 95% after 24 hours. This indicated a faster reaction than analogous reactions involving the catechol-containing methacrylamides (*e.g.* FR-MA-49/51, 81% after 22.5 h). The

molecular weight of the copolymer was 35500 g mol^{-1}, similar to that of the MMA/ADMA copolymers, but greater than the MMA/DMA equivalent. The SEC chromatogram was broad and monomodal, with a hint of a low molecular weight shoulder (Figure 2.23). No evidence of significant chain coupling was observed.

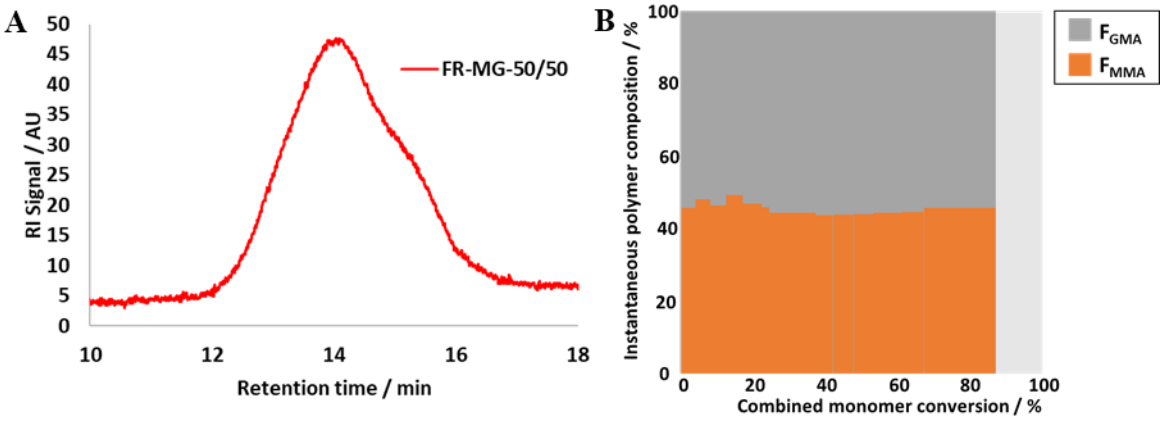

Figure 2.23. A) SEC RI chromatogram of FR-MG-50/50, eluent THF B) Evolution of copolymer composition for FR-MG-50/50.

The final composition of FR-MG-50/50 was 46/54 (mol% MMA/GMA). Samples collected throughout the reaction indicated that the copolymer composition remained consistently close to 50 % MMA at the start of the reaction, but the GMA content of the average copolymer chain increased as the reaction progressed (Figure 2.23B). This indicated the monomers were consumed at very similar rates, with a slight preference towards incorporation of GMA. This compositional drift was not as pronounced as seen in the reactions involving the methacrylamide monomers ADMA and DMA, which is expected as, generally, non H-bonding methacrylates in FR polymerisations polymerise at similar rates.[61] The slight preference for GMA incorporation over MMA has been previously reported. Reported reactivity ratios for FR polymerisation of these monomers in bulk were $r_{MMA} = 0.80$, $r_{GMA} = 1.05$, which suggest that the polymerisation is expected to be nearly random, but some compositional drift may be expected.[66] The results also agree with the reactivity ratios calculated when the same monomers were polymerised using ATRP in anisole ($r_{MMA} = 0.85$, $r_{GMA} = 1.24$).[67] Moreover, it has been reported that methacrylic monomers with cyclic pendant groups (such as GMA) have a higher rate of propagation (k_p) than MMA.[83]

The second copolymer, FR-HG-89/11, was synthesised in DMF. The low GMA mole fraction was chosen to allow direct comparison in subsequent copolymer testing with the most commonly used molar ratios of GMA in the DMA containing terpolymers (*e.g.*

FR-HGD-80/10/10-(DMF)). FR-HG-89/11 reached 83% conversion after 18.5 h, which indicates a similar rate of reaction compared to FR-HGA-80/10/10-(DIOX) (86% conversion after 24 h) and FR-HGD-80/10/10-(DMF) (75% conversion after 15 h). The SEC trace illustrates a multimodal distribution with a molecular weight and dispersity which were very high, particularly in comparison with the HEMA homopolymer, FR-H. Two lower molecular weight peaks were observed, similar to the HEMA/DMA copolymers, which were assigned to significant termination by combination, as discussed previously. However, a high molecular weight peak was observed in the SEC RI chromatogram (Figure 2.23), similar to that observed for FR-HGD-80/10/10-(DIOX). This suggests some chain coupling occurred in the copolymer, which is likely to be caused by GMA. However, this was not observed for other copolymers containing GMA, and thus could have occurred after the polymerisation – suggesting potential reactivity of the copolymer upon storage. Changes in solubility of polymers containing GMA are discussed further in Chapter 5.

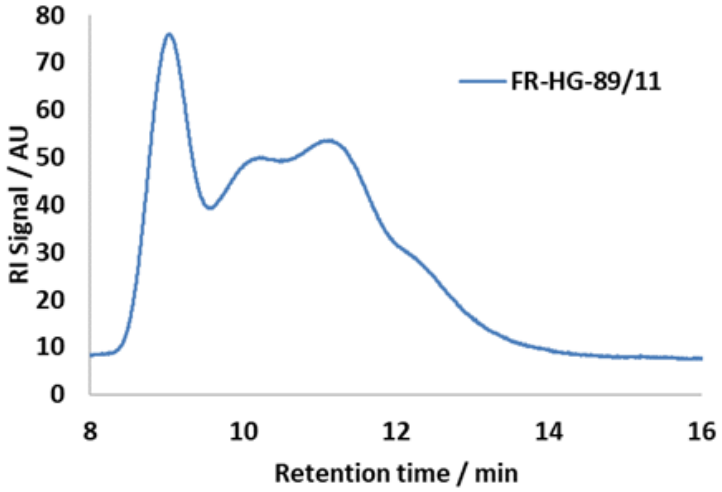

Figure 2.24. SEC RI chromatogram of FR-HG-89/11, eluent DMF.

The final composition of FR-HG-89/11 was 78/22, indicating GMA was preferentially incorporated into the copolymer. A previous report indicated the reactivity ratios of HEMA and GMA at 60 °C in DMF were $r_{HEMA} = 0.74$, $r_{GMA} = 1.00$, using a benzoyl peroxide initiator.[84] This implies the composition of FR-HG-89/11 is unsurprising as some degree of compositional drift favouring the incorporation of GMA would be expected.

2.5 Conclusion

In the preceding chapter the synthesis of DMA and ADMA and the copolymerisation of both DMA and ADMA with methacrylate comonomers has been investigated.

The synthesis of DMA was optimised, giving a maximum yield of 67%. A fast workup method using precipitation and crystallisation was compared to column chromatography and column chromatography was determined to be the only workup which provided sufficiently pure DMA monomer. Subsequent protection of DMA as an acetonide gave a maximum yield of 81%. The monomers were subsequently used in FR (co)polymerisations to generate a library of catechol-containing functional copolymers.

The polymerisation of DMA yielded homopolymers which quickly turned brown and became insoluble on exposure to air, almost certainly due to oxidation of the catechol side chains and subsequent crosslinking. DMF proved to be a more appropriate polymerisation solvent than 1,4-dioxane, due to improved solubility of DMA, and allowed a DMA homopolymer of relatively high M_n (59800 g mol^{-1}) to be synthesised. Free-radical homopolymerisation of ADMA was carried out but was extremely sensitive to impurities and monomer conversion was slow, reaching only 20% after 24 hours. The retarded homopolymerisation rate was probably due to impurities in the ADMA produced as by-products of the DMA synthesis. The extremely low M_n indicated the formation of mostly very short oligomeric chains, although limited evidence for the production of a small fraction of longer homopolymer chains was visible in the SEC chromatogram.

For the first time, to the best of our knowledge, reactivity ratios were estimated for the copolymerisation of ADMA with i) MMA and ii) GMA. The values obtained by the NLLS method for the MMA/ADMA reaction were $r_{MMA} = 2.21 \pm 0.26$ and $r_{ADMA} = 0.17 \pm 0.03$, and for the GMA/ADMA copolymerisation $r_{GMA} = 1.96 \pm 0.49$ and $r_{ADMA} = 0.18 \pm 0.08$. The reactivity ratios demonstrated that in both cases the methacrylate monomer is preferentially incorporated at all monomer feed ratios. This is in large part due to the inherent lower reactivity of methacrylamides when polymerised with methacrylates, but possibly enhanced due to relatively poor solvation of ADMA in 1,4-dioxane. The reactivity ratios also indicated that under the conditions used, there was very little difference between the reactivity of the two methacrylate monomers.

A library of co- and terpolymers containing ADMA and a small family of methacrylate comonomers was successfully synthesised, introducing a variety of functional groups. As expected, given the reactivity ratios, significant compositional drift was observed during polymerisation, with the methacrylate monomer being consumed in preference but ADMA incorporated increasingly throughout the reaction. In several reactions, NMR analysis of

samples collected early in the polymerisations indicated a surprisingly high fraction of ADMA, which suggested significant experimental error in the composition measurements at the early stages of reaction.

Deprotection of ADMA and ADMA-containing copolymers was successful using TFA in chloroform. Copolymers of ADMA with MMA and the less-polar SMA were both deprotected successfully, evidenced by ^{1}H NMR spectroscopy. However, it was not possible to remove the protecting groups from a copolymer containing GMA, without the formation of a gel. This was attributed to chain coupling due to the ring opening of the epoxide functional groups resulting in probable crosslinking.

Co- and terpolymers containing DMA were also synthesised. The compositional drift appeared to be very similar to that observed for analogous copolymers comprising ADMA. Bimodal SEC RI chromatograms were observed for copolymers of DMA with HEMA and PEGMEM, but also a HEMA homopolymer. The higher molecular weight peak was attributed to chain termination *via* chain combination; however, a firm cause was not established for this result. For HEMA/DMA copolymers, a trend for reduction in M_n with increasing DMA mole fraction was observed, suggesting that significant chain transfer occurred from the propagating radical to the catechol monomer. Similarly high dispersities with low molecular weights were observed for terpolymers comprising HEMA, DMA and GMA. A copolymer of MMA and DMA and terpolymer of MMA, DMA and GMA had very low molecular weight, which was attributed to significant chain transfer occurring due to reaction of the catechol in DMA side chains with the propagating radical. This was attributed to due to a lack of monomer stabilisation from H-bonding or steric hindrance.

Finally, two methacrylate copolymers, FR-MG-50/50 and FR-HG-89/11 were synthesised for use as control copolymers for coatings testing (described in Chapters 4 and 5). As expected, little compositional drift was observed for either polymerisation. A high molecular weight peak was observed for FR-HG-89/11, suggesting chain coupling may have occurred due to the epoxide group in GMA side chains.

2.6 References

1. M. S. Kharasch, F. Kawahara and W. Nudenberg, *J. Org. Chem.*, 1954, **19**, 1977-1990.
2. J. S. Wright, E. R. Johnson and G. A. DiLabio, *J. Am. Chem. Soc.*, 2001, **123**, 1173-1183.
3. N. Patil, C. Jérôme and C. Detrembleur, *Prog. Polym. Sci.*, 2018, **82**, 34-91.
4. E. Faure, C. Falentin-Daudré, C. Jérôme, J. Lyskawa, D. Fournier, P. Woisel and C. Detrembleur, *Prog. Polym. Sci.*, 2013, **38**, 236-270.
5. *WO Pat.*, WO2009147007-A2, 2009.
6. J. Yang, J. Keijsers, M. van Heek, A. Stuiver, M. A. Cohen Stuart and M. Kamperman, *Polym. Chem.*, 2015, **6**, 3121-3130.
7. J. Yang, M. A. Cohen Stuart and M. Kamperman, *Chem. Soc. Rev.*, 2014, **43**, 8271-8298.
8. A. A. A. Smith, A. Hall, V. Wu and T. Xu, *Acs Macro Letters*, 2019, **8**, 36-40.
9. J. J. Benkoski, G. H. Fredrickson and E. J. Kramer, *J. Polym. Sci., Part B: Polym. Phys.*, 2001, **39**, 2363-2377.
10. D. Payra, Y. Fujii, S. Das, J. Takaishi and M. Naito, *Polym. Chem.*, 2017, **8**, 1654-1663.
11. S.-W. Kuo, H.-C. Kao and F.-C. Chang, *Polymer*, 2003, **44**, 6873-6882.
12. G. Jayashima Reddy, S. Venkata Naidu and A. V. Rami Reddy, *J. Appl. Polym. Sci.*, 2003, **90**, 2179-2186.
13. J. Brandrup and E. H. Immergut, *Polymer Handbook*, Wiley Interscience, 3rd edn., 1989.
14. M. Kucharski and R. Lubczak *J. Appl. Polym. Sci.*, 1997, **64**, 1259-1265.
15. G. Saini, A. Leoni and S. Franco, *Die Makromolekulare Chemie*, 1971, **147**, 213-218.
16. T. R. Rooney and R. A. Hutchinson, *Ind. Eng. Chem. Res.*, 2018, **57**, 5215-5227.
17. S. Beuermann, *Macromol. Rapid Commun.*, 2009, **30**, 1066-1088.
18. J. Yang, I. Bos, W. Pranger, A. Stuiver, A. H. Velders, M. A. Cohen Stuart and M. Kamperman, *J. Mater. Chem. A*, 2016, **4**, 6868-6877.
19. K. Nagai, *Appl. Catal., A*, 2001, **221**, 367-377.
20. J. Feng, O. O. Oyeneye, W. Z. Xu and P. A. Charpentier, *Ind. Eng. Chem. Res.*, 2018, **57**, 15654-15662.
21. P. F. Holmes, M. Bohrer and J. Kohn, *Prog. Polym. Sci.*, 2008, **33**, 787-796.
22. D. Debnath, J. A. Baughman, S. Datta, R. A. Weiss and C. Pugh, *Macromolecules*, 2018, **51**, 7951-7963.
23. H. Shinoda, P. J. Miller and K. Matyjaszewski, *Macromolecules*, 2001, **34**, 3186-3194.
24. J. P. Montheard, M. Chatzopoulos and D. Chappard, *J. Macromol. Sci. Rev. Macromol. Chem. Phys.*, 1992, **C32**, 1-34.
25. J. V. M. Weaver, I. Bannister, K. L. Robinson, X. Bories-Azeau, S. P. Armes, M. Smallridge and P. McKenna, *Macromolecules*, 2004, **37**, 2395-2403.
26. H. Mori, O. Wakisaka, A. Hirao and S. Nakahama, *Macromol. Chem. Phys.*, 1994, **195**, 3213-3224.
27. C. Pietsch, M. W. M. Fijten, H. M. L. Lambermont-Thijs, R. Hoogenboom and U. S. Schubert, *J. Polym. Sci., Part A: Polym. Chem.*, 2009, **47**, 2811-2820.
28. N. Patil, C. Falentin-Daudré, C. Jérôme and C. Detrembleur, *Polym. Chem.*, 2015, **6**, 2919-2933.

29. E. M. Muzammil, A. Khan and M. C. Stuparu, *RSC Advances*, 2017, **7**, 55874-55884.
30. J. Kalal, F. Svec and V. Marousek, *J. Polym. Sci., Part C: Polym. Symp.*, 1974, 155-166.
31. E. R. Kenawy, F. I. Abdel-Hay, A. El-Shanshoury and M. H. El-Newehy, *J. Polym. Sci., Part A: Polym. Chem.*, 2002, **40**, 2384-2393.
32. Y. Iwakura, T. Kurosaki, N. Ariga and T. Ito, *Die Makromolekulare Chemie*, 1966, **97**, 128-138.
33. S. Akgöl, G. Bayramoğlu, Y. Kacar, A. Denizli and M. Y. Arıca, *Polym. Int.*, 2002, **51**, 1316-1322.
34. G. Bayramoglu, A. U. Senel and M. Y. Arica, *J. Appl. Polym. Sci.*, 2007, **104**, 672-679.
35. Z. Lei, J. Gao, X. Liu, D. Liu and Z. Wang, *ACS Appl. Mater. Interfaces*, 2016, **8**, 10174-10182.
36. X. W. Fan, L. J. Lin, J. L. Dalsin and P. B. Messersmith, *J. Am. Chem. Soc.*, 2005, **127**, 15843-15847.
37. H. Lee, B. P. Lee and P. B. Messersmith, *Nature*, 2007, **448**, 338-341.
38. Y. S. Choi, H. Kang, D. G. Kim, S. H. Cha and J. C. Lee, *ACS Appl. Mater. Interfaces*, 2014, **6**, 21297-21307.
39. K. Niederer, C. Schüll, D. Leibig, T. Johann and H. Frey, *Macromolecules*, 2016, **49**, 1655-1665.
40. G. V. Dizon, Y. N. Chou, L. C. Yeh, A. Venault, J. Huang and Y. Chang, *J. Colloid Interface Sci.*, 2018, **529**, 77-89.
41. M. Liu, G. Zeng, K. Wang, Q. Wan, L. Tao, X. Zhang and Y. Wei, *Nanoscale*, 2016, **8**, 16819-16840.
42. T. W. Greene and P. G. M. Wuts, *Protective Groups in Organic Chemistry*, Wiley, 2nd edn., 1991.
43. V. Soloshonok and H. Ueki, *Synthesis*, 2008, **5**, 693-695.
44. S. Hong, Y. S. Na, S. Choi, I. T. Song, W. Y. Kim and H. Lee, *Adv. Funct. Mater.*, 2012, **22**, 4711-4717.
45. J. Wang, M. N. Tahir, M. Kappl, W. Tremel, N. Metz, M. Barz, P. Theato and H.-J. Butt, *Adv. Mater.*, 2008, **20**, 3872-3876.
46. H. J. Meredith and J. J. Wilker, *Adv. Funct. Mater.*, 2015, **25**, 5057-5065.
47. H. N. Nguyen, E. T. Nadres, B. G. Alamani and D. F. Rodrigues, *J. Mater. Chem. B*, 2017, **5**, 6616-6628.
48. D. E. Clark, *Chemical Health and Safety*, 2001, **8**, 12-22.
49. N. A. Boulding, J. M. Millican and L. R. Hutchings, *Polymer Chemistry*, 2019, **10**, 5665-5675.
50. F. R. Mayo and F. M. Lewis, *J. Am. Chem. Soc.*, 1944, **66**, 1594-1601.
51. T. Kelen, F. Tudos and B. Turcsanyi, *Polym. Bull. (Berlin)*, 1980, **2**, 71-76.
52. K. F. Odriscoll and P. M. Reilly, *Makromol. Chem.*, 1987, **10**, 355-374.
53. A. L. Polic, T. A. Duever and A. Penlidis, *J. Polym. Sci., Part A: Polym. Chem.*, 1998, **36**, 813-822.
54. D. W. Behnken, *J. Polym. Sci., Part A: Gen. Pap.*, 1964, **2**, 645-648.
55. G. Odian, *Principles of Polymerization*, Wiley, 4th edn., 2004.
56. Y. Tsukahara, N. Hayashi, X. L. Jiang and Y. Yamashita, *Polym. J. (Tokyo, Jpn.)*, 1989, **21**, 377-391.
57. J. Schrooten, I. Lacik, M. Stach, P. Hesse and M. Buback, *Macromol. Chem. Phys.*, 2013, **214**, 2283-2294.
58. E. Koyama, F. Sanda and T. Endo, *Macromol. Chem. Phys.*, 1997, **198**, 3699-3707.

59. M. A. Hegazy, S. H. El-Hamouly, M. M. Azab, S. I. Beshir and M. A. Zayed, *Polymer Science Series B*, 2014, **56**, 182-190.
60. A. Scott and A. Penlidis, *Processes*, 2018, **6**.
61. R. Ferrari, T. R. Rooney, M. Lupi, P. Ubezio, R. A. Hutchinson and D. Moscatelli, *Macromol. Biosci.*, 2013, **13**, 1347-1357.
62. G. J. Reddy, M. M. Reddy, G. R. Reddy, S. V. Naidu and A. V. R. Reddy, *Des. Monomers Polym.*, 2008, **11**, 581-591.
63. K. Demirelli, E. Kaya and M. C. Coskun, *J. Appl. Polym. Sci.*, 2006, **99**, 3344-3354.
64. A. Natalello, J. N. Hall, E. A. Eccles, S. M. Kimani and L. R. Hutchings, *Macromol. Rapid Commun.*, 2011, **32**, 233-237.
65. L. R. Hutchings, P. P. Brooks, D. Parker, J. A. Mosely and S. Sevinc, *Macromolecules*, 2015, **48**, 610-628.
66. M. S. Gluckman, M. J. Kampf, J. L. Obrien, T. G. Fox and R. K. Graham, *J. Polym. Sci.*, 1959, **37**, 411-423.
67. D. Neugebauer, K. Bury and M. Wlazło, *J. Appl. Polym. Sci.*, 2012, **124**, 2209-2215.
68. A. J. Scott and A. Penlidis, *Eur. Polym. J.*, 2018, **105**, 442-450.
69. M. A. Dube and A. Penlidis, *Polymer*, 1995, **36**, 587-598.
70. R. E. Parker and N. S. Isaacs, *Chem. Rev. (Washington, DC, U. S.)*, 1959, **59**, 737-799.
71. A. Stepuk, J. G. Halter, A. Schaetz, R. N. Grass and W. J. Stark, *Chem. Commun. (Cambridge, U. K.)*, 2012, **48**, 6238-6240.
72. D. Payra, M. Naito, Y. Fujii, N. L. Yamada, S. Hiromoto and A. Singh, *RSC Adv.*, 2015, **5**, 15977-15984.
73. A. R. Sasikala, A. GhavamiNejad, A. R. Unnithan, R. G. Thomas, M. Moon, Y. Y. Jeong, C. H. Park and C. S. Kim, *Nanoscale*, 2015, **7**, 18119-18128.
74. A. D. Smith, E. Lester, K. J. Thurecht, J. El Harfi, G. Dimitrakis, S. W. Kingman, J. P. Robinson and D. J. Irvine, *Ind. Eng. Chem. Res.*, 2010, **49**, 1703-1710.
75. L. Jiang, W. Y. Huang, X. Q. Xue, H. J. Yang, B. B. Jiang, D. L. Zhang, J. B. Fang, J. H. Chen, Y. Yang, G. Q. Zhai, L. Z. Kong and S. F. Wang, *Macromolecules*, 2012, **45**, 4092-4100.
76. L. R. C. Barclay, C. E. Edwards and M. R. Vinqvist, *J. Am. Chem. Soc.*, 1999, **121**, 6226-6231.
77. K. Liang and R. A. Hutchinson, *Macromol. Rapid Commun.*, 2011, **32**, 1090-1095.
78. A. Matsumoto, A. Ueda, H. Aota and J. Ikeda, *Eur. Polym. J.*, 2002, **38**, 1777-1782.
79. K. Matyjaszewski and T. P. Davis, *Handbook of Radical Polymerization*, John Wiley & Sons, 2003.
80. Y. Nakamura and S. Yamago, *Macromolecules*, 2015, **48**, 6450-6456.
81. Y. Nakamura, T. Ogihara, S. Hatano, M. Abe and S. Yamago, *Chem.--Eur. J.*, 2017, **23**, 1299-1305.
82. J. B. L. de Kock, A. M. Van Herk and A. L. German, *J. Macromol. Sci., Polym. Rev.*, 2001, **C41**, 199-252.
83. S. Beuermann, M. Buback, T. P. Davis, N. Garcia, R. G. Gilbert, R. A. Hutchinson, A. Kajiwara, M. Kamachi, I. Lacik and G. T. Russell, *Macromol. Chem. Phys.*, 2003, **204**, 1338-1350.
84. D. Mohan, G. Radhakrishnan, S. Rajadurai and K. T. Joseph, *J. Polym. Sci., Part C: Polym. Lett.*, 1990, **28**, 307-314.

Chapter 3 Synthesis of statistical and block copolymers containing catechol functional groups using RAFT copolymerisation

3.1 Introduction

3.1.1 General requirements for a successful RAFT polymerisation

Reversible addition-fragmentation chain transfer (RAFT) polymerisation is a useful approach for synthesis of (co)polymers with controlled molecular weight and dispersity. As RAFT polymerisation has become a more established technique over the two decades since its discovery, some general guidelines have been established which enable the set-up of a successful RAFT reaction. According to Perrier in his 2018 "user guide" review,[1] a successful RAFT polymerisation is defined by a "predictable molecular weight, low molar mass dispersity (*Đ*), high end-group fidelity, and capacity for continued chain growth." A short summary of the conditions required to achieve a polymerisation which adheres to the above definition follows:

1) Selection of appropriate R- and Z- groups in the RAFT agent (see species **1** in Figure 1.3, Chapter 1) is critical to maintaining control of dispersity and molecular weight by tuning the rate of fragmentation. Fast re-initiation by the R-group is critical to the effective set-up of the RAFT main equilibrium. The Z-group remains on the chain end of the majority of chains and controls the rate of fragmentation in the RAFT main equilibrium. The activity of the RAFT agent must be tuned to match that of the monomer. RAFT agent structure is discussed in more detail in Chapter 1.
2) A low radical concentration must be used with respect to chain transfer agent (CTA). This is because the proportion of dead chains (chains without a RAFT end group) can be predicted at the start of the reaction, depending only on the number of initiator-derived radicals.[1] To maintain an acceptable number fraction of living chains, RAFT agent to initiator molar ratios of >5:1 are usually used.[1, 2]
3) Chain propagation should proceed at an acceptable rate, as at long timescales the loss of polymer end group fidelity becomes an issue and termination becomes more likely.[3] This requires the selection of reaction conditions and a radical source such that the radical concentration is kept relatively low with respect to CTA concentration, but the rate of propagation is high.
4) The generation of radicals by the initiator should be rapid, as if significant numbers of radicals are generated by the initiator throughout the polymerisation, control

over dispersity and molecular weight will decrease. This is achieved by controlling the temperature or by use of a radical initiator with a high dissociation constant.

5) The RAFT agent must be stable to degradation under the selected reactions conditions. Although most RAFT agents are stable in a wide variety of solvents, some (*e.g.* dithiobenzoates) can undergo hydrolysis in water or strongly nucleophilic solvents.
6) A relatively wide range of molecular weights can be achieved under RAFT normal conditions (up to ~100000 g mol^{-1}), however targeting very high molecular weights increases the proportion of dead chains and thus reduces control. The targeted DP depends on the molar feed ratio of monomer to CTA ($[mon]_0$:$[CTA]_0$).

3.1.2 RAFT polymerisation of catechol-containing monomers

Dopamine methacrylamide (DMA) is a monomer used to introduce catechol side chains into copolymers; the free radical polymerisation of DMA is discussed in Chapter 2. It is widely accepted that catechols are radical scavengers, *e.g. tert*-butyl catechol is used as an inhibitor of radical polymerisation.[4, 5] It is therefore somewhat surprising that radical polymerisation is possible with unprotected catechol monomers. When using reversible-deactivation radical polymerisation (RDRP), the impact of radical scavenging is heightened due to the low radical concentrations employed. Polymerisation of unprotected DMA using RDRP has, however, been reported. Patil *et. al.* reported that in the majority of cases, the use of unprotected DMA in RAFT copolymerisation is limited to a monomer mole fraction of ~40 %.[6] Above this limit, control over dispersity and molecular weight diminishes and insoluble deposits form which are attributed to crosslinking due to reaction of the catechol group with the propagating radical.[7]

RAFT polymerisation has been used to synthesise copolymers of DMA with other methacrylamides[8-11] and methacrylates[12, 13] with reasonable control of dispersity. For example, a copolymer of MMA and DMA (20 mol% DMA) was synthesised using the RAFT agent 2-cyano-2-propyl benzodithioate (CPDB) in DMF (Đ = 1.20, M_w = 16000 g mol^{-1}).[13] The rate of reaction was fairly slow, with a 70% yield of recovered copolymer after 17 h, though a full kinetic study was not carried out. The resulting copolymer was used to bind to iron oxide nanoparticles with a borate-containing drug, taking advantage of the versatile reactivity of the catechol side chains.

In a further example, DMA was copolymerised with dimethylaminoethyl methacrylate (DMAEMA), using single electron transfer RAFT (SET-RAFT) polymerisation.[12]

Copolymers were synthesised with DMA monomer feed mole fractions of 17% and 29% and the reactions were quenched at <55% conversion, resulting in low incorporation of DMA (6.2% and 16.3% respectively) and reasonably low dispersities (1.28 and 1.36 respectively). The resulting copolymers were used to prepare porous membranes by self-assembly. It was also observed that homopolymerisation of DMA under these conditions proceeded to over 60% conversion but produced a homopolymer which was poorly soluble in DMF and THF, implying crosslinking had occurred during the polymerisation.

DMA was also copolymerised with N-[3-(dimethylamino)propyl] methacrylamide in DMF.[10] Very good control of dispersity was achieved using benzyl 2-hydroxyethyl carbonotrithioate as a RAFT agent (Đ = 1.05). The target molecular weight was not indicated by the authors, but calculation from the stated methods indicated good control of molecular weight - a measured M_w of 6633 g mol^{-1} against a theoretical mass of 7750 g mol^{-1}. In contrast to the copolymerisation of DMA with methacrylate monomers (see Chapter 2), DMA was incorporated in preference to N-[3-(dimethylamino)propyl] methacrylamide; in one iteration a 20% DMA mole fraction in the feed led to a mole fraction of 29% DMA in the resulting copolymer. This highlights the importance of the polymerisable group on comonomer reactivity, as discussed in Chapter 2.

RAFT polymerisation has also been used to synthesise copolymers using monomers bearing protected catechol side chains.[6] The synthesis of an ADMA homopolymer was reported by Detrembleur *et al.* in step one of the synthesis of a poly(ADMA-*block*-PEGMEM) diblock copolymer in DMF.[14] They conducted a study into the homopolymerisation kinetics of ADMA using 4-cyano-4-(phenylcarbonothioylthio)pentanoic acid (CTP) as a RAFT agent. RAFT polymerisation of ADMA using a molar feed ratio of 75:1:0.15 [mon]:[CTA]:[AIBN] at 70 °C (where [mon], [CTA] and [AIBN] refer to the mole equivalents of monomer, CTA and AIBN respectively) led to a long inhibition period and retardation of homopolymerisation kinetics; monomer conversion was <15% after 12 h. A subsequent increase in the mole equivalents of initiator with respect to CTA to 1:0.4 at 70 °C resulted in increased monomer conversion but a loss of control of dispersity and molecular weight. No explanation was offered by the authors, but it can be speculated that the higher radical concentration led to increased bimolecular termination and many dead chains. The temperature was increased to 80 °C, presumably in an attempt to increase the rate of monomer conversion and reduce the inhibition period, although the authors do not state their reasoning. To control the

radical concentration, the initiator was also changed from AIBN to 1,1′-azobis(cyclohexanecarbonitrile) (ACHN) because of the longer half-life of ACHN. A deviation from the expected *pseudo*-first order kinetics and a colour change from pink to brown suggested that hydrolysis/thermal degradation of the RAFT agent occurred under these conditions. To avoid degradation of the RAFT agent the reaction temperature was reduced to 60 °C, and the mole equivalents of initiator were increased relative to CTA to give molar ratios of 75:1:0.75 ([mon]:[CTA]:[AIBN]) in an attempt to maintain the rate of reaction. The higher than usual molar ratio of initiator to RAFT agent was necessary to ensure sufficient radicals were generated at the start of the reaction, considering the reduced temperature; the half-life of AIBN at 60 °C is 20 h. These conditions ensured the requirement for a low radical concentration (see section 3.1.1) was still met. 70% monomer conversion was reported after 8 h reaction time. The reaction at 60 °C resulted in good control of the dispersity of poly(ADMA), evidenced by a dispersity of 1.2. The M_n was calculated using polystyrene standards (reported M_n = 14000 g mol^{-1}), so the M_n values were treated as relative rather than absolute, thus control of molecular weight could only be inferred through the linear increase of M_n as a function of conversion. Although not discussed by the authors, radicals would have been formed continuously throughout the polymerisation due to the slow homolysis of AIBN which in turn, would lead to the formation of monomer chains throughout the reaction and an increased dispersity. However, the compromise appeared to provide satisfactory control of the polymerisation.

A similar use of a low [CTA]:[I] ratio, at a lower temperature, has been reported by Stenzel *et al.*[15] who reported the homopolymerisation of another bulky acrylamide monomer, 2-methacrylamido glucopyranose (MAG). The reaction was carried out in a solvent mixture of *N,N'*-dimethylacetamide and water (9:1 v/v). CTP was used as the RAFT agent with molar ratios of 100:1:0.5 ([mon]:[CTA]:[I]). The temperature was reduced to 60 °C to reduce the rate of RAFT agent hydrolysis. Good control of dispersity was reported (Đ = 1.23) with a linear increase of M_n with conversion after an inhibition period. M_{nSEC} was apparently higher than the theoretical value by a factor of ~2, but this was attributed to an error in the SEC analysis due to the difference in hydrodynamic volume between the poly(MAG) sample and the polystyrene standards. Hydrolysis of the RAFT agent, leading to a pink to brown colour change in some instances, was attributed to primary amine-containing impurities arising from the monomer synthesis. Considering the argument of Stenzel *et al.*, it could be speculatively suggested that the ADMA polymerisation reported

by Detrembleur and described above could also have been compromised by traces of unreacted dopamine remaining in the monomer.

3.2 Aims

In the work describe in this chapter, RAFT polymerisation was used first to reproduce and then extend the previously reported work on the use of CTP for ADMA.[14] Then (for the first time to the best of the author's knowledge) the same (or similar) conditions were explored using CTP to copolymerise methacrylate monomers with ADMA and DMA in statistical copolymers. The synthesis of novel block copolymers is also reported. These catechol-containing (co)polymers were compared with analogous (co)polymers synthesised using free radical polymerisation and selected copolymers used to assess the influence of copolymer composition and molecular weight in coatings for biosensing applications.

The aims of the work reported in this chapter were:

1. To synthesise homopolymers of ADMA using the RAFT agent CTP with periodically collected samples to allow a qualitative investigation into the copolymerisation kinetics, control of dispersity and molecular weight. The temperature and reaction solvent were modified to optimise the polymerisation. Synthesis of MMA, GMA and SMA homopolymers were also carried out under the conditions necessary for polymerisation of ADMA. The reactions were used to assess the possibility of synthesising (diblock) copolymers of ADMA with methacrylate comonomers.

2. To synthesise a library of statistical copolymers containing ADMA for use as functional adhesive coatings. ADMA-containing statistical copolymers synthesised by RAFT polymerisation have not been previously reported (to the best of the author's knowledge). MMA, SMA and HEMA were used as comonomers to allow the solubility of the resulting copolymers to be tuned. GMA was investigated as a reactive monomer to enable the reactive functional group to immobilise biomolecules in later work (Chapter 5). Additionally, a terpolymer containing HEMA, GMA and ADMA was synthesised using RAFT polymerisation to compare directly with the terpolymers produced by free radical polymerisation discussed in Chapter 2.

3. To synthesise terpolymers comprising HEMA, GMA and (unprotected) DMA using RAFT polymerisation. The extent of control over the dispersity and molecular weight in

the presence of unprotected DMA was investigated. It is hypothesised that such terpolymers could be more readily applied to coating applications than those containing ADMA as they do not require deprotection after polymerisation.

4. To further explore the impact of monomer sequence and chain architecture on functional adhesive copolymers by the synthesis of two novel diblock copolymers. A functional diblock copolymer comprising MMA and ADMA was synthesised. A functional diblock copolymer consisting of ADMA (block A) and a statistical copolymer of HEMA and GMA (block B) was also synthesised for comparison with the poly(HEMA-*stat*-ADMA-*stat*-GMA) statistical terpolymers. The diblock copolymers were prepared to explore the hypothesis that improved adhesion and reactive functional group availability could be obtained from a copolymer with the adhesive catechol moieties concentrated at one end of the copolymer. If immobilised on a surface by the adhesive end a "brush" type structure could be formed, enhancing the opportunity for the GMA to immobilise target molecules from solution.

3.3 Experimental

3.3.1 Materials

4-Cyano-4-(phenylcarbonothioylthio)pentanoic acid (CTP, >97%) was supplied by Sigma-Aldrich, UK and used as received. *N*,*N*-dimethylformamide (DMF, anhydrous, 99.8%) was supplied by Fisher Scientific, UK and used as received. Azobisisobutyronitrile (AIBN, 98%) was supplied by Sigma-Aldrich, UK and recrystallised from methanol before use. 1,4-dioxane (99.8%), glycidyl methacrylate (GMA, 97%), 2-hydroxyethyl methacrylate (HEMA, 97%), and methyl methacrylate (MMA, 99%) were supplied by Sigma-Aldrich, UK and passed through a column of activated alumina column before use to purify and remove inhibitor. Stearyl methacrylate (SMA, 97%) was supplied by TCI UK and used as received. Dimethyl sulfoxide-d_6 (DMSO, 99.9% D atom) was supplied by Sigma-Aldrich, UK and used as received. Deuterated chloroform (99.8% D atom) was supplied by Apollo Scientific, UK, and used as received. DMA and ADMA were synthesised as previously described (Chapter 2).

3.3.2 Polymer Synthesis

3.3.2.1 Procedure for RAFT homopolymerisation of ADMA in DMF - RAFT-A-(DMF)

ADMA (0.5 g, 1.91 mmol), CTP (21 mg, 0.08 mmol) and AIBN (9 mg, 0.05 mmol) in anhydrous DMF (5 mL) were added to a 50 mL Schlenk flask. A sample was taken, and

the reaction mixture was degassed via at least three freeze-pump-thaw cycles and back-filled with nitrogen. The flask was immersed in a preheated oil bath at 60 °C. The reaction was allowed to proceed for 15 h before a final sample was taken. The reaction mixture before workup was a pink solution. The reaction mixture was poured into methanol, causing precipitation of a pink solid, which was collected and dried overnight under vacuum. Yield = 0.14 g, 28% M_n = 1700 g mol^{-1}, Đ = 1.20. ^{1}H NMR ($CDCl_3$, 400 MHz) δ (ppm) = 7.83, 7.51, 7.39 (3s, 5H, Ph-**H**, *RAFT agent end group*), 6.60 (m, 3H, Ph-**H**), 5.94 (s, 1H, N**H**-CH_2), 3.32 (s, 2H, NH-C**H$_2$**), 2.68 (s, 2H, C**H$_2$**-Ph), 1.75 (br m, 8H, O-C-C**H$_3$** *acetonide group*, C**H$_2$**-C-CH_3 *polymer main chain protons*), 1.07–0.95 (br m, 3H, CH_2-C-C**H$_3$**, *methacrylamide methyl group*).

3.3.2.2 Procedure for RAFT polymerisation of ADMA in 1,4-dioxane, RAFT-A-(DIOX)

A homopolymer of ADMA was prepared according to the procedure described above (3.3.2.1) using ADMA (0.5 g, 1.91 mmol), CTP (7 mg, 0.03 mmol), AIBN (3 mg, 0.02 mmol) in 1,4-dioxane (1.5 mL). The reaction was sampled under positive nitrogen pressure after 0, 2, 4, 8, 23, 28, 32 and 48 h. The reaction was allowed to proceed for 53 h before a final sample was taken. The homopolymer was precipitated in methanol. Yield = 0.03 g, 6%, M_n = 32500 g mol^{-1}, Đ = 1.05. ^{1}H NMR ($CDCl_3$, 400 MHz) δ (ppm) as 3.3.2.1.

3.3.2.3 Procedure for RAFT homopolymerisation of MMA, RAFT-M-(DIOX/60C)

A homopolymer of MMA was prepared according to the procedure described above (3.3.2.1) using MMA (1.0 g, 10.0 mmol), CTP (37 mg, 0.13 mmol) and AIBN (16 mg, 0.10 mmol) in 1,4-dioxane (2 mL). The reaction was allowed to proceed for 7 h before a final sample was taken. The homopolymer was precipitated in methanol. Yield = 0.46 g, 46%, M_n = 8300 g mol^{-1}, Đ = 1.07. ^{1}H NMR ($CDCl_3$, 400 MHz) δ (ppm) = 7.89, 7.53, 7.36 (3s, 5H, Ph-**H**, *RAFT agent end group*), 3.62 (m, 3H, C-O-C**H$_3$** *MMA side chain*), 1.92 (s, 2H, C**H$_2$**-C-CH_3 *polymer main chain protons*), 1.04 – 0.85 (m, 3H, CH_2-C-C**H$_3$**, *methacrylate methyl group*).

3.3.2.4 Procedure for RAFT homopolymerisation of MMA, RAFT-M-(DIOX/70C)

A homopolymer of MMA was prepared according to the procedure described above (3.3.2.1) using MMA (1.0 g, 10.0 mmol), CTP (28 mg, 0.10 mmol) and AIBN (2 mg, 0.01 mmol) in 1,4-dioxane (9 mL) at 70 °C. The reaction was sampled under positive

nitrogen pressure after 0 and 5 h. The reaction was allowed to proceed for 24 h before a final sample was taken. The homopolymer was precipitated in methanol. Yield = 0.67 g, 67%, M_n = 15200 g mol^{-1}, Đ = 1.04. ^{1}H NMR ($CDCl_3$, 400 MHz) δ (ppm) as 3.3.2.3.

3.3.2.5 Procedure for RAFT homopolymerisation of MMA, RAFT-M-(DIOX)-2

A homopolymer was prepared according to the procedure described above (3.3.2.1) using MMA (1.0 g, 10.0 mmol), CTP (37 mg, 0.13 mmol) and AIBN (16 mg, 0.10 mmol) in 1,4-dioxane (9 mL). The reaction was allowed to proceed for 20 h before a final sample was taken. The homopolymer was precipitated in methanol. Yield = 0.70 g, 70%, M_n = 10750 g mol^{-1}, Đ = 1.07. ^{1}H NMR ($CDCl_3$, 400 MHz) δ (ppm) as 3.3.2.3.

3.3.2.6 Procedure for RAFT homopolymerisation of SMA, RAFT-S-(DIOX/60C)

A homopolymer of SMA was prepared according to the procedure described above (3.3.2.1) using SMA (0.68 g, 2.00 mmol), CTP (7 mg, 0.03 mmol) and AIBN (3 mg, 0.02 mmol) in 1,4-dioxane (2 mL). The reaction was allowed to proceed for 7 h before a final sample was taken. The homopolymer was precipitated in methanol. Yield = 0.48 g, 70%, M_n = 28850 g mol^{-1}, Đ = 1.20. ^{1}H NMR ($CDCl_3$, 400 MHz) δ (ppm) = 7.86, 7.53, 7.36 (3s, 5H, Ph-**H**, *RAFT agent end group*), 3.92 (s, 2H, O-C**H$_2$**-CH_2), 1.92 – 1.81 (s, 2H, C**H$_2$**-C-CH_3 *polymer main chain protons*), 1.61 (s, 2H, O-CH_2-C**H$_2$**-), 1.31 (m, 30H, O-CH_2-CH_2-(C**H$_2$**)$_{15}$-), 1.13 - 0.89 (m, 6H, CH_2-C-C**H$_3$**, *methacrylate methyl group* and $(CH_2)_{15}$-C**H$_3$** *SMA side chain*).

3.3.2.7 Procedure for RAFT homopolymerisation of GMA, RAFT-G-(DIOX/60C)

A homopolymer of GMA was prepared according to the procedure described above (3.3.2.1) using GMA (2 g, 14.0 mmol), CTP (52 mg, 0.18 mmol) and AIBN (23 mg, 0.14 mmol) in 1,4-dioxane (2 mL). The reaction was allowed to proceed for 7 h before a final sample was taken. The homopolymer was precipitated in methanol. Yield = 1.58 g, 79%, M_n = 15450 g mol^{-1}, Đ = 1.19. ^{1}H NMR ($CDCl_3$, 400 MHz) δ (ppm) = 7.87, 7.53, 7.36 (3s, 5H, Ph-**H**, *RAFT agent end group*), 4.31, 3.82 (2s, 1H, O-C**H$_2$**-CH), 3.25 (s, 1H, O-C**H**-CH_2 *epoxide ring*), 2.87, 2.66 (2s, 1H, O-CH-C**H$_2$** *epoxide ring*), 1.90 (s, 2H, C**H$_2$**-C-CH_3 *polymer main chain protons*), 1.10 – 0.94 (m, 3H, CH_2-C-C**H$_3$**, *methacrylate methyl group*).

3.3.2.8 Procedure for RAFT homopolymerisation of GMA, RAFT-G-(DIOX/70C)

A homopolymer of GMA was prepared according to the procedure described above (3.3.2.1) using GMA (1 g, 7.00 mmol), CTP (39 mg, 0.14 mmol) and AIBN (2 mg,

0.01 mmol) in 1,4-dioxane (9 mL) at 70 °C. The reaction was allowed to proceed for 15 h before a final sample was taken. The homopolymer was precipitated in methanol. Yield = 0.51 g, 51%, M_n = 12950 g mol^{-1}, Đ = 1.16. ^{1}H NMR ($CDCl_3$, 400 MHz) δ (ppm) as 3.3.2.7.

3.3.2.9 Procedure for RAFT statistical copolymerisation of MMA and ADMA, RAFT-MA-90/10

A copolymer of MMA and ADMA was prepared according to the procedure described above (3.3.2.1) using MMA (0.50 g, 5.00 mmol), ADMA (0.14 g, 0.55 mmol), CTP (20 mg, 0.07 mmol) and AIBN (9 mg, 0.06 mmol) in 1,4-dioxane (2 mL). The reaction was allowed to proceed for 7 h before a final sample was taken. The copolymer was precipitated in methanol. Yield = 0.40 g, 63%, M_n = 13600 g mol^{-1}, Đ = 1.06. ^{1}H NMR ($CDCl_3$, 400 MHz) δ (ppm) = 7.89, 7.53, 7.36 (s, 2H, Ph-**H** *RAFT agent end group*), 6.69 – 6.60 (m, 3H, Ph-**H**), 5.67 (s, 1H, N**H**-CH_2), 3.59 (m, 3H, C-O-C**H$_3$** *MMA*), 3.33 (s, 2H, NH-C**H$_2$**-CH_2), 2.70 (s, 2H, CH_2-C**H$_2$**-Ph), 1.92 - 1.83 (m, 2H, C**H$_2$**-C-CH_3 *polymer main chain protons*), 1.68 (br m, 6H, O-C-C**H$_3$** *acetonide group*), 1.03 - 0.86 (m, 3H, CH_2-C-C**H$_3$**, *methacrylamide / methacrylate methyl groups*).

3.3.2.10 Procedure for RAFT statistical copolymerisation of MMA and ADMA, RAFT-MA-50/50

A copolymer of MMA and ADMA was prepared according to the procedure described above (3.3.2.1) using MMA (0.08 g, 0.80 mmol), ADMA (0.21 g, 0.80 mmol), CTP (6 mg, 0.02 mmol) and AIBN (3 mg, 0.02 mmol) in 1,4-dioxane (2 mL). The reaction was allowed to proceed for 7 h before a final sample was taken. The copolymer was precipitated in methanol. Yield = 0.20 g, 69%, M_n = 12850 g mol^{-1}, Đ = 1.14. ^{1}H NMR ($CDCl_3$, 400 MHz) δ (ppm) as 3.3.2.9.

3.3.2.11 Procedure for RAFT statistical copolymerisation of GMA and ADMA, RAFT-GA-90/10

A copolymer of GMA and ADMA was prepared according to the procedure described above (3.3.2.1) using GMA (0.40 g, 2.82 mmol), ADMA (0.08 g, 0.31 mmol), CTP (11 mg, 0.04 mmol) and AIBN (5 mg, 0.03 mmol) in 1,4-dioxane (2 mL). The reaction was allowed to proceed for 7 h before a final sample was taken. The copolymer was precipitated in methanol. Yield = 0.38 g, 79%, M_n = 25100 g mol^{-1}, Đ = 1.23. ^{1}H NMR ($CDCl_3$, 400 MHz) δ (ppm) = 7.89, 7.53, 7.39 (3s, 2H, Ph-**H** *RAFT agent end group*), 6.68 – 6.60 (m, 3H, Ph-**H**), 5.65 (s, 1H, N**H**-CH_2), 4.31, 3.82 (2s, 1H, O-C**H$_2$**-CH), 3.36 (s, 2H,

NH-C**H**$_2$), 3.25 (s, 1H, O-C**H**-CH_2 *epoxide ring*), 2.86 (s, 1H, O-CH-C**H**$_2$ *epoxide ring*), 2.68 (s, 2H, C**H**$_2$-Ph), 1.98 (s), 1.91 (s, 2H, C**H**$_2$-C-CH_3 *polymer main chain protons*), 1.70 (br m, 6H, O-C-CH_3 *acetonide* group), 1.10 - 0.95 (m, 3H, CH_2-C-C**H**$_3$, *methacrylamide methyl group*).

3.3.2.12 Procedure for RAFT statistical copolymerisation of SMA and ADMA, RAFT-SA-90/10

A copolymer of SMA and ADMA was prepared according to the procedure described above (3.3.2.1) using SMA (0.75 g, 2.22 mmol), ADMA (0.06 g, 0.22 mmol), CTP (9 mg, 0.03 mmol) and AIBN (4 mg, 0.02 mmol) in 1,4-dioxane (2 mL). The reaction was allowed to proceed for 7 h before a final sample was taken. The copolymer was precipitated in methanol. Yield = 0.53 g, 65%, M_n = 32000 g mol^{-1}, Đ = 1.07. ^{1}H NMR ($CDCl_3$, 400 MHz) δ (ppm) = 7.87, 7.53, 7.36 (3s, 2H, Ph-**H** *RAFT agent end group*), 6.66 – 6.59 (m, 3H, Ph-**H**), 5.68 (s, 1H, N**H**-CH_2), 3.92 (s, 2H, O-C**H**$_2$-CH_2 (SMA)), 3.34 (s, 2H, NH-C**H**$_2$), 2.68 (s, 2H, C**H**$_2$-Ph), 1.92 – 1.81 (s, 2H, C**H**$_2$-C-CH_3 *polymer main chain protons*), 1.69 (br m, 6H, C-CH_3 *acetonide group*), 1.62 (s, 2H, O-CH_2-C**H**$_2$-), 1.30 (m, 30H, O-CH_2-CH_2-(C**H**$_2$)$_{15}$), 1.12 - 0.90 (m, 6H, CH_2-C-C**H**$_3$, *methacrylate / methacrylate methyl group* and (CH_2)$_{15}$-C**H**$_3$).

3.3.2.13 Procedure for RAFT statistical copolymerisation of SMA and ADMA, RAFT-SA-50/50

A copolymer of SMA and ADMA was prepared according to the procedure described above (3.3.2.1) using SMA (0.17 g, 0.50 mmol), ADMA (0.13 g, 0.50 mmol), CTP (4 mg, 0.01 mmol) and AIBN (2 mg, 0.01 mmol) in 1,4-dioxane (2 mL). The reaction was allowed to proceed for 7 h before a final sample was taken. The copolymer was precipitated in methanol. Yield = 0.10 g, 33%, M_n = 15250 g mol^{-1}, Đ = 1.14. ^{1}H NMR ($CDCl_3$, 400 MHz) δ (ppm) as 3.3.2.12.

3.3.2.14 Procedure for RAFT statistical copolymerisation of HEMA and ADMA, RAFT-HA-90/10

A copolymer of HEMA and ADMA was prepared according to the procedure described above (3.3.2.1) using HEMA (1.17 g, 9.00 mmol), ADMA (0.26 g, 1.00 mmol), CTP (37 mg, 0.13 mmol) and AIBN (16 mg, 0.10 mmol) in anhydrous DMF (14 mL). The reaction was allowed to proceed for 21.5 h before a final sample was taken. The copolymer was precipitated in diethyl ether. Yield = 0.97 g, 67%, M_n = 9700 g mol^{-1}, Đ = 1.38. ^{1}H NMR (DMSO-d6, 400 MHz) δ (ppm) = 7.81, 7.62, 7.47 (3s, 2H, Ph-**H** *RAFT agent end*

group), 6.72 – 6.58 (m, 3H, Ph-**H**), 4.82 (s, 1H, CH_2-O**H**), 3.89 (s, 2H, O-C**H₂**-CH_2), 3.58 (s, 2H, O-CH_2-C**H₂**), 3.32 (s, 2H, NH-C**H₂**), 1.78 (br m, 6H, C-CH_3 *acetonide group*), 1.62 (s, 2H, C**H₂**-C-CH_3 *polymer main chain protons*), 0.94 - 0.78 (br m, 3H, CH_2-C-C**H₃**, *methacrylamide methyl group*).

3.3.2.15 Procedure for RAFT statistical terpolymerisation of HEMA, GMA and ADMA, RAFT-HGA-80/10/10

A terpolymer of HEMA, GMA and ADMA was prepared according to the procedure described above (3.3.2.1) using HEMA (1.04 g, 8.00 mmol), GMA (0.14 g, 1.00 mmol), ADMA (0.26 g, 1.00 mmol), CTP (37 mg, 0.13 mmol) and AIBN (16 mg, 0.10 mmol) in anhydrous DMF (14 mL). The reaction was allowed to proceed for 21.5 h before a final sample was taken. The terpolymer was precipitated in diethyl ether. Yield = 0.83 g, 58%, M_n = 10850 g mol^{-1}, Đ = 1.32. ^{1}H NMR (DMSO-d6, 400 MHz) δ (ppm) = 7.81, 7.62, 7.51 (3s, 2H, Ph-**H** *RAFT agent end group*), 6.72 – 6.60 (m, 3H, Ph-**H**), 4.82 (s, 1H, CH_2-O**H**), 4.26 (s, 1H, O-C**H₂**-CH *GMA*), 3.89 (s, 2H, O-C**H₂**-CH_2 *HEMA*), 3.73 (s, 1H, O-C**H₂**-CH *GMA*), 3.58 (s, 2H, O-CH_2-C**H₂** *HEMA*), 3.36 (s, 2H, NH-C**H₂**), 3.20, 2.89 (2s, 1H, O-CH-C**H₂** *epoxide ring*), 2.67 (s, 2H, C**H₂**-Ph), 2.59 (s, 1H, O-CH-C**H₂** *epoxide ring*), 1.80 (br m, 6H, C-CH_3 *acetonide*), 1.62-1.48 (s, 2H, C**H₂**-C-CH_3 *polymer main chain protons*), 0.95 - 0.78 (br m, 3H, CH_2-C-C**H₃**, *methacrylamide / methacrylate methyl groups*).

3.3.2.16 Procedure for RAFT statistical terpolymerisation of HEMA, GMA and DMA, RAFT-HGD-80/14/6

A terpolymer of HEMA, GMA and DMA was prepared according to the procedure described above (3.3.2.1) using HEMA (1.04 g, 8.00 mmol), GMA (0.14 g, 1.00 mmol), DMA (0.22 g, 1.00 mmol), CTP (37 mg, 0.13 mmol) and AIBN (16 mg, 0.10 mmol) in anhydrous DMF (12 mL). The reaction was allowed to proceed for 21 h before a final sample was taken. The terpolymer was precipitated in diethyl ether. Yield = 0.79 g, 56%, M_n = 10100 g mol^{-1}, Đ = 1.44. ^{1}H NMR (DMSO-d6, 400 MHz) δ (ppm) = 8.67 (2s, 2H, Ph-O**H**), 7.82, 7.62, 7.51 (3s, 2H, Ph-**H** *RAFT agent end group*) 6.64 – 6.41 (m, 3H, Ph-**H**), 4.80 (s, 1H, CH_2-O**H**), 4.59 (s, 1H, N**H**-CH_2), 4.27 (s, 1H, O-C**H₂**-CH *GMA*), 3.91 (s, 2H, O-C**H₂**-CH_2 *HEMA*), 3.73 (s, 1H, O-C**H₂**-CH *GMA*), 3.58 (s, 2H, O-CH_2-C**H₂** *HEMA*), 3.33 (s, 2H, NH-C**H₂**), 3.20, 2.89 (2s, 1H, O-CH-C**H₂** *epoxide ring*), 2.65 (s, 2H, C**H₂**-Ph), 2.50 (s, 1H, O-CH-C**H₂** *epoxide ring*), 1.62-1.48 (s, 2H, C**H₂**-C-CH_3 *polymer main chain*), 0.95 - 0.79 (br m, 3H, CH_2-C-C**H₃**, *methacrylamide / methacrylate methyl groups*).

3.3.2.17 Procedure for RAFT statistical terpolymerisation of HEMA, GMA and DMA, RAFT-HGD-80/10/10

A terpolymer of HEMA, GMA and DMA was prepared according to the procedure described above (3.3.2.1) using HEMA (1.04 g, 8.00 mmol), GMA (0.14 g, 1.00 mmol), DMA (0.22 g, 1.00 mmol), CTP (19 mg, 0.07 mmol) and AIBN (8 mg, 0.05 mmol) in anhydrous DMF (13 mL). The reaction was allowed to proceed for 23.5 h before a final sample was taken. The terpolymer was precipitated in diethyl ether. Yield = 1.02 g, 73%, M_n = 20000 g mol^{-1}, Đ = 1.55. ^{1}H NMR (DMSO-d6, 400 MHz) δ (ppm) as 3.3.2.16.

3.3.2.18 Procedure for RAFT statistical terpolymerisation of HEMA, GMA and DMA, RAFT-HGD-74/13/13

A terpolymer of HEMA, GMA and DMA was prepared according to the procedure described above (3.3.2.1) using HEMA (1.04 g, 8.00 mmol), GMA (0.14 g, 1.00 mmol) and DMA (0.22 g, 1.00 mmol), CTP (37 mg, 0.13 mmol), and AIBN (4 mg, 0.03 mmol) in anhydrous DMF (12 mL) at 70 °C. The reaction was allowed to proceed for 24 h before a final sample was taken. The terpolymer was precipitated in diethyl ether. Yield = 0.86 g, 61%, M_n = 24950 g mol^{-1}, Đ = 2.18. ^{1}H NMR (DMSO-d6, 400 MHz) δ (ppm) as 3.3.2.16.

3.3.2.19 Procedure for RAFT block copolymerisation of ADMA with poly(MMA) macro-RAFT agent, RAFT-M-*b*-A-DIOX

A block copolymer was prepared according to the procedure described above (3.3.2.1) using ADMA (0.20 g, 0.77 mmol), poly(MMA) (RAFT-M-(DIOX)-2) (0.11 g, 0.01 mmol) and AIBN (1 mg, 0.01 mmol) in 1,4-dioxane (2 mL). The reaction was allowed to proceed for 7 h before a final sample was taken. The diblock copolymer was precipitated in methanol. Yield = 0.06 g, 19%, M_n = 14600 g mol^{-1}, Đ = 1.14. ^{1}H NMR ($CDCl_3$, 400 MHz) δ (ppm) = 6.69 – 6.60 (m, 3H, Ph-**H**), 5.84 (s, 1H, NH-C**H$_2$**), 3.60 (m, 3H, C-O-C**H$_3$**), 3.31 (s, 2H, NH-C**H$_2$**), 2.66 (s, 2H, C**H$_2$**-Ph), 1.94 – 1.81 (s, 2H, C**H$_2$**-C-CH_3 *polymer main chain protons*), 1.65 (br m, 8H, O-C-C**H$_3$** *acetonide group*), 1.04 – 0.85 (m, 3H, CH_2-C-C**H$_3$**, *methacrylamide / methacrylate methyl groups*).

3.3.2.20 Procedure for RAFT block copolymerisation of HEMA and GMA with poly(ADMA) macro-RAFT agent, RAFT-A-*b*-(HG-90/10)

A block copolymer was prepared according to the procedure described above (3.3.2.1) using HEMA (0.33 g, 2.50 mmol), GMA (0.04 g, 0.31 mmol), poly(ADMA) (RAFT-A-(DMF)) (64 mg, 0.01 mmol) and AIBN (2 mg, 0.01 mmol) in anhydrous DMF (3.5 mL). The reaction was allowed to proceed for 24 h before a final sample was taken.

The diblock copolymer was precipitated in methanol. Yield = 0.04 g, 11%, M_n = 38300 g mol^{-1}, Đ = 1.14. ^{1}H NMR (DMSO-d6, 400 MHz) δ (ppm) as 3.3.2.15.

3.3.3 Characterisation methods

3.3.3.1 Size exclusion chromatography (SEC)

Molecular weight and dispersity data were obtained by SEC using a Viscotek TDA 302 with refractive index, viscosity, and light scattering detectors. 2 × 300 mm PLgel 5 μm mixed C-columns (with a linear range of molecular weight from 200 to 2,000,000 g mol^{-1}) were used and THF as the eluent with a flow rate of 1.0 mL min^{-1} at a temperature of 35 °C, or dimethylformamide (DMF) with 0.1% of lithium bromide with a flow rate of 1.0 mL^{-1} at a temperature of 70 °C.

The molecular weights were obtained by triple detection SEC with light scattering, using a dn/dc value of 0.085 mL g^{-1} for poly(MMA) in THF, 0.084 mL g^{-1} for poly(GMA) in THF, 0.075 mL g^{-1} for SMA in THF and 0.076 mL g^{-1} for poly(HEMA) in DMF.[16] The dn/dc for poly(ADMA) in THF, 0.125 mL g^{-1}, was obtained by measuring two samples of poly(ADMA) in THF with accurately determined concentration. Unless otherwise specified, the dn/dc value of the monomer with the greatest mole fraction in a copolymer was used to calculate molecular weight. Where indicated, the molecular weights were obtained from the RI detector and a conventional calibration curve constructed using nine reference polystyrene standards (Polymer Laboratories, M_n between 580-1112000 g mol^{-1}, Đ ≤ 1.11).

3.3.3.2 Nuclear magnetic resonance (NMR) spectroscopy

^{1}H NMR spectra were recorded on a Bruker-400 MHz spectrometer using $CDCl_3$ or DMSO d_6 as a solvent. Spectra were referenced to the trace proton peaks present in $CDCl_3$ (7.26 ppm) or DMSO d_6 (2.50 ppm). NMR spectra were analysed using MestReNova (Mestrelab Research, Spain). Dinitrobenzene (DNB) or DMF were used as internal standards in NMR experiments.

3.4 Results and Discussion

The synthesis of (co)polymers containing ADMA and DMA was investigated using RAFT polymerisation as a means to access advanced architectures such as diblock copolymers, with the intention to control dispersity and molecular weight.

3.4.1 Synthesis of homopolymers by RAFT polymerisation

Homopolymers of ADMA, MMA, GMA and SMA were synthesised using RAFT polymerisation in order to establish suitable conditions for the controlled polymerisation of these monomers using similar conditions, and in some cases to prepare macro-RAFT agents for the synthesis of diblock copolymers.

3.4.1.1 Synthesis of poly(ADMA) using RAFT polymerisation

Dithiobenzoate RAFT agents are suitable for the controlled polymerisation of methacrylate and methacrylamide monomers. A large number of such RAFT agents are exemplified by Barner-Kowollik in "The Handbook of RAFT Polymerisation"[2] including CTP, which was used in the current work. The controlled polymerisation of ADMA using CTP in DMF has been previously reported[14] and the aim of this work was to repeat and expand on the reported procedure, and then analyse the outcome of using similar conditions to polymerise the other methacrylate monomers mentioned above. Upon the formation of the RAFT pre-equilibrium, the pentanoic acid-functionalised R-group of CTP should have good solubility in the polar solvents used herein (DMF and 1,4-dioxane). The electron-withdrawing cyano-group weakens the C-S bond meaning that the R-group is a good radical leaving group and the concentration of R$^{\bullet}$ should increase rapidly. Rapid re-initiation should then occur due to the high reactivity of the monomers towards R$^{\bullet}$, which is a condition of a successful RAFT polymerisation, as described in section 3.1.1. A reaction scheme for the RAFT polymerisation of ADMA is presented in Scheme 3.1.

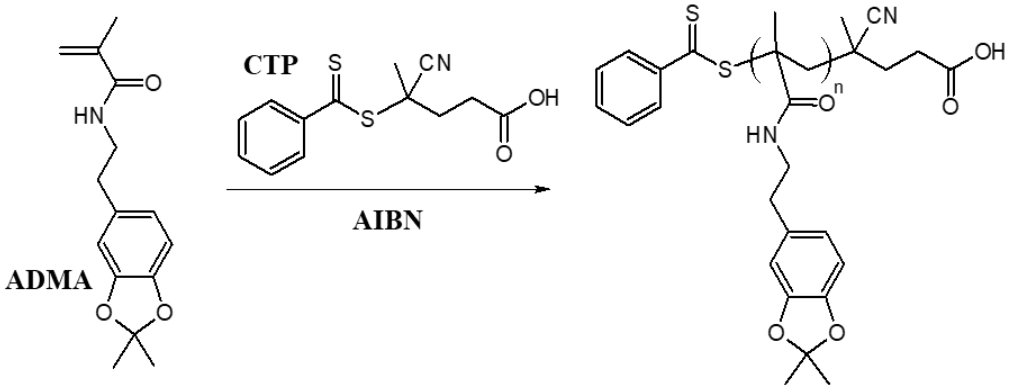

Scheme 3.1. Reaction scheme for the RAFT polymerisation of ADMA using CTP

The relationship between the predicted and measured molecular weight can be used to infer the control afforded by the RAFT polymerisation. Theoretical number average molecular weight (M_{nTheo}) can be calculated using the following equation (3.1):

$$M_{nTheo} = \frac{[mon]_0 \times M_{mon} \times p}{[CTA]_0 + df([I]_0(1 - e^{k_d t}))} + M_{CTA} \quad \textbf{3.1}$$

where p is the monomer conversion, $[mon]_0$ and $[CTA]_0$ are the amounts of monomer and CTA in the feed respectively, and M_{mon} and M_{CTA} are the relative molecular mass of the monomer and CTA respectively. The initiator term, $df([I]_0(1-e^{k_d t}))$, refers to the number of initiator derived chains, where d is the average number of chains formed by each chain termination (depending on the ratio of termination by combination and disproportionation), f is the initiator efficiency, t is time, and k_d is the rate coefficient for initiator decomposition. In practice, by following the guidelines outlined in Section 3.1.1, a well-designed reaction should have a low number of initiator-derived chains, so Equation 3.1 is commonly simplified to:

$$M_{nTheo} = \frac{[mon]_0 \times M_{mon} \times p}{[CTA]_0} + M_{CTA} \quad \textbf{3.2}$$

A target M_n can therefore be calculated prior to the reaction using Equation 3.2, using an estimated value for monomer conversion, p.[17] M_{nTheo} is then calculated with the experimentally derived value of p after the reaction. Several assumptions are associated with Equations 3.1 and 3.2:[1] i) that the rate of radical generation from the initiator is rapid; ii) that the RAFT main-equilibrium is rapidly established, so that the majority of the chains begin growing in the same time frame; iii) that no other undesired reactions occur such as irreversible chain transfer or bimolecular termination; iv) that the RAFT agent is completely consumed in the pre-equilibrium reaction, such that $[CTA]_0$ accurately predicts the number of RAFT agent-derived chains formed;[18] and v) that the RAFT agent is 100% pure.[19]

In the current work, number average molecular weight data was obtained using SEC with triple detection calibration and using a dn/dc value for the monomer with the highest mole fraction in each case (M_{nSEC}). M_{nSEC} can be compared to M_{nTheo} to assess the control over the molecular weight afforded by the RAFT agent using a molecular weight factor (MWF):

$$MWF = \frac{M_{nSEC}}{M_{nTheo}} \quad \textbf{3.3}$$

where M_{nTheo} is the theoretical molecular weight calculated using Equation 3.2. An MWF value of 1 would indicate Equation 3.2 predicts the M_n perfectly.

Unless otherwise stated, monomer conversion was calculated by comparison of normalised integrals arising from the vinyl peaks of residual monomer in ^{1}H NMR samples according to Equation 2.1 (Chapter 2). The signal arising from DMF was used as an internal standard to normalise the integrals. In cases where a final reaction sample could not be obtained, monomer conversion is estimated from the % yield of the recovered (co)polymer. In these cases, experimental error in conversion may be significantly higher than calculation of conversion by NMR.

The conditions used for the polymerisation of ADMA and the characteristics of the resulting homopolymers are summarised in Table 3.1. Polymers in this thesis are referred to individually using a code where the first element describes the type of polymerisation, *e.g.* RAFT, and the second denotes the monomers used. Further information is then included for the avoidance of ambiguity between samples *e.g.* monomer feed mole fraction, solvent or reaction temperature. For example, RAFT-MA-90/10 refers to a copolymer of MMA and ADMA with a 90/10 molar feed ratio of monomers, synthesised using RAFT polymerisation.

Table 3.1. Summary of reaction conditions, monomer conversion and molecular weight data for poly(ADMA) synthesised using RAFT polymerisation.

Homopolymer	Time / h	ρ /%	[mon]: [CTA]:[I]	M_{nTheo} / g mol^{-1}	M_{nSEC} / g mol^{-1}	MWF	Đ
RAFT-A-(DMF)	24	38	25:1:0.75	2800	1700	0.61	1.20
RAFT-A-(DIOX)	53	88	75:1:0.75	17200	32500	1.89	1.05

In the current investigation, initial conditions for the RAFT polymerisation of ADMA (25:1:0.75 [ADMA]:[CTP]:[AIBN] at 60 °C) were chosen to reflect the molar ratios that led to controlled polymerisation reactions in the reported synthesis of poly(ADMA), described in Section 3.1.2.[14] A low [ADMA]:[CTP] ratio was selected to target a low M_n for potential use in block copolymer synthesis. The data in Table 3.1 shows that the RAFT polymerisation of ADMA in DMF (RAFT-A-(DMF)) resulted in a rather low monomer conversion after 24 h – 38% – calculated according to Equation 2.1. This conversion was significantly lower than the value from the previously reported procedure which achieved 70% conversion in 8 h, under conditions which were identical to those used in the current study with the exception of the [mon]:[CTA] ratio. The previous study used a [mon]:[CTA] ratio of 75:1[14] whereas a much lower [mon]:[CTA] ratio of 25:1 was used in the current

study. Thus, the low conversion of RAFT-A-(DMF) may have been due to rate retardation arising from the high CTA concentration, commonly observed for dithiobenzoate RAFT agents.[20] Additionally, as impurities arising from dopamine were detected in the mass spectrum of ADMA (see Chapter 2), radical scavenging may have reduced the radical concentration and therefore the rate of reaction, although careful purification of the monomer means this is a less likely explanation.

RAFT-A-(DMF) was analysed using triple detection SEC in THF. A dn/dc value of 0.12 mL g^{-1} for poly(ADMA) was calculated using SEC using two samples of RAFT-A-(DMF) with accurately determined concentration – this value of dn/dc was used to calculate the M_n of RAFT-A-(DMF). The dispersity was reasonably narrow (Đ = 1.20), especially considering the low molecular weight, and that a unimodal distribution was observed. However, the measured M_{nSEC} (1700 g mol^{-1}) was smaller than the M_{nTheo} of 2800 g mol^{-1} (calculated using Equation 3.2) by a factor of 0.61. In RAFT polymerisation, a low observed M_n with respect to M_{nTheo} is usually attributed to a large number of initiator-derived chains in the reaction (see Equation 3.1). In this case the very low conversion introduces more error into the SEC measurements due to the poor light scattering signal intensity and determining the actual molecular weight control is subject to this error. Further experimental error could have been introduced *via* inaccurate calculation of the dn/dc due to potential impurities in the homopolymer. Overall, considering the low conversion and resulting low molecular weight, the homopolymer synthesis could be regarded to be under reasonable control.

Peaks between 7.3 and 7.9 ppm in the ^{1}H NMR spectrum for RAFT-A-(DMF) (Figure 3.1) confirmed the presence of the RAFT end-group. The ratio of the integrals of the end-group protons to the aromatic protons on the monomer repeat unit would indicate a number average degree of polymerisation (DP) of 19 if all chains comprised terminal RAFT groups. The provisional NMR-determined DP is much larger than the SEC-determined DP (~7), suggesting around half of the chains retained the terminal RAFT Z-group at the end of the reaction (although this is subject to the significant aforementioned experimental error in SEC measurement of low M_n homopolymers and error in NMR calculation).

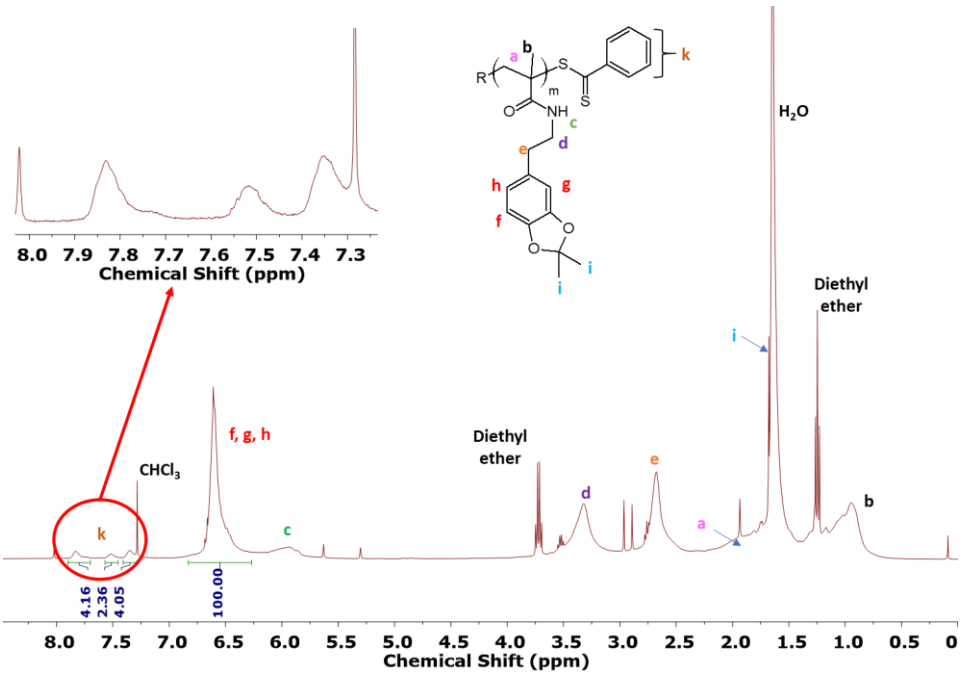

Figure 3.1. ^{1}H NMR spectrum for RAFT-A-(DMF) with inset expanded region of the RAFT agent peaks. R = initiator or RAFT agent R-group.

RAFT homopolymerisation of ADMA was also conducted using 1,4-dioxane as the solvent (RAFT-A-(DIOX)). The solvent was changed to 1,4-dioxane to allow closer comparison with FR-A, the equivalent free radical polymerisation of ADMA in 1,4-dioxane at 70 °C, which also experienced slow monomer conversion – 20% after 24 h. In that case low conversion was attributed to radical scavenging impurities in the monomer (see Chapter 2). RAFT polymerisation of ADMA under these conditions had not previously been reported. The [mon]:[CTA] ratio was increased to 75:1 and the reaction time increased to allow the reaction to progress to a higher conversion and molecular weight. Although the solvent usually has only a minor effect on the rate of reaction and dispersity of RAFT polymerisations,[20, 21] because of the multiple changes between the two reactions the outcome of RAFT-A-(DIOX) and RAFT-A-(DMF) cannot be directly compared.

Samples were periodically withdrawn from the reaction, analysed by ^{1}H NMR, and a kinetic plot of $\ln([mon]_0/[mon])$ *vs*. time was produced (Figure 3.2). Good correlation of the data to a linear fit would indicate *pseudo*-first order kinetics (*i.e.* the absence of significant termination implies the concentration of propagating radicals is constant); a method commonly used to identify a functioning RAFT equilibrium.[22, 23] An initial period of very slow conversion (~4 h) was observed. This phenomenon, known as an inhibition period, has been widely reported, especially for polymerisation reactions using

dithiobenzoate RAFT agents such as CTP,[20, 24] although the inhibition period is usually <100 min. The inhibition period occurs before the main RAFT equilibrium is established and could be due to either slow re-initiation of monomer by the R˙ radical in the RAFT pre-equilbrium[17] or excessive stabilisation of the pre-equilibrium RAFT adduct by the phenyl Z-group (**2** in Scheme 1.3, Chapter 1).[23]

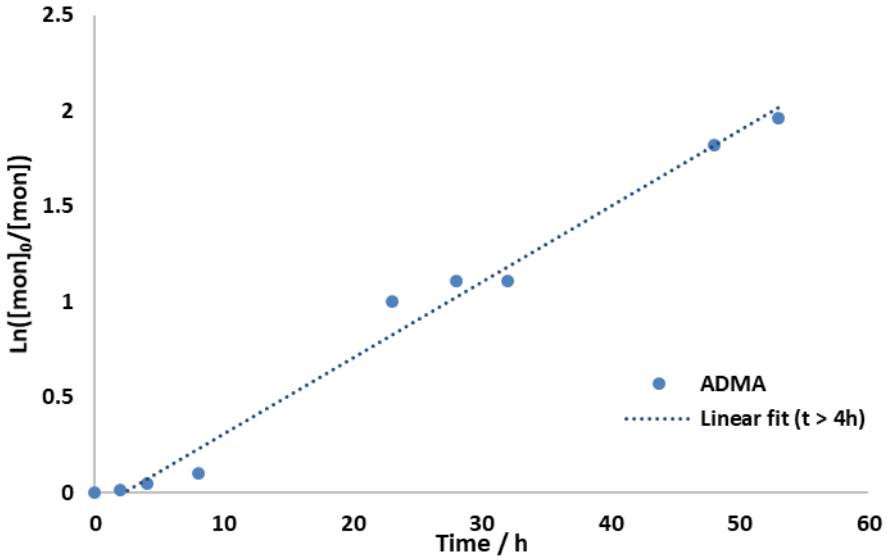

Figure 3.2. Kinetic plot of the RAFT polymerisation of ADMA (RAFT-A-(DIOX)).

Linear regression was used to plot a line of best fit on Figure 3.2, only considering the data when t > 4 h (after the inhibition period). In the case of a controlled reaction with no inhibition period the line of best fit should cross the *x*-axis at t = 0. Accordingly, following an inhibition period, the line of best fit should intersect the *x*-axis at the point at which monomer conversion begins to increase. The fitted line on Figure 3.2 intersected the *x*-axis around t = 2 h (just before the end of the inhibition period), indicating there was little deviation from *pseudo*-first order kinetics, allowing for the potential error in NMR measurements. This suggested that radical scavenging was minimal and thus any impurities arising from the ADMA synthesis had a negligible effect on the RAFT polymerisation. RAFT-A-(DIOX) reached 88% conversion after 53 h. The monomer conversion after 23 h was 63%, indicating faster monomer consumption compared to RAFT-A-(DMF) (38% after 24 h). This could be due to the increase in [mon]:[CTA] ratio from 25:1 to 75:1, which may reduce rate retardation.[20]

SEC analysis indicated the dispersity of the final homopolymer was very narrow (Đ = 1.05). Unlike the synthesis of ADMA in DMF (RAFT-A-(DMF)), M_{nSEC} (32500 g mol^{-1}) was higher than M_{nTheo} (17200 g mol^{-1}) by a factor of 1.89. Errors

associated with the SEC measurement (poor light scattering signal) are significantly reduced due to the higher molecular weight of RAFT-A-(DIOX). The poor prediction of RAFT-A-(DIOX) molecular weight, despite the narrow dispersity, indicated a violation of the assumptions made when using Equation 3.2. The most likely factor causing an underestimation of the molecular weight is the incomplete consumption of RAFT agent, resulting in the generation of fewer polymer chains under RAFT-control. This could be due to a low partition coefficient, ϕ, in the RAFT pre-equilibrium (see Equation 1.26 – 1.29, Chapter 1), leading to fewer than predicted RAFT agent-derived chains.[17] Additionally, radical scavenging from impurities in ADMA arising from dopamine (as demonstrated in Chapter 2) would reduce the amount of active RAFT agent, although, as previously mentioned, the *pseudo*-first order kinetics observed in Figure 3.2 suggest this effect is minimal.

Whilst it cannot be claimed that conditions are optimised in terms of reaction rate and control of molecular weight, RAFT polymerisation of ADMA has nevertheless been shown to provide narrow dispersity homopolymer chains, *via* two alternative sets of reaction conditions, which could be taken forward for potential use as macro-RAFT agents in block copolymer synthesis.

3.4.1.2 Synthesis of methacrylate homopolymers using RAFT polymerisation

Having established suitable conditions for the RAFT polymerisation of ADMA – a methacrylamide – based on previously reported procedures, an investigation was carried out to establish if the same conditions would be suitable for the polymerisation of MMA and for the first time (to the best of our knowledge) attempts would be made to synthesise homopolymers of SMA and GMA using CTP as the RAFT agent.

Table 3.2. Summary of reaction conditions, monomer conversion and molecular weight data for poly(MMA), poly(SMA) and poly(GMA) synthesised using RAFT polymerisation.

Homopolymer	Time / h	ρ /%	[mon]: [CTA]:[I]	M_{nTheo} / g mol^{-1}	M_{nSEC} / g mol^{-1}	MWF	Đ
RAFT-M-(DIOX/60C)	7	46[a]	75:1:0.75	3700	8300	2.24	1.07
RAFT-M-(DIOX/60C)-2	20	70[a]	75:1:0.75	5550	10750	1.94	1.07
RAFT-M-(DIOX/70C)	24	75	100:1:0.1	7800	15200	1.95	1.04
RAFT-S-(DIOX/60C)	7	70[a]	75:1:0.75	17900	28850	1.61	1.20
RAFT-G-(DIOX/60C)	7	79[a]	75:1:0.75	8450	15450	1.83	1.19
RAFT-G-(DIOX/70C)	15	58	50:1:0.1	4100	12950	3.16	1.16

[a] Monomer conversion from % recovered yield of homopolymer.

The RAFT polymerisation of MMA has been widely reported[25-27] including *via* the use of CTP as the RAFT agent. In one such example, Guillaneuf *et al*. reported the synthesis of poly(MMA) in 1,4-dioxane, using 4,4'-azobis(cyanopentanoic acid) as an initiator and CTP as RAFT agent at 80 °C.[28] The targeted DP was 10, with a [mon]:[CTA] ratio of 9:1. The high temperature led to some RAFT agent degradation, which was reported to be solvent independent. The reported dispersity was relatively narrow (1.2). The authors did not report M_n, claiming a lack of appropriate calibration standards, but bimodal distributions were observed in the SEC after 6 h. The lower molar mass peak was attributed to unreacted RAFT agent. The presence of unreacted RAFT agent would in-turn have led to higher-than-predicted values for the M_n.

In another example, poly(MMA) was synthesised in bulk, using CTP as the RAFT agent, AIBN as an initiator, at 80 °C.[29] The use of a low initiator molar ratio (100:1 [CTA]:[I]) and short reaction times allowed the polymerisation to be quenched at low conversion (25%) after 1.5 h. The resulting homopolymer was well controlled with a dispersity of 1.18 and the molecular weight (2500 g mol^{-1}) was very close to the theoretical value at the reported monomer conversion. This evidence indicates that CTP could be used to produce poly(MMA) with low dispersity and good control of M_n. In this case, no thermal degradation of the RAFT agent was reported, which could be due to the shorter reaction time.

In the current study, a homopolymer of MMA (RAFT-M-(DIOX/60C)) was synthesised in 1,4-dioxane, at 60 °C, using molar ratios of 75:1:0.75 [MMA]:[CTP]:[AIBN]. After 7 hours, the reaction was quenched and a pink powdery solid was collected in a 46% yield.

The recovered yield of homopolymer was used to calculate monomer conversion, which could introduce significant experimental error, so the results must be considered with caution. SEC indicated an M_{nSEC} of 8300 g mol^{-1}, which was greater than the M_{nTheo} of 3700 g mol^{-1} by a factor of 2.24, however, the dispersity was narrow (1.07). The high MWF was similar to that observed for RAFT-A-(DIOX). The cause of M_n underestimation was likely to be analogous to ADMA – unconsumed RAFT agent. Despite the compositional drift observed between methacrylamide and methacrylate monomers (Chapter 2), they are both considered "more active monomers" in terms of reactivity with RAFT agents.[1] Thus, the same RAFT agent, in this case CTP, would be expected to behave effectively with both methacrylamides and methacrylates. A similar underestimation of M_{nTheo} has also been reported for the bulk polymerisation of GMA using CPDB as RAFT agent.[30] It was reported that decreasing the [mon]:[CTA] ratio from 100:1 to 65:1 led to greater deviation between M_{nSEC} from M_{nTheo}, an effect that was attributed to i) incomplete RAFT agent consumption or ii) impure RAFT agent. Further evidence for unconsumed RAFT agent is provided above in the discussion of unreacted RAFT agent in the polymerisation of MMA reported by Guillaneuf *et al*.[28]

The polymerisation of MMA was repeated using the same conditions, but the reaction allowed to proceed for 20 h to obtain higher monomer conversion (RAFT-M-(DIOX/60C)-2). The dispersity of the two reactions were identical and the latter experiment resulted in a significantly higher yield (70%). The comparatively lower MWF of RAFT-M-(DIOX/60C)-2 (1.94) could be due to the higher conversion reducing the relative impact of any inhibition period on the observed M_n.

A further homopolymer of MMA was synthesised using an alternative set of reaction conditions: at 70 °C (RAFT-M-(DIOX/70C)) and with a reduced initiator molar ratio. The low initiator molar ratio/higher temperature combination is desirable compared to the previous high initiator mole ratio at a lower temperature, as fewer radicals are generated throughout the reaction. The reaction was carried out in 1,4-dioxane using molar ratios of 100:1:0.1 [MMA]:[CTP]:[AIBN]. A sample of RAFT-M-(DIOX/70C) withdrawn after 5 h yielded a $\ln([mon]_0/[mon])$ value of 0.18, indicating that the inhibition period, if any, in the MMA polymerisation was much shorter than the ~4h observed for the ADMA polymerisation (although direct comparisons of the reactivity with the RAFT agent cannot be drawn as the reaction conditions had been changed). SEC analysis of RAFT-M-(DIOX/70C) indicated a low dispersity (Đ = 1.04) which suggested the new conditions still

afforded good control over the dispersity of poly(MMA). The MWF was 1.95, which indicated molecular weight control was very similar to RAFT-M-(DIOX/60C) and RAFT-M-(DIOX/60C)-2. Furthermore, the monomer conversion of 75% after 24 h indicated the rate of monomer conversion was not significantly affected by the change in conditions. Overall, the change in conditions did not appear to affect the polymerisation, although the effect of each individual change cannot be isolated.

A homopolymer of SMA was also synthesised to compare the conditions used to polymerise MMA with a more hydrophobic monomer, carrying a non-polar C18 alkyl chain. An SMA homopolymer synthesised using RAFT polymerisation has been reported previously[31] using CPDB as the RAFT agent, toluene as solvent and with molar ratios of 20:1:0.2 [mon]:[CTA]:[I]. In that case the reaction was allowed to proceed at 70 ^{o}C for 16 h at which point the resulting homopolymer had an M_n of 6450 g mol^{-1}, compared to an M_{nTheo} of 7000 g mol^{-1} (assuming 100% monomer conversion) and a dispersity of 1.15, which can be considered to be well controlled. Synthesis of poly(SMA) using CTP has not been reported previously to the best of our knowledge.

In the current investigation, the polymerisation of SMA was carried out using CTP as the RAFT agent (RAFT-S-(DIOX/60C). The reaction was carried out at 60 °C using 1,4-dioxane and molar ratios were 75:1:0.75 [SMA]:[CTP]:[AIBN]. SEC data (see Table 3.2) indicated that the dispersity was relatively well controlled (Đ = 1.20). M_{nSEC} was 28850 g mol^{-1}, which was higher than M_{nTheo} (17900 g mol^{-1}) by a factor of 1.61. A possible cause for this could be more efficient recovery of poly(SMA) from methanol due to the lower polarity of the homopolymer compared to poly(MMA); incomplete recovery of poly(MMA) when precipitated in methanol has been previously reported, wherein very low molecular weight chains but also high molecular weight, highly branched chains were slightly soluble in methanol.[32] Thus recovery by precipitation in methanol may lead to reduced yields and an over-estimation of the actual molar mass, due to a loss of low molecular weight chains. Moreover, the small scale of the reaction could have resulted a reduction in recovered yield, due to the reduced efficiency of recovering a small amount of precipitated polymer. Incomplete recovery of poly(MMA) could result in an underestimation of conversion, potentially obscuring similar poly(MMA) and poly(SMA) conversion, which would indicate similar reactivity of the two monomers. It is likely that incomplete consumption of RAFT agent remained the predominant cause for the poor molecular weight prediction as the radical reactivity is expected to be similar for the

methacrylate monomers used in this study. Furthermore, the underestimation of MMA conversion would lead to overestimation of M_{nTheo} and therefore a higher MWF in this case, indicating the control of the MMA homopolymerisation could be slightly better than suggested above.

A homopolymer of GMA (RAFT-G-(DIOX/60C) was also synthesised using identical conditions to that used for the synthesis of RAFT-S-(DIOX/60C). The resulting poly(GMA) was collected in a yield of 79% after 7 h, representing an increased yield compared to the polymerisations of MMA. SEC analysis of the product indicated a relatively low dispersity (Đ = 1.19). However, the M_{nSEC} of 15450 g mol^{-1} was once again higher than M_{nTheo} (8450 g mol^{-1}) by a factor of 1.83. This deviation from molecular weight control is similar to the observations made for SMA, MMA and ADMA polymerised in 1,4-dioxane and suggests a common factor between the loss of control in the homopolymer syntheses.

A further homopolymer of GMA was synthesised (RAFT-G-(DIOX/70C)) using a higher [CTP]:[AIBN] ratio to investigate an alternative set of reaction conditions (50:1:0.1 of [GMA]:[CTP]:[AIBN] in 1,4-dioxane at 70 °C), conditions which were similar to those used for the polymerisation of MMA (RAFT-M-(DIOX/70C)). The rate of homopolymerisation was slow, only reaching 59% conversion after 16 h, although SEC analysis indicated reasonable control of dispersity (Đ = 1.16) however, both of the GMA homopolymers had higher dispersity values than the poly(MMA) samples. As a higher value of the chain transfer coefficient (C_{tr}, see Equation 1.26) is associated with greater control of dispersity, it could be speculated that the reduced control for GMA compared to MMA could be due to a higher k_p for GMA, which has been reported in free radical polymerisation.[33]

M_{nSEC} was significantly higher than M_{nTheo}, by a factor of 3.16. The increased MWF with lower [mon]:[CTA] was in agreement with the previously discussed report for poly(GMA) synthesis,[30] although as the initiator concentration was also changed, the precise reason for the MWF increase cannot be identified. An increase in rate retardation and inhibition has been observed when molar ratio of monomer to RAFT agent is decreased, and assigned to inhibition due to the RAFT agent, which may disrupt the pre-equilibrium.[20] Therefore, it may be speculated that the interference with the pre-equilibrium may cause loss of

molecular weight control, particularly in the case of a lower [mon]:[CTA] (and thus higher molar ratio of RAFT agent).

In summary, MMA, GMA and SMA homopolymers were synthesised under conditions which had not previously been explored. Narrow dispersities were obtained in all cases which suggests that the equilibrium was functioning well, and termination was supressed. However, incomplete consumption of RAFT agent resulted in a deviation from the anticipated molecular weight control.

3.4.2 Synthesis of statistical co/terpolymers containing ADMA by RAFT polymerisation

Due to the many potential polymer architectures (block, star etc) available *via* RAFT polymerisation, statistical copolymerisations are reported less regularly. Despite this, the synthesis of statistical copolymers by RAFT copolymerisation is potentially useful as (almost) all chains grow statistically throughout the whole polymerisation, termination is limited, and whilst compositional drift may still occur, a controlled statistical copolymerisation will result in copolymers in which all chains have almost identical monomer composition.[34] The use of two or more monomers with dissimilar reactivity ratios is expected to result in the synthesis of gradient copolymers (*i.e.* with statistically predictable compositional heterogeneity along copolymer chains).[2] This approach has been used to synthesise gradient copolymers which are capable of phase separation or self-assembly.[34] Gradient copolymers have also been shown to have different crystallinity and morphology compared to (random) statistical copolymer analogues.[35] Thus the synthesis of gradient copolymers allows greater scope to investigate the effect of monomer sequence distribution on the physical and chemical properties of such functional copolymers compared to block copolymers or copolymers synthesised by FR polymerisation.

A series of statistical copolymers comprising ADMA and a methacrylate comonomer (MMA, GMA, SMA or HEMA), previously unreported to the best of our knowledge, were synthesised using RAFT polymerisation. Additionally, a terpolymer comprising HEMA, GMA and ADMA was synthesised. The extent of ADMA incorporation in these co/terpolymers is compared with the free radical equivalents reported in Chapter 2.

The reactivity ratios for the free radical copolymerisation of ADMA with i) MMA and ii) GMA in 1,4-dioxane at 70 °C were determined, discussed in Chapter 2 and have been reported in a recently published manuscript.[36] The reactivity ratios were i) $r_{MMA} = 2.21 \pm 0.26$ and $r_{ADMA} = 0.17 \pm 0.03$ and ii) $r_{GMA} = 1.96 \pm 0.49$ and $r_{ADMA} = 0.18 \pm 0.08$. The

reactivity ratios indicated in both cases that the methacrylate comonomer is polymerised preferentially at all monomer feed mole ratios, resulting in significant compositional drift. Reactivity ratios are not expected to change significantly when switching between free radical and RAFT reactions (except at very low conversion where the relative affinity of the monomers for the RAFT agent may affect the composition).[2] Thus, no attempt to estimate reactivity ratios during RAFT polymerisation was made. Assuming the reactivity ratios of ADMA in copolymerisation with MMA/GMA are indeed the same in RAFT and FR polymerisation, the expected compositional drift would lead to a gradient in comonomer composition along the copolymer chains. Thus, the chains would initially be comprised predominantly of the methacrylate monomer whilst ADMA would be increasingly incorporated as the mole fraction of ADMA in the instantaneous monomer feed increased.

Having established suitable conditions for the RAFT polymerisation of ADMA, specifically using molar ratios of [mon]:[CTA]:[I] = 75:1:0.75 at 60 °C, statistical copolymerisation reactions of ADMA with methacrylate comonomers were carried out using similar conditions (see Table 3.3).

Table 3.3. Data for a series of statistical RAFT copolymerisations. The molar feed ratios were [mon]:[CTA]:[I] = 75:1:0.75 and temperature was 60 °C in all cases.

Copolymer	Time / h	ρ / %	Composition of copolymer[b]	M_{nTheo} / g mol^{-1}	M_{nSEC} / g mol^{-1}	MWF	Đ
RAFT-MA-90/10	7	63[a]	90/10	5750	13600	2.37	1.06
RAFT-MA-50/50	7	69[a]	57/43	9650	12870	1.33	1.14
RAFT-GA-90/10	7	78[a]	90/10	10700	25100	2.35	1.23
RAFT-SA-90/10	7	65[a]	93/7	22700	31980	1.41	1.07
RAFT-SA-50/50	7	33[a]	59/41	20500	15250	0.74	1.14
RAFT-HA-90/10	24	89	93/7	13150	9700	0.74	1.38
RAFT-HGA-80/10/10	22	94	80/12/8	11700	10850	0.93	1.32

[a] Monomer conversion from % recovered yield of collected copolymer. [b] Relative to order of monomers in copolymer name, calculated by ^{1}H NMR

Two poly(MMA-*stat*-ADMA) copolymers were synthesised in 1,4- dioxane at 60 °C using RAFT polymerisation. Molar feed ratios of 90/10 and 50/50 (MMA/ADMA) were selected to investigate the effect of monomer feed molar ratio on the dispersity and M_n of the

resulting copolymers, as well as on the final copolymer composition when each reaction was terminated after 7 hours.

SEC analysis of RAFT-MA-90/10 (see Table 3.3) indicated a very narrow dispersity (1.06), however M_{nSEC} was higher than M_{nTheo} by a factor of 2.37. This finding is perhaps not surprising considering the similar observations for the previously discussed RAFT homopolymerisations of both MMA and ADMA under the same conditions. The dn/dc value of MMA was used for molar mass analysis, as the low mole fraction of ADMA should not significantly affect the dn/dc, although this is a source of minor error in the M_n calculations.

NMR analysis was used to calculate the composition of the final copolymers using Equation 2.3, as described previously in Chapter 2. The monomer composition of RAFT-MA-90/10 was the same as in the monomer feed (see Table 3.3), which is slightly surprising given the significant difference in reactivity ratios and the incomplete reaction; a lower incorporation of ADMA might have been expected. However, as previously discussed, the accuracy of the calculations could be affected by significant potential experimental errors, particularly in using the recovered yield as a proxy for conversion, potentially resulting in an underestimation of conversion and an overestimate of M_{nTheo}. In reality, the actual conversion is likely to be significantly higher than the apparent conversion based on recovered yield and this may explain the level of ADMA incorporation and high MWF.

The analogous copolymer synthesised by free radical polymerisation (FR-MA-90/10, see Chapter 2) had a final composition of 92/8 (mol% MMA/ADMA) with a 93% monomer conversion, and the FR copolymerisations had significant incorporation of ADMA throughout the reaction. As such, the composition of RAFT-MA-90/10 can be considered to be within the expected range.

When the molar ratio of ADMA in the feed was increased (RAFT-MA-50/50), M_{nSEC} was higher than M_{nTheo} by a factor of 1.33. This was surprisingly low when compared to the homopolymer MWF values. A source of potential error arises from the use of the dn/dc for MMA to calculate M_{nSEC}. SEC data can be reanalysed using a calculated dn/dc value according to Equation 3.4:

$$\left(\frac{dn}{dc}\right)_C = W_A\left(\frac{dn}{dc}\right)_A + W_B\left(\frac{dn}{dc}\right)_B \qquad \textbf{3.4}$$

where W_A and W_B are weight fractions of the monomer units in the copolymer and C is the copolymer.[37] The dn/dc value for the MMA and ADMA homopolymers were used and a copolymer dn/dc of 0.112 mL g^{-1} was calculated. Recalculation of M_n yielded an MWF value of 1.01. This indicated excellent control over the molecular weight was achieved. NMR analysis of the final copolymer indicated the composition of the final copolymer was 57/43 (mol% MMA/ADMA). This reflected the difference in reactivity ratios between the two monomers and was very similar to the equivalent copolymer synthesised by free radical polymerisation (FR-MA-50/50) which had a composition of 55/45 (mol% MMA/ADMA).

A copolymer of ADMA with GMA (RAFT-GA-90/10) was also synthesised under the same conditions – see Table 3.3. SEC analysis indicated that the M_{nSEC} was higher than M_{nTheo} by a factor of 2.35 – very similar to the equivalent MMA/ADMA copolymer. Similar errors to those discussed above may have also affected the data. A relatively narrow dispersity (1.23) was measured for RAFT-GA-90/10, albeit poorer than the equivalent copolymerisation of MMA and ADMA (Đ = 1.06 for RAFT-MA-90/10). The increase in dispersity when MMA was replaced with GMA was also observed when comparing the homopolymerisations of MMA (Đ = 1.07 for RAFT-M-(DIOX/60C)) and GMA (Đ = 1.19 for RAFT-G-(DIOX/60C)) under identical conditions and was speculatively attributed to the higher k_p of GMA.[33]

Analysis of the copolymer using ^{1}H NMR again indicated the final copolymer composition was 90/10 (GMA/ADMA). Therefore, for copolymers of both GMA and MMA with ADMA, incorporation of 10 mol% ADMA did not significantly impact the dispersity, and ADMA was incorporated well into the copolymers. Considering the potential errors discussed previously, the molecular weight control was not significantly worse in the copolymers than the equivalent homopolymers.

To further expand the library of catechol-containing copolymers, two statistical copolymers of SMA and ADMA were synthesised under exactly the same conditions (RAFT-SA-90/10 and RAFT-SA-50/50 – see Table 3.3). SEC analysis indicated the dispersity of RAFT-SA-90/10 was low (Đ = 1.07) and similar to that observed for the copolymerisations of MMA and ADMA. M_{nSEC} was higher than M_{nTheo} by a factor of only 1.41, which was an improvement compared to copolymers of ADMA with MMA and GMA. A lower MWF for copolymers of SMA with respect to the MMA and GMA was

also observed in the synthesis of homopolymers, indicating increased control over the molecular weight. However, as a result of the use of recovered yield as a proxy for conversion, reduced experimental error is expected for SMA-containing copolymers as they are recovered from methanol more efficiently than MMA and GMA-containing copolymers. Therefore, the M_{nTheo} value is more accurate for copolymers comprising SMA, and the MWF closer to 1. In this case, incorporation of ADMA in the copolymer was again very similar to the previously discussed gradient copolymers, reaching a final mole ratio of 93/7.

For RAFT-SA-50/50, the molecular weight obtained was in reasonable agreement with the expected molar mass. M_{nSEC} was lower than the M_{nTheo} by a factor of 0.74. This was analogous with the reduction of MWF when the proportion of ADMA was increased to 50 mol% in the MMA/ADMA polymerisation. It was hypothesised that the reduction in the MWF could be also be due to the error in actual dn/dc, as the dn/dc for MMA was used in both cases. This would result in a different value from SEC analysis. However, recalculation using a dn/dc of 0.092 mL g^{-1}, obtained from Equation 3.4, resulted in an even lower MWF of 0.69. No reasonable explanation could be found for the extremely low yield for RAFT-SA-50/50 (33%). Compared to RAFT-SA-90/10, the dispersity of RAFT-SA-50/50 increased to 1.14, although it remained in the same range as the homopolymer of SMA (RAFT-S-(DIOX/60C), Đ = 1.20).

To further expand the library of copolymers to include an example with a more hydrophilic character, a copolymer of ADMA and HEMA (RAFT-HA-90/10) was also synthesised under identical conditions. Due to the insolubility of poly(HEMA) in 1,4-dioxane, it was necessary to use DMF as a solvent. The conversion of RAFT-HA-90/10 was expected to be similar to the previously described ADMA-containing copolymers, which only reached a maximum of 78% conversion, although as the conversion was calculated only from recovered yield, these values may underestimate the true conversion. As such, for RAFT-HA-90/10, NMR was used to obtain a more accurate conversion and the reaction time was increased to 24 hours to ensure the reaction reached a high monomer conversion compared to the previously described copolymer syntheses. SEC analysis of RAFT-HA-90/10 indicated a somewhat higher dispersity (Đ = 1.38), indicating poor dispersity control relative to the previously discussed ADMA copolymers. The cause of the poor dispersity control is unclear, but it could be speculated that the longer reaction time for RAFT-HA-90/10 may have led to an increase in side reactions such as bimolecular

termination, resulting in a higher dispersity. In comparison, the methacrylate homopolymer syntheses discussed in section 3.4.1.2 reached high conversion after only 7 h and maintained good control of dispersity. M_{nSEC} was lower than M_{nTheo} by a factor of 0.74, indicating reasonable control of the molecular weight. The observed and theoretical molar mass were thus in reasonable agreement in light of the previously discussed potential errors. The dramatic decrease in MWF indicates improved control of the polymerisation when using DMF as a solvent and HEMA as a monomer. This could indicate that increased H-bonding from HEMA increased the stability of the propagating radical and thus reduced side reactions, as previously reported[38] and discussed in Chapter 2.

NMR analysis indicated the total monomer conversion of RAFT-HA-90/10 was 89% after 24 h and the final molar composition was 93/7 (HEMA/ADMA). This was in the range observed for the previous copolymerisations and indicated a copolymer with a slight gradient in monomer composition was formed. When the reaction was quenched, 34 % of the residual monomer was ADMA, strongly supporting the assertion that a gradient copolymer was formed.

Finally, a terpolymer comprising of HEMA, GMA and ADMA (RAFT-HGA-80/10/10) was synthesised. Reaction time, temperature and the ratio of [mon]:[CTP]:[AIBN] were identical to RAFT-HA-90/10 (DMF, 24 h, 60 °C, 75:1:0.75 [mon]:[CTP]:[AIBN]). The MWF of 0.94 indicated excellent control of the molecular weight, subject to the errors which have been discussed previously. However, as monomer conversion was calculated by NMR, rather than inferred from recovered yield the potential experimental error is significantly reduced in this case. The dispersity, 1.32, indicated reasonable dispersity control, although poor compared to the ADMA copolymers with MMA, GMA and SMA and similar to that of the HEMA/ADMA copolymer (RAFT-HA-90/10).

NMR analysis of RAFT-HGA-80/10/10 indicated a total monomer conversion of 95% and a final composition of 82/10/7. This suggests a similar degree of compositional drift to that seen for RAFT-HA-90/10. Furthermore, NMR analysis of the reaction mixture at the time of termination indicated that 53 % of the residual monomer was ADMA. This strongly suggested the synthesis of gradient copolymer chains with HEMA and GMA incorporated in preference at the start of the chains, and an increasing concentration of ADMA towards the end of the chains.

3.4.3 Synthesis of statistical terpolymers by RAFT polymerisation containing DMA, HEMA and GMA

As discussed in Chapter 2, deprotection of the ADMA monomer repeat units in a copolymer also containing GMA repeat units presented a significant challenge, since the trifluoroacetic acid used as the deprotecting reagent could result in ring-opening of the epoxide groups. Therefore, the synthesis of statistical copolymers using unprotected DMA was attempted. As discussed previously, the synthesis of copolymers comprising unprotected DMA has been reported, however the mole fraction of DMA was limited to ~40% to prevent crosslinking due to the formation of a network of aryloxy bonds between DMA side chains, instigated by radical scavenging reactions (see Chapter 2).[6] To the best of our knowledge, the syntheses of statistical copolymers of DMA or ADMA with one or more comonomer(s) have not been previously compared under identical RAFT polymerisation conditions. Herein, the synthesis of three terpolymers consisting of HEMA, GMA and DMA using RAFT polymerisation is reported for comparison with RAFT-HGA-80/10/10 and for potential further study in coating applications. The conditions and results for the terpolymerisations are reported in Table 3.4.

Table 3.4. Statistical terpolymers containing HEMA, GMA and DMA by RAFT polymerisation in DMF.

Terpolymer	ρ /%	Composition	M_{nTheo} / g mol^{-1}	M_{nSEC} / g mol^{-1}	MWF	Đ
RAFT-HGD-80/14/6[a]	96	79/16/5	10100	16800	1.66	1.44
RAFT-HGD-80/10/10[b]	95	73/21/5	20000	30650	1.53	1.55
RAFT-HGD-74/13/13[c]	92	78/14/8	9700	24950[d]	2.57	2.18

a) 60 °C, [mon]:[CTP]:[AIBN] =75:1:0.75. b) 60 °C, [mon]:[CTP]:[AIBN] =150:1:0.75. c) 70 °C, [mon]:[CTP]:[AIBN] =75:1:0.2. d) M_{nSEC} calculated relative to PS conventional calibration

The first terpolymer, RAFT-HGD-80/14/6, was synthesised using identical conditions to the analogous terpolymerisation comprising ADMA (RAFT-HGA-80/10/10): DMF solvent, 60 °C, [mon]:[CTP]:[AIBN] of 75:1:0.75 for 24 h. SEC analysis gave M_{nSEC} of 16800 g mol^{-1} and a dispersity of 1.44. The SEC data indicated a further deterioration in control of dispersity compared to the already borderline dispersity control of RAFT-HGA-80/10/10, which could be caused by the radical scavenging by DMA. The dispersity could also be affected by radical side reactions caused by the catechol functionality including irreversible chain coupling or crosslinking.[6] In contrast to the excellent molecular weight control observed for RAFT-HGA-80/10/10, the M_{nSEC} for

RAFT-HGD-80/14/6 was higher than M_{nTheo} (10100 g mol^{-1}) by a factor of 1.66. Again, this could be due to radical scavenging from the DMA reducing the incorporation of the RAFT agent.

The reaction reached a combined monomer conversion of 96% in 24 h indicating there was no strong rate retardation in the presence of DMA, despite the suspected radical scavenging. The final terpolymer composition, based on NMR analysis, was 79/16/5, showing that all three monomers had been incorporated into the chain. The final (unreacted) monomer feed contained 38% DMA, 56% HEMA and 6% GMA, clearly showing that, as expected from the compositional drift observed in Chapter 2, HEMA and GMA were polymerised in preference to DMA.

A second HEMA/GMA/DMA terpolymer (RAFT-HGD-80/10/10) was synthesised using the same reaction conditions as RAFT-HGD-80/14/6 (DMF solvent, 60 °C, 24 h). However, the molar ratio of [mon]:[CTP]:[AIBN] was adjusted to 150:1:0.75, to alter the target molecular weight. SEC analysis of the resulting terpolymer suggested that the RAFT polymerisation yielded poor dispersity control (Đ = 1.55), as this approached the range expected for a free radical copolymerisation. In contrast, M_{nSEC} was higher than the M_{nTheo} by a factor of 1.53, virtually the same as RAFT-HGD-80/14/6. Considering the error associated with the SEC data, the outcome of both polymerisations can be considered rather similar. Some crosslinking was evident in the SEC chromatogram in the form of high molecular weight shoulders, which increased in intensity as the feed mole fraction of DMA in the terpolymers in Table 3.4 increased (see Figure 3.3). These high molecular weight shoulders were also observed in analogous terpolymers synthesised using free radical (FR) polymerisation (Chapter 2), which were assigned to chain coupling caused by intermolecular reaction of a catechol side-chain radical with other DMA side-chains. The MWF of both terpolymers was much higher than RAFT-HGA-80/10/10. This suggested the presence of unprotected DMA significantly reduced control over molecular weight, which could indicate side reactions occurred between DMA and RAFT agent when the RAFT pre-equilibrium was set up, resulting in incomplete RAFT agent usage. The presence of the high molecular weight peaks for RAFT-HGA-80/10/10 would also increase the MWF.

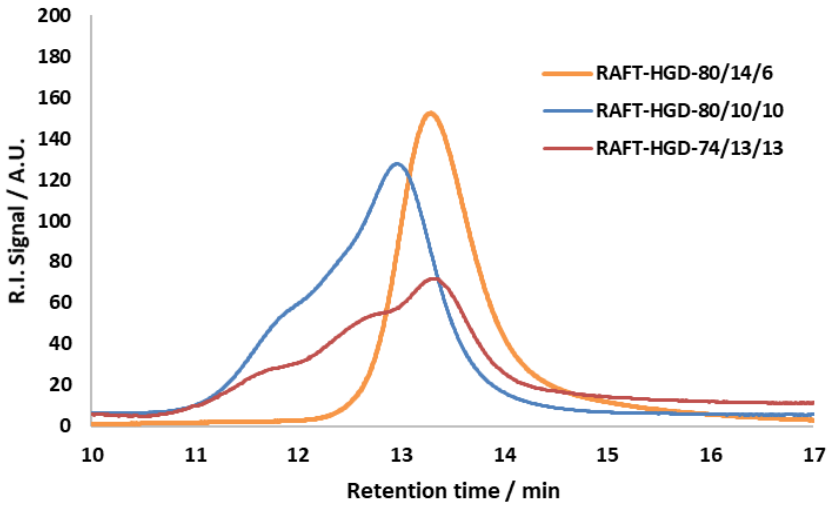

Figure 3.3. SEC chromatogram for statistical terpolymers RAFT-HGA-80/14/6, RAFT-HGA-80/10/10 and RAFT-HGA-74/13/13

The total (final) monomer conversion of RAFT-HGD-80/10/10 was 95%, and the final molar composition was 73/21/5. DMA comprised 25% of the residual monomer in the final sample (66% HEMA, 9% GMA). This strongly suggested a gradient copolymer was formed.

A further terpolymer, RAFT-HGD-74/13/13, was synthesised using modified reaction conditions, which were similar to those used for RAFT-M-(DIOX/70C). The temperature was increased to 70 °C and the [mon]:[CTP]:[AIBN] was adjusted to 75:1:0.2. The reduced mole fraction of initiator should generate less radicals throughout the reaction and was used in an attempt to reduce dispersity. However, SEC analysis of the resulting terpolymer revealed an M_{nSEC} of 24950 g mol^{-1} (MFW = 2.57) and a dispersity of 2.18, clearly indicating that this polymerisation was less, rather than more, controlled. It should be pointed out though, that a weak light scattering signal in the SEC analysis meant that M_{nSEC} was obtained using a conventional calibration with PS standards, and as such this value should be treated with some caution. In an attempt to quantify the potential inaccuracy RAFT-HGD-80/14/6 was also analysed using the same conventional calibration, resulting in an M_n value of 22800 g mol^{-1} (from 30650 g mol^{-1} using triple detection), indicating the true molecular weight of RAFT-HGD-74/13/13 was likely to be over 30000 g mol^{-1}. This effectively means the MWF of HGD 74/13/13 was even higher. The molecular weight of RAFT-HGD-74/13/13 can be thus considered uncontrolled, probably due to side reactions between the DMA and RAFT agent at the higher reaction temperature. The composition

of RAFT-HGD-74/13/13, obtained by NMR, was 78/14/8, indicating the DMA was not fully incorporated and a gradient terpolymer structure is likely.

In summary, terpolymers of HEMA, GMA and DMA were successfully synthesised, albeit with poor dispersity control in comparison to RAFT-HGA-80/10/10, which was ascribed to DMA-instigated chain-coupling side reactions. Polymerisation with a low temperature and high mole fraction of initiator afforded more control of the polymerisation.

3.4.4 Synthesis of diblock copolymers using RAFT polymerisation

RAFT polymerisation enables the synthesis of block copolymers using a wide variety of monomers. Block copolymers are valuable as the advanced polymer architecture can deliver physical properties which differ in comparison to statistical copolymers and can lead to microphase separation,[39] self-assembly,[14, 40] and many other specialised properties.[41]

In a RAFT copolymerisation, the first (α) block acts as a macro-RAFT agent for the synthesis of the second (β) block. In a macro-RAFT agent, the α-polymer chain serves as a macro-R group for the initiation of the β-block; as such, the α-polymer chain must be a good homolytic leaving group and be able to efficiently reinitiate a polymerisation of the β-block.[18] In practice this means that "more activated monomers" (MAMs) should be polymerised first (to form the α-block) with respect to "less activated monomers" (see description in Section 1.5.2). Furthermore, when designing block copolymers from two MAMs, monomers which produce tertiary radicals in the propagating chain (*e.g.* methacrylates and methacrylamides) should be polymerised before those which produce more reactive secondary radicals (*e.g.* acrylates and acrylamides).

The monomers used in the current work are methacrylates and methacrylamides; both produce relatively stable tertiary propagating radicals and should thus be effective as macro-chain transfer agents for each other. Methacrylamides are more able to donate electron density to stabilise the propagating radical than methacrylates and thus methacrylamides may appear a more logical choice for use as a macro-RAFT agent. It has been reported that in the diblock copolymerisation of compatible MAMs (for example ADMA and PEGMEM) that either monomer can be used to prepare the first block and achieve control over M_n and Đ.[14] However, the same report states it is more effective to first prepare the block with the lowest desired DP to avoid loss of control.

Diblock copolymers comprising a block of catechol-containing monomer (DMA or ADMA) were synthesised for a comparison of their properties with statistical copolymers. It was expected that block copolymers may lead to improved copolymer performance over statistical copolymers in the context of the desired application of using the catechol functionalities to adhere to a surface by the "grafting to" method.[6] Reactive side chains (*e.g.* epoxides) could be included in the brush as demonstrated in Figure 3.4A, which may be more available in the "brush" conformation (see Figure 3.4B) than the equivalent monomer repeat units in a statistical copolymer, which may result in loops, as demonstrated in Figure 3.4C.

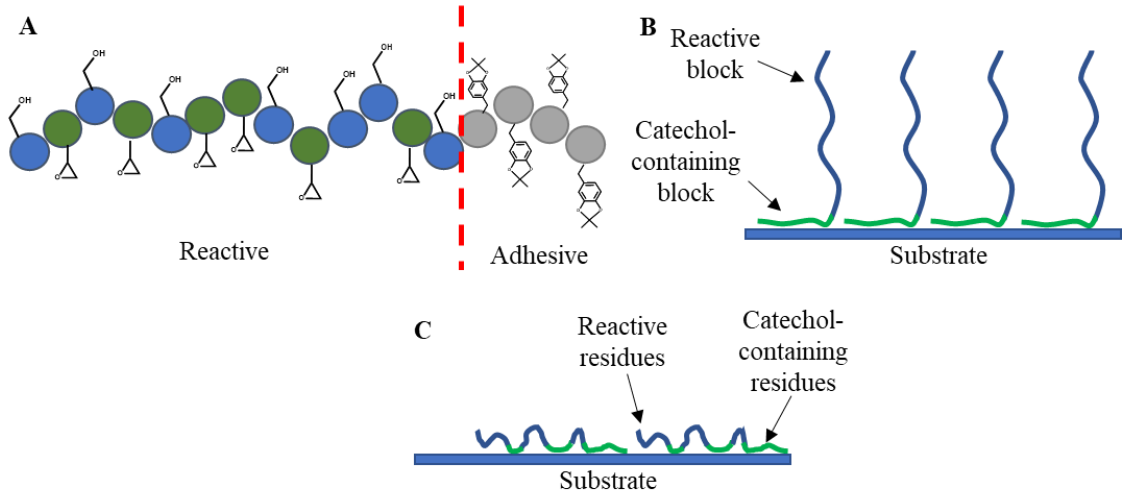

Figure 3.4. A) Schematic representation of block copolymer RAFT-A-*b*-(HG-90/10). B) Schematic of hypothesised mode of adhesion of catechol-containing block copolymer. C) Schematic of hypothesised mode of adhesion of catechol-containing gradient copolymer.

In the current work, the synthesis of block copolymers was attempted using blocks formed from both methacrylate and methacrylamide monomers as macro-RAFT agents. A summary of the conditions and block copolymer characteristics can be found in Table 3.5. For the diblock copolymers it was necessary to modify the naming system. For instance, the name "RAFT-A-*b*-(HG-90/10)" indicates a diblock copolymer in which the α-block is synthesised using ADMA and the β-block with a statistical copolymer of HEMA and GMA comprising a 90/10 molar feed ratio. Results for the α-block homopolymers are discussed above in Section 3.4.1 and reported in Table 3.1.

Table 3.5. Data for diblock copolymers by RAFT polymerisation, synthesised at 60 °C, [CTA]:[I] = 1:0.75

Block copolymer	Block	[Mon]: [CTA]	Time / h	M_{nTheo} / g mol^{-1}	M_n / g mol^{-1}	MWF	Đ
RAFT-M-*b*-A	α[a]	75:1	20	5550	10750	1.94	1.07
	α + β	75:1	20	16600	14600	0.88	1.14
RAFT-A-*b*-(HG-90/10)	α[b]	25:1	24	2800	1700	0.61	1.20
	α + β	200:1	20	28500	38300	1.34	1.14

a) α-block = RAFT-M-(DIOX60C)-2 – see Table 3.2. b) α-block = RAFT-A-(DMF) – see Table 3.1.

A diblock copolymer (RAFT-M-*b*-A) was synthesised using MMA as the α-block and ADMA as the β-block. Molar ratios of [mon]:[CTA]:[I] were 75:1:0.75 [mon]:[CTA]:[I] (1,4-dioxane, 60 °C, 20h). The poly(MMA) α-block was recovered by precipitation in methanol in 70% yield. SEC indicated the dispersity was well-controlled (Đ = 1.07) however, as previously observed and discussed the homopolymerisation of MMA resulted in an M_{nSEC} which was larger than M_{nTheo} by a factor of 1.94. The recovered homopolymer was dried in a vacuum oven to remove residual solvent then used as a macro RAFT agent to initiate the polymerisation of ADMA. The polymerisation of ADMA to form the β-block only reached 28% conversion in 20 h. This led to a value for M_{nTheo} for the block copolymer of 16600 g mol^{-1}, which equated to a DP of 21 for the ADMA in the β-block. However, the DP is subject to the assumption that no ADMA homopolymer is formed in the β-block synthesis. A poly(ADMA) peak is observed in the SEC (Figure 3.5), so the DP of 21 is clearly not accurate.

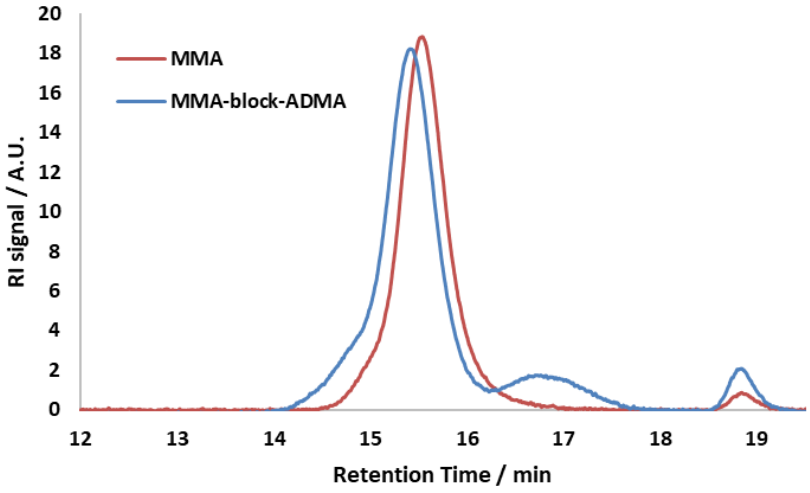

Figure 3.5. SEC chromatogram of block copolymer of MMA and ADMA (RAFT-M-(DIOX)-2 and RAFT-M-*b*-A)

When the RAFT-M-*b*-A block copolymer was analysed by SEC (Figure 3.5), the major peak at retention time 15.5 min corresponded to M_{nSEC} = 14600 g mol^{-1} and Đ = 1.14, indicating in an increase in molar mass of about 4000 g mol^{-1} compared to the macroRAFT agent and a slight increase in dispersity. It is also clear that the peak had shifted to shorter retention time with respect to the macroRAFT agent, as expected. Furthermore, the MWF (0.88) was fairly close to 1. However, a bimodal distribution with a second peak at low M_n (16.5 min) was also observed, which could suggest the formation of a low molar mass ADMA homopolymer. This suggests that although a block copolymer was formed, the macro-RAFT agent was not ideal for significant chain extension. This could have been caused by limited end-group fidelity of the macroRAFT agent, which in turn would lead to a significant proportion of ADMA chains being formed by reaction with initiator-derived radicals. The ^{1}H NMR spectrum of the block copolymer confirmed the presence of both ADMA and MMA (11 mol% ADMA, Figure 3.6).

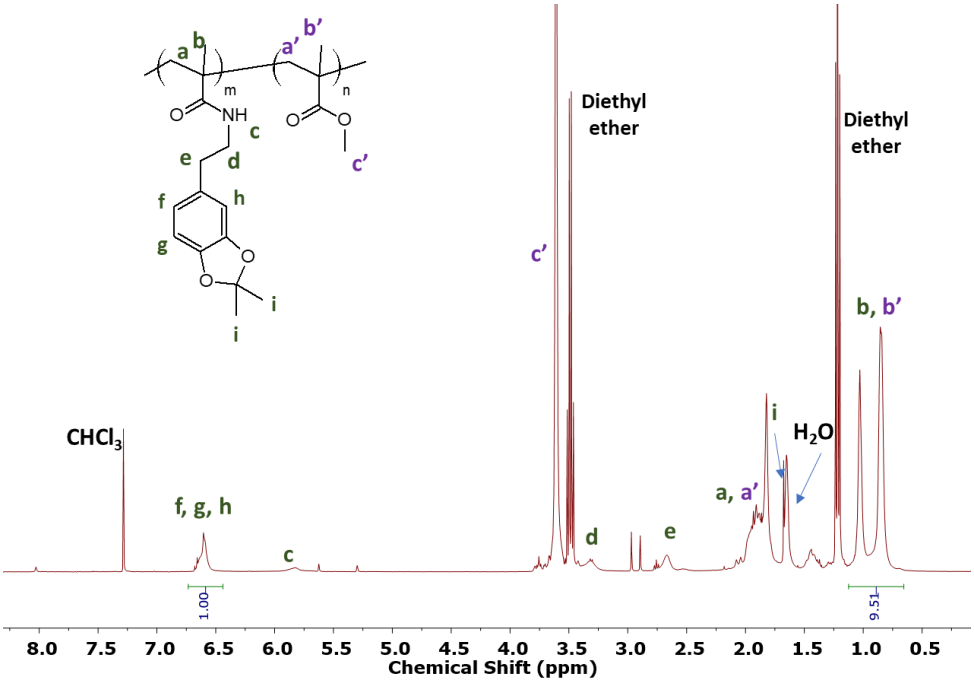

Figure 3.6. ^{1}H NMR spectrum of RAFT-M-*b*-A

As discussed previously, HEMA was used to produce a copolymer with enhanced hydrophilicity/polarity with respect to MMA, and therefore increased solubility of the resulting copolymer in polar solvents such as methanol. GMA was also used to introduce reactive functionality into the copolymers for subsequent reaction with biomolecules in the desired biosensing applications. The same approach was applied to the synthesis of diblock copolymers, and thus a diblock copolymer was synthesised (RAFT-A-*b*-(HG-90/10))

using ADMA as the α-block and a statistical copolymer of GMA and HEMA for the β-block.

RAFT-A-(DMF), described in section 3.4.1.1, was used as the α-block macroRAFT agent. A low mole fraction of monomer to macroRAFT agent was used, DMF was used as the solvent and the reaction was allowed to proceed for 24 h (25:1:0.75 [mon]:[CTA]:[I], DMF, 60 °C). These changes were all motivated by an attempt to maximise the number of active chains in the α-block. For the α-block, a 25:1 [mon]:[CTA] molar ratio was used to target a low molecular weight macro-RAFT agent, which would subsequently enable synthesis of a block copolymer with roughly 10 mol% ADMA. This would enable comparison of the block terpolymer properties with statistical terpolymers with a similar monomer composition. The ^{1}H NMR spectrum, shown in Figure 3.1 clearly indicates the retention of the RAFT agent end groups *via* characteristic signals at 7.3 – 7.9 ppm assigned to protons on the phenyl ring of the Z-group (see section 3.4.1.1).

For the β-block, a statistical copolymer of HEMA and GMA was synthesised using the α-block as a macro RAFT agent (RAFT-A-*b*-(HG-90/10)). Previous work had demonstrated the unsuitability of 1,4-dioxane for the polymerisation of HEMA, so DMF was used for the synthesis of this block copolymer. A high molar ratio of monomer to macro RAFT agent was used to target ~10% mole fraction of ADMA in the final block copolymer (200:1:0.75 [mon]:[CTA]:[I], DMF, 60 °C, 20 h). Monomer conversion reached 91% in 24 h. Peaks arising from the side chains of all 3 monomers are visible in the ^{1}H NMR spectrum *e.g.* 6.72 – 6.60 ppm (DMA), 3.89 ppm (HEMA) and 4.26 ppm (GMA) (see Figure 3.7 for full assignment of peaks). The final block copolymer molar composition was 77/17/6 (H/G/A), confirming the macro RAFT agent was incorporated in the diblock copolymer.

RAFT-A-*b*-(HG-90/10) was analysed by SEC, which indicated M_{nSEC} = 38300 g mol^{-1} and Đ = 1.14. The narrow dispersity suggested the synthesis was well-controlled, however M_{nSEC} was higher than M_{nTheo} by a factor of 1.34, indicating relatively good molecular weight control. The slight loss of control could be due to the reduced RAFT end-group fidelity of the macroRAFT agent, which would lead to inactive chains of ADMA, which would in turn lead to a concomitant higher molar mass for the β-block chains (Figure 3.1). However, despite some tailing, no significant peak for the ADMA homopolymer or residual RAFT agent was observed in the SEC RI trace of the block copolymer (Figure

3.8), further supporting a successful block copolymerisation. The synthesis of RAFT-A-*b*-(HG-90/10) offered good evidence of successful block copolymer synthesis.

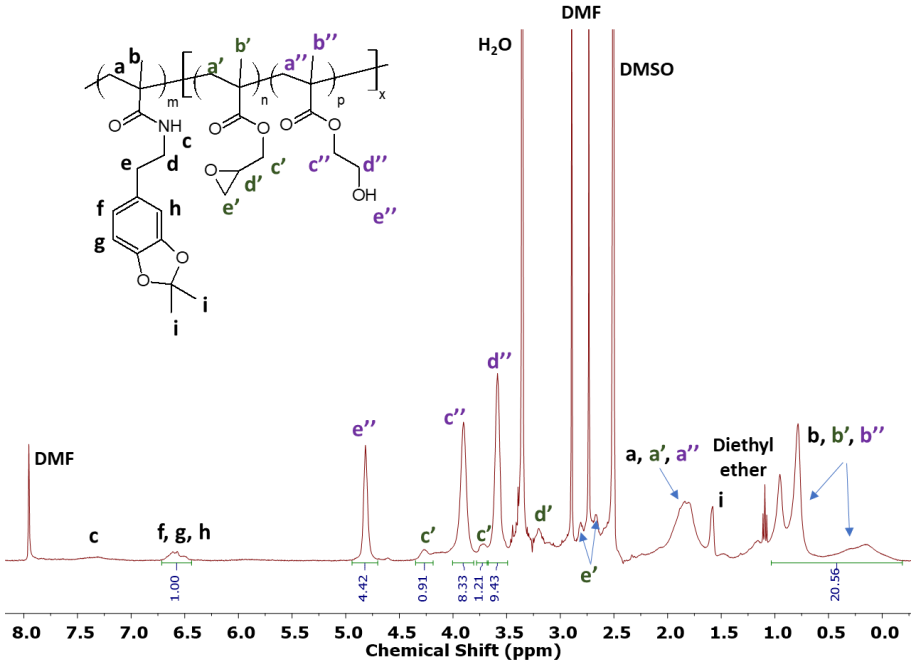

Figure 3.7. ^{1}H NMR spectrum for RAFT-A-*b*-(HG-90/10)

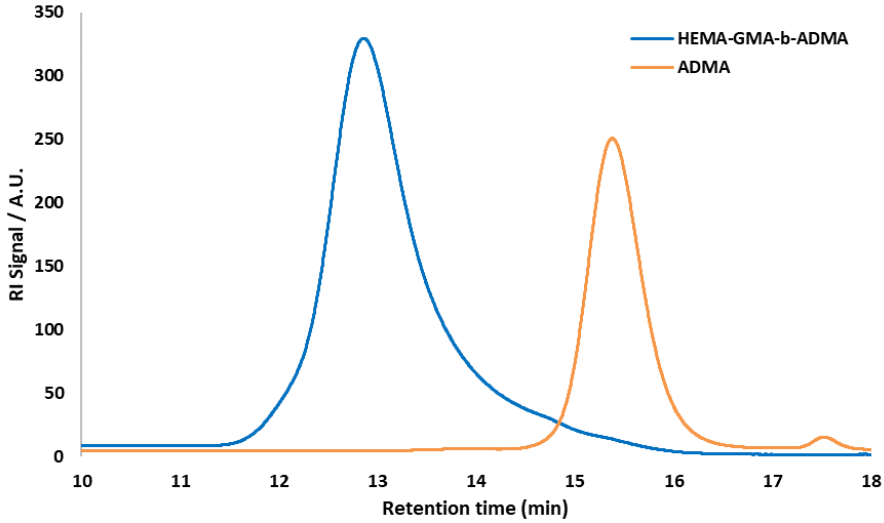

Figure 3.8. RI SEC chromatogram of copolymer of HEMA and GMA and addition of ADMA block RAFT-A-(DMF) and RAFT-A-*b*-(HG-90/10)

3.5 Conclusion

In this chapter, RAFT polymerisation, using CTP as a RAFT agent, was used to synthesise homo-, co- and ter- polymers containing ADMA and DMA. The conditions required to achieve control over the molecular weight and dispersity were investigated. Generally,

good control over dispersity was achieved but control over molecular weight was not optimal.

RAFT polymerisation of ADMA in DMF and 1,4-dioxane yielded homopolymers with good control over dispersity. However, relatively poor control over molecular weight was indicated by a low MWF. It was concluded that the lack of control over molecular weight for the RAFT-A-(DMF) was due to the very low conversion. It was suspected the low conversion was caused by rate retardation due to the relatively high molar ratio of CTA to monomer. In contrast, RAFT-A-(DIOX) went to higher conversion and had a high MWF. The reason for the higher conversion was not clear but was likely to be due to a combination of a reduction in retardation from the higher mole ratio of CTP and a longer reaction time. The high MWF was attributed to incomplete consumption of RAFT agent. This would lead to the formation of fewer propagating chains and hence a higher-than-expected M_n. Despite this, the polymerisation showed *pseudo*-first order polymerisation kinetics, which implied a controlled reaction.

RAFT polymerisation of SMA, MMA and GMA in 1,4-dioxane yielded homopolymers with good control over dispersity, but relatively poor control over molecular weight. It was concluded that the conditions used for the synthesis of RAFT-A-(DIOX) were appropriate for synthesising methacrylate homopolymers with good dispersity control. However, similar to the synthesis of RAFT-A-(DIOX), the MWF was high. The consistently high MWF suggested a common cause for the lack of control, which was again attributed to poor RAFT agent consumption. The use of alternative conditions for the synthesis of homopolymers, in which [CTA]:[I] ratio and temperature were increased, was found to have a minimal effect on control of dispersity or molecular weight and both approaches were considered viable.

Copolymers of ADMA with MMA, GMA, SMA and HEMA and poly(HEMA-*stat*-GMA-*stat*-ADMA) were also synthesised. Narrow dispersities (≤ 1.23) were observed for the copolymers containing MMA, GMA and SMA. Deviation from molecular weight control was observed for the MMA, GMA and SMA copolymers, similar to that observed for the methacrylate homopolymers, and it was concluded that the same cause was likely. In contrast, the HEMA co- and terpolymers were synthesised with excellent molecular weight control, which was attributed to the change in solvent. However, a slight loss of dispersity control ($Đ \leq 1.38$) was observed for the HEMA-containing copolymers. It was also

concluded that the slightly larger dispersities were due to side reactions arising from the longer reaction times used. The extent of monomer compositional drift in RAFT-HA-90/10 and RAFT-HGA-80/10/10 was found to agree closely with the value for the equivalent terpolymer synthesised by free radical copolymerisation. The novel copolymers were useful options from an application perspective.

Attempts to synthesise statistical terpolymers comprising HEMA, GMA and DMA were less successful. Control of dispersity for RAFT-HGD-80/14/6 and RAFT-HGD-80/10/10 was much diminished (>1.5), indicating DMA has a negative effect on control in copolymerisations under the conditions used, probably due chain coupling *via* aryloxy bond formation between catechol side-chains. Control of molecular weight remained reasonable, albeit with M_{nSEC} higher than M_{nTheo}. The high MWF was also attributed to incomplete RAFT agent consumption. Synthesis of RAFT-HGD-74/13/13, using alternative conditions resulted in particularly poor control of polymerisation. It was concluded that side reactions between DMA and the RAFT agent at the higher temperature led to the reduced control. Nevertheless, these statistical terpolymers removed the need for deprotection of ADMA when used in applications testing, so were deemed potentially useful.

Two catechol-containing diblock copolymers were also synthesised. Poly(MMA-*b*-ADMA) was synthesised; poly(MMA) was used as a macro-RAFT agent for the synthesis of the β-block. It was concluded that the block copolymer was a good candidate for a functional adhesive, as it had a narrow dispersity and excellent molecular weight control, although evidence of a small amount of residual poly(MMA) homopolymer was observed. Finally, a functional adhesive block copolymer was synthesised: Poly(ADMA-*b*-(HEMA-*stat*-GMA)). Good control of dispersity and reasonable molecular weight control was observed. If the protecting group was successfully removed, the block copolymers could be used as coatings, potentially forming a brush-like structure. These block copolymers present an interesting avenue for potential future research.

3.6 References

1. S. Perrier, *Macromolecules*, 2017, **50**, 7433-7447.
2. C. Barner-Kowollik, *Handbook of RAFT Polymerization*, Wiley-VCH, 2008.
3. G. Moad, *Polym. Chem.*, 2017, **8**, 177-219.
4. K. K. Georgieff, *J. Appl. Polym. Sci.*, 1965, **9**, 2009-2018.
5. L. R. C. Barclay, C. E. Edwards and M. R. Vinqvist, *J. Am. Chem. Soc.*, 1999, **121**, 6226-6231.
6. N. Patil, C. Jérôme and C. Detrembleur, *Prog. Polym. Sci.*, 2018, **82**, 34-91.
7. J. Yang, J. Keijsers, M. van Heek, A. Stuiver, M. A. Cohen Stuart and M. Kamperman, *Polym. Chem.*, 2015, **6**, 3121-3130.
8. L. Li, B. Yan, L. Zhang, Y. Tian and H. Zeng, *Chem Commun (Camb)*, 2015, **51**, 15780-15783.
9. H. Zhang, T. Zhao, B. Newland, P. Duffy, A. N. Annaidh, E. D. O'Cearbhaill and W. Wang, *J. Mater. Chem. B*, 2015, **3**, 6420-6428.
10. X. Xue, G. Pasparakis, N. Halliday, K. Winzer, S. M. Howdle, C. J. Cramphorn, N. R. Cameron, P. M. Gardner, B. G. Davis, F. Fernandez-Trillo and C. Alexander, *Angew Chem Int Ed Engl*, 2011, **50**, 9852-9856.
11. I. Louzao, C. Sui, K. Winzer, F. Fernandez-Trillo and C. Alexander, *Eur J Pharm Biopharm*, 2015, **95**, 47-62.
12. J. Wang, H. Zhu, G. Chen, Z. Hu, Y. Weng, X. Wang and W. Zhang, *Macromol. Rapid Commun.*, 2014, **35**, 1061-1067.
13. A. GhavamiNejad, A. R. K. Sasikala, A. R. Unnithan, R. G. Thomas, Y. Y. Jeong, M. Vatankhah-Varnoosfaderani, F. J. Stadler, C. H. Park and C. S. Kim, *Adv. Funct. Mater.*, 2015, **25**, 2867-2875.
14. N. Patil, C. Falentin-Daudré, C. Jérôme and C. Detrembleur, *Polym. Chem.*, 2015, **6**, 2919-2933.
15. S. Pearson, N. Allen and M. H. Stenzel, *J. Polym. Sci., Part A: Polym. Chem.*, 2009, **47**, 1706-1723.
16. J. Brandrup and E. H. Immergut, *Polymer Handbook*, Wiley Interscience, 3rd edn., 1989.
17. G. Moad, E. Rizzardo and S. H. Thang, *Aust. J. Chem*, 2005, **58**, 379-410.
18. D. J. Keddie, *Chem. Soc. Rev.*, 2014, **43**, 496-505.
19. R. Plummer, Y. K. Goh, A. K. Whittaker and M. J. Monteiro, *Macromolecules*, 2005, **38**, 5352-5355.
20. C. Barner-Kowollik, M. Buback, B. Charleux, M. L. Coote, M. Drache, T. Fukuda, A. Goto, B. Klumperman, A. B. Lowe, J. B. McLeary, G. Moad, M. J. Monteiro, R. D. Sanderson, M. P. Tonge and P. Vana, *Journal of Polymer Science Part a-Polymer Chemistry*, 2006, **44**, 5809-5831.
21. M. Benaglia, E. Rizzardo, A. Alberti and M. Guerra, *Macromolecules*, 2005, **38**, 3129-3140.
22. A. Goto and T. Fukuda, *Prog. Polym. Sci.*, 2004, **29**, 329-385.
23. S. Perrier, C. Barner-Kowollik, J. F. Quinn, P. Vana and T. P. Davis, *Macromolecules*, 2002, **35**, 8300-8306.
24. D. J. Keddie, G. Moad, E. Rizzardo and S. H. Thang, *Macromolecules*, 2012, **45**, 5321-5342.
25. G. Moad, E. Rizzardo and S. H. Thang, *Aust. J. Chem.*, 2006, **59**, 669-692.
26. G. Moad, E. Rizzardo and S. H. Thang, *Aust. J. Chem.*, 2009, **62**, 1402-1472.
27. G. Moad, E. Rizzardo and S. H. Thang, *Aust. J. Chem.*, 2012, **65**, 985-1076.

28. E. Hosseini Nejad, P. Castignolles, R. G. Gilbert and Y. Guillaneuf, *J. Polym. Sci., Part A: Polym. Chem.*, 2008, **46**, 2277-2289.
29. E. V. Chernikova, A. V. Tarasenko, E. S. Garina and V. B. Golubev, *Polym. Sci. Ser. A*, 2008, **50**, 353-364.
30. C. S. Gudipati, M. B. H. Tan, H. Hussain, Y. Liu, C. He and T. P. Davis, *Macromol. Rapid Commun.*, 2008, **29**, 1902-1907.
31. Y. Pei, L. Thurairajah, O. R. Sugita and A. B. Lowe, *Macromolecules*, 2014, **48**, 236-244.
32. F. Isaure, P. A. G. Cormack and D. C. Sherrington, *J. Mater. Chem.*, 2003, **13**, 2701-2710.
33. S. Beuermann, M. Buback, T. P. Davis, N. Garcia, R. G. Gilbert, R. A. Hutchinson, A. Kajiwara, M. Kamachi, I. Lacik and G. T. Russell, *Macromol. Chem. Phys.*, 2003, **204**, 1338-1350.
34. T. J. Neal, D. L. Beattie, S. J. Byard, G. N. Smith, M. W. Murray, N. S. J. Williams, S. N. Emmett, S. P. Armes, S. G. Spain and O. O. Mykhaylyk, *Macromolecules*, 2018, **51**, 1474-1487.
35. P. Kratochvil and J. Stejskal, *Polimery*, 2001, **46**, 761-767.
36. N. A. Boulding, J. M. Millican and L. R. Hutchings, *Polymer Chemistry*, 2019, **10**, 5665-5675.
37. S. Mori and H. G. Barth, *Size Exclusion Chromatography*, Springer Science & Business Media, 2013.
38. K. Liang and R. A. Hutchinson, *Macromol. Rapid Commun.*, 2011, **32**, 1090-1095.
39. H. C. Kim, S. M. Park and W. D. Hinsberg, *Chem. Rev. (Washington, DC, U. S.)*, 2010, **110**, 146-177.
40. C. Liu, P. Ni, X. Fang and X. Zhou, *Colloid Polym. Sci.*, 2008, **287**, 45-55.
41. F. H. Schacher, P. A. Rupar and I. Manners, *Angew. Chem., Int. Ed.*, 2012, **51**, 7898-7921.

Chapter 4 Optimisation of the deposition of catechol-containing polymer films on model substrates

4.1 Introduction

4.1.1 Coating methodologies

A multitude of methods exist to apply thin (co)polymer films onto substrate surfaces. They include drop-casting, spray-coating, spin-coating, dip-coating, immersion-coating and surface-initiated polymerisation. In this work, spin-coating is utilised as a reliable method to obtain controllable, continuous thin films and immersion-coating is explored as a facile, non-mechanical coating method which takes advantage of the adhesive catechol functionality present in the copolymers.

4.1.1.1 Spin-coating

Spin-coating is widely used in industry, especially in the manufacture of semiconductors, to deposit polymer coatings with controllable film thickness. The substrate, fully wetted with a solution of polymer, is rotated on a sample stage at speeds of $10^3 – 10^5$ revolutions per minute (rpm) until the carrier solvent has evaporated and a thin film has formed.

The spin-coating process has four stages (Figure 4.1).[1-3] First, a polymer solution is placed on a substrate (Figure 4.1A). The substrate must normally be fully wetted by the solution or defects could occur. The second stage involves acceleration of the substrate to the desired rotational velocity, during which excess solution is ejected from the spinning disc, leaving a thin layer of polymer solution (Figure 4.1B). Vortices occur in the solution until it becomes thin enough to co-rotate with the substrate, at which point the viscous shear drag balances the rotational acceleration. The third stage sees gradual thinning of the film as the rotational motion forces the solvent towards the edge of the substrate, and droplets of polymer solution are ejected from the disc (Figure 4.1C). Viscous forces dominate the thinning at this point. In the fourth stage, the viscosity of the film increases dramatically, and evaporation dominates the thinning process (Figure 4.1D). Rotational flow is minimal in this stage, but continued rotation is important to remove remaining solvent.

Further steps may be added after the four initial stages to fully dry or anneal the coatings. The physics of the spin-coating process are complex, as many forces are involved including inertia and centrifugal forces, and many properties of the solution must be considered, such as non-Newtonian behaviour, surface tension and volatility.

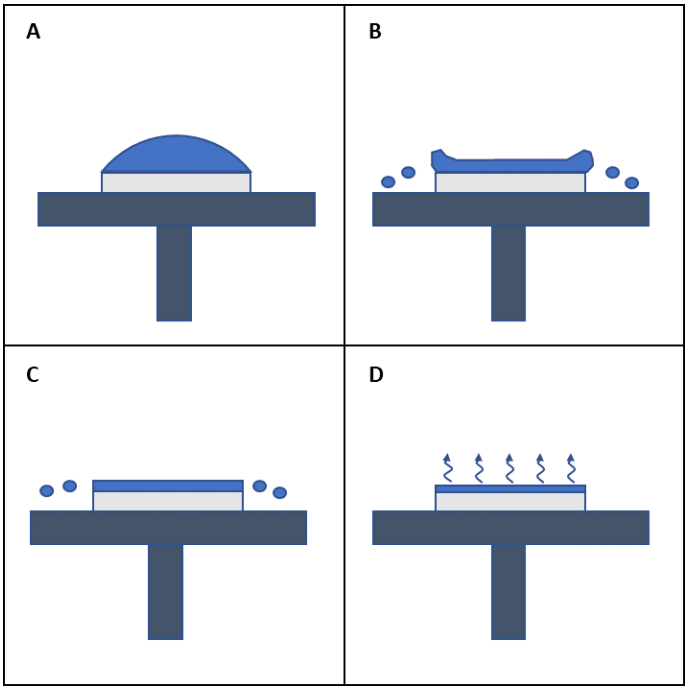

Figure 4.1. Spin-coating process. A) Solution loading B) Acceleration of the substrate C) Thin film formation D) Evaporation-dominated drying.

Defects can be introduced at each stage of the coating process. They include non-continuous films, striations (radial waves or banding) on the surface of the film and edge effects and can be caused by many factors, not all of which are fully understood.[4] Thus, control over the coating conditions is essential for the deposition of uniform films.

4.1.1.2 Immersion-coating

Immersion-coating involves the self-assembly of a coating on a surface which is fully immersed in a polymer solution. In the literature this process is, somewhat confusingly, sometimes often also termed "dip-coating",[5] which usually refers to the commonly used industrial technique involving mechanical removal of a substrate from a polymer solution.[6] For the avoidance of confusion, the self-assembly procedure will be referred to as immersion-coating in the discussion herein.

Immersion-coating is advantageous compared to traditional dip-coating as no mechanical action is required for the former, reducing the potential for defects. Immersion-coating requires a polymer with chemical properties which allow the chains to spontaneously adhere to a substrate surface in solution. Catechol-containing copolymers are particularly suitable for immersion-coating to many surfaces because of the strongly adhesive functionality in solution.[7] Careful control of conditions such as copolymer composition, pH, solvent and temperature have allowed catechol-containing copolymers to be deposited

on many surfaces.[8, 9] Despite the many possible adhesion mechanisms of the catechol group, the ideal conditions for adhesion vary for each combination of copolymer and substrate, so optimisation of conditions is crucial.[10]

4.1.2 Surface analysis techniques

4.1.2.1 Spectroscopic ellipsometry

Spectroscopic ellipsometry (referred to herein as ellipsometry) is a non-destructive technique which is used for characterising transparent thin films, including polymer films. Ellipsometry can provide data about a number of polymer properties, including film thickness, roughness, dielectric properties, swelling, and optical properties, as well as the adsorption of biomolecules or other particles onto the surface *in-situ*.[11, 12]

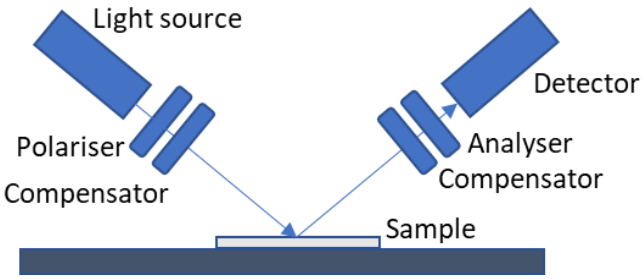

Figure 4.2. Schematic of basic spectroscopic ellipsometer set-up.

In an ellipsometry experiment, polarised light is passed through a semi-transparent film and reflected from the substrate surface into a detector. The changes in polarisation of the light as it passes through the film are used to fit a model, allowing the film thickness and refractive index to be estimated. The most basic set-up for a spectroscopic ellipsometer includes a light source (which can be single or multiple wavelength), a polarising element (polariser and compensator), an analyser, and a detector (Figure 4.2). The more wavelengths of light and angles of incidence used, the more accurate the generated model can be, hence modern ellipsometers scan using multiple wavelengths and light source angles for each measurement.

Many enhancements can be added to ellipsometry, such as a liquid cell for *in-situ* measurements, and combination with infra-red (IR) spectroscopy or quartz-crystal microbalance (QCM), enabling the use of ellipsometry as a sophisticated tool for studying polymer films.[13]

4.1.2.2 Atomic force microscopy

The atomic force microscope was first described in 1986, as a development of the technologies used in a profilometer and a scanning tunnelling microscope.[14] An AFM set

up consists of a probe with a cantilever and sharp tip, controlled by a feedback loop. The tip is scanned across a solid substrate mounted on a piezoelectric scanner (Figure 4.3). One of two types of experiment are commonly used: contact mode, where the tip is in constant contact with the surface, or tapping mode, where the tip is oscillated near its resonant frequency to reduce damage on soft surfaces. A laser, directed at the end of the cantilever and reflected into a detector is used to record the bending of the cantilever (contact mode) or the change in oscillation amplitude and phase (tapping mode).[15] AFM is a valuable technique for surface/film analysis and allows the non-destructive imaging of surface topography to Ångstrom resolution in ambient conditions.

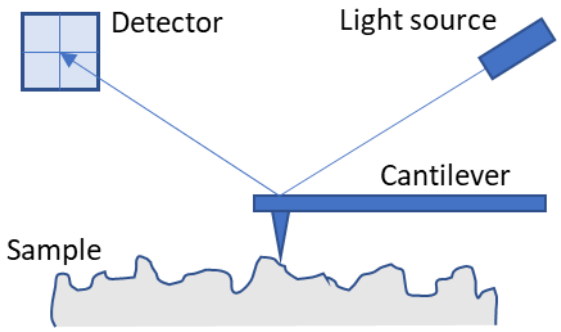

Figure 4.3. Schematic of an AFM set up.

AFM and ellipsometry are considered complementary techniques, as AFM provides direct measurement of roughness and lateral variation in the X-Y direction, whereas ellipsometry provides a non-destructive measure of the film thickness and refractive index. In tandem, the two techniques can give a useful insight into polymer film thickness and topography.

4.2 Aims

The aims of the work reported in this chapter were:

1. To investigate the solubility of selected homo-, co- and terpolymers comprising a variety of methacrylate comonomers. The results of the brief solubility study were used to identify appropriate dopamine methacrylamide (DMA)-containing co- and terpolymers to be used as coatings. A suitable polymer should be soluble in highly polar solvents (*e.g.* methanol or dimethylformamide (DMF)) to enable its deposition in microfluidic devices where the use of solvents such as tetrahydrofuran (THF) and chloroform is inappropriate.

2. To optimise conditions for spin-coating of a series of copolymers from methanol solution onto silicon wafer substrates. The impact of copolymer composition and molecular weight on the topography and film thickness of copolymer thin films, including

identification of defects in the film, were investigated using ellipsometry and AFM. The effect of spin-speed, acceleration of the disc and solution concentration on film thickness and topography was also considered.

3. To optimise conditions for copolymer spin-coating from DMF solution onto silicon wafer substrates, and to compare these coatings with the same copolymer films deposited using methanol. Additionally, high molecular weight copolymer containing an increased mole fraction of DMA were spin-coated to investigate the effect of increased solution viscosity on film thickness and topography.

4. To optimise conditions for immersion-coating of catechol containing copolymers. Copolymer coatings were deposited from solutions of DMF with 1% (v/v) pyridine to elucidate the effect of DMA inclusion and molecular weight on the deposition of copolymer films. It was hypothesised that pyridine should cause oxidation of the catechol, which may increase the coating thickness via crosslinking of the copolymer chains.

4.3 Experimental

4.3.1 Investigation of (co)polymer solubility in various solvents

A sample of (co)polymer (2 mg) was weighed into a 3 mL vial, and 2 mL solvent added. The vials were sealed and placed on rollers overnight. (Co)polymer solubility was assessed visually and judged by the presence/absence of any visible polymer or cloudiness in the solution. For each (co)polymer sample, the solvents investigated were water, methanol, ethanol, isopropyl alcohol (IPA), acetone, chloroform, DMF, THF, toluene, diethyl ether and hexane.

4.3.2 Substrate preparation method

Substrates were prepared using one of two methods.

Method A. Silicon wafers were cleaned by immersion for 30 min in a flask containing 250 mL dichloromethane (DCM), before immersion for 30 minutes in 250 mL piranha solution (1:3 mixture of hydrogen peroxide and sulfuric acid) and then rinsed by immersion in 250 mL milliQ water. The cleaned wafers were stored for up to 24 h in milliQ water before coating to prevent contamination, before being dried in a stream of nitrogen.

Method B. Silicon wafers were cleaned by sequential immersion for 30 seconds in 50 mL of dichloromethane, THF, water and isopropanol, dried in a stream of nitrogen, and then exposed to oxygen plasma for 120 seconds.

4.3.3 Spin-coating experiments

Copolymers were spin-coated onto substrates using either a POLOS 200 spin-coater or a Laurell WS-650MZ-23NPP spin-coater. Copolymers were dissolved in methanol or DMF, at solution concentrations from 0.5% to 2% (w/v) and then passed through a 0.45 µm syringe filter. The cleaned silicon wafers were immobilised on the stage of the spin-coater using a vacuum pump and sufficient copolymer solution was applied to ensure the entire surface of the substrate was wetted. Spin speeds were varied between 1000 and 4000 rpm at acceleration rates of between 100 and 600 rpm s^{-1}. The parameters used for individual experiments are specified below. The spin duration was set to 75 s.

4.3.4 Immersion-coating experiments

Copolymers were dissolved in methanol, a methanol/THF 50/50% (v/v) mixture or DMF, at a solution concentration of between 0.75% and 8% (w/v). In some experiments, 1% (v/v) pyridine was added to the copolymer solution. Silicon wafers were immersed in the copolymer solutions and left on rollers overnight. After removal from the copolymer solution, the wafers were rinsed with fresh solvent (DMF or methanol) to remove unbound copolymer and then dried overnight under vacuum.

4.3.5 Ellipsometry measurements

Film thickness measurements were carried out using a variable angle spectroscopic ellipsometer (J. A. Woollam VASE M2000). A wavelength range of 400-1600 nm was used, and measurements were taken with incident light angles of 60, 65, 70 and 75 degrees. The data was processed using completeEASE software (J. A. Woollam Co. Inc., Lincoln, USA) using the Cauchy model. For film thickness values smaller than 10 nm, fixed values of A = 1.52 and B = 0.006 were used for the real and imaginary components of the refractive index unless otherwise indicated.

4.3.6 AFM experiments

Unless otherwise specified, AFM measurements were carried out using a Bruker Multimode 8 scanning probe microscope in tapping mode. Images were processed and analysed using NanoScope Analysis (x86). 2^{nd} order flattening was carried out to minimise artefacts arising from sample levelling or imperfectly flat motion from the AFM cantilever tip. Where indicated, AFM measurements were carried out by Andreas Janke, Leibniz-Institut für Polymerforschung, Dresden, Germany. Measurements were carried out in the peak force tapping mode by a Dimension FASTSCAN (Bruker-Nano, USA) using silicon nitride sensors FASTSCAN-C (Bruker, USA) with a nominal spring constant of 0.7 N/m and tip radius of 5 nm. The setpoint was 0.08 V.

4.4 Results and Discussion

In the following sections, the deposition of copolymers onto silicon wafer substrates is discussed in detail. Preceding this, the solubility of selected copolymers introduced in Chapters 2 and 3 is discussed, the results of which informed the selection of copolymers used for deposition of coating.

4.4.1 Investigation of (co)polymer solubility in various solvents

Throughout Chapters 2 and 3, the copolymerisation of various methacrylate monomers with DMA and acetonide-protected DMA (ADMA) was reported. One criterion for the selection of the methacrylate comonomers was their polarity. Monomers with a wide polarity range were investigated to enable use of the resulting copolymers in a wide variety of industrial applications. As such, the solubility of a selection of the synthesised (co)polymers (see Chapters 2 and 3) was investigated, by monitoring their dissolution (or otherwise) in various solvents at 1 mg mL^{-1} concentration. Solubility was assessed by the presence or absence of any visible (undissolved) polymer in the test vial after 24 hours at room temperature. Thus, these results should be considered only a qualitative survey of (co)polymer solubility. A full solubility profile would require determination of the Hildebrand or Hansen solubility parameters for each (co)polymer,[16] but in this case a simplified study was sufficient to determine which copolymers were suitable for further testing. Solubility of (co)polymers comprising up to three monomers from HEMA, MMA, PEGMEM, SMA, DMA, ADMA and GMA were investigated. Solubility test results are presented in Table 4.1. The naming system used to refer to individual copolymer samples in Chapters 2 and 3 is retained to avoid confusion whereby, for example, the name FR-HGD-80/10/10 signifies a terpolymer synthesised by free radical polymerisation (FR), with monomers HEMA, GMA and DMA (HGD) and a monomer molar feed ratio of 80/10/10.

Table 4.1. Results for (co)polymer solubility testing. Each (co)polymer immersed in solvent at concentration of 1 mg mL^{-1} and stirred overnight.

(Co)polymer[a] / Solvent[b]	FR-H	FR-G	FR-D-(DMF)	RAFT-A-(DIOX)	RAFT-HGD-80/14/6	FR-HGD-80/10/10	FR-MD-90/10	FR-MGA-52/26/22	FR-PD-71/29	FR-SA-90/10
	M_n / g mol^{-1}									
	17250	220600	95300	32500	16800	43400	37000	42700	9700	93300
Water	×	×	×	×	×	×	×	×	×	×
DMF	✓	×	✓	✓	✓	✓	✓	✓	✓	×
Methanol	✓	×	✓	×	✓	✓	×	×	✓	×
Ethanol	✓	×	✓	×	✓	✓	×	×	✓	×
Acetone	×	✓	×	✓	×	×	✓	✓	×	×
IPA	×	×	×	×	×	×	×	×	×	×
THF	×	✓	×	✓	×	×	✓	✓	×	✓
Chloroform	×	✓	×	✓	×	×	✓	✓	×	✓
Diethyl Ether	×	×	×	×	×	×	×	×	×	✓
Toluene	×	✓	×	×	×	×	×	×	×	✓
Hexane	×	×	×	×	×	×	×	×	×	×

a) Abbreviations of monomers in (co)polymer names: H = HEMA, G = GMA, D = DMA, A = ADMA, M = MMA, P = PEGMEM, S = SMA. b) Solvents in order of decreasing dielectric constant.

The solubility of a homopolymer of HEMA, FR-H (17250 g mol^{-1}, Đ = 2.67), was tested to ensure the results from the current test method were concordant with solubility reports in the literature. FR-H was soluble in methanol, ethanol and DMF. The solubility profile of FR-H agrees well with the report of Hirao *et al.*[17] and the survey by Brandrup *et al.*,[18] indicating the applicability of the basic test method used here. The solubility test was repeated using a homopolymer of GMA (FR-G) which indicated solubility of FR-G in acetone, toluene, chloroform and THF. The solubility of GMA homopolymers is unsurprisingly very similar to other methacrylate homopolymers bearing short-chain, low-polarity side chains, such as poly(MMA).[18]

No formal solubility testing of a DMA homopolymer has been reported in the literature, and thus FR-D-(DMF) was included in the study. Extensive crosslinking of DMA homopolymers and copolymers containing mole fractions of DMA of >50%, has been reported. The crosslinking is reported to occur upon oxidation of the catechol functionality.[19] This could complicate the assessment of polymer solubility. For example, a DMA homopolymer was reported to be insoluble in "most common organic solvents" and showed insufficient solubility in DMF to obtain a molecular weight by SEC.[20] In another report, the solubility of a DMA homopolymer was not discussed, but the authors were able to obtain molecular weights using SEC (7550 g mol^{-1}, solvent unreported).[21]

In the current investigation, FR-D-(DMF) (95300 g mol^{-1}) was found to be soluble in polar solvents such as methanol, ethanol and DMF. The contrast between our finding and the literature report suggests that the solubility of poly(DMA) may vary significantly depending on molecular weight and the degree of oxidative crosslinking. It could thus be hypothesised, albeit tentatively, that (uncrosslinked) poly(DMA) has a similar solubility profile to poly(HEMA) and should not strongly affect the solubility of HEMA/DMA copolymers.

Inclusion of GMA in HEMA/GMA/DMA terpolymers would reduce the polymer polarity, however the impact is expected to be low as GMA is a minor component. The solubility profile of two HEMA/GMA/DMA terpolymers – RAFT-HGD-80/14/6 (16800 g mol^{-1}, Đ = 1.43) and FR-HGD-80/10/10 (43400 g mol^{-1}, Đ = 3.23) – was investigated. These particular examples were chosen as they were promising candidates for thin film deposition, having been designed according to the criteria discussed in previous chapters, and had different molecular weights and dispersity.

The solubility of RAFT-HGD-80/14/6 and FR-HGD-80/10/10 was found to be identical to FR-H under the restricted conditions used here, indicating that the copolymer solubility was not strongly affected by the particular changes to composition (*i.e.* inclusion of DMA and GMA). The solubility was also relatively unaffected by the variation in molecular weight and dispersity, but without further investigation it is impossible to isolate the potential effect of molecular weight/dispersity/composition on solubility.

The HEMA-containing polymers in this study appeared to swell, but not dissolve, in water. Poly(HEMA) is generally considered to be water insoluble (due to the hydrophobic backbone),[22] although it has been shown that short poly(HEMA) chains of less than 10000 g mol^{-1} can be dissolved in water.[23] Swelling of higher molecular weight poly(HEMA) in water may arise due to hydrophobic domains and extensive intermolecular H-bonding, which impede the dissolution of the homopolymer.[24] Light crosslinking (chain coupling) during polymerisation of HEMA can also be caused by a common impurity, ethylene glycol dimethacrylate (EGDMA); this may also have contributed to poly(HEMA) swelling instead of dissolving, or at least slowing the timescale of dissolution in case of a low concentration of EGDMA.[22] Inhibitor was removed from HEMA prior to homopolymer synthesis by passing the monomer through a column of silica, which may not be selective enough to remove traces of EGDMA, so some chain coupling of this type is possible.

The solubility of an ADMA homopolymer (RAFT-A-(DIOX)) was also investigated. The homopolymer was found to be soluble in DMF, THF, acetone and chloroform. This demonstrated, as expected, that the ADMA homopolymer is soluble in less polar solvents than DMA. This is due to the protection of the polar hydroxyl groups of the catechol functionality with the non-polar acetonide group.

MMA was also widely used in the current work (see Chapters 2 and 3). Poly(MMA) is the most widely studied methacrylate polymer, and is reported to be soluble in acetone, chloroform, THF and DMF.[16, 18] The solubility of FR-MD-90/10 and FR-MGA-52/26/22 was investigated and found to show similar solubility to an MMA homopolymer. Intermolecular interactions may be increased due to the catechol functionality in DMA,[25] however it was demonstrated above that the DMA homopolymers tend to dissolve in more polar solvents than poly(MMA). Again, the effect of competing factors (molecular weight/intermolecular forces/dispersity) on solubility could not be isolated under the

investigated conditions, so there is significant uncertainty associated with the measurements. The solubility of MGA-52/26/22 was similar to poly(MMA) despite having significantly different monomer composition; however, this finding was expected as MMA, GMA and ADMA homopolymers are soluble in a similar range of solvents.

Finally, to demonstrate the range of polymer solubility in the library of catechol-containing copolymers discussed in Chapters 2 and 3, the solubility of representative examples of copolymers with the low polarity stearyl methacrylate (S) monomer (FR-SA-90/10) and high polarity PEGMEM (FR-PD-71/29) were investigated. FR-SA-90/10 was only soluble in toluene, chloroform, THF and diethyl ether due to the non-polar aliphatic pendant groups in SMA. In stark contrast, FR-PD-71/29, which contained polar poly(ethylene glycol) pendant groups, was only soluble in methanol, ethanol and DMF. Surprisingly, FR-PD-71/29 swelled in water rather than dissolving. PEGMEM is widely used to synthesise water-soluble copolymers,[26] however, copolymers of PEGMEM and DMA are water-insoluble as evidenced by a report of formation of spherical micelles of poly(DMA-*b*-PEGMEM) in water.[27] Therefore the water-insolubility of FR-PD-71/29 can be attributed to the DMA, and the swelling could be due to strong intermolecular interaction arising from the catechol functional groups on DMA.

4.4.2 Cleaning and preparation of silicon wafer substrates

Silicon wafer was chosen as a model substrate due to its exceptional flatness and low surface roughness (<0.5 nm). It has been widely studied and reported in the literature and films deposited on the silicon wafer surface can be easily characterised by many analytical techniques. When depositing a polymer film, it is important that the substrate is clear from impurities and debris and – especially when spin-coating – that the substrate is fully wetted by the polymer solution. The coating experiments described in this chapter were carried out at two sites and the silicon wafer substrates were cleaned by one of two methods depending on the equipment available at each site. Unless otherwise indicated, silicon wafers were prepared by cleaning with DCM followed by treatment using piranha solution (3:1 sulfuric acid and hydrogen peroxide). Piranha solution oxidises organic residues, allowing them to be dissolved or washed off. A further consequence of this treatment is the formation of polar SiOH groups on the substrate surface[28] which promoted full wetting of the substrates with polar organic solvents such as methanol and DMF. Clean silicon wafers were stored in ultrapure water for up to 24 h to prevent contamination of the surfaces.

Alternatively, silicon wafers were cleaned by washing with several organic solvents, including DCM, and treatment with air plasma. Air plasma treatment is also a commonly used method for cleaning substrates[29] and oxidises organic contaminants by the generation of oxygen and hydroxyl radicals and consequently leads to a mixture of siloxane (Si-O-Si) and silanol (SiOH) groups on the wafer surface.[30] The adsorption of the non-ionic polymer poly(N-vinylpyrrolidone) at neutral pH has previously been shown to be very similar when plasma- or piranha solution-treated silicon wafers were compared, so the surface treatment used was not expected to have a significant impact on the coating performance in the present study.[28]

4.4.3 Details of (co)polymers used in the optimisation of film deposition

Solubility of the HEMA/GMA/DMA copolymers in polar solvents such as methanol and ethanol made them excellent candidate copolymers for deposition in MMA-containing microfluidic devices. Furthermore, the reported non-fouling properties of HEMA[31] are ideal for coatings which, after adhesion of antibodies through the GMA functionality, would be exposed to a range of biomolecules. A series of (co)polymers, all containing mole fractions of at least 73% HEMA, were selected for further testing (see Table 4.2). All were statistical copolymers synthesised either by free radical (FR) or RAFT polymerisation.

Table 4.2. Polymers used in spin-coating and immersion-coating. Constituent monomers and monomer molar feed ratios are indicated in the name of each polymer.

(Co)polymer	M_n/g mol^{-1}	Đ	Copolymer composition/mol% [a]
FR-HGD-80/10/10	43400	3.23	83/12/6
FR-HD-90/10-(DMF)	13650	3.18	92/0/8
FR-HG-89/11	133500	4.26	78/22/0
RAFT-HGD-74/13/13	24950	2.18	78/14/8
FR-HGD-58/9/33	110650	3.48	68/12/20
FR-H	17250	2.67	-
FR-HD-70/30-(DMF)	3050	14.27	75/0/25

[a] Copolymer compositions are given relative to the order of monomers in the name of the polymer

4.4.4 Optimisation of spin-coating methodology and thin film characterisation by AFM and ellipsometry

Spin-coating, a process widely used in industry, was chosen to cast the copolymers onto silicon wafer with the aim of obtaining uniform thin films. Initial objectives were to i) identify suitable coating conditions to achieve smooth, uniform coatings, ii) identify ways

to control the film thickness of the copolymer coatings and thus iii) evaluate the suitability of the copolymer films for potential industrial applications. AFM was used to assess the nanometre-scale topography (roughness) of the films, whilst film thickness was measured by ellipsometry.

Despite the relative simplicity of the experimental set-up, modelling of ellipsometry data is non-trivial.[13] Ellipsometry can be described in terms of the change in polarisation upon reflection of a polarised laser reflected from a sample and is described by the two ellipsometric angles: Δ and Ψ. The ellipsometric angles are the usual output from an ellipsometric measurement and are related using the "fundamental equation of ellipsometry" (Equation 4.1):

$$\mathbf{tan\Psi e^{i\Delta}} = \frac{\mathbf{R_p}}{\mathbf{R_s}} = \boldsymbol{\rho} \qquad \textbf{4.1}$$

where R_p and R_s are the parallel and perpendicular parts of the total complex refraction coefficient, ρ. In ellipsometric measurements, a model is created by estimating Δ and *tan*Ψ over a range of wavelengths and angles. The model is iterated to fit the obtained values and thus determine the desired film property (*e.g.* film thickness or refractive index (RI)). Scanning a large wavelength range increases the likelihood that an accurate model can be generated.

The mean squared error (MSE) of the fit is determined by the ellipsometry software. MSE is a statistical estimator used as a measure of how well the model fits the observed data, by calculating the bias and standard error of the observed data.[32] The magnitude of the MSE is used as an indicator of the quality of the fit, where a smaller MSE implies a better fit. The MSE function used is given in Equation 4.2

$$MSE = \sqrt{\frac{\mathbf{1}}{\mathbf{2N-M}}\sum_{\boldsymbol{i=1}}^{\boldsymbol{N}}\left[\left(\frac{\boldsymbol{\Psi_i^{Mod}-\Psi_i^{Exp}}}{\boldsymbol{\sigma_{\Psi,i}^{Exp}}}\right)^{\mathbf{2}}+\left(\frac{\boldsymbol{\Delta_i^{Mod}-\Delta_i^{Exp}}}{\boldsymbol{\sigma_{\Delta,i}^{Exp}}}\right)^{\mathbf{2}}\right]} \qquad \textbf{4.2}$$

where *Mod* and *Exp* refer to the experimental and modelled values, Ψ and Δ refer to the ellipsometric angles and σ to the standard deviation of the experimental values.[33]

The native oxide layer on a silicon wafer is a well understood and reproducible surface,[13, 32] which has a highly contrasting refractive index (1.45) compared to the silicon wafer itself (3.78). This allows the film thickness of the oxide layer to be modelled with very low uncertainty (MSE of ≤1). A reference clean wafer measured with the ellipsometer used in

this work had a native oxide film thickness of 1.63 ± 0.001 nm and an MSE of 1.034. The silicon oxide layer thickness was subsequently used in the model used to calculate the film thickness of the spin-coated copolymers described herein.

The MSE of models fitted for copolymer coatings should ideally be as close to zero as possible, but in reality, MSE values < 1 are often impossible to achieve due to film surface heterogeneity and any other defects in the film. MSE values between 1 and 5 are considered excellent for thin films.[32] Film thickness measurements of copolymer coatings with an MSE within 1 order of magnitude of silicon oxide (*i.e.* <10) were considered acceptable and valid in this work, and copolymer films with an MSE of >10 were considered to have been (relatively) poorly modelled and, whilst still a useful guide to film thickness, should be considered with caution.

The uncertainty of ellipsometric modelling increases for measurements of films thinner than 15 nm, as in this range the copolymer RI and film thickness become coupled parameters *i.e.* their values cannot be determined independently of each other.[32, 34] An estimated value for thin-film copolymer RI can be obtained *via* multiple measurements of thicker films of the same copolymer or by the use of advanced modelling techniques, but these methods were impractical given the scope of the project. Thus, for coated substrates where preliminary measurements indicated a film thickness of <15 nm, film thickness was calculated using fixed values of A = 1.52 and B = 0.006 for the real and imaginary parts of the RI respectively. These values were chosen based on the characterisation of thicker films of the same composition, assuming RI should not change significantly for very thin films. As estimated RI data was used to allow measurement of thin films, the uncertainty associated with thickness measurements of very thin films is high compared to thicker films with low MSE values.

Surface roughness/heterogeneity can also affect the accuracy of the model used to fit the ellipsometric data. Light scattering from the surface, caused by increased surface roughness, and the introduction of domains of different RI (due to the air between surface peaks), can cause large differences between the predicted and measured data, and hence large MSE values.[35, 36] Again, this can be overcome using advanced modelling in some cases to provide truly accurate representations of film thicknesses.

4.4.4.1 Characterisation of blank silicon wafer substrates by AFM and ellipsometry

Prior to deposition of copolymer films, the topography of the uncoated silicon wafer surface was analysed by AFM to provide context for subsequent copolymer thin film analysis. The roughness, defined as the average absolute deviation about the mean film height (R_a), of 0.11 nm and a maximum peak-trough distance (Z-range) of 8.17 nm were both calculated using the AFM analysis software. The very low R_a indicates an extremely homogeneous surface, however the slightly larger Z-range is likely to be due to deposition of dust or other organic contaminants which are extremely difficult to avoid unless substrates are prepared in a clean room.[37]

The film thickness of the native oxide on the blank silicon wafer was determined to be 1.63 ± 0.00 nm. The model fitted the data extremely well, giving an MSE of 1.034 (Figure 4.4).

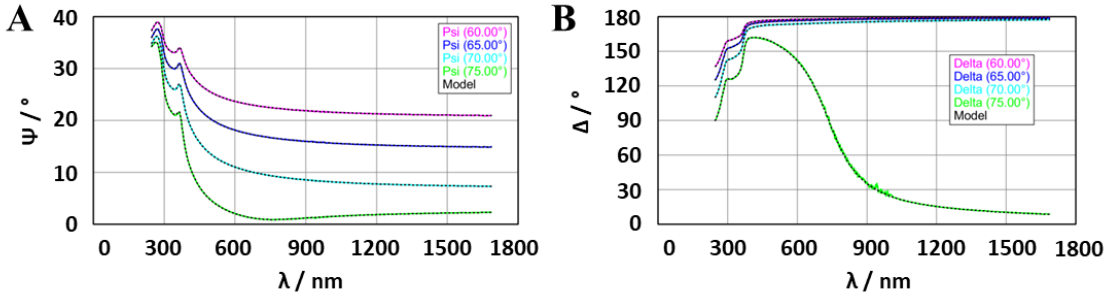

Figure 4.4. Ellipsometric data for the native oxide layer on a silicon wafer measured at four angles of incidence. A) Ψ *vs.* λ. B) Δ vs. λ.

4.4.4.2 Characterisation of copolymer films spin-coated from methanol

Initially, the use of methanol as a spin-coating solvent was investigated. All of the copolymers included in the study are soluble in methanol up to at least 2.0% (w/v) concentration, and the high volatility allowed efficient removal of residual solvent from the resulting films under vacuum. FR-HGD-80/10/10, FR-HD-90/10-(DMF), FR-HG-89/11 and RAFT-HGD-74/13/13 were spin-coated onto silicon wafer substrates using copolymer solution concentrations in the range of 0.5 – 2.0% (w/v). Spin-speeds of 1000 – 4000 rpm were used and the disc was accelerated at a rate of between 100 – 600 rpm s^{-1}.

Ellipsometry was used to measure the thickness and AFM used to measure the topography of the resulting copolymer films. When fitting the ellipsometry data, it was necessary to restrict the wavelength range to 400 – 1600 nm, as the copolymers absorbed radiation in the UV region of the spectrum due to the aromatic ring in DMA.

An opaque or iridescent border could be seen around the perimeter of all coated substrates due to edge effects – the perturbation of the air caused by the edges and corners of the rectangular substrate which led to uneven evaporation close to the outer limits of the substrate.[38] When measuring film thickness using ellipsometry, the laser spot was directed at the centre of the substrate to avoid this particular defect.

4.4.4.2.1 Analysis of spin-coated films of FR-HGD-80/10/10 using ellipsometry and AFM

Spin-coating parameters and ellipsometry results for substrates spin-coated with FR-HGD-80/10/10 are presented in Table 4.3. The following discussion considers in turn the effect of spin-speed, acceleration and solution concentration on film thickness and heterogeneity, followed by studying the observed film heterogeneity in more detail. In this chapter, coatings are numbered sequentially as they are discussed to allow them to be referenced in the text.

Table 4.3. Ellipsometry data for films of FR-HGD-80/10/10, spin-coated from methanol onto silicon wafer.

Coating Code	Soln. Conc. / % (w/v)	Spin Speed / rpm	Accel. / rpm s^{-1}	Film thickness/nm	MSE	RI (real part)
1	0.50	1000	400	2	1.30	1.60
2	0.75	1000	400	50	71.66	1.51
3	0.75	1000	400	58	53.41	1.50
4	0.75	4000	400	42	2.68	1.45
5	0.75	4000	600	61	2.97	1.40
6	0.75	4000	600	37	1.11	1.49
7	2.00	1000	400	150	78.38	1.54
8	2.00	1000	400	145	77.68	1.54
9	2.00	4000	400	148	99.82	1.53
10	2.00	4000	400	165	73.00	1.53

The data in Table 4.3 shows that the measured film thickness of identical pairs of coatings varied significantly. Coatings 2 and 3, 5 and 6, 7 and 8, and 9 and 10 were prepared under identical conditions and yet the film thickness varied by as much as 65% for "identical" thinner films and 10% for thicker films. Several of the coatings had low MSE values despite having significantly different film thickness, which indicated the fit of the data was good and the variation was very unlikely to be due to measurement error.[32] Thus, the poor repeatability was more likely to have been caused by highly heterogeneous film topography. Under normal circumstances, film thickness variations of <10 nm could be attributed to changes in spin-coating parameters,[11] however in this case the poor

repeatability meant only variations in the order of tens of nanometres could be considered significant enough to attribute to parameter changes.

The contrasting MSE values can be better understood by comparing the ellipsometric data and model fit from samples yielding differing MSE values. A poor fit is shown in Figure 4.5A and B (Coating 2, MSE = 71.66), in which the region between 300 and 400 nm is poorly modelled, as shown by the clearly poor agreement between the experimental data (solid coloured lines) and modelled data (dashed black lines). In contrast, the fit in Figure 4.5C and D (Coating 4, MSE = 2.97), which had a similar film thickness, the model is fitted extremely well, resulting in a low MSE.

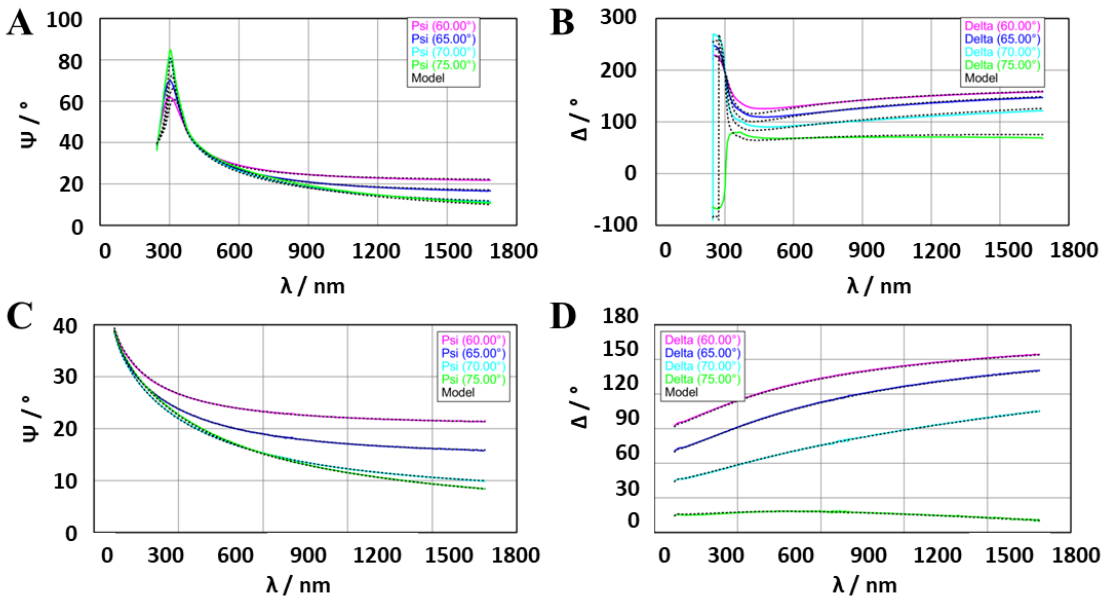

Figure 4.5. Ellipsometry data for polymer films A) Coating 2, Ψ *vs.* λ, B) Coating 2, Δ *vs.* λ, C) Coating 4, Ψ *vs.* λ, B) Coating 4, Δ *vs.* λ.

4.4.4.2.1.1 Effect of spin-speed on film thickness of FR-HGD-80/10/10 coatings

Two spin-coating speeds were used in the experiments – 1000 and 4000 rpm. Coatings 2, 3 and 4 were prepared under identical conditions (0.75% (w/v) terpolymer concentration and 400 rpm s^{-1} acceleration) but with some variation in spin speed. The film thickness of coatings 2 (1000 rpm), 3 (1000 rpm) and 4 (4000 rpm) were 50 nm, 58 nm and 42 nm respectively; differences in film thickness were not significant enough to correlate with spin-speed. However, it is notable that the MSE values of coatings 2 (71.66) and 3 (53.41) are much larger than coating 4 (2.68). As high MSE is linked to light scattering from the surface, this suggested the surface roughness was significantly lower at higher spin speeds.

Furthermore, for coatings 7, 8, 9 and 10 – two pairs of films coated at different spin speeds under otherwise identical conditions – the measured thickness is very similar, varying by only a few percent (148 – 165 nm). MSE values of 78.38 and 77.68 for coatings 7 and 8 compared to 99.82 and 73.00 for coatings 9 and 10, suggested no correlation between MSE and spin-speed in this case. Furthermore, the ability to accurately compare the effect of spin speed on film thickness is reduced for coatings 7 – 10 due to the high MSE values, which indicated a poor fit, so the data must be considered with appropriate caution.

No correlation between spin speed and film thickness was observed, which is contrary to the accepted literature precedent.[39, 40] The influence of spin-speed on polymer film thickness can be evaluated by considering the relationship between the "flow" phase (Figure 4.1C), and the "evaporation" phase (Figure 4.1D) of the drying process.[41] The relationship is determined by Equation 4.3:

$$\frac{dh}{dt} = -2Kh^3 - e \qquad \textbf{4.3}$$

where the flow term ($-2Kh^3$) describes the flow of the solution, in which h is the instantaneous fluid thickness and K is a flow constant defined by Equation 4.4:

$$K = \frac{\rho\omega^2}{3\eta} \qquad \textbf{4.4}$$

where η is the fluid viscosity, ρ is the fluid density and ω is the spin-speed. The second component of Equation 4.3 is the evaporation term, e, defined by Equation 4.5:

$$e = C\sqrt{\omega} \qquad \textbf{4.5}$$

where C is a proportionality constant depending on the airflow above the disc.

As the flow term in Equation 4.3 has a cubic dependence on fluid thickness, the evaporation term becomes rapidly more important as film thickness decreases. Eventually, the value of the flow term becomes insignificant and drying becomes evaporation driven. Film thickness changes at this stage are very small, as polymer is no longer removed from the disc and solvent content in the film is low.

Due to the squared relationship between ω (spin speed) and the flow constant K (Equation 4.4), thinner coatings should be obtained by faster rotation of the substrate *i.e.* faster rotation leads to the ejection of more polymer from the disc during the "flow" phase.[39] It was thus somewhat surprising that no correlation was observed between film thickness and

spin-speed in this case. However, the heterogeneity of the terpolymer films implied by the high MSE values could have masked any variation in film thickness, as repeatability of the coatings was poor.

4.4.4.2.1.2 Effect of spin-coating acceleration on film thickness of FR-HGD-80/10/10 coatings

In the current investigation, there was only one set of coatings (4, 5 and 6) for which the acceleration was modified (from 400 rpm s^{-1} to 600 rpm s^{-1}) whilst all other parameters were kept constant. No systematic trend was observed, as an increase in acceleration resulted in increased film thickness for 5, but decreased film thickness for 6. As there was no further data that could be compared, there is insufficient data to fully assess the impact of spin acceleration on solutions of FR-HGD-80/10/10.

Usually, the acceleration of the coating is considered not to have a significant effect on film thickness in spin-coating.[39, 42] However, if the rate of acceleration is too slow, the point at which evaporative drying becomes dominant over solution flow may occur before maximum rotational velocity is achieved. This effectively freezes film thickness at a lower "final" spin-speed.[41] When using volatile solvents, the acceleration is often selected such that the coating reaches maximum rotational velocity within 5 s, however, the acceleration rate necessary to reach the maximum spin speed before film thickness is frozen depends on many factors and is difficult to predict. The (relatively) low acceleration rate used for the 4000 rpm coatings (reaching maximum rotational velocity in 6.7 – 10 s) could also account for the lack of correlation between spin speed and film thickness, as the effective "final" spin speed may have been lower than 4000 rpm.

4.4.4.2.1.3 Effect of terpolymer solution concentration on film thickness of FR-HGD-80/10/10 coatings

The effect of terpolymer solution concentration on film thickness was also considered. Coatings 1, 2, 7 and 8 were prepared using identical parameters (1000 rpm spin speed, 400 rpm s^{-1} acceleration) but solution concentration was varied. Film thickness increased from 2 nm at 0.50% (w/v) terpolymer concentration (coating 1), to 61 nm at 0.75% (w/v) (coating 2), and to 150 nm and 145 nm at 2.00% (w/v) (coatings 7 and 8 respectively). The same trend was also evident for substrates spin-coated with speeds of 4000 rpm. Film thickness increased from 42 nm (coating 4, 0.75% (w/v)) to 148 nm and 165 nm for coatings 9 and 10 respectively (2.00% (w/v)). An increase in solution concentration clearly

led to a significant increase in film thickness. This is expected due to the higher concentration, and hence viscosity, η, of polymer.[43, 44] Increased η reduces the value of the flow constant, K, in Equation 4.4, and thus reduces the rate of film thinning predicted by Equation 4.3. The outcome is a non-linear relationship between film thickness and solution concentration.

The measured RI of several films was unusually low (<1.5). An RI of about 1.52 would be expected for a homogeneous poly(HEMA) film,[45] compared to 1.00 for air and 1.33 for water. A possible explanation for variation of RI in the described films is the presence of air voids in the terpolymer films, which would reduce the measured RI of the film. Air voids are further indicators of heterogeneous film surfaces. The unusual RI values appear more prominently in thinner films, so the film heterogeneity could be increased in these coatings.

High MSE values were obtained for terpolymer coatings deposited from solutions with a concentration of 2% (w/v). High MSE values are indicative of a poor model fit.[32] This is often due to surface roughness, which supported the suggestion that the coated surfaces were heterogeneous and likely to scatter light. The heterogeneity is likely to be caused by macroscopic surface defects such as striations (lines forming a radial pattern from the centre to the edge of the substrate). Striations have been shown to significantly scatter light[46, 47] and, because of their periodicity, can also diffract light in some cases,[48] both of which would cause deviations from the expected ellipsometric angles. Striations were observed in some spin-coated substrates with a periodicity of around 0.25 mm (see example in Figure 4.6).

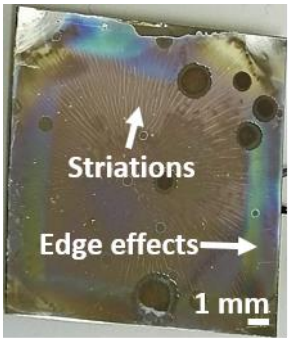

Figure 4.6. Typical example of defects on a preliminary test for spin-coating of FR-HGD-80/10/10. Polymer-free spots on the film are due to solvent testing and not the spin-coating process.

Previous studies have indicated that striations may be caused by capillary forces due to the Marangoni effect (see Figure 4.7).[4, 46, 47] In very thin films, surface tension gradients can

be caused by local random variations in film thickness. Liquid flows towards regions of high surface tension by capillary action, forming convection cells and amplifying the evaporation-driven composition differences. As solvent evaporation is faster from the low-surface tension regions, wave-like defects are formed on the surface. Any concentration gradients would be exacerbated as the polymer reaches its solubility limit. Jamming of the highly concentrated polymer can occur before relaxation to a uniform film is possible, therefore fixing the defects in the film.[49-51] Often, annealing the polymer film at elevated temperature is used to increase the rate of surface relaxation,[52] but in the current work exposure to high temperatures was avoided to prevent ring-opening of the epoxide functional groups in the film.

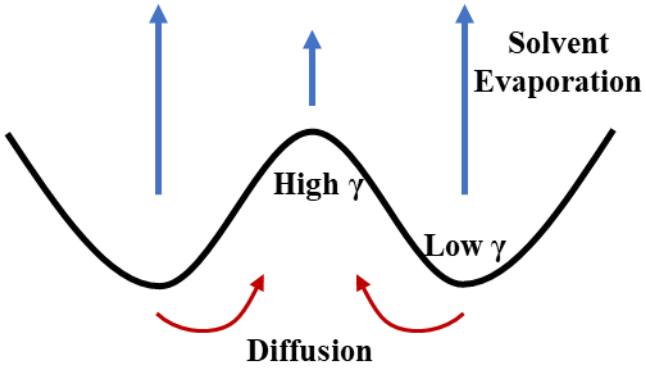

Figure 4.7. Schematic of striations formed due to regions of high and low surface tension on a drying polymer film, where γ is surface tension.

Additionally, in a drying film, rapid solvent evaporation can create gradients in solution concentration or temperature through the film.[53] In temperature-driven variations, the Marangoni effect occurs above a critical Marangoni number (Ma) defined by Equation 4.6:

$$Ma = -\frac{d\gamma}{dT}\frac{h\Delta T}{\eta\alpha} \qquad 4.6$$

where γ is the surface tension, η is the solution viscosity, α is the thermal diffusivity and ΔT the temperature gradient through the film from bottom to top.[54] Due to the high vapour pressure of methanol, fast evaporation leads to high ΔT values, so the Marangoni effect is likely to occur.

4.4.4.2.1.4 Analysis of spin-coated FR-HGD-80/10/10 films using AFM

To further investigate the surface topography (roughness) of the FR-HGD-80/10/10 terpolymer films, AFM images were collected for a selection of spin-coated substrates with different film thicknesses. Coating 6 (4000 rpm, 600 rpm s^{-1}, 0.75% (w/v)) had a film

thickness of 37 nm, coating 5 (4000 rpm, 600 rpm s^{-1}, 0.75% (w/v)) had a thickness of 61 nm and coating 7 (1000 rpm, 400 rpm s^{-1}, 2.00% (w/v)) had a thickness of 150 nm.

The AFM images are shown in Figure 4.8. The R_a (roughness) and Z-range (peak-to-trough range), determined by AFM, and the ellipsometric film thickness and MSE are reported in Table 4.4. The AFM Z-range can be greater than the ellipsometry-derived film thickness, especially in porous coatings, as ellipsometry measures an averaged film thickness over the laser spot (diameter around 1 mm), whereas AFM measures peaks and troughs to nanometre resolution and the Z-range is not averaged. Considered together, the Z-range, R_a and ellipsometry-derived film thickness can be used to develop an enhanced understanding of the film features.

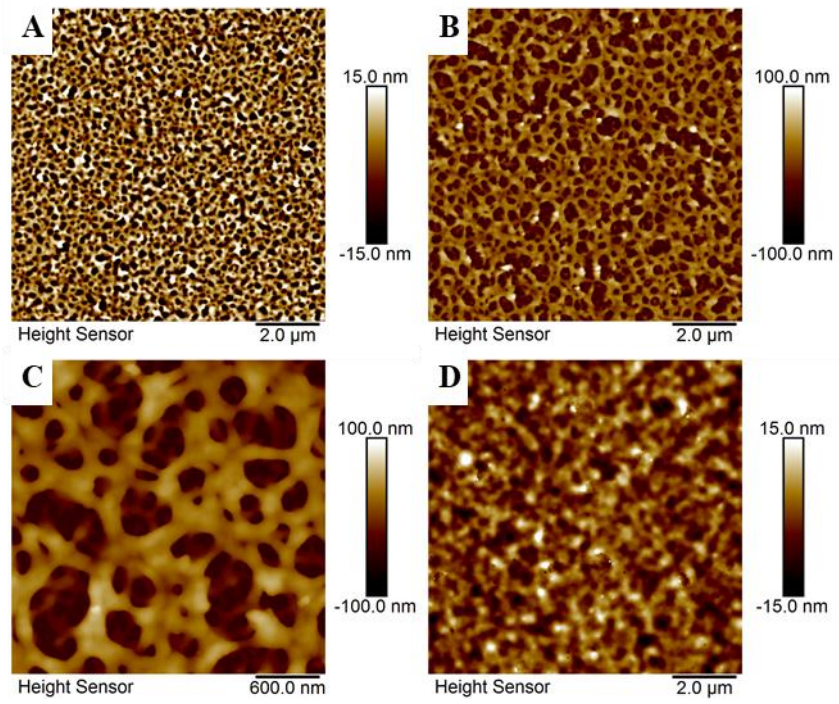

Figure 4.8. 2D AFM images of films of FR-HGD-80/10/10, spin-coated from a solution in methanol. A) 37 nm film, coating 6 B) 61 nm film, coating 5 C) 61 nm film, coating 5 (enlarged section) D) 150 nm film, coating 7. AFM measurements carried out by Andreas Janke, IPF, Dresden.

The AFM images shown in Figure 4.8 clearly show that the resulting terpolymer coating in each case was porous with irregular size pores of diameter 0.1 – 2 µm. The pores visible in coating 6 (Figure 4.8A, 37 nm) had a diameter of around 0.2 µm. The R_a and Z-range were large (9.79 nm and 86.43 nm respectively), despite a low MSE value of 1.11. The pores observed on coating 5 (Figure 4.8B, 61 nm), had a diameter of 0.5 µm, larger than coating 6 despite identical spin-coating parameters. The R_a (25.13 nm) and Z-range (183.33 nm) were also much larger than for coating 6, indicating a more heterogeneous

surface. The greatly increased roughness for coating 5 also correlates well with the larger observed film thickness for coating 5 compared to coating 6. An expanded region of the image of coating 5 (Figure 4.8C) shows more clearly how the porous, sponge-like structure penetrates the film. The different pore size and roughness for the two identical spin-coated coatings indicated that the defects can vary significantly.

Table 4.4. Roughness data from the AFM images in Figure 4.8. Silicon wafers coated with FR-HGD-80/10/10 Film thickness was obtained by ellipsometry.

Coating	Ellipsometry		AFM	
Code	Film Thickness / nm	MSE	R_a / nm	Z-range / nm
6	37	1.11	9.79 ± 1.67	86.43 ± 11.70
5	61	2.97	25.13 ± 0.25	183.33 ± 26.50
7	150	78.38	3.23 ± 0.24	54.97 ± 9.75

The AFM image of coating 7 (150 nm, 2.00% (w/v) concentration) is shown in Figure 4.8D. Many small pores with a diameter of around 0.5 µm can be observed. While the pore diameter was not significantly different to coating 5, the Z-range is much lower (54.97 nm), indicating a less heterogeneous film was formed in coating 7. Additionally, the AFM R_a was smaller (3.23 nm) for the thicker film (coating 7) compared to the R_a for the thinner films (9.79 nm and 25.13 for 6 and 5 respectively). The small R_a and Z-range for coating 7 appeared counter-intuitive, as thicker films, coated from higher solution concentrations were generally associated with increased MSE from ellipsometry. This suggested that the ellipsometric MSE and AFM R_a are not directly related. As the size of the pores was of the same order of magnitude as the wavelength of light used for the ellipsometry measurements, light scattering may be expected from these surfaces. However, the ellipsometric MSE, which can be considered an indirect measure of the light scattering, was low for coatings 5 and 6, indicating light scattering due to the porous surfaces was not significant. Ellipsometric MSE may therefore be affected more significantly by the presence of striations *i.e.* high MSE values may only be associated with macroscale defects and have little correlation with porosity.

Due to the lack of correlation between porosity and high MSE, we suggest that the observed striations and porosity are not directly related and have distinct causes. Porous spin-coated films have been previously observed and various causes have been discussed in the literature.[55] One hypothesis is that that rapid solvent evaporation will lead to a

surface concentration gradient and hence the formation of a "skin" of polymer at the surface of the drying film.[40] As the "skin" retards solvent evaporation, mechanical stress from the liquid layer below causes buckling and defects due to solvent evaporating through cracks in the film. However, as it has been predicted that skin formation does not occur below a minimum film thickness of at least 200 nm,[56] this mechanism is deemed unlikely in this case. An alternative hypothesis attributes porosity to the Marangoni effect, discussed above in the context of striation formation.[51] This effect results in regularly-spaced holes in the film, usually several microns in diameter, where extreme gradients in surface tension occur. However, in the current work the pores formed have a small diameter (~500 nm) and are irregular, so it is considered unlikely that they are caused by the Marangoni effect. The pores appear to bear more resemblance to a phase-separated structure. These structures have been commonly observed when spin-coating a block copolymer with domains of different solubility,[57] upon spinodal-like dewetting of a polymer from a surface[58, 59] or upon solvent-induced phase separation of a multilayer film.[60] In a previously reported study, "phase separation, surface irregularity and cloudiness" was observed when spin-coating poly(HEMA-*co*-ethyl methacrylate), with HEMA mole fraction >50%, from a 10% (w/v) solution in methanol. The nature of the surface irregularities was not discussed, nor the possibility of spin-coating from more dilute polymer solutions. Moreover, in the same study it was observed that changing the solvent to DMF resulted in smooth, optically transparent coatings (although the film topography was not investigated in detail).[45]

It is therefore speculated that the pores in the coatings described in this chapter are most likely caused by poor solubility of the copolymers in methanol, particularly when the solution reaches a higher polymer concentration due to solvent evaporation. Thus, the polymer may precipitate before the end of the usual flow stage while a significant amount of solvent still remains. The precipitation can be described as analogous to a phase separation in which the two phases are polymer and solvent. Continued rapid evaporation of the methanol from the solvent "phase" leads to the formation of air voids or pores in the film, as the polymer is unable to flow. It is important to note that while the striations and porosity will be treated as independent phenomena, due to the complexity of the system it is quite possible that they share causes and the models proposed are somewhat simplified.

The polymer appears not to wet the surface of the silicon wafer upon precipitation in presence of methanol, in the in the short timescale of the spin-coating, which is attributed

to the strong H-bonding interaction between the methanol and surface silanol/siloxane groups. Thus, the use of methanol in this investigation could significantly influence the formation of defects (striations and pores). Use of a less volatile solvent or reduction of the temperature to further reduce the rate of evaporation could mitigate the formation of defects.[53, 55] To further study the phase separation of these DMA-containing copolymers from methanol, a cloud point analysis could be conducted to determine the concentration at which the copolymers become insoluble.[61]

It is worth noting that macroporous films such as those observed in Figure 4.8 (defined as having pore sizes from 50 – 1000 nm) have various uses such as in membranes and for chemical scaffolds due to their high surface area.[62, 63] If the porosity could be reliably and reproducibly predicted or templated through coating preparation such as nanolithography, this could present a facile approach towards generating macroporous materials. An example of such an approach is the "breath figure" technique, a hierarchical templating technique using water droplets as templates, which has been used to form macroporous membranes from inorganic nanoparticles coated with a catechol-containing copolymer.[64]

4.4.4.2.2 Analysis of spin-coated films of copolymer FR-HD-90/10-(DMF) using ellipsometry and AFM

FR-HD-90/10-(DMF) was also spin-coated onto silicon wafer, whilst modifying the same parameters as for FR-HGD-80/10/10 (section 4.4.4.2.1). The spin-coating parameters, ellipsometry film thickness and MSE are reported in Table 4.5.

Table 4.5. Ellipsometry data for films of FR-HD-90/10-(DMF), spin-coated from methanol onto silicon wafer.

Coating Code	Soln Conc /% (w/v)	Spin Speed / rpm	Accel. / rpm s^{-1}	Film thickness / nm	MSE	RI (real part)
11	0.50	1000	400	26	5.13	1.52
12	0.75	1000	100	49	17.71	1.53
13	0.75	1000	400	45	2.28	1.52
14	0.75	4000	600	36	1.04	1.50
15	0.75	4000	600	40	1.91	1.49
16	2.00	1000	400	118	35.14	1.52
17	2.00	1000	400	119	36.59	1.52
18	2.00	4000	400	116	39.30	1.53
19	2.00	4000	400	109	32.42	1.52

4.4.4.2.2.1 Effect of spin-speed on film thickness of FR-HD-90/10-(DMF) coatings

To study the impact of spin speed on film thickness, coatings 16 and 17 (1000 rpm, 2.00% (w/v) copolymer concentration, 400 rpm s^{-1}) can be compared with coatings 18 and 19 (4000 rpm, other parameters constant). All four spin-coated substrates have measured film thicknesses between 109 and 118 nm, indicating there is no discernible difference in film thickness due to spin speed under these conditions. This is similar to the observation for films of FR-HGD-80/10/10.

4.4.4.2.2.2 Effect of spin-coating acceleration on film thickness of FR-HD-90/10-(DMF) coatings

There was only one pair of coatings (12 and 13) for which the acceleration was modified whilst all other parameters were kept constant; in this case from 100 rpm s^{-1} to 400 rpm s^{-1}. Whilst the film thickness of coatings 12 and 13 were similar (49 and 45 nm respectively), coating 12 (100 rpm s^{-1}) had an MSE of 17.71 compared to coating 13 (400 rpm s^{-1}) which had an MSE of only 2.28. The difference in MSE is significant and could indicate the production of a fewer striations when the acceleration rate is high. In support of this suggestion, a previous report claimed increased acceleration rates during spin-coating reduced the amplitude of striations.[65] In the case of coating 12, the low acceleration rate of 100 rpm s^{-1} and final spin speed of only 1000 rpm, could cause the effective "final" rotation rate to be fixed at a low value – insufficient to prevent the formation of defects. A very low spin speed has also been linked with an increase in striation height.[47] However, as there is only one set of coatings to compare, this explanation can only be considered speculative without further data.

4.4.4.2.2.3 Effect of copolymer solution concentration on film thickness of FR-HD-90/10-(DMF) coatings

Coatings 11, 13, 16 and 17 used identical spin-coating parameters (1000 rpm spin speed, 400 rpm s^{-1} acceleration) but varying solution concentration. It is clear from the data in Table 4.5 that an increase in solution concentration led to an increase in film thickness from 26 nm (0.50% w/v), to 45 nm (0.75% w/v), and a further increase to 118 nm and 119 nm for coatings 16 and 17 respectively (2.00% (w/v)). These findings are consistent with the results reported above (Table 4.3) for films of FR-HGD-80/10/10.

Coatings 13 (FR-HD-90/10-(DMF)) and 3 (FR-HGD-80/10/10) were spin-coated using different copolymers under the same conditions (1000 rpm, 400 rpm s^{-1}, 0.75 % w/v). The

low MSE value of 2.28 for coating 13 is in contrast to that of coating 3, which had an MSE of 71.66. As high MSE was previously linked to the presence of striations, FR-HD-90/10-(DMF) appeared to exhibit fewer such defects.

The extent of film heterogeneity (in this case striations) remaining in the dry film is considered to be determined by whether the polymer film is able to relax before jamming occurs *i.e.* flow to relieve the surface concentration gradients – a process termed "levelling". However, if solvent evaporation is fast or levelling is slow there is often insufficient time for levelling before polymer jamming occurs and flow ceases. Kumar *et. al.* considered the levelling time, τ_{level}, as analogous to the spreading of a droplet on a surface such that:[51]

$$\boldsymbol{\tau_{level} = \frac{\eta L^{*}}{\gamma \theta^{m}}} \qquad \textbf{4.7}$$

where η is viscosity, L* is the characteristic length scale of the droplet, γ is surface tension and θ the contact angle of the fluid, which is raised to a positive exponent *m*.

The likelihood of levelling occurring can be described using the ratio, λ, between τ_{level}, and evaporation time, τ_{evap}:

$$\boldsymbol{\lambda = \frac{\tau_{level}}{\tau_{evap}}} \qquad \textbf{4.8}$$

where

$$\boldsymbol{\tau_{evap} = \frac{\rho h}{E}} \qquad \textbf{4.9}$$

where ρ is the density of the polymer solution, *h* is film thickness, *E* is solvent evaporation rate. Thus, considering $h / L^{*} \approx \theta$ and rearranging gives:

$$\boldsymbol{\lambda \propto \frac{\eta E}{\gamma \theta^{m+1} \rho}} \qquad \textbf{4.10}$$

When λ > 1, more time is required to create a level film than is available during solvent evaporation. From Equation 4.10, it can be observed that a faster evaporation rate E, or greater viscosity η will increase λ, indicating a relatively longer levelling time, meaning any defects are more likely to remain in the final film. Thus, the substrate coated with the lower molecular weight copolymer (FR-HD-90/10-(DMF)) may have a lower MSE due to a macroscopically smoother surface. This arises because a lower solution viscosity would

lead to a lower value of λ, implying more time was available for any striations to relax before jamming occurred.

FR-HD-90/10-(DMF) and FR-HGD-80/10/10 have a significantly different molecular weight: M_n = 13650 g mol^{-1} and 43400 g mol^{-1} respectively. The mole fraction of DMA of both copolymers is very similar. FR-HD-90/10-(DMF) had a slightly larger mole fraction HEMA than FR-HGD-80/10/10 (92 mol% and 83 mol% respectively). This may increase intermolecular H-bonding and hence viscosity of FR-HD-90/10-(DMF), although the difference is expected to be relatively small. Therefore, the differences between copolymer spin-coating behaviour are most likely due to differences in molecular weight, which will influence solution viscosity and solubility. Thus, according to Equation 4.10, a lower molecular weight and concomitant lower solution viscosity of FR-HD-90/10-(DMF) compared to FR-HGD-80/10/10 could explain the lower value of MSE and the inferred reduced presence of striations.

4.4.4.2.2.4 Analysis of spin-coated FR-HD-90/10-(DMF) films using AFM

The topography of two copolymer films, prepared under identical conditions from FR-HD-90/10-(DMF) and FR-HGD-80/10/10, was compared using AFM analysis (coatings 15 and 6 respectively, 4000 rpm, 600 rpm s^{-1}, 0.75% (w/v)). The AFM image of coating 15 (Figure 4.9A) shows a smooth, uniform film, with a very low R_a (0.21 ± 0.03 nm) and Z-range (5.50 ± 3.04 nm), whereas the AFM image of coating 6 (Figure 4.9B) is porous and starkly different. Methanol was used as the solvent in both cases, however there was a significant difference in copolymer molecular weight; the M_n of FR-HGD-80/10/10 was greater than FR-HD-90/10-(DMF) by a factor of ~3. It is likely that the lower molecular weight copolymer has increased solubility and therefore precipitates later in the spin-coating process. Therefore, any phase separation would not have a chance to become significant before jamming occurs, resulting in a non-porous structure. The copolymer composition could also affect the solubility to some extent, with the higher proportion of H-bonding monomers increasing the solubility of FR-HD-90/10-(DMF) with respect to FR-HGD-80/10/10 and reducing the probability of copolymer dewetting.

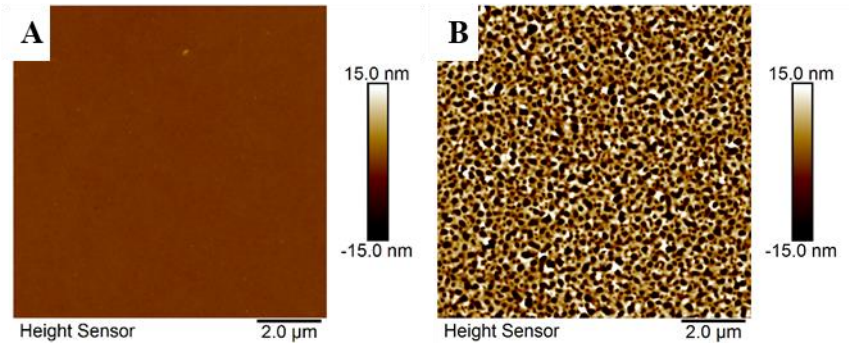

Figure 4.9. A) 2D AFM image of films of FR-HD-90/10-(DMF), spin-coated from a 0.75% (w/v) solution in methanol, 4000 rpm, 600 rpm s^{-1}. B) AFM image of FR-HGD-80/10/10, film 6. Images obtained by Andreas Janke, IPF, Dresden.

4.4.4.2.3 Analysis of spin-coated films of copolymer FR-HG-89/11 using ellipsometry and AFM

FR-HG-89/11 (M_n = 133500 g mol^{-1}) was also spin-coated onto silicon wafer to allow an investigation into the impact of the same parameters as for copolymers FR-HGD-80/10/10 and FR-HD-90/10-(DMF). The spin-coating parameters and ellipsometry results for silicon wafer coated with films of copolymer FR-HG-89/11 are given in Table 4.6.

Table 4.6. Ellipsometry data for films of copolymer FR-HG-89/11, spin-coated from methanol onto silicon wafer.

Coating Code	Soln Conc /% (w/v)	Spin Speed / rpm	Accel. / rpm s^{-1}	Film thickness / nm	MSE	RI (real part)
20	0.50	1000	400	47	9.64	1.52
21	0.75	1000	400	56	3.04	1.49
22	0.75	1000	400	53	5.20	1.51
23	0.75	4000	600	44	1.32	1.49
24	0.75	4000	600	48	2.48	1.48
25	2.00	1000	400	145	63.24	1.51
26	2.00	1000	400	140	55.78	1.51
27	2.00	4000	400	151	65.86	1.52
28	2.00	4000	400	140	69.37	1.51

4.4.4.2.3.1 Effect of spin-speed, acceleration and solution concentration on film thickness of FR-HG-89/11 coatings

It is clear that the key variable that impacts upon both film thickness and MSE is the solution concentration – other parameters once again seem to have little or no impact on the outcome (Table 4.6). Thus, as the solution concentration of FR-HG-89/11 increased from 0.50% to 2.00% w/v the film thickness increased approximately threefold from 47 nm to ~145 nm. Once again, the increase in film thickness was accompanied by a significant

increase in MSE from single digits values at low concentration to an average of 63.6 at 2.0% w/v.

4.4.4.2.3.2 Analysis of spin-coated FR-HG-89/11 films using AFM

An AFM image was collected for coating 24 (Figure 4.10, 4000 rpm, 600 rpm s^{-1}, 0.75% (w/v)). A smooth, uniform film was observed, which was very similar to the observation for FR-HD-90/10-(DMF) (coating 15, Figure 4.9). R_a and Z-range were very low (0.20 ± 0.01 nm and 8.58 nm ± 4.55 nm respectively).

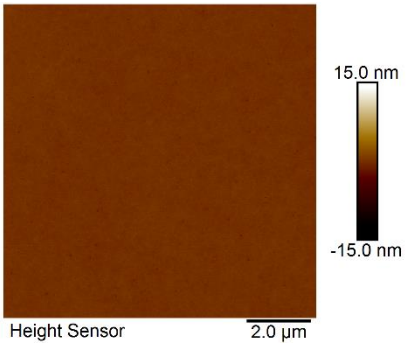

Figure 4.10. 2D AFM image of films of FR-HG-89/11, spin-coated from a 0.75% (w/v) solution in methanol, 4000 rpm, 600 rpm s^{-1}. AFM measurements carried out by Andreas Janke, IPF, Dresden.

As it is suggested that solubility is the primary parameter determining the presence or absence of pores, when the solvent is unchanged the factors which contribute to solubility should be considered. The M_n of FR-HG-89/11 is nearly 10 times that of FR-HD-90/10 which suggests molecular weight is not the only molecular feature determining the solubility. Ruiz-Molina *et al.* reviewed the literature on catechol adhesion and determined that the presence of the functional group increases cohesion in copolymers through intermolecular interactions.[25] In one instance, Kamperman *et al.* reported that in copolymers of DMA and 2-methoxyethyl methacrylate, a concentration of around 5 mol% DMA provided the best adhesion to glass. This was attributed to crosslinking via the catechol groups, which provided a surface attachment and copolymer cohesion to resist delamination, however a higher fraction of DMA actually decreased the adhesive strength as the copolymer became more brittle and the contact area between copolymer and surface decreased.[20] Additionally, it has been shown that many phenolic small molecules undergo significant intermolecular hydrogen bonding in solution.[66] Thus, we speculate that that the cohesive effect of the DMA in copolymers FR-HGD-80/10/10 and FR-HD-90/10-(DMF) due to significantly increased intermolecular interactions in the (concentrated) drying film also caused a significant increase in effective molecular weight, leading to increased

viscosity and decreased solubility. The multiple hydrogen bonds from catechol groups should form stronger intermolecular interactions with respect to the H-bonding interactions between catechol and methanol molecules. The absence of DMA from FR-HG-89/11 can thus account for the smooth film in Figure 4.10.

4.4.4.2.4 Analysis of spin-coated films of terpolymer RAFT-HGD-74/13/13 using ellipsometry and AFM

Finally, RAFT-HGD-74/13/13 (M_n = 24950 g mol^{-1}) was also spin-coated onto silicon wafer, with similar parameters modified as for FR-HGD-80/10/10, FR-HD-90/10-(DMF) and FR-HG-89/11 discussed in the previous sections. The spin-coating parameters and ellipsometry results for silicon wafer substrates spin-coated with FR-HG-89/11 are given in Table 4.7.

Table 4.7. Ellipsometry data for films of RAFT-HGD-74/13/13, spin-coated from methanol onto silicon wafer.

Coating Code	Soln Conc /% (w/v)	Spin Speed / rpm	Accel. / rpm s^{-1}	Film thickness / nm	MSE	RI (real part)
29	0.50	1000	400	34	17.13	1.54
30	0.75	1000	400	39	5.84	1.59
31	0.75	1000	400	41	3.37	1.54
32	0.75	4000	600	42	1.49	1.51
33	0.75	4000	600	44	1.78	1.50
34	2.00	1000	400	111	24.88	1.52
35	2.00	1000	400	121	37.37	1.52
36	2.00	4000	400	106	35.31	1.52
37	2.00	4000	400	118	36.70	1.54

4.4.4.2.4.1 Effect of spin-speed, acceleration and solution concentration on film thickness of RAFT-HGD-74/13/13 coatings

Once again, it is clear that solution concentration is the key variable in determining film thickness (Table 4.7). Upon increase of the solution concentration from 0.5% to 2.0% (w/v) (coatings 29, 34 and 35) the film thickness increased by a factor of around 4. Likewise, the MSE was low (>6) for the substrates spin-coated with 0.75% w/v solution, but much higher for the films coated from 2.00% solutions.

4.4.4.2.4.2 Analysis of spin-coated RAFT-HGD-74/13/13 films using AFM

An AFM image was collected for coating 33 (Figure 4.11A, 4000 rpm, 600 rpm s^{-1}, 0.75% (w/v)) to compare with previously obtained images of films coated using the same parameters. The AFM image shows a smooth, uniform film, which had very low R_a

(0.25 ± 0.02 nm) and Z-range (3.41 ± 0.86 nm). This was very similar to the observation for FR-HD-90/10-(DMF) (coating 15, Figure 4.9) and FR-HG-89/11 (coating 24, Figure 4.10), which were deposited using the same spin-coating parameters. That RAFT-HGD-74/13/13 resulted in a smooth film under these conditions (Figure 4.11A), whereas FR-HGD-80/10/10 resulted in a porous film, can be possibly attributed to increased solubility of RAFT-HGD-74/13/13, as the molecular weight is lower by a factor of ~2 and the DMA content is very similar.

An AFM image was also collected for coating 29, to determine whether non-porous coatings were also produced at low spin speeds, considering the surprisingly high MSE values (Figure 4.11B, 1000 rpm, 400 rpm s^{-1}, 0.50% (w/v)). Surprisingly, the two AFM images of the RAFT-HGD-74/13/13 coatings are dramatically different. The AFM image of coating 29 (Figure 4.11B) shows large pores with a diameter of around 2 µm. R_a and the Z-range are fairly large (5.27 nm and 40.67 nm respectively), indicating the diameter of the pores is much greater than the film thickness and significant regions of the substrate surface could be exposed. The presence of a porous surface indicates that, despite the low molecular weight of RAFT-HGD-74/13/13, phase separation was significant. This is surprising, as the polymer concentration of the solution used to deposit coating 29 was lower than coating 33 (which gave a smooth coating), and one would assume that solubility would not be worsened by a reduced concentration.

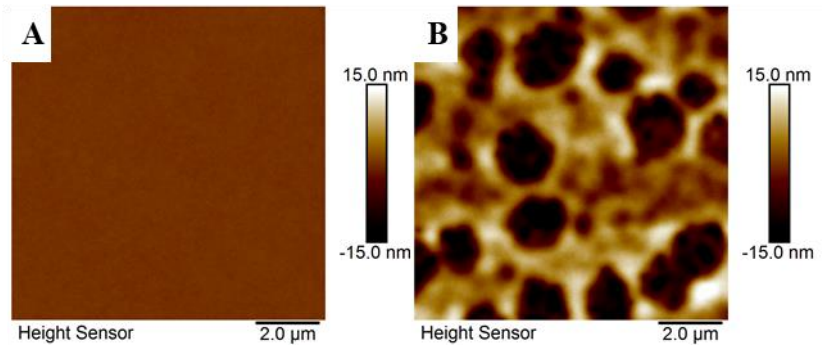

Figure 4.11. 2D AFM images of RAFT-HGD-74/13/13 terpolymer films, spin-coated from methanol solvent. A) 44 nm film, coating 33. B) 34 nm film, coating 29.

As multiple variables were altered simultaneously, and in the absence of further AFM data to fully investigate each variable, it is impossible to determine the precise cause of porosity in film coating 29 in Figure 4.11B. Moreover, there is no evidence that any copolymer used in this work could be spin-coated from methanol at 1000 rpm without the formation of pores; the other example of a film spin-coated at the same spin-coating speed was

coating 7 (Figure 4.8D), which was also porous but was created using a higher solution concentration. It was shown above that flow and evaporation are slower at a lower spin-speed (Equation 4.3). It could therefore be the case that after the solubility limit is reached (and the polymer precipitates), the phase separated structure has longer to coarsen and large pores are formed. In summary it is concluded that due to the presence of multiple defects, methanol is not an ideal choice of solvent for deposition of these copolymers. Due to time constraints, further work focused on changing the spin-coating solvent to achieve a more stable system.

4.4.4.2.5 Analysis of film thickness differences between the copolymer films

From the data discussed in sections 4.4.4.2.1 to 4.4.4.2.4 it was clear that when spin-coating copolymer films from methanol, film thickness showed a marked dependence on solution concentration, however there was no apparent correlation between spin speed or acceleration and film thickness. The trend of increased average film thickness with greater solution concentration can be clearly observed for all copolymers in Figure 4.12. The average film thickness of the lowest molecular weight copolymer, FR-HD-90/10-(DMF) (M_n = 13650 g mol^{-1}), increased by 172%; from 43 nm at 0.5% concentration to 116 at 2%. Likewise, the average film thickness of RAFT-HGD-74/13/13 (M_n = 24950 g mol^{-1}) increased by 175% upon the same change in concentration; from 42 nm to 114 nm. A very similar, though slightly larger film thickness increase of 186% was seen for FR-HGD-80/10/10 (M_n = 43400 g mol^{-1}); from 49 nm to 152 nm. The average film thickness increased for FR-HG-89/11 (M_n = 133500 g mol^{-1}) was almost identical to FR-HGD-80/10/10; increasing by 187% from 50 nm to 144 nm.

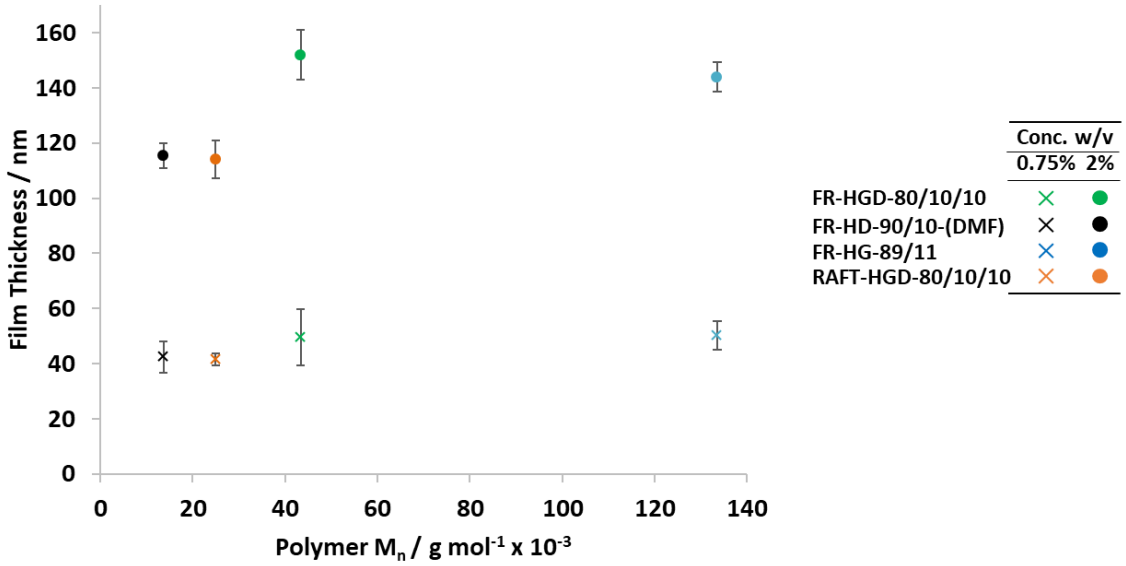

Figure 4.12. Average film thickness plotted against copolymer M_n for spin-coated copolymers at two concentrations. Crosses = 0.75% w/v, circles = 2% w/v.

Considering different copolymers deposited from solutions of the same concentration, the film thickness appeared to scale with molecular weight in a non-linear fashion. The difference between copolymers can be rationalised by considering the copolymer composition. Copolymers containing DMA appear to show a weak trend towards increased film thickness with increasing molecular weight. FR-HG-89/11 does not follow this trend, which suggests that the presence of DMA may increase the film thickness of the copolymer coating, due to increased viscosity because of the strong intermolecular H-bonding afforded by the catechol side chains.

It also became apparent that for copolymers deposited at 2% (w/v) solution concentration, MSE and copolymer film thickness were correlated (Figure 4.13). At 2% (w/v) solution concentration, all the films displayed striations. Striation amplitude has been shown to increase with increasing film thickness, as increased film thickness increases the Marangoni number (see Equation 4.6).[4, 67] Thus, MSE will increase with film thickness due to the greater light scattering caused by the increasing amplitude of the striations. In contrast, at 0.75% (w/v) solution concentration the MSE values generally do not vary significantly with film thickness; this is attributed to the deposition of smooth, striation-free films. However, the outlier is the FR-HGD-80/10/10, coated at 1000 rpm (coatings 2 and 3, average film thickness 54 nm, average MSE = 62). The MSE is significantly higher than the other copolymers, coated under the same conditions, which has been attributed earlier in this chapter to striations arising from the combined high molecular weight and

H-bonding from DMA. This evidence supports the previous suggestion that high MSE is linked to the presence of striations.

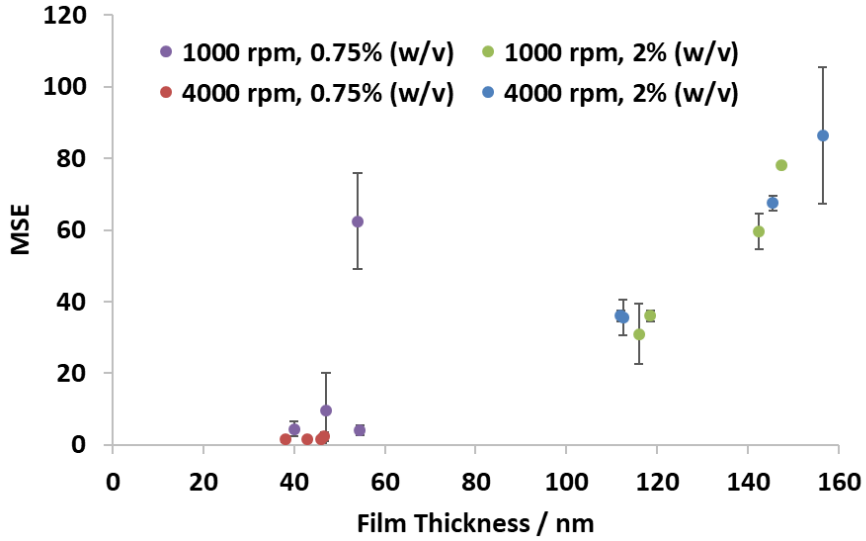

Figure 4.13. Film thickness vs MSE for copolymer films coated at different spin-speeds and solution concentrations.

4.4.4.3 Characterisation of copolymer films spin-coated from DMF

The porosity of some films reported in section 4.4.4.2 could significantly affect the suitability of the coatings for the applications targeted here, especially when using substrates such as nickel, which should not be exposed directly to biomolecules or cells. As the diameter of the pores are larger than the film thickness in all cases, the substrate may still be exposed. To ensure complete coverage and even functionalisation of a substrate surface, deposition of a smooth, uniform film would be preferable. As such, subsequent spin-coating experiments were carried out using DMF as the solvent for copolymer solutions. DMF was chosen as it is a good solvent for all copolymers under investigation and is much less volatile than methanol. It has been previously reported that solvent evaporation rate significantly impacts film roughness.[51] Reduced solvent volatility should reduce the likelihood of striations arising due to Marangoni instabilities, as slower evaporation reduces the temperature gradient across the film (ΔT, Equation 4.6). Were such instabilities to occur, a low rate of solvent evaporation would allow more time for defect levelling before the film structure becomes fixed.

Increased solubility of the copolymers in DMF may also decrease the probability of phase separation occurring and pores forming in the films. A previous report had noted that smooth films of poly(HEMA-co-ethyl methacrylate) of around 1 µm were obtained by spin-coating 10% (w/v) copolymer solutions from DMF at 4000 rpm.[45]

4.4.4.3.1 Analysis of copolymer films spin-coated from DMF using ellipsometry and AFM

0.75% (w/v) DMF solutions of FR-HGD-80/10/10, FR-HD-90/10-(DMF), FR-HG-89/11 and RAFT-HGD-74/13/13 were used to spin-coat thin films using a variety of spinning parameters. The impact of using DMF as the solvent on the roughness and uniformity of the resulting coatings was assessed using ellipsometry and AFM. The results are presented in Table 4.8. Solutions with 0.75% (w/v) concentration were selected because spin-coating using methanol solutions of the same concentration gave the lowest MSE values.

Table 4.8. Ellipsometry data for dry copolymer films. Spin-coated from 0.75% (w/v) copolymer solution in DMF onto silicon wafer.

Coating Code	Copolymer	Spin Speed / rpm	Accel / rpm s^{-1}	Film thickness / nm	MSE	RI (real part)
38	FR-HGD-80/10/10	1000	200	18	0.81	1.50
39	FR-HGD-80/10/10	2000	200	13	0.08	1.48
40	FR-HGD-80/10/10	2000	400	13	1.01	1.53
41	FR-HGD-80/10/10	4000	400	10	0.84	1.50
42	FR-HGD-80/10/10	4000	600	9	0.88	1.54
43	FR-HD-90/10-(DMF)	4000	600	4	0.98	1.69
44	FR-HG-89/11	4000	600	12	0.96	1.46
45	RAFT-HGD-74/13/13	4000	600	7	0.79	1.48

4.4.4.3.1.1 Effect of spin-speed, acceleration and solution concentration on films spin-coated from DMF

Five substrates were coated with FR-HGD-80/10/10 using increasing spin-speeds (from 1000 to 4000 rpm) and acceleration (from 200 to 600 rpm s^{-1}) to ensure that in each case the combination of spin speed and acceleration ensured that the time taken to reach maximum spin speed was 5 – 10 seconds. This range was chosen to roughly match the acceleration time used for the 4000 rpm coatings from methanol, which generally gave smooth coatings. The resulting films were much thinner than films obtained under identical spinning conditions from methanol solution. For example, the film thickness of coating 42 (DMF, 4000 rpm, 600 rpm s^{-1}) was 9 nm and the analogous film spin-coated from methanol (coating 6) was 37 nm. Likewise, the film thickness of coating 41 was 10 nm (DMF, 4000 rpm, 400 rpm s^{-1}) and the equivalent coating from methanol (coating 4) had a film thickness of 42 nm.

Equations 4.3 and 4.4, discussed in section 4.4.4.2.1, predict that the rate of film thinning depends on the spin speed, instantaneous film thickness, solution density and solution

viscosity. The predicted rate of film thinning for DMF solutions should be slower than methanol solutions due to the higher viscosity of DMF (DMF = 0.92 mPa s and methanol = 0.59 mPa s at 293 K). Thus, thicker films would be expected when using DMF. This is mitigated somewhat by the higher density of DMF (0.94 g cm^{-3}) compared to methanol (0.79 g cm^{-3}), due to the inversely proportional relationship between density and film thinning rate. Equations 4.3 and 4.4 do not consider the evaporation rate, yet Torkelson *et al.* reported that for films with a thickness of <200 nm (*i.e.* for all of the films considered in this work), the rate of solvent evaporation becomes increasingly significant. This in effect means more solvent is ejected from the disc for less volatile solvents before evaporation becomes important, such that less volatile solvents result in thinner films.[38] Thus, the final thickness of films coated from volatile solvents (such as methanol) is often underpredicted by Equation 4.3 due to excessive evaporation in the flow stage, which reduces the amount of time before jamming occurs. Due to the very thin films targeted in the current work, the reduced volatility of DMF compared to methanol is likely to be responsible for the observed thinner films.

Films of FR-HGD-80/10/10 were spin-coated from DMF at 1000 rpm (coating 38) to produce a film of 18 nm thickness, at 2000 rpm to produce two films of 13 nm (coatings 39 and 40) and at 4000 rpm spin-speed to produced coatings of 9 and 10 nm (coatings 41 and 42 respectively). The range of film thickness values was very narrow (9 – 18 nm) compared to the differences observed for substrates spin-coated from methanol using identical parameters. However, the MSE values were very low (≤ 1.01), indicating the model could be fitted well, indicating good reliability of the data. The MSE values may also be reduced due to the coupling of the RI and film thickness for very thin films (>15 nm), meaning fewer constraints are fitted.

Table 4.8 also shows ellipsometric film thickness data for coatings of FR-HD-90/10-(DMF) (coating 43), FR-HG-89/11 (coating 44) and RAFT-HGD-74/13/13 (coating 45), spin-coated from 0.75% (w/v) solutions from DMF. Spin-coating parameters identical to coating 42 were used (4000 rpm speed, 600 rpm s^{-1} acceleration). The film thickness of the coating from FR-HD-90/10-(DMF) was only 4 nm, from FR-HG-89/11 was 12 nm, from RAFT-HGD-74/13/13 was 7 nm and MSE all values were <1. As discussed previously, the uncertainty of measurements of very thin coatings is increased, however it can be suggested with caution that although the absolute film thickness values are smaller, the trends agree well with the findings from section 4.4.4.2.5, in which thinner films were

produced by solutions of low M_n copolymers (FR-HD-90/10-(DMF) and RAFT-HGD-74/13/13), due to their lower viscosity and a thicker film was obtained from the high M_n copolymer (FR-HG-89/11) due to increased viscosity.

4.4.4.3.1.2 Analysis of films spin-coated from DMF using AFM

In all cases the films cast from DMF solutions were free from visible striations although edge effects persisted (an example is shown in Figure 4.14A). The MSE values were consistently low (<1) which could also be attributed to the low volatility of DMF, either due to the absence of Marangoni flows due to low ΔT, or to the additional relaxation time afforded by the slow evaporation.[4, 39] The smooth films increased the confidence associated with the film thickness data in Table 4.8; the large uncertainty in the film thickness measurements for films cast from methanol was probably due to the presence of striations on the coatings.

To investigate the impact of spin-coating from DMF on the surface topography of the resulting films, coating 42 (FR-HGD-80/10/10, 4000 rpm) was then analysed using AFM (Figure 4.14B). This coating was chosen as it had been produced using the same spin-coating parameters as the substrates coated from methanol solutions which were analysed previously by AFM.

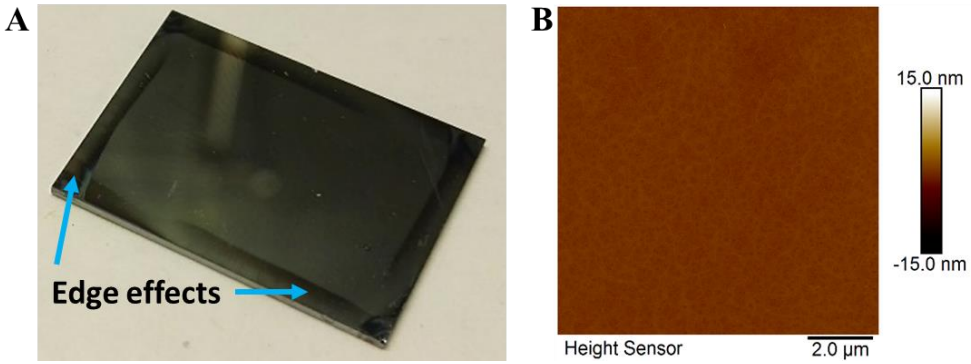

Figure 4.14. A) Photograph of coating 42, FR-HGD-80/10/10 spin-coated on silicon wafer from 0.75% (w/v) solution in DMF. B) 2D AFM image of coating 42. AFM image obtained by Andreas Janke, IPF, Dresden.

In contrast to the analogous films spin-coated from methanol (coating 6, Figure 4.8A), in which a porous coating was observed, the AFM image for coating 42 appeared uniform and smooth. Increased solubility of the copolymers in DMF would reduce the likelihood of phase separation occurring and porous structures forming. Additionally, reduced H-bonding between DMF and siloxane groups on the wafer surface may enable increased

interaction between copolymer chains and the coating. The image in Figure 4.14 has a low R_a (0.30 ± 0.01 nm) and Z-range (10.60 ± 4.68 nm), suggesting a smooth coating.

4.4.4.3.2 Investigation of the impact of solution viscosity on film roughness when spin-coating from DMF

The films discussed in the preceding section (4.4.4.3.1) were spin-coated from DMF, using 0.75% copolymer solution concentrations. The copolymers each contained relatively low mole fractions of DMA. Coatings with thicknesses of <20 nm and low MSE (<2) were obtained.

In a further experiment, FR-HGD-58/9/33 (M_n = 110650 g mol^{-1}) was spin-coated on air plasma treated silicon wafer from a 2% (w/v) copolymer solution in DMF (coating 46). NMR analysis indicated that despite the feed ratio indicated in the copolymer name, FR-HGD-58/9/33 comprised 15 mol% DMA. Thus, the DMA mole fraction and M_n of FR-HGD-58/9/33 were higher than FR-HGD-80/10/10 (M_n of 43400 g mol^{-1} and 6% DMA). The solution concentration was also increased compared to the previously discussed copolymer coatings from DMF (Table 4.8). It was anticipated that the combined impact of an increase in DMA content (as previously speculated), M_n and solution concentration would lead to significantly increased solution viscosity. Thus, FR-HGD-58/9/33 was used to investigate the limits of producing homogenous films from copolymer solutions in DMF. FR-HGD-58/9/33 remained soluble in DMF at 2% (w/v) concentration and surprisingly, spin-coating (4000 rpm, 600 rpm^{-1}) yielded a film without visible striations.

Optical microscopy and AFM analysis were used to analyse the topography of the resulting films (Figure 4.15). As AFM only measures surface topography, film thickness could not be measured directly. To overcome this, the film was scratched with forceps which displaced a channel of the copolymer film from the substrate. By careful positioning of the AFM tip (using optical microscopy, Figure 4.15A) at the edge of the scratch, an image was obtained which included areas of both the scratched region and the pristine copolymer film (Figure 4.15B).

Using the AFM analysis software, the height profile, indicated by orange/red/blue arrows on Figure 4.14B, was analysed to obtain a cross-sectional chart (Figure 4.15C). The orange/red/blue coloured lines in Figure 4.15C represent the varying height of the film along the direction indicated by the arrows on the AFM image (Figure 4.15B). By comparing the average heights of the scratched region (black dashed horizontal line at

~20nm) and the copolymer film region (black solid line) indicated in Figure 4.15C the film thickness was estimated at 25 nm. At the boundary of the scratched region and the pristine copolymer region, the scratching process resulted in the formation of an elevated ridge of displaced copolymer (indicated on Figure 4.15B). This ridge, up to 100 nm in height was ignored when estimating the film thickness. The same method was used to estimate film thickness using AFM where indicated in subsequent examples.

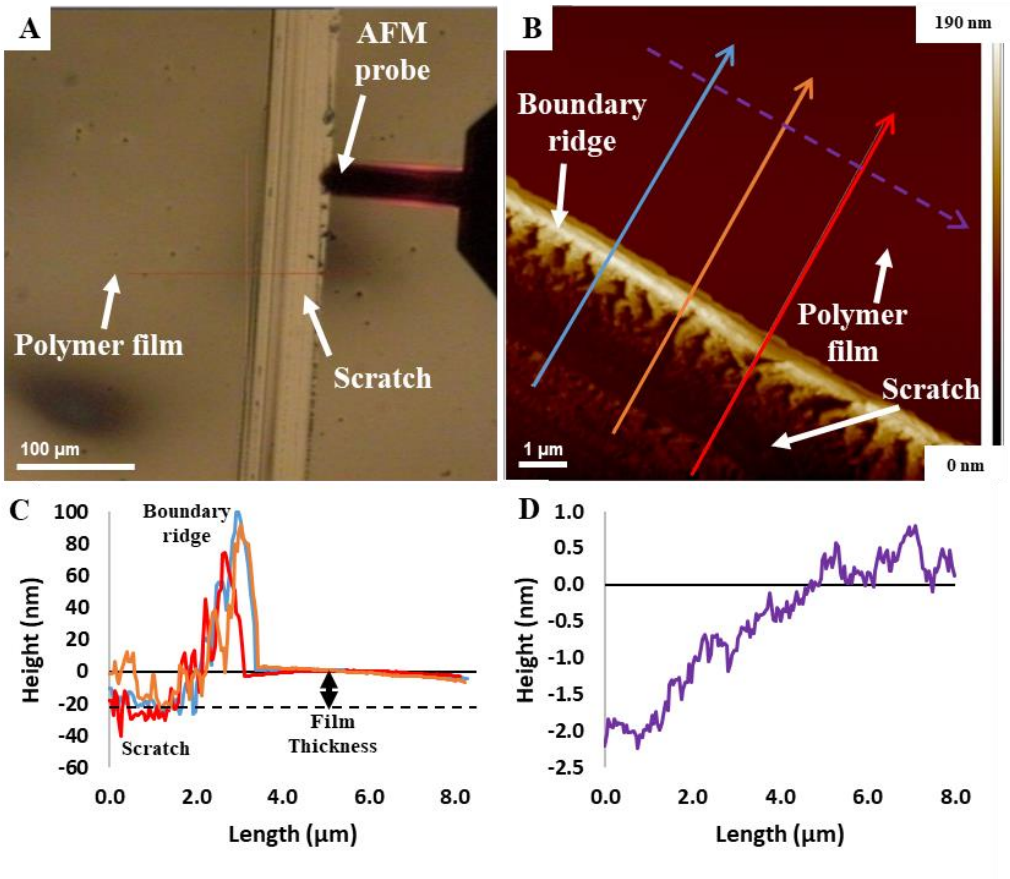

Figure 4.15. Scratched film of copolymer FR-HGD-58/9/33 spin-coated from DMF. A) Optical microscope image. B) 2D AFM image. C) Cross section height data for solid lines (red, orange and blue) on image B. D) Cross section height data for dashed line (purple) on image B.

By obtaining a cross-sectional profile in the direction parallel to the scratch (Figure 4.15B, dashed purple line) it was possible to demonstrate the low surface roughness of the copolymer film, with height variation of <3nm over 8 µm distance (Figure 4.15D). The R_a of the smooth film was 0.59 nm and Z-range 12.6 nm, indicating the exceptional homogeneity and smoothness of the copolymer films deposited from DMF. This confirmed that DMF is a good solvent for the deposition of smooth films from HEMA/DMA copolymer solutions with a wide range of concentrations, molecular weight and DMA content.

To ensure that the estimated film thickness was not influenced by damage to the silicon wafer caused by scratching, the same method was used to scratch and analyse a blank silicon wafer (Figure 4.16).

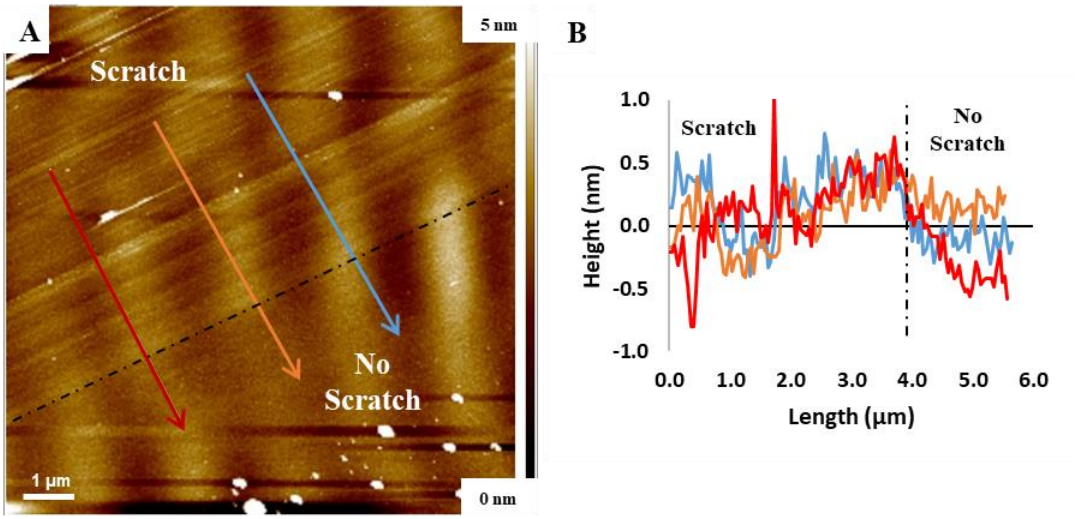

Figure 4.16. A) AFM image of scratched blank wafer. The black dashed line indicates the boundary between the scratched and non-scratched regions B) Cross-sectional depth profile of the coloured lines on image A.

The coloured lines on Figure 4.16A indicate the location of measurements used for the height profile (Figure 4.16B). Figure 4.16B demonstrates that the pristine part of the wafer surface was extremely flat (<0.5 nm peak height). Some deposits of around 10 nm can be observed on the AFM image (in the unscratched region), which can be attributed to dust as the preparation and measurement was not carried out in a clean-room environment. The scratched area has marginally increased peak heights, though they are generally still <1 nm. The R_a was 0.23 nm, only slightly greater than a clean, unscratched silicon wafer (R_a = 0.11 nm). The low profile of the scratch confirmed the method was appropriate to obtain cross sections of the polymer layers.

4.4.5 Optimisation of immersion-coating and thin film characterisation with AFM and ellipsometry

There exists a large amount of data attesting to the ability of the catechol functional group to bind to surfaces through a variety of interactions.[25] Adhesion of poly(PEGMEM-co-DMA) to a gold electrode in solution has previously been quantified using quartz crystal microbalance.[27] Furthermore, catechol-containing copolymers have been immobilised on nanoparticles in solution.[68, 69] As such, it was hypothesised that copolymer samples containing DMA could be deposited on a surface by immersion of a silicon wafer substrate in a polymer solution. A short investigation was therefore carried out to i) identify

appropriate conditions to enable surface adhesion of DMA-containing copolymer samples, ii) attempt to correlate the resulting polymer film thickness and uniformity with copolymer composition and molecular weight, and thus iii) evaluate the suitability of the copolymer films for potential industrial applications.

4.4.5.1 Analysis of immersion-coating from copolymer solutions in DMF and pyridine

Preliminary testing of immersion-coating using methanol and a solution of methanol and THF as solvents yielded heterogeneous and inconsistent films. This was attributed to hydrogen bonding between the hydroxyl groups in methanol and the silicon wafer substrate, reducing the likelihood of polymer adsorption to the surface. It has been reported that polymer adsorption to a substrate can be compromised if the solvent interacts strongly with the substrate.[70] DMF was selected as an alternative to methanol since DMF, unlike methanol, will not H-bond with the substrate surface. However, preliminary tests using DMF as a solvent did not yield polymer films. It has been reported that immersion-coating of catechol-containing films was possible at pH 8.5 as the oxidation of the catechol groups to the quinone form led to crosslinking and increased copolymer cohesion.[8] The quinones may undergo crosslinking to form a network, increasing the cohesion of the copolymer.[10, 25] Pyridine was used to adjust the pH. It was selected as the base to avoid reactions which readily occur between epoxides and primary or secondary amines.[71] Thus, DMF containing pyridine as a basic additive was used with a view to inducing partial oxidation of the catechol groups to quinones in an attempt to produce thicker and more homogeneous films. Oxidation could occur in solution or on the substrate surface, but it was hypothesised that in both cases the increased inter-chain interactions would increase surface immobilisation.

In a previous report, low molecular weight catechol-terminated PEG (M_n = 5000 g mol^{-1}) was deposited by immersion of TiO_2 and Nb_2O_5 substrates in aqueous polymer solutions, leading to film thicknesses of 1 – 2 nm formed via strong metal oxide-catechol interactions.[9] However, deposition of the same polymers on SiO_2 led to film thicknesses of <0.4 nm. The affinity of the catechol groups for the surfaces was reported to be strongest at pH values close to the isoelectric point for each substrate (~pH 2 for SiO_2). In the current investigation, use of strongly acidic solutions to encourage bonding of polymers to SiO_2 would result in ring-opening of the epoxide, so basic conditions were used as an alternative approach favouring oxidative crosslinking of the catechols. Furthermore, copolymers with a higher DMA content were used (FR-HGD-58/9/33 and FR-HD-70/30-(DMF)) to more

easily elucidate the influence of the catechol group on copolymer deposition. FR-HG-89/11 and a HEMA homopolymer (FR-H) were also included as catechol-free controls. The surface topography and film thickness of the films deposited from DMF were analysed using AFM. Film thickness and roughness data is presented in Table 4.9.

Table 4.9. Film thickness data, estimated using AFM, for polymer coatings, 2% (w/v) solution in DMF with 1% (v/v) pyridine.

Coating	Polymer	Film thickness / nm	R_a / nm	Z-range / nm
47	FR-HGD-58/9/33	5	1.27	25.5
48	FR-HD-70/30-(DMF)	< 1	0.35	30.3
49	FR-HG-89/11	2	0.48	13.4
50	FR-H	0	0.11	9.51

FR-HGD-58/9/33 was deposited onto silicon wafer from a 2% (w/v) solution in DMF containing 1% (v/v) pyridine (coating 47). During the coating process, a solution colour change from colourless to light brown suggested oxidation of the catechol groups had occurred. In the AFM image (Figure 4.17A) a scratch can be observed in the top left corner of the wafer. The boundary between the scratched and non-scratched areas is indicated with a purple dashed line. The estimated depth of the scratch is 5 nm, using the lowest points in the scratched and non-scratched areas of the cross-sectional profile (Figure 4.17B). This clearly indicated the presence of a polymer coating on the silicon wafer. Moreover, large peaks were observed in the scratched area due to ridges (~50 nm high) arising from polymer displaced by the scratching process. The unscratched area of the polymer coating appeared to be relatively homogeneous, but with some deposits of ~10 nm. This was supported by analysis of an unscratched area of the film, which had a low R_a of 1.27 nm and a Z-range of 25.5 nm, marked on the image with a blue box.

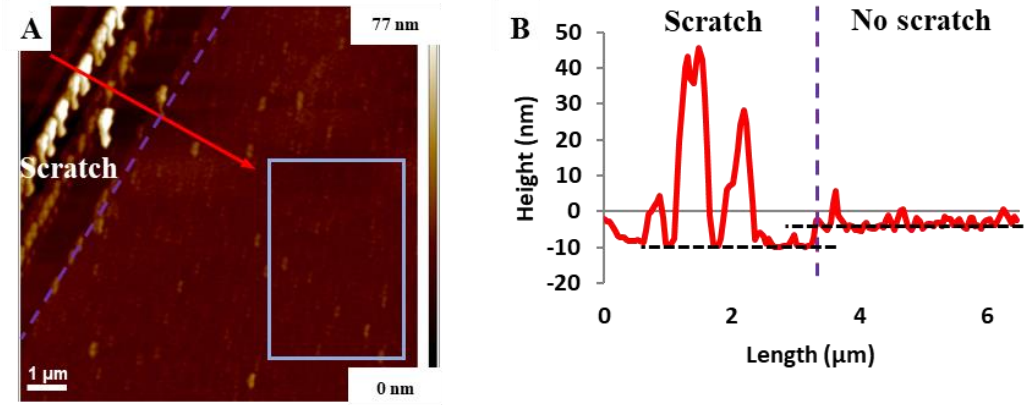

Figure 4.17. A) AFM image of scratched film of FR-HGD-58/9/33, immersion-coated from DMF with pyridine on silicon wafer. Blue squares indicate region of roughness measurement. B) Height profile corresponding to red arrow on image A.

AFM analysis of the scratched coating of FR-HD-70/30-(DMF) indicated the film thickness was <1 nm (although the scratch can clearly be observed in Figure 4.18). This could suggest only a monolayer was present on the film surface. Despite the larger mole fraction of DMA in the copolymer (25%), the coating of FR-HD-70/30-(DMF) was much thinner than FR-HGD-58/9/33 (15% DMA). The molecular weights of FR-HGD-58/9/33 and FR-HD-70/30-(DMF) were very different (110650 g mol^{-1}, 68/12/20 compared to 3050 g mol^{-1}, 75/25). It was suspected that FR-HD-70/30-(DMF) was a branched, low molecular weight copolymer which may result in low viscosity and fewer entanglements (see Chapter 2).[72] The result could be indicative of the vast difference in molecular size and entanglements; both copolymers bind to the surface, but the thickness of a layer of FR-HGD-58/9/33 is greater. In the unscratched area of FR-HD-70/30-(DMF), R_a was 0.35 nm and the Z-range 30.3 nm, indicating a generally more homogeneous film compared to FR-HGD-58/9/33, but with some deposits still present.

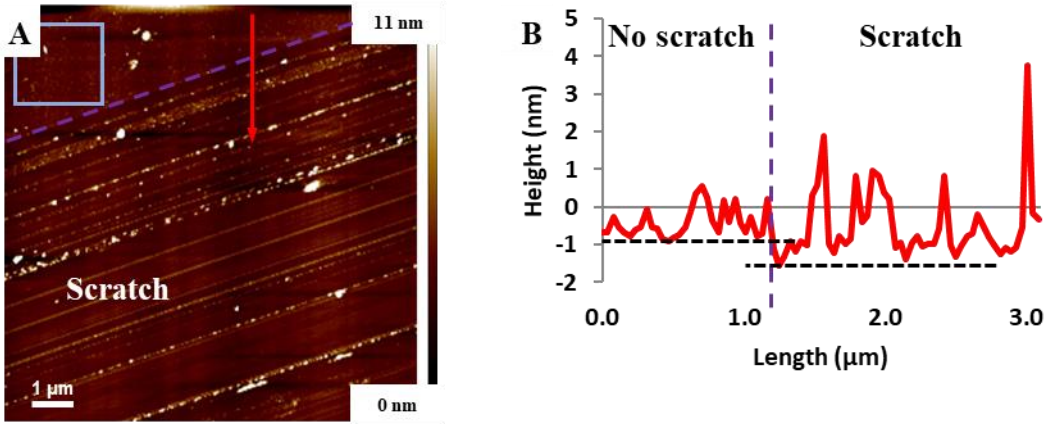

Figure 4.18. A) AFM image of scratched film of FR-HD-70/30-(DMF), immersion-coated from DMF with pyridine on silicon wafer. Blue squares indicate region of roughness measurement. B) Height profile corresponding to red arrow on image A.

The AFM image of immersion-coated FR-HG-89/11 (Figure 4.19) shows a clear scratch where a copolymer film has been displaced; analysis indicated the presence of a very thin copolymer film. The presence of a polymer film is perhaps surprising given the lack of catechol groups in the copolymer. This could indicate that FR-HG-89/11 can be deposited on the silicon wafer surface *via* a large number of H-bonding interactions between the hydroxyl functionalities in HEMA and silanol groups on the silicon wafer surface. In the case of FR-HG-89/11, retention of the adsorbed copolymer on the surface could have been enhanced because of the high molecular weight of the copolymer (133500 g mol^{-1}). Furthermore, with such apparently thin films, it could also be the case that the copolymer is weakly adsorbed to the surface and copolymer chains were not fully removed by the

rinsing process due to the large molecular weight. It has been reported that polymer absorption on oxides increases with molecular weight, although this dependency is stronger in a poor solvent than a good solvent.[70] Despite the larger molecular weight of FR-HG-89/11, the comparatively thicker coating of FR-HGD-58/9/33 suggests DMA may be playing an active role in increasing film thickness, although this cannot be proven from the current limited data. It is hypothesised that the presence of DMA is likely to enhance copolymer cohesion by oxidative chain coupling. In the unscratched area of FR-HG-89/11, R_a was 0.48 nm and the Z-range 13.4 nm, indicating fewer large peaks compared to FR-HGD-58/9/33, and a more homogeneous film.

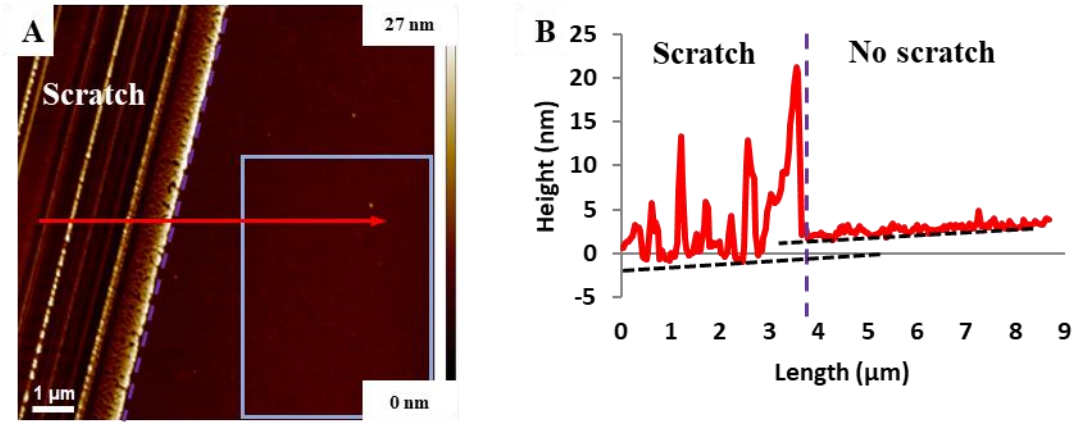

Figure 4.19. A) AFM image of scratched film of FR-HG-89/11, immersion-coated from DMF with pyridine on silicon wafer. Blue squares indicate region of roughness measurement. B) Height profile corresponding to red arrow on image A.

AFM analysis of the substrate exposed to FR-H (Figure 4.20) showed only a faint sign of a scratch in the bottom-right corner, with a small number of peaks arising from the scratching process. No film was observed on the wafer, and the R_a of 0.11 nm and Z-range of 9.51 nm was very similar to a blank silicon wafer. The molecular weight of FR-H (17250 g mol^{-1}) is much lower than FR-HGD-58/9/33 and FR-HG-89/11, but larger than FR-HD-70/30-(DMF), so the combination of relatively low molecular weight and lack of the strong H-bonding ability of DMA catechol side chains probably renders FR-H only able to adsorb very weakly on the substrate. Thus, any chains that were weakly adsorbed may have been more easily removed from the surface by rinsing.

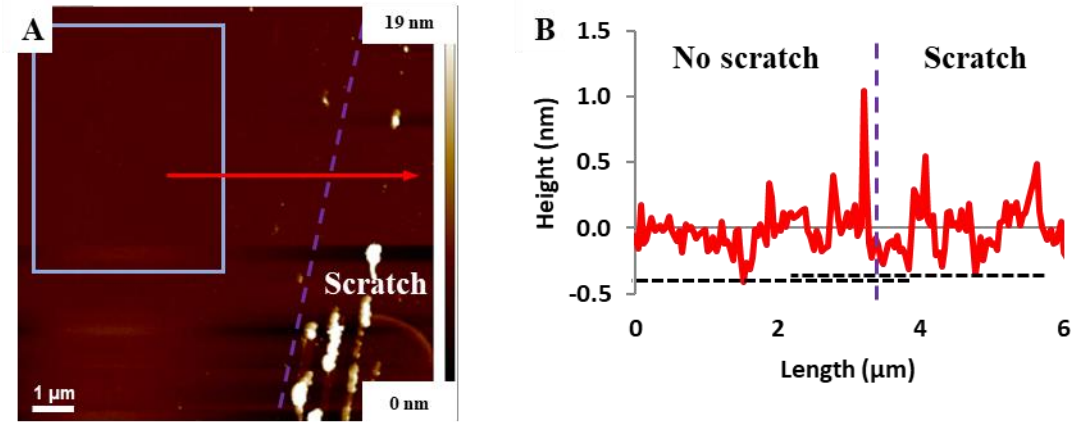

Figure 4.20. A) AFM image of scratched film of FR-H, immersion-coated from DMF with pyridine on silicon wafer. Blue squares indicate region of roughness measurement. B) Height profile corresponding to red arrow on image A.

In summary, a coating of FR-HGD-58/9/33 could be deposited on silicon wafer from a DMF solution containing pyridine, but the factors influencing deposition could not be isolated in this short study. Although not optimised in the current study, this approach could be further explored with the intention of immobilising ultra-thin coatings of DMA-containing copolymers on silicon wafers or alternative substrates directly from a solution.

4.5 Conclusion

The solubility of copolymers comprising a variety of monomers was investigated. It was concluded that terpolymers containing a high mole fraction of HEMA (RAFT-HGD-80/14/6 and FR-HGD-80/10/10) had the same solubility profile as a homopolymer of HEMA (FR-H) despite the addition of DMA and the less polar GMA. The copolymers of MMA and (A)DMA investigated had the same solubility profile as MMA homopolymers; generally soluble in polar aprotic solvents, but insoluble in polar protic and non-polar solvents. The wide solubility range in the library of synthesised polymers was demonstrated by considering an SMA/ADMA copolymer, which was soluble in lower polarity solvents such as toluene and diethyl ether. Copolymers containing HEMA were selected for further study because of their excellent solubility profile for the potential industrial applications.

Spin-coating of FR-HGD-80/10/10, FR-HD-90/10-(DMF), FR-HG-89/11 and RAFT-HGD-74/13/13 from methanol solutions was subsequently investigated. Coatings of FR-HGD-80/10/10 showed defects in the film. Striations were attributed to the Marangoni effect, due to concentration gradients forming in the polymer solution during the spin-coating process, causing waves to from on the surface of the film. Films exhibiting

striations were generally identifiable by high ellipsometric MSE. It was noted that in general, films coated from solutions of 0.75% (w/v) exhibited fewer striations than those coated from solutions of higher polymer concentrations, as judged by the ellipsometric MSE. It would seem reasonable to expect that the reduction in viscosity (at lower concentration) allowed levelling of the polymer to occur prior to striations becoming fixed.

For some coatings, porosity was also observed by AFM and was attributed to phase separation of the polymer and solvent when the concentration was increased as a result of solvent evaporation. In the case of FR-HGD-80/10/10, we believe that the combination of a high molecular weight polymer and DMA induced cohesion, which decreased solubility, such that phase separation occurred before the evaporation was complete. At the end of the flow phase the polymer topography became fixed and the remaining solvent evaporated, resulting in the formation of pores. It was concluded that the causes of striations and porosity were distinct because high ellipsometric MSE did not correlate well with the presence of porous films. However, due to the complex nature of the system, the two forms of defects cannot be decoupled with certainty.

The impact of various spin-coating parameters was explored (spin speed, acceleration, solution concentration) and variation of these parameters resulted in films with widely varying thickness; from 26 – 165 nm. However, interrogation of the data indicated that there was little evidence of any correlation between film thickness and spin-speed/acceleration and thus variation in thickness (for spin-coated films of the same polymer) was primarily attributed to variation in solution concentration. It was concluded that increasing concentration resulted in increased solution viscosity which in turn caused less polymer to be ejected from the disc, yielding coatings with greater film thickness.

When comparing films spin-coated using the same spinning parameters (spin speed, acceleration, concentration), but using different copolymers, film thickness appeared to depend on solution viscosity, which in turn was largely (but not solely) dependent on copolymer molecular weight and solution concentration. In some cases the mole fraction of DMA in the polymers may have played a role, in so much that the presence of DMA may have increased viscosity due to strong intermolecular H-bonding from the catechol functional group.

Copolymers FR-HGD-80/10/10, FR-HD-90/10-(DMF), FR-HG-89/11 and RAFT-HGD-74/13/13 were also spin-coated from DMF, which clearly resulted in films which were

thinner and more homogeneous than the analogous films spin-coated from methanol. This was attributed primarily to the reduced rate of evaporation of DMF compared to methanol and the increased solubility of the polymers in DMF compared to methanol. Films free of striations were produced from all polymers at 0.75% (w/v) solution concentration due to the reduced evaporation rate of the less volatile solvent. Furthermore, no porosity was observed in the films, probably due to the increased solubility of the polymers in the DMF solution. Additionally, FR-HGD-58/9/33 was spin-coated on to silicon wafer using a 2% (w/v) DMF solution. Despite the potentially increased viscosity due to high molecular weight and intermolecular H-bonding arising from the high DMA content, AFM indicated the coating was exceptionally smooth and free of defects. It was thus concluded that DMF could be used to produce smooth films over a wide range of copolymer compositions and solution concentrations, and clearly gave better outcomes than methanol.

Immersion-coating was also investigated. Substrates were immersion-coated using FR-HGD-58/9/33, FR-HD-70/30-(DMF), FR-HG-89/11 and FR-H using a solution of DMF and pyridine. It was hoped that the basic solution would promote oxidative chain coupling of DMA to occur, increasing the cohesion of the films, which was indicated by the appearance of a brown colour in the solution. AFM indicated a thin film of FR-HGD-58/9/33 was deposited with film thickness of ~5 nm. AFM also suggested the presence of very thin coatings of FR-HD-70/30-(DMF) and FR-HG-89/11, however due to the inconsistent coatings, factors influencing the deposition could not be properly determined. Further investigation is required to determine optimised conditions for deposition of these polymers by immersion.

4.6 References

1. D. Meyerhofer, *J. Appl. Phys.*, 1978, **49**, 3993-3997.
2. A. G. Emslie, F. T. Bonner and L. G. Peck, *J. Appl. Phys.*, 1958, **29**, 858-862.
3. C. J. Lawrence, *Physics of Fluids*, 1988, **31**, 2786.
4. D. P. Birnie, *J. Mater. Res.*, 2001, **16**, 1145-1154.
5. H. Lee, S. M. Dellatore, W. M. Miller and P. B. Messersmith, *Science*, 2007, **318**, 426-430.
6. C. J. Brinker, G. C. Frye, A. J. Hurd and C. S. Ashley, *Thin Solid Films*, 1991, **201**, 97-108.
7. C. X. Wang, A. Braendle, M. S. Menyo, C. W. Pester, E. E. Perl, I. Arias, C. J. Hawker and D. Klinger, *Soft Matter*, 2015, **11**, 6173-6178.
8. Q. Wei, T. Becherer, R. C. Mutihac, P. L. Noeske, F. Paulus, R. Haag and I. Grunwald, *Biomacromolecules*, 2014, **15**, 3061-3071.
9. B. Malisova, S. Tosatti, M. Textor, K. Gademann and S. Zurcher, *Langmuir*, 2010, **26**, 4018-4026.
10. Q. Wei and R. Haag, *Materials Horizons*, 2015, **2**, 567-577.
11. E. Bittrich and K.-J. Eichhorn, in *Polymer Surface Characterization*, ed. L. Sabbatini, De Gruyter, 2014.
12. W. A. McGahan, B. Johs and J. A. Woollam, *Thin Solid Films*, 1993, **234**, 443-446.
13. K. Hinrichs and K.-J. Eichhorn, *Ellipsometry of Functional Organic Surfaces and Films*, Springer, 2014.
14. G. Binnig, C. F. Quate and C. Gerber, *Phys. Rev. Lett.*, 1986, **56**, 930-933.
15. S. N. Magonov and D. H. Reneker, *Annu. Rev. Mater. Sci.*, 1997, **27**, 175-222.
16. M. Vayer, A. Vital and C. Sinturel, *Eur. Polym. J.*, 2017, **93**, 132-139.
17. H. Mori, O. Wakisaka, A. Hirao and S. Nakahama, *Macromol. Chem. Phys.*, 1994, **195**, 3213-3224.
18. J. Brandrup and E. H. Immergut, *Polymer Handbook*, Wiley Interscience, 3rd edn., 1989.
19. N. Patil, C. Jérôme and C. Detrembleur, *Prog. Polym. Sci.*, 2018, **82**, 34-91.
20. J. Yang, J. Keijsers, M. van Heek, A. Stuiver, M. A. Cohen Stuart and M. Kamperman, *Polym. Chem.*, 2015, **6**, 3121-3130.
21. H. N. Nguyen, E. T. Nadres, B. G. Alamani and D. F. Rodrigues, *J. Mater. Chem. B*, 2017, **5**, 6616-6628.
22. F. J. Holly, *J. Biomed. Mater. Res.*, 1975, **9**, 315-326.
23. J. V. M. Weaver, I. Bannister, K. L. Robinson, X. Bories-Azeau, S. P. Armes, M. Smallridge and P. McKenna, *Macromolecules*, 2004, **37**, 2395-2403.
24. D. E. Gregonis, G. A. Russell, J. D. Andrade and A. C. Devisser, *Polymer*, 1978, **19**, 1279-1284.
25. J. Saiz-Poseu, J. Mancebo-Aracil, F. Nador, F. Busque and D. Ruiz-Molina, *Angew. Chem., Int. Ed.*, 2019, **58**, 696-714.
26. S. Han, M. Hagiwara and T. Ishizone, *Macromolecules*, 2003, **36**, 8312-8319.
27. N. Patil, C. Falentin-Daudré, C. Jérôme and C. Detrembleur, *Polym. Chem.*, 2015, **6**, 2919-2933.
28. W. M. de Vos, B. Cattoz, M. P. Avery, T. Cosgrove and S. W. Prescott, *Langmuir*, 2014, **30**, 8425-8431.
29. P. Frantz and S. Granick, *Langmuir*, 1992, **8**, 1176-1182.
30. E. Spruijt, P. M. Biesheuvel and W. M. de Vos, *Physical Review E*, 2015, **91**, 11.
31. C. Zhao, L. Li, Q. Wang, Q. Yu and J. Zheng, *Langmuir*, 2011, **27**, 4906-4913.

32. W. Ogieglo, H. Wormeester, K. J. Eichhorn, M. Wessling and N. E. Benes, *Prog. Polym. Sci.*, 2015, **42**, 42-78.
33. J. A. Woollam, B. D. Johs, C. M. Herzinger, J. N. Hilfiker, R. A. Synowicki and C. L. Bungay, presented in part at the Optical Metrology: A Critical Review, 1999.
34. P. Nestler and C. A. Helm, *Opt Express*, 2017, **25**, 27077-27085.
35. D. E. Aspnes, J. B. Theeten and F. Hottier, *Phys. Rev. B*, 1979, **20**, 3292-3302.
36. D. Lehmann, F. Seidel and D. R. T. Zahn, *SpringerPlus*, 2014, **3**, 82.
37. K. Choi, S. Ghosh, J. Lim and C. M. Lee, *Appl. Surf. Sci.*, 2003, **206**, 355-364.
38. D. B. Hall, P. Underhill and J. M. Torkelson, *Polym. Eng. Sci.*, 1998, **38**, 2039-2045.
39. L. L. Spangler, J. M. Torkelson and J. S. Royal, *Polym. Eng. Sci.*, 1990, **30**, 644-653.
40. D. E. Bornside, C. W. Macosko and L. E. Scriven, *J. Appl. Phys.*, 1989, **66**, 5185-5193.
41. D. P. Birnie, S. K. Hau, D. S. Kamber and D. M. Kaz, *J. Mater. Sci.: Mater. Electron.*, 2005, **16**, 715-720.
42. W. J. Daughton and F. L. Givens, *J. Electrochem. Soc.*, 1982, **129**, 173-179.
43. W. W. Flack, D. S. Soong, A. T. Bell and D. W. Hess, *J. Appl. Phys.*, 1984, **56**, 1199-1206.
44. J. Q. Xu, Y. J. Liu, J. S. He, R. P. Zhang, B. Zuo and X. P. Wang, *Soft Matter*, 2014, **10**, 8992-9002.
45. D. S. Walker, K. Balasubramanian and W. M. Reichert, *J. Appl. Polym. Sci.*, 1993, **49**, 2147-2155.
46. D. T. W. Toolan and J. R. Howse, *J. Mater. Chem. C*, 2013, **1**, 603-616.
47. S. Sakka and H. Kozuka, *Handbook of Sol-Gel Science and Technology. 1. Sol-Gel Processing*, Springer Science & Business Media, 2005.
48. D. E. Haas and D. P. Birnie, *J. Mater. Res.*, 2001, **16**, 3355-3360.
49. P. Muller-Buschbaum, J. S. Gutmann, M. Wolkenhauer, J. Kraus, M. Stamm, D. Smilgies and W. Petry, *Macromolecules*, 2001, **34**, 1369-1375.
50. C. M. Hansen, *Ind. Eng. Chem. Prod. Res. Develop.*, 1970, **9**, 282-286.
51. K. E. Strawhecker, S. K. Kumar, J. F. Douglas and A. Karim, *Macromolecules*, 2001, **34**, 4669-4672.
52. R. L. Jones, T. J. Hu, C. L. Soles, E. K. Lin, R. M. Reano and D. M. Casa, *Nano Lett.*, 2006, **6**, 1723-1728.
53. D. P. Birnie, 3rd, *Langmuir*, 2013, **29**, 9072-9078.
54. D. P. Birnie, *Journal of Materials Research*, 2011, **16**, 1145-1154.
55. P. D. Fowler, C. Ruscher, J. D. McGraw, J. A. Forrest and K. Dalnoki-Veress, *Eur. Phys. J. E*, 2016, **39**, 90.
56. P. G. de Gennes, *Eur. Phys. J. E*, 2001, **6**, 421-424.
57. S. Yoo, J. H. Kim, M. Shin, H. Park, S. Y. Lee and S. Park, *Science Advances*, 2015, **1**, 7.
58. R. Xie, A. Karim, J. F. Douglas, C. C. Han and R. A. Weiss, *Phys. Rev. Lett.*, 1998, **81**, 1251-1254.
59. C. Bollinne, S. Cuenot, B. Nysten and A. M. Jonas, *Eur. Phys. J. E*, 2003, **12**, 389-395.
60. J. D. Mendelsohn, C. J. Barrett, V. V. Chan, A. J. Pal, A. M. Mayes and M. F. Rubner, *Langmuir*, 2000, **16**, 5017-5023.
61. A. Briddick, R. J. Fong, E. F. D. Sabattie, P. X. Li, M. W. A. Skoda, F. Courchay and R. L. Thompson, *Langmuir*, 2018, **34**, 1410-1418.

62. S. P. Adiga, C. Jin, L. A. Curtiss, N. A. Monteiro-Riviere and R. J. Narayan, *WIREs Nanomed. Nanobiotechnol.*, 2009, **1** 568–581.
63. W. Y. Zhang, Q. Zhao and J. Y. Yuan, *Angewandte Chemie-International Edition*, 2018, **57**, 6754-6773.
64. Y. Saito, M. Shimomura and H. Yabu, *Macromol Rapid Commun*, 2014, **35**, 1763-1769.
65. P. Frasch and K. H. Saremski, *Ibm Journal of Research and Development*, 1982, **26**, 561-567.
66. M. Kavanoz, N. O. Pekmez and M. Can, *J. Appl. Polym. Sci.*, 2016, **133**, 12.
67. H. Kozuka and M. Hirano, *J. Sol-Gel Sci. Technol.*, 2000, **19**, 501-504.
68. E. Vasilaki, M. Kaliva, N. Katsarakis and M. Vamvakaki, *Applied Surface Science*, 2017, **399**, 106-113.
69. A. R. Sasikala, A. GhavamiNejad, A. R. Unnithan, R. G. Thomas, M. Moon, Y. Y. Jeong, C. H. Park and C. S. Kim, *Nanoscale*, 2015, **7**, 18119-18128.
70. L. T. Lee and P. Somasundaran, *Langmuir*, 1989, **5**, 854-860.
71. L. Shechter, J. Wynstra and R. P. Kurkjy, *Ind. Eng. Chem.*, 1956, **48**, 94-97.
72. D. Yan, C. Gao and H. Frey, *Hyperbranched Polymers: Synthesis, Properties, and Applications*, John Wiley & Sons, 2011.

Chapter 5 Characterisation of the properties of functional, catechol-containing thin copolymer films

5.1 Introduction

Herein the results of investigations into the properties of thin film coatings of copolymers comprising HEMA, DMA and GMA are reported with the aim of identifying suitable candidates for industrial exploitation in devices for biosensing. The desirable properties were resistance to delamination or dissolution of the copolymer films in water and the ability to immobilise an antibody directly from an aqueous solution. As such, surface analysis techniques were selected to gain an understanding of the physical and chemical properties of the films, including contact angle analysis, in-situ ellipsometry, electrokinetic streaming potential and quartz crystal microbalance (QCM) measurements.

5.1.1 Contact angle measurements

Measurement of the contact angle of a liquid on a solid surface is widely used to calculate surface energy and other properties.[1] Usually, a liquid droplet is placed on a surface and the angle measured at the interface between the three phases: gas, liquid and solid. The contact angles measured at the advancing or receding edge of a moving droplet can be used to infer additional surface properties such as surface roughness.[2]

The technique used to measure contact angles in the current investigation is known as axisymmetric drop shape analysis-profile (ADSA-P). ADSA-P was first described in 1983 by Neumann *et al*, building on earlier work to develop a user-friendly and accurate method to measure contact angles.[3, 4] The relationship between the surface tension and the shape of a liquid droplet is used to infer the surface energy at the liquid-surface interface. Compared to the more facile sessile drop method of measuring static contact angles, ADSA-P provides additional information such as accurate measurement of the advancing and receding contact angles and the droplet surface tension.

In an ADSA-P experiment, a drop of a fluid is constrained such that the surface tension can be measured; the constraining factors can be volume and radius in the case of a pendant drop, (Figure 5.1A) or constrained sessile drop (Figure 5.1B) or volume and angle in the case of an unconstrained sessile drop (Figure 5.1C) or captive bubble (Figure 5.1D). The captive-bubble experiment was used in this work.

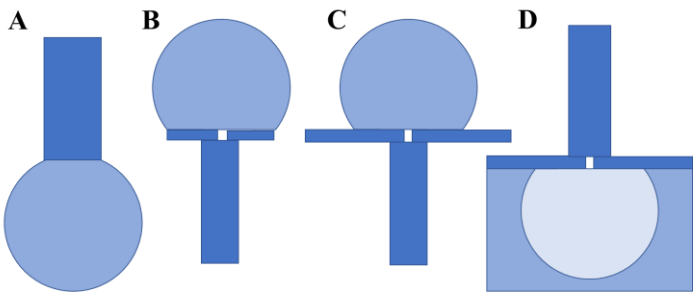

Figure 5.1. Schematic representing four methods of ADSA-P. A) Pendant drop, B) Constrained sessile drop, C) Unconstrained sessile drop, D) Captive bubble.

The schematic in Figure 5.2 shows the set-up of the captive bubble experiment. A coated substrate is suspended face-down in a liquid bath and air is injected through a hole in the substrate using a syringe pump. An air bubble is thus trapped underneath the sample. Contact angle and liquid surface tension can be determined by analysing a video of the air bubble with computer software. The captive bubble method is particularly useful for analysing gels or gel-like materials as coatings can be measured in their swollen state when surrounded by various liquid media.[1, 5]

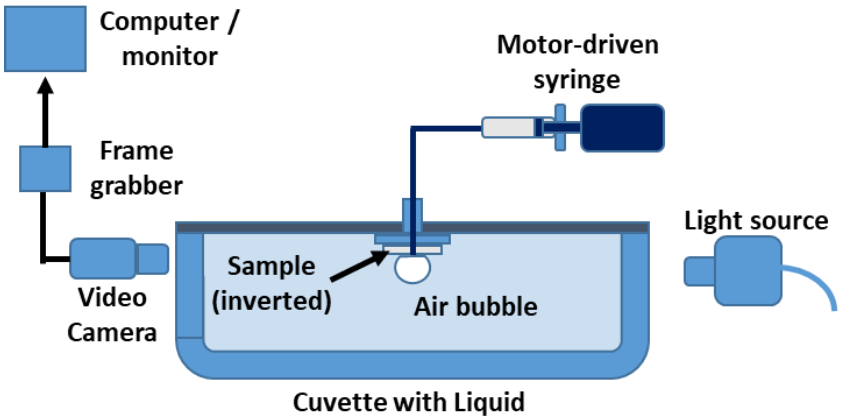

Figure 5.2. Diagram of a captive bubble ADSA-P experimental set-up.

5.1.2 Electrokinetic streaming potential (zeta potential) measurements

The zeta potential (ζ), or electrokinetic potential, of a system is an important parameter in colloid and surface science, which describes the electrical potential in the double layer at the interface between solution and particle or surface.[6] This electrokinetic potential can directly affect the interaction between a polymer film surface and potential analytes in solution.

Two types of measurement are generally used to determine the zeta-potential of polymer surfaces or colloids: electroosmotic mobility and streaming potential.[7] In an electroosmotic mobility experiment, a current is applied across a colloidal dispersion in a capillary, and a

flow is induced due to the electrokinetic potential of the solution. In a streaming potential experiment, an analyte is coated on the walls of a capillary through which the electrolyte solution is flowed (Figure 5.3A). The movement of ions in the shear plane next to the electrical double layer induces a current (Figure 5.3B), which can be measured to determine the electrokinetic potential of the surface. Streaming current measurements were used in this work as the method is more appropriate for polymer films.

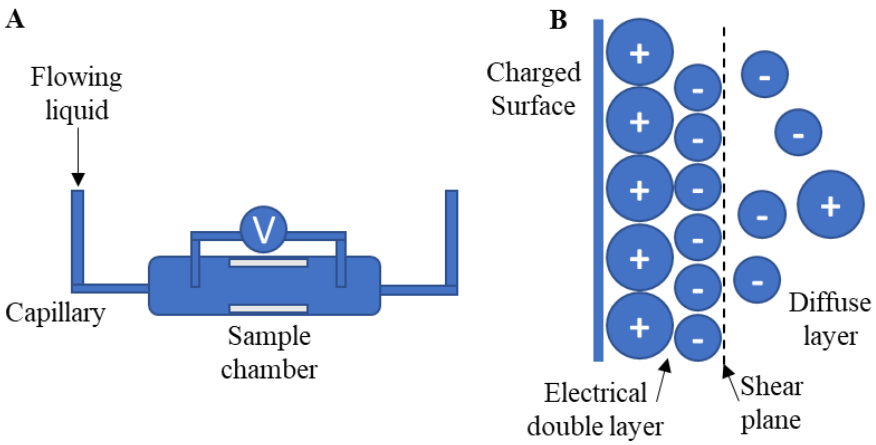

Figure 5.3. A) Schematic of a streaming potential electrokinetic measurement B) Schematic representation of the electrical double layer at a solid-liquid interface.

Various properties of the polymer coating can be inferred by the streaming potential experiment. The zeta potential at various electrolyte pH values can be used to estimate the presence of dissociable functional groups at the polymer film surface and predict ion adsorption processes influenced by the surface chemistry.[6] Swelling and dissolution of the polymer films may also be detected. Thus, understanding the surface interactions of copolymer coatings may help rationalise the influence of the polymer composition and the binding behaviour of antibodies on the surface of the film.

5.1.3 In-situ spectroscopic ellipsometry

The principles behind spectroscopic ellipsometry have been explained in detail in Chapter 4. Here, in-situ ellipsometry is used to model the dynamic swelling of copolymer films and the deposition of an antibody onto swollen copolymer films. The technique has been reported in the literature and is valuable as the film thickness and refractive index of the film or deposited layer can be calculated simultaneously, allowing the dynamics of swelling and deposition behaviour to be considered in detail.[8, 9] A polymer-coated sample is immobilised in a sample cell which is designed especially to reduce interference from the cell on the path of the incident and reflected beams. The cell is then filled with a solvent

under controlled conditions and the sample is scanned by the laser at regular intervals to determine the dynamic film behaviour. A schematic of the setup is shown in Figure 5.4.

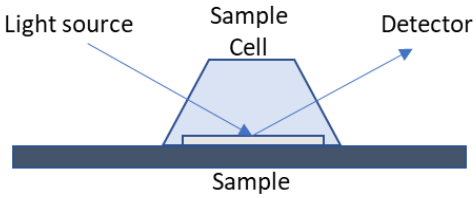

Figure 5.4. Schematic of the set-up for in-situ ellipsometry.

5.1.4 Quartz crystal microbalance measurements

A quartz crystal microbalance with dissipation monitoring (QCM-D) measures energy dissipation upon binding of an analyte to an oscillating quartz crystal. It relies on the piezoelectric effect on quartz crystals to accurately determine the mass of a substance adhering to the crystal surface, which can subsequently be used to infer film thickness.[10, 11] Data is obtained as a change in electrode resonant frequency upon a change in mass and a dissipation shift representing energy loss arising from the viscoelasticity of an attached film. The energy dissipation is modelled to identify the mass or thickness of the surface coverage. It is sensitive enough to detect small molecule monolayers yet can also detect the adhesion of more massive substances such as polymer films and much larger masses still, such as cells. QCM-D has commonly been used to analyse the binding of polymers or biomolecules to a substrate surface.[12-14] In the current investigation, QCM-D is used to study film thickness and stability upon immobilisation of anti-aflatoxin antibody on a copolymer film.

5.2 Aims

The aims of the work reported in this chapter were:

1. To conduct a study to determine the change in solubility upon storage of selected copolymers in bulk. Copolymers were stored at -18 °C, 4 °C and 35 °C and their solubility in methanol regularly tested over the course of 6 weeks. Storage conditions which allowed the copolymers to remain soluble in methanol over the medium to long term were identified and differences in copolymer stability correlated to copolymer composition.

2. To characterise the physical properties of four copolymers, and investigate their surface energy and degree of swelling in water. Advancing and receding contact angles were obtained using ADSA-P to infer the surface energy of the copolymer films. The contact angles were correlated with copolymer composition. The contact angle hysteresis was used

to infer the ability of the copolymers to undergo conformational rearrangement to reduce the free energy of the system. Electrokinetic potential measurements were also used to assess the surface charge on the films at various pH levels. The electrokinetic potential of the films can be correlated to copolymer composition and the physical properties of the copolymers. In-situ ellipsometry was used to investigate dynamic swelling of the copolymer films in the presence of an aqueous buffer solution as a function of copolymer composition and to indicate the stability of copolymer films on the surface of a silicon wafers *i.e.* if they delaminate or redissolve.

3. To monitor the immobilisation of anti-aflatoxin antibody on films of a suitable candidate copolymer. In-situ ellipsometry was used to measure the change in film thickness upon exposure of the copolymer film to the antibody. A similar experiment was carried out using QCM-D to characterise the film thickness when an antibody solution was flowed through a QCM-D cell containing a copolymer-coated quartz crystal.

5.3 Experimental

5.3.1 Materials

Phosphate buffered saline (PBS) tablets, sodium phosphate monobasic (99%) and sodium phosphate dibasic (99%) were all obtained from Merck, Germany and used as received. Anti-aflatoxin M1 antibody A16A-1 was supplied by AntiProt, Puchheim, Germany, stored at 4 °C and used within 4 weeks.

5.3.2 Testing of copolymer solubility upon storage

For each copolymer under investigation, three solid samples (0.1g) were placed into 10 mL vials, sealed and stored either at -18 °C, 4 °C or 35 °C. After 1, 2 and 6 weeks, a 2 mg sample of the copolymer stored at each temperature was transferred to a 2 mL vial, and 2 mL methanol added. The vial was placed on rollers to allow the polymer and solvent to mix. After 1 hour, copolymer solubility was judged by the visual presence of any turbidity.

5.3.3 Ellipsometry measurements

Ellipsometry measurements were carried out using a Woollam M2000 spectroscopic ellipsometer. For in-air measurements, a wavelength range of 300-1600 nm was used, and measurements were obtained using incident angles of 60, 65, 70 and 75°. The data was processed using completeEASE software (J.A. Woollam Co. Inc., Lincoln, USA) using the Cauchy model. For film thickness values smaller than 10 nm, fixed values of A = 1.52 and B = 0.006 were used for the refractive index (n) unless indicated.

PBS solution (pH 7.4, 0.01 mol dm^{-3}) was obtained by dissolving one PBS tablet in 200 mL deionised water. A 0.01 mol dm^{-3} solution of PBS contains 0.01 mol dm^{-3} phosphate buffer, 0.0027 mol dm^{-3} potassium chloride and 0.137 mol dm^{-3} sodium chloride.

Sodium phosphate buffer solution (pH 7.4, 0.001 mol dm^{-3}) was obtained by dissolving 0.109 g of sodium phosphate dibasic and 0.031 g of sodium phosphate monobasic in 1L deionised water.

In-situ ellipsometry measurements were carried out using a 3 mL volume glass cuvette with walls at 68° angles. All measurements were taken at room temperature. Dry measurements were taken with the coated wafer outside and inside the cuvette to correct for window effects, and the wafer was secured with a PTFE support. PBS buffer solution (pH 7.4, 0.01 mol dm^{-3}) was then added and the degree of swelling measured at regular intervals (scans were performed constantly and each scan took ~18 s). When the film thickness value had become stable, at least 3 further measurements were recorded at different points on the film to obtain an average degree of swelling, over a wavelength range of 370-900 nm.

Antibody adhesion measurements were carried out using a 1.3 mL glass cuvette with walls at 70° angles. Dry measurements were taken with the coated wafer outside and inside the cuvette to correct for window effects, and the wafer was secured with a PTFE support. 1.3 mL sodium phosphate buffer solution at (pH 7.4, 0.001 mol dm^{-3}) was then added and measurements were recorded every ~45 s. When the thickness had become stable, 0.2 mL of buffer solution was removed using a syringe. 100 µL of a solution of anti-aflatoxin antibody (1 mg mL^{-1} in 0.001 mol dm^{-3} NaPB) was then introduced and the cell refilled with buffer solution to give a total antibody concentration of 0.08 mg mL^{-1}. Measurements of film thickness were recorded again, every ~45 s until the value became stable, and a single further measurement was taken with a wavelength range of 370-900 nm. 0.1 mL aliquots of antibody solution were then removed and replaced with buffer solution until the antibody concentration was reduced to 0.04 mg mL^{-1} and measurements were then recorded every ~45 s until a stable value was reached. A final measurement was taken with a wavelength range of 370-900 nm.

5.3.4 Electrokinetic streaming potential measurements

All electrokinetic measurements were carried out by Anja Caspari, Leibniz-Institut für Polymerforschung (IPF) Dresden e.V., Dresden, Germany. Electrokinetic streaming

potential measurements were carried out using a SurPASS 3 (Anton Paar GmbH, Graz). For these measurements an adjustable gap cell, equipped with Ag/AgCl electrodes, was used. A measuring channel was built between two spin-coated silicon wafers, fixed between two electrodes. The measuring fluid was streamed through this channel. The pH-dependence of zeta potential was determined in the presence of 0.001 mol/L KCl solution. The measurements were started at neutral pH and were adjusted with HCl or KOH.

5.3.5 Contact angle measurements

Contact angle measurements were carried out by Kathrin Pöschel, IPF, Dresden, Germany using the ADSA-P contact angle method described below.

Specially prepared silicon wafers – laser-cut 20 mm x 20 mm squares with a 1 mm diameter central hole – were spin coated as described in Chapter 4 to obtain film thicknesses of around 150 nm (1000 rpm, 400 rpm s^{-1}, 2% copolymer solution in methanol). Each copolymer-coated wafer was immersed, face-down, in water and the copolymer coating allowed to equilibrate for at least 30 minutes. Air was injected through the sample using a syringe pump connected to a needle, causing a bubble of air to be trapped on the underside of the copolymer-coated wafer. The volume of the captive air bubble was increased and decreased using the syringe pump and the advancing and receding contact angles of the air bubble measured using a camera linked to computer software. For each polymer sample, three silicon wafers were spin coated, and the bubble expansion/retraction cycle was repeated at least three times for each coated silicon wafer.

5.3.6 QCM analysis

QCM measurements were carried out using a Q-Sense E4 flow cell device. Three SiO_2-coated, gold-plated quartz crystal electrodes were spin-coated with copolymer and the resulting copolymer films dried under vacuum. The electrodes were then mounted in the flow cell, and buffer solution (0.001 mol dm^{-3} sodium phosphate buffer, pH 7.4) was passed through the cells at a flow rate of 0.1 mL/min until a stable frequency was observed. The solution was then switched to a 0.025 mol dm^{-3} solution of anti-aflatoxin antibody in the previously used buffer solution and passed through the cells until a stable frequency was obtained. The solution was then switched back to buffer solution and the process was repeated. After each measurement, the cell was washed with 0.1 mol dm^{-3} HCl and Millipore water before air was pumped into the system. Data was processed using QSense Dfind (Biolin Scientific, Sweden) using the Sauerbrey model.

5.4 Results and Discussion

5.4.1 Influence of temperature and storage time on the solubility of copolymers containing HEMA with GMA and/or DMA

Spin-coating and immersion-coating of a range of homo-, co- and terpolymers comprising HEMA and, in some cases, GMA and DMA were described in Chapter 4. It was observed that in some cases, the copolymers (particularly the terpolymers) became insoluble in methanol following storage at room temperature for several weeks. The solubility of a variety of the copolymer samples was investigated after prolonged storage, in bulk, at -18 °C, 4 °C and 35 °C, to establish if a correlation existed between solubility and the composition of the copolymer. Their solubility in methanol (1 mg/mL) was tested after 1, 2 and 6 weeks. Solubility was defined as the absence of any visible solid copolymer after stirring 2 mg of copolymer in 2 mL of methanol for 1 hour.

The copolymer compositions, molecular weights and solubility test results for those samples tested are shown in Table 5.1.

Table 5.1. Solubility of selected copolymer samples after storage in bulk at a range of temperatures. Solubility tested in a 1 mg mL^{-1} solution in methanol after 1 h stirring.

Polymer	Comp-osition	M_n / g mol^{-1}	Solubility in methanol (✓ or ×)								
			-18 °C			4 °C			35 °C		
			1w	2w	6w	1w	2w	6w	1w	2w	6w
RAFT-H	-	11150	✓	✓	✓	✓	✓	✓	✓	✓	✓
FR-HD-90/10-(DMF)	92/8	13600	✓	✓	✓	✓	✓	✓	✓	✓	✓
FR-HG-89/11	78/22	133500	✓	✓	✓	✓	×	×	×	×	×
FR-HGD-80/10/10-(DMF)	79/14/7	43400	✓	✓	✓	✓	✓	×	×	×	×
RAFT-HGD-80/10/10	73/21/5	30650	✓	✓	✓	✓	✓	×	×	×	×

All of the samples were comprised of a majority of HEMA. A homopolymer of HEMA (RAFT-H, M_n = 11150 g mol^{-1}) was synthesised for comparison to the copolymers containing GMA and DMA. RAFT-H was synthesised in DMF and used a molar feed ratio of 150:1:0.2 [mon]:[CTA]:[I]. Copolymers (FR-HG-89/11 and FR-HD-90/10-(DMF)) and

terpolymers (RAFT-HGD-80/10/10 and FR-HGD-80/10/10-(DMF)) were also investigated.

All samples stored at -18 °C remained soluble throughout the investigation, suggesting that -18 °C is an appropriate storage temperature for these samples in the medium term.

Of the samples stored at 4 °C, all remained soluble after one week. However, after two weeks, FR-HG-89/11 became completely insoluble in methanol. After six weeks at 4°C, all copolymers containing GMA had become insoluble, whereas those containing no GMA – RAFT-H and FR-HD-90/10-(DMF) – remained soluble. When the copolymers became insoluble, swelling was observed (qualitatively), suggesting a crosslinked network had formed. The results clearly indicated a correlation between GMA content and a reduction in solubility upon storage at 4 °C. FR-HG-89/11 became insoluble faster than the other GMA-containing copolymers FR-HGD-80/10/10-(DMF) and RAFT-HGD-80/10/10. As the polymer mol% GMA was similar in each case, the difference in solubility could be attributed to the high molecular weight of FR-HG-89/11. As discussed in Chapter 2, the presence of a high molecular weight peak in the SEC chromatogram of FR-HG-89/11 indicated some chain coupling had already occurred during synthesis and initial storage of FR-HG-89/11, which supports the argument that the reduction in solubility is due to the formation of a crosslinked network.

It has been reported that a homopolymer of GMA can be stored for an extended period of time under ambient conditions at room temperature without crosslinking or loss of solubility,[15] so it appears likely that the instability may be due to a crosslinking reaction between GMA and HEMA. A possible explanation could be nucleophilic addition of hydroxyl groups from HEMA to the epoxide ring of GMA (Scheme 5.1).[16] Reaction between an epoxide and alcohol can proceed without catalysis at high temperature, although the reaction is slow,[17] and hydrogen bonding groups can catalyse the addition of alcohol to epoxide. It is therefore possible that the high concentration of hydroxyl groups in copolymers comprising a high mole fraction of HEMA causes slow crosslinking of such copolymers, a process that would likely occur more readily at higher temperaratures.[18] The results suggested that there was no significant impact of DMA on the stability of the copolymers, however H-bonding from the catechol functionality could contribute towards catalysis of the crosslinking reaction or the catechol side chain could act as the nucleophile in place of the primary alcohol of HEMA. The proposed reaction would require a source

of H^+ ions, which could be present in small amounts due to adsorption of water by the hygroscopic HEMA, or the carboxylic acid end-group of the copolymers synthesised using RAFT polymerisation. The hydroxyl groups in catechol could provide another source of H^+ ions, although the relatively high pK_a of dopamine (pK_{a1} = 9.05) suggests the DMA side chains should remain largely protonated.

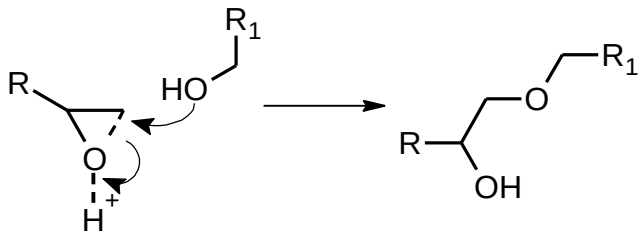

Scheme 5.1. Crosslinking reaction between epoxide and primary alcohol. R and R_1 = aromatic/aliphatic group

The solubility test results for the polymers stored at 35 °C showed a similar but accelerated trend to those stored at 4 °C. After only 1 week at 35 °C, all samples containing GMA had become insoluble in methanol. In contrast, the samples containing no GMA (RAFT-H and FR-HD-90/10-(DMF)) remained soluble throughout the 6-week testing period. This reinforced the correlation between reduced solubility and GMA *via* a probable crosslinking mechanism.

5.4.2 Characterisation of surface properties of films on exposure to water

For industrial applications involving the immobilisation and use of antibodies it is generally necessary to use aqueous solution as the medium. Copolymer films which have been deposited onto substrates may display varying behaviour when exposed to water at various pH values, including swelling, delamination, dissolution and changes to their surface energy or surface charge.

Spin-coated copolymer films were therefore studied using contact angle analysis, in-situ ellipsometry and electrokinetic potential measurements to determine the effect of copolymer composition and molecular weight on the properties of each copolymer upon exposure of the film to aqueous solutions. Table 5.2 is included to show the composition and molecular weight data for the copolymers discussed herein.

Table 5.2. Copolymers used in spin-coating and immersion-coating reactions. Monomers and monomer feed molar ratios are indicated in the name of each copolymer.

Copolymer	Copolymer composition[a] / mol%	M_n / g mol^{-1}	Đ
FR-HGD-80/10/10	83/12/6	43400	3.23
FR-HD-90/10-(DMF)	92/0/8	13650	3.18
FR-HG-89/11	78/22/0	133500	4.26
RAFT-HGD-74/13/13	78/14/8	24950	2.18

[a]**Copolymer composition quoted in the order: H/G/D.**

5.4.2.1 Contact angle analysis of copolymer films

Contact angle measurements were carried out using the axisymmetric drop shape analysis – profile analysis technique (ADSA-P) with the captive bubble method and water as the contact fluid.[1]

In a captive bubble experiment, the contact angle (θ) of a bubble of air on a solid surface, surrounded by a liquid continuous phase, is used to study the interaction between the solid-liquid, liquid-vapour and solid-vapour interfaces. It should be noted that "inverse" contact angles are measured in the captive bubble experiment as the phases are inverted compared to a standard sessile drop experiment. As such, the contact angles are always measured in terms of the liquid to aid comparison with other methods (see Figure 5.5).

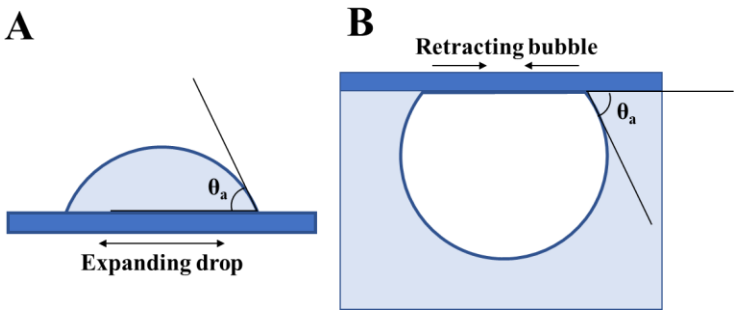

Figure 5.5. Schematic demonstrating the difference in measurement of advancing contact angle for: A) an expanding sessile drop and B) a retracting captive bubble (inverse contact angle).

As the bubble displaces liquid from the solid surface, (liquid) contact angles vary between high wettability ($0° < \theta < 90°$) and low wettability ($\theta > 90°$) states. In the case of "full wetting", the contact between the bubble and the solid substrate is minimised, so the measured contact angle is $\theta = 0°$. However, in cases of low wettability, the interaction between the bubble and the surface is more favourable and the contact area is maximised. All situations other than full wetting can be described by the interfacial tensions γ_{sl}, γ_{lv} and

γ_{sv} (for the solid-liquid, liquid-vapour and solid-vapour interfaces respectively) as described by Young's relationship (Equation 5.1):

$$\cos\theta = \frac{\gamma_{sv} - \gamma_{sl}}{\gamma_{lv}} \qquad \textbf{5.1}$$

The interfacial tensions and the resulting contact angle are determined by the chemical and physical properties of the interfaces involved. For an ideal surface (*i.e.* no chemical heterogeneity or surface roughness), this relationship predicts a single contact angle under a given set of environmental conditions. For a real (non-ideal) surface, a difference is observed between the contact angle at the front and rear of moving droplet (either on a tilted substrate or when movement is simulated by changing the volume of the droplet). The forward angle is called the advancing angle, θ_a, and the rearward is the receding angle, θ_r. The difference between the two is the hysteresis, θ_{hyst} (see Equation 5.2).[1]

$$\theta_{hyst} = \theta_a - \theta_r \qquad \textbf{5.2}$$

In a captive bubble experiment, θ_a is measured when the volume of the air bubble is decreasing. This is analogous to measuring the advancing angle in an expanding droplet of water in air (see Figure 5.5). Likewise, θ_r is measured when the volume of the air bubble is increasing.

Generally, hysteresis is caused by surface heterogeneity (roughness or chemical heterogeneity) or (polymer) surface rearrangement.[19] In smooth polymer films, it has been shown that hysteresis can be influenced by local reorganisation of the functional groups at the polymer film surface (Figure 5.6).[20, 21] Surface rearrangement can often be observed within the timescale of a contact angle experiment (seconds).[22] However, such rearrangement is determined by the mobility of surface groups, and hence reduced in highly crosslinked polymers but increased in swollen polymers. Except in special cases, bulk rearrangement of polymers does not usually occur in the timescale of the contact angle experiments used in this work, but may be observed over extended periods (many hours or days)[23] or by using elevated temperatures to increase chain mobility.[21]

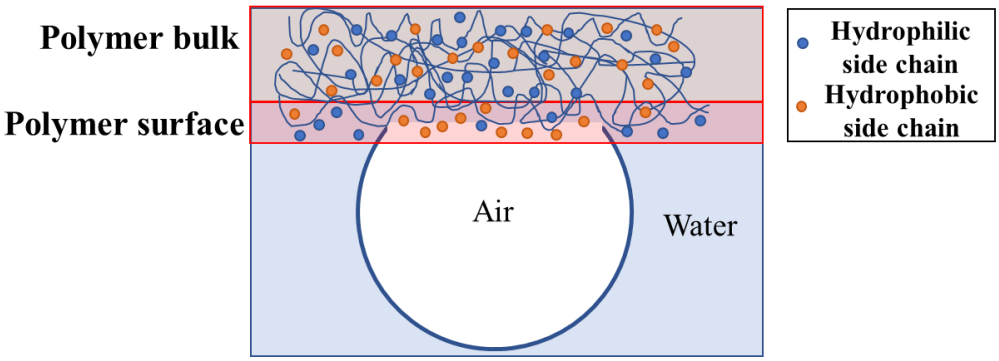

Figure 5.6. Schematic representing reorganisation of the polymer surface region to allow hydrophobic chains to face the polymer-air interface.

It has been previously reported that poly(HEMA) films show high hysteresis, even when the surface is free from significant roughness.[24, 25] A high advancing contact angle (60° – 90°, higher than hydrophobic poly(MMA) in some cases) is observed, indicating that, in air, poly(HEMA) adopts a conformation in which the hydrophobic backbone is predominantly exposed to the air-polymer interface.[26-28] This has been demonstrated experimentally using x-ray photoelectron spectroscopy.[29] However, the receding contact angle is low (0° – 20°), which suggests the chains are able to rearrange in the presence of water to allow the hydrophilic hydroxyl groups to point towards the water-polymer interface.[26] The swelling of the poly(HEMA) layer plasticises the film and allows for increased surface polymer segment mobility. Differences in the extent of hysteresis arise from the preparation method and degree of crosslinking in the poly(HEMA), which affect the ability of the chains to rearrange their surface conformation.[26] Thomas *et al.* reported that copolymerisation of HEMA with hydrophobic comonomers affected the contact angle hysteresis.[28] Copolymers of HEMA with MMA or ethyl methacrylate showed decreased hysteresis, as the average chain length of the average monomer side chain increased, due to the increasing mobility of the surface groups in the copolymer. It has also been reported that poly(vinylmethylsiloxane) elastomers, modified by grafting mercaptoalkanol groups of varying alkyl length to the vinyl side-chain, exhibited reduced contact angle hysteresis and slower rearrangement kinetics when the alkyl chain length was increased.[22] This was attributed to increasing crystallinity and reduced surface mobility of the copolymer chains.

Copolymers FR-HGD-80/10/10, FR-HD-90/10-(DMF), FR-HG-89/11 and RAFT-HGD-74/13/13 were spin coated (1000 rpm, 400 rpm s^{-1}, 2 % solution in methanol) onto laser-cut silicon wafers, designed especially for ADSA-P measurements. A small hole in the centre of the wafer allowed a needle to pass through and an air bubble to be injected underneath the wafer, as per the captive bubble experimental set up (Figure 5.2). Contact

angle measurements using the ADSA-P method were carried out to determine the advancing and receding contact angles of the captive bubble on the copolymer surface, with distilled water as the continuous phase. The copolymer films were immersed in the water for at least 30 minutes before each measurement to allow swelling of the copolymer to occur and the copolymer films to equilibrate in their swollen state. The films showed no sign of delamination during the testing, indicating they were adhered well to the surface of the substrate. The contact angle (θ), bubble radius (r) and bubble volume (V) data from a captive bubble measurement of each copolymer are shown in Figure 5.7. The bubble volume is the independent variable in the captive bubble experiment.

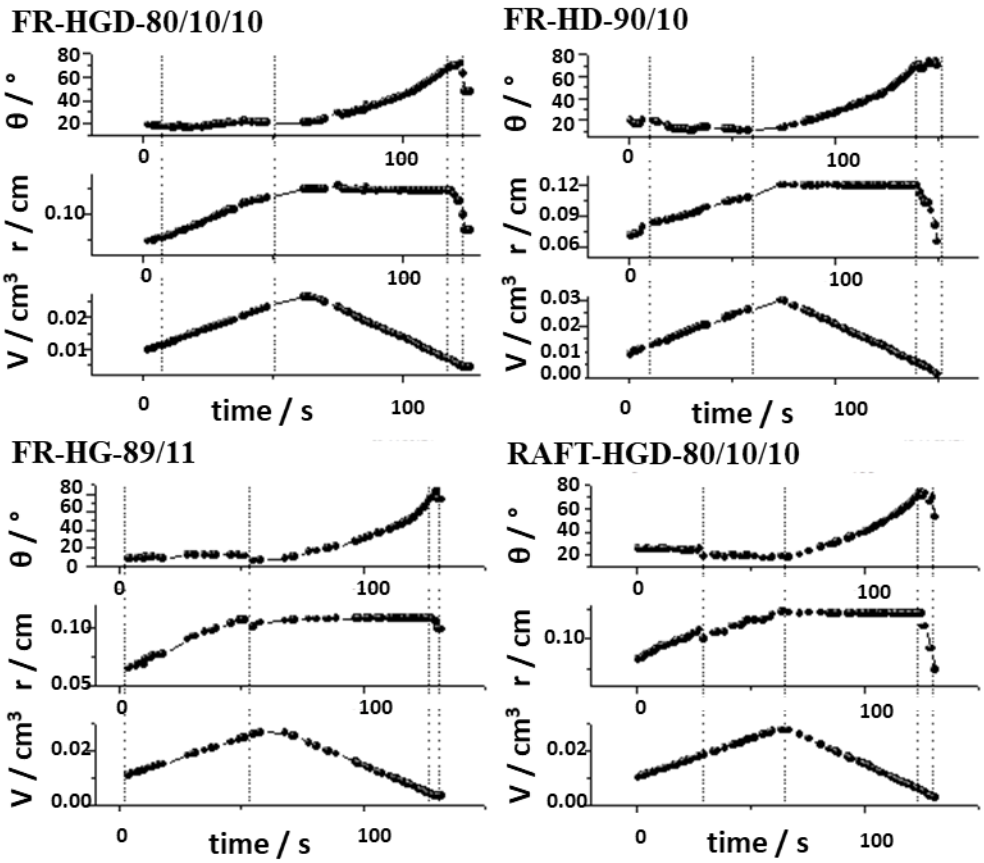

Figure 5.7. Data for ADSA-P measurement of copolymers FR-HGD-80/10/10, FR-HD-90/10-(DMF), FR-HG-89/11 and RAFT-HGD-74/13/13. Top – Contact angle (θ) vs time / s. Middle – Radius of bubble (r) vs time / s. Bottom – Volume of bubble (V) vs time. Measurement carried out by Kathrin Pöschel, IPF Dresden.

It should be noted that, as contact angle hysteresis can be increased by roughness or chemical heterogeneity of the surface,[1] the contact angles of the samples could also be influenced by any defects in the films. As the spin-coating conditions used for these samples were shown to produce porous films for FR-HGD-80/10/10, the contact angle results should be treated with a degree of caution, as the experimental error could be greater

and reproducibility reduced compared to perfectly smooth films. However, the maximum roughness (as measured by AFM – all R_a < 25 nm, see Chapter 4) for each of the relevant copolymers was much lower than the threshold value for feature depth to affect hysteresis; thought to be ~100 nm.[30, 31] Therefore, for the purposes of this discussion, the films can be considered "smooth". Furthermore, the experiments were carried out in the swollen copolymer state, where chain mobility is increased, and consequently surface pore size will be reduced or the pores may disappear entirely.[32]

In each case, the volume of the bubble was steadily increased for 60 s and then decreased, as seen in the bottom of the three data sets for each copolymer shown in Figure 5.7. When volume increased, either the bubble radius increased or contact angle decreased and the reverse was true when volume decreased. These trends are used to determine the advancing and receding contact angles; the regions in which these are calculated are marked by the two sets of vertical dotted lines (first θ_r and then θ_a).

The general trends for θ, r and V were similar for each polymer. Considering FR-HGD-80/10/10 as an example, the bubble radius, r, expanded smoothly as bubble volume, V, increased, while the (receding) contact angle remained constant at 21° (see Figure 5.7). This smooth expansion indicated any surface roughness had a limited effect on the contact angle as an inhomogeneous surface may have resulted in contact-line slipping, whereby the radius increases in several rapid bursts.[1] Upon decrease of the bubble volume, the bubble radius stayed constant at 0.15 cm, but the (advancing) contact angle increased from 21° to 65°. This phenomenon is termed contact line pinning and is the source of contact angle hysteresis.[2] A difference in advancing and receding angles is a consequence of pinning; the advancing angle is measured at the point that the droplet radius begins to change. Pinning is often due to a change in the polymer conformation, whereby the contact line does not change while the polymer equilibrates to its lowest energy conformation in the new medium.[33] At the end of the measurements, after the receding angle had been reached, the bubble radius rapidly decreased. The length of time that the radius remained constant provides an indication of the extent of the hysteresis.

Contact line pinning is evident for all four copolymer samples, in particular FR-HG-89/11, for which the bubble radius does not have time to retreat to zero before the end of the measurement. This indicated the copolymer films showed significant contact angle hysteresis. To further investigate the source of the hysteresis and thus the relationship

between surface properties and structure (composition and molar mass) of each copolymer, the advancing (θ_a) and receding (θ_r) contact angles were calculated using the ADSA-P software (Figure 5.8). At least eight contact angle measurements were obtained for each copolymer to obtain the mean value for θ_a and θ_r. The error bars represent one standard deviation from the mean.

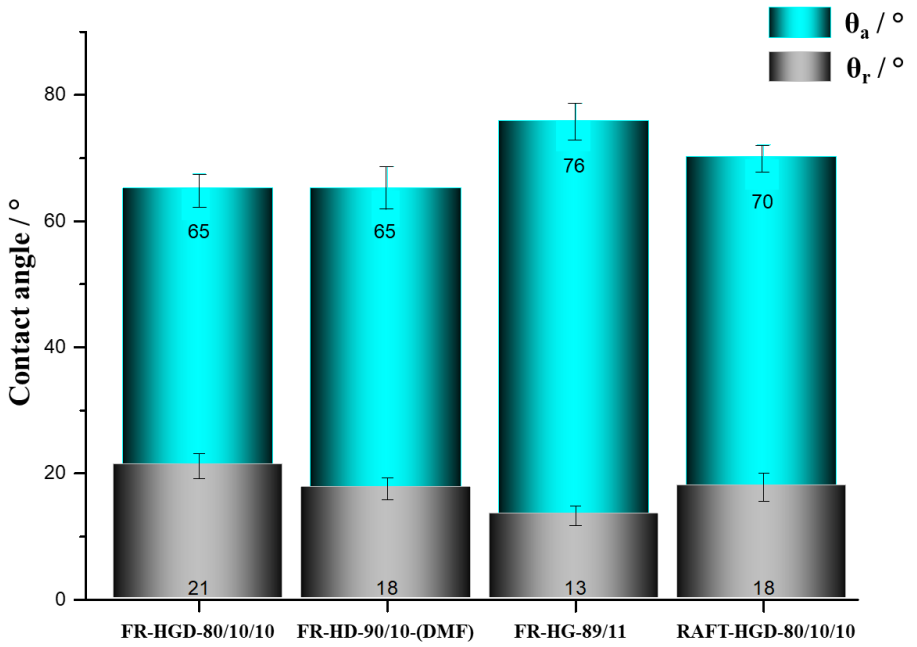

Figure 5.8. ADSA-P captive bubble contact angle measurements. Advancing (blue) and receding (grey) angles in water. Measurement carried out by Kathrin Pöschel.

The data in Figure 5.8 indicates θ_a and θ_r for the copolymers studied. The results are hereby rationalised in terms of copolymer composition and its effect on surface reorganisation. The influence of surface roughness is not considered further as it is considered negligible in the context of these experiments, however, it should be considered that even small deviations from perfectly smooth films may affect the contact angles slightly and increase the experimental error.

The observed contact angles of FR-HGD-80/10/10 and FR-HD-90/10-(DMF) are very similar, with an identical θ_a of 65° and θ_r of 21° and 18° respectively. The similar θ_r supports the suggestion that, in water, significant swelling of both copolymers enabled rapid conformational rearrangement to allow the hydrophilic groups to point towards the interface with water.[20] It has been reported in the literature that surface rearrangement can occur very rapidly, although the timescale of diffusion of chains in the copolymer film may be in the order of several hours.[23] This suggests that the rearrangement is very local and can be attributed largely to the side chains of the monomer repeat units found at the

polymer surface. This in turn would suggest that any difference in the molecular weight between the copolymers is unlikely to significantly affect hysteresis. The θ_r of FR-HD-90/10-(DMF) is slightly lower than FR-HGD-80/10/10, but considering the errors associated with the measurements including surface heterogeneity and experimental variation, the difference is not significant. When considering θ_a, the presence of the (slightly polar) GMA side chains appeared to have little influence on the surface properties. As the advancing contact angle was identical for both copolymers (65^o), it would seem likely that the hydrophobic methacrylate/methacrylamide backbone played a significant role in determining θ_a. Both copolymers showed smaller hysteresis values than are typical for poly(HEMA) (44° and 47° respectively compared to 60 – 70° for poly(HEMA)).[24-26] This suggests that the surface mobility of the copolymer chains was reduced due to the DMA and GMA comonomer side chains.

There is a noticeable increase in contact angle hysteresis when FR-HG-89/11 (63°) is compared to FR-HGD-80/10/10 and FR-HD-90/10-(DMF). For FR-HG-89/11, θ_a was 76° but θ_r was only 13°. The comparatively larger value of θ_a indicates the air-exposed surface of FR-HG-89/11 is more hydrophobic than FR-HGD-80/10/10 and FR-HD-90/10-(DMF). The key difference between FR-HG-89/11 and the preceding copolymers is the absence of DMA side chains. The presence of DMA, although a minor component, could significantly reduce the surface mobility of the copolymer chains: it is bulky and inflexible, and can form strong H-bonding or even π-stacking interactions with adjacent chains.[34] Thus, the absence of catechol bulk and cohesive interactions allows FR-HG-89/11 to more quickly rearrange to present a more hydrophilic surface in the presence of water and hydrophobic surface in the presence of air. The contact angle hysteresis of FR-HG-89/11 is in the range expected for poly(HEMA), which suggested that the presence of 22 mol% GMA had little or no impact on the mobility of the surface chains. This may be due to the similar size and polarity of the HEMA and GMA side chains.

RAFT-HGD-74/13/13 had an intermediate hysteresis value (52°) compared to the previously discussed copolymers. RAFT-HGD-74/13/13 appeared not able to rearrange its conformation to the same extent as FR-HG-89/11, as evidenced by the comparatively lower hysteresis. The reduced mobility is most likely due to the presence of DMA, as suggested above for FR-HGD-80/10/10 and FR-HD-90/10-(DMF). θ_a (70°) was higher than FR-HGD-80/10/10 and FR-HD-90/10-(DMF), but θ_r (18°) was very similar, indicating that the copolymer presents a similarly hydrophilic surface after rearrangement

due to contact with the water, but then rearranged to present a more hydrophobic surface in air. It was previously reported that the identity of a RAFT end-group could have a significant impact on the swelling and contact angle of two otherwise identical poly(*N*-propyl methacrylate) films, with a similar molecular weight and the same RAFT agent as RAFT-HGD-74/13/13.[35] The authors speculated that aggregation of the RAFT end groups could affect the mechanical properties of the film, however, the cause of the unexpected behaviour was not satisfactorily determined. Thus, we speculate that the high θ_a could be due to the presence of the RAFT end group, which contains a bulky, hydrophobic phenyl group, which may be present at the surface of the film in the presence of air. The DMA content of RAFT-HGD-74/13/13 is identical to FR-HD-90/10-(DMF) and 2% greater than FR-HGD-80/10/10 and, so it is slightly surprising that the hysteresis for RAFT-HGD-74/13/13 is greater.

In summary, the findings indicate that all of the copolymers display significant hysteresis, probably due to local conformational changes in the presence of water in order to reduce surface energy, which render the copolymer surfaces more hydrophilic. The modest difference in hysteresis of FR-HG-89/11 compared to FR-HGD-80/10/10, FR-HD-90/10-(DMF) and RAFT-HGD-74/13/13 is primarily assigned to reduced mobility of the chains at the surface of the other copolymer films arising from the catechol groups in DMA, which restricts surface rearrangement, due to H-bonding and steric bulk. A more in-depth study would be required to fully elucidate the individual contributions of surface roughness and chemical composition in both the swollen and dry states.

5.4.2.2 Electrokinetic potential measurements of copolymer films

Electrokinetic streaming potential measurements using aqueous solutions with a range of pH values were carried out to further characterise the behaviour of the copolymer films. The surface charge of a polymer film in a buffer solution may influence the interaction between the polymer film and biomolecules, which may also carry charged sites.[36]

The zeta potential (ζ) of a surface is calculated according to the Smoluchowski equation (Equation 5.3) by measuring the potential difference between two electrodes in a channel for a given pressure difference:

$$\zeta = \frac{dU}{dp}\frac{\eta\kappa}{\varepsilon_r\varepsilon_0} \qquad 5.3$$

where U is the streaming potential (the potential difference between the two electrodes), p is the pressure in the channel, ε_r and ε_0 are the relative permittivity of the liquid and the permittivity of a vacuum respectively, η and κ are the viscosity and the conductivity respectively of the measuring fluid. For the avoidance of confusion, it should be stated that the literature convention is to refer to a zeta potential value which becomes more negative as "increasing" and accordingly, the most negative value is referred to as a "maximum". For consistency, the same convention is used herein.

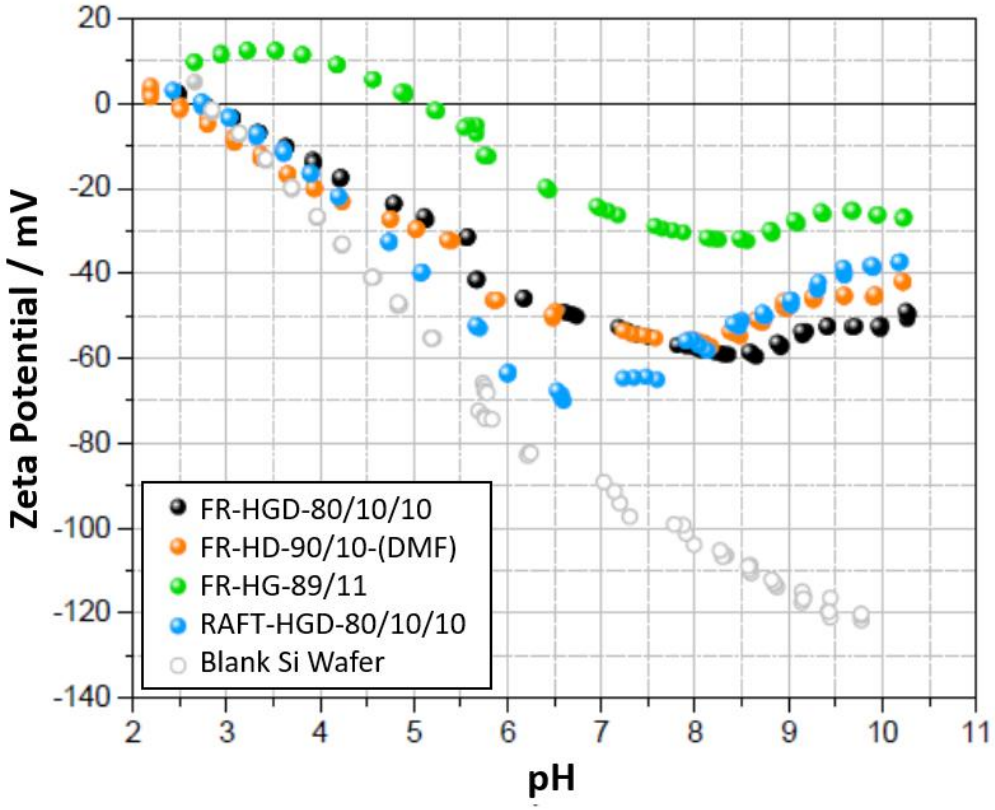

Figure 5.9. Zeta potential measurements of spin-coated films of FR-HGD-80/10/10, FR-HD-90/10-(DMF), FR-HG-89/11 and RAFT-HGD-74/13/13 on silicon wafer and a blank silicon wafer. Measurements carried out by Anja Caspari, IPF Dresden.

Films of FR-HGD-80/10/10, FR-HD-90/10-(DMF), FR-HG-89/11 and RAFT-HGD-74/13/13 were spin-coated onto silicon wafers (4000 rpm, 600 rpm s^{-1}, 0.75% copolymer solution in methanol), and the streaming potential was measured for each, over a range of pH values from 2 – 10.5 (adjusted using aqueous solutions of KOH and HCl). The resulting data for the four copolymers and a blank silicon wafer are shown in Figure 5.9. For copolymers FR-HD-90/10-(DMF), FR-HG-89/11 and RAFT-HGD-74/13/13 the aforementioned spin-coating parameters had previously produced thin, homogenous films (36 – 61 nm) with low ellipsometric MSE values (<6). However, the same conditions

produced porous films of FR-HGD-80/10/10 (see Chapter 4). Inhomogeneity of copolymer films may affect the repeatability of electrokinetic measurements slightly,[37] although at first glance, the results for FR-HGD-80/10/10 appear to be in the same range as the other copolymers studied.

The zeta potential results for FR-HGD-80/10/10 and FR-HD-90/10-(DMF) (black and orange data points respectively) were very similar across the entire pH range. Both copolymers showed identical negative electrokinetic potential at pH 7, which is consistent with the very similar water contact angle data observed for these two copolymers (section 5.4.2.1). The negative values arise from the retention of anions (OH^-) by the copolymer film, a commonly observed phenomenon even in non-ionic copolymers such as MMA.[38] The anions bind preferentially over water, especially on hydrophobic surfaces, reflecting the free energy gain of liberating water from a hydrophobic surface.[24, 39, 40]

The isoelectric points (IEPs) of both copolymers, where $\zeta = 0$, occurred at pH 2.5. The isoelectric point can be considered as the point at which the charge on the copolymer surface (including contributions from adsorbed ions) is net zero. The similar IEPs of FR-HGD-80/10/10 and FR-HD-90/10-(DMF) suggest that the GMA in FR-HGD-80/10/10 has no significant effect on ζ. This is consistent with the findings in the contact angle measurements reported above, where GMA appeared to have little effect on the wettability of the polymer films.

The zeta potential of FR-HGD-80/10/10 and FR-HD-90/10-(DMF) became more negative as pH was increased above the IEP, reaching a maximum of -60 mV at pH 8. This is due to functional groups which dissociate to form anions (in this case the HEMA and DMA hydroxyl groups). However, beginning at around pH 8, the zeta potential of both copolymers became less negative with increasing pH. Usually, the zeta potential of copolymer films with such acidic dissociable groups becomes more negative before plateauing at alkaline pH values.[41] However, in hydrogels with functional groups that dissociate to form anions (*e.g.* carboxylic acid or hydroxyl groups), zeta potential can become less negative due to pH-influenced swelling.[42] This swelling arises from repulsion between the anionic functional groups upon their dissociation, and the trapping of electrolytes from the solution in the diffuse layer formed by the swollen film. The hydroxyl groups on a primary alcohol such as HEMA will be >99% protonated at pH 7.4, but some deprotonation will occur at high pH (the pK_a of a primary alcohol is ~ 16). However, using

the pK_a of dopamine (pK_{a1} = 9.05 and pK_{a2} = 11.98),[43] it can be inferred the OH groups on the catechol side chains of DMA should remain 98% protonated at pH 7.4, but significant deprotonation can occur during the experiment at higher pH. Thus, in the two copolymers under discussion, the reduced zeta potential at high pH can be attributed to pH-induced swelling, particularly due to DMA. At pH 10.5, the zeta potential of FR-HD-90/10-(DMF) was lower than FR-HGD-80/10/10 by ~10 mV. The slightly lower zeta potential for FR-HD-90/10-(DMF) than FR-HGD-80/10/10 could reflect additional swelling. FR-HD-90/10-(DMF) comprises a greater mole fraction of HEMA side chains than FR-HGD-80/10/10, which could lead to more repulsion compared to the (non-dissociable) GMA. Furthermore, as GMA was suspected to cause gradual crosslinking in the polymer films, as discussed in previously (see section 5.4.1), the lack of GMA in FR-HD-90/10-(DMF) could also impact the swelling of the polymer. As the density of crosslinking in a polymer film is strongly correlated to the degree of swelling,[44, 45] any crosslinking in FR-HGD-80/10/10 introduced during synthesis or storage of the copolymers may result in reduced swelling upon increase in pH. The swelling behaviour of the copolymers is discussed further in section 5.4.2.3 below.

The trend for RAFT-HGD-74/13/13 differed slightly from FR-HGD-80/10/10 and FR-HD-90/10-(DMF); the zeta potential maximum for RAFT-HGD-74/13/13 occurred at lower pH (6.5) and with a more negative zeta potential (-70 mV), indicating greater anion retention. However, the IEP for RAFT-HGD-74/13/13 (pH 2.5) was almost identical to FR-HGD-80/10/10 and FR-HD-90/10-(DMF). The lower pH of the zeta potential maximum could be due to the lower pK_a of the ionisable carboxylic acid terminal RAFT groups of RAFT-HGD-74/13/13 compared to the hydroxyl groups of HEMA and DMA. Carboxylic acid end-groups have been shown to have sufficient influence on the surface charge to influence the zeta potential of copolymer films.[46, 47] It has also been reported that ionisable end groups increase the repulsion between chains at high pH, increasing the pH-dependent swelling,[48] which could also be the case in this work. This supports the suggestion made in the previous section that the RAFT end-groups are able to impact on the film properties, leading to unexpected behaviour of the RAFT polymer. Accordingly, the large decrease in zeta potential in the alkaline pH range for RAFT-HGD-74/13/13 could be due to repulsion between the terminal RAFT groups.

The behaviour of FR-HG-89/11 is significantly different to the other copolymers investigated in this work, as was observed in the contact angle experiments (section

5.4.2.1). The IEP, at pH 5, indicates a net neutral surface charge at higher pH than FR-HGD-80/10/10, FR-HD-90/10-(DMF) and RAFT-HGD-74/13/13. Since FR-HG-89/11 contains no DMA monomer, these results suggest that that the anionic character of the copolymers is increased by the presence of DMA, due to the lower pk_a in comparison with HEMA.[34] Accordingly, the extent of pH-induced swelling at alkaline pH is also smaller for FR-HG-89/11 than the other copolymers in this study, as the repulsion arising from dissociated DMA phenoxide groups is absent. The zeta potential for FR-HG-89/11 became positive at pH values below the IEP (<5), indicating retention of cations by the film.[38] This can be attributed to hydronium ion retention, which is characteristic of hydrophilic copolymers, including HEMA, at pH values below the IEP.[49] As all of the copolymers contain HEMA, this effect would be expected for each copolymer included in this study, indeed perhaps more strongly for the copolymers containing DMA, given the strong ability of catechol to bind cations.[50] However, it is unclear if this is the case for the other three copolymers, as their IEPs were close to the end of the investigated pH range.

In summary, the zeta potential results show that copolymer composition has a clear impact on the surface charge. The presence of DMA reduced the IEP of the copolymers, whereas GMA had little effect. This information is relevant to the ultimate aim for the coating when considering the conditions which may be used to enable immobilisation of antibodies on the film. As an antibody must be used close to biological pH (~7.4) to prevent denaturing, it is clear that the antibody will be in competition with adsorbed ions on the copolymer surface and, although the GMA should covalently bind the antibodies, electrostatic repulsion from adsorbed ions may reduce the likelihood of the proteins approaching the copolymer surface.[51]

5.4.2.3 In-situ ellipsometry measurements of copolymer films immersed in buffer solution

In-situ ellipsometry can be used to measure the dynamic swelling or deswelling behaviour of a copolymer film (matrix) by a solvent by monitoring the change in film thickness and refractive index in real time after immersion in a solvent.[8] In the previous section, electrokinetic measurements suggested the copolymer films exhibited pH-dependent swelling behaviour. To further investigate the swelling of the copolymer films, in-situ ellipsometry was used to monitor swelling in an aqueous buffer solution at pH 7.4.

If the proportion of solvent increases in a swollen matrix, and the refractive index (n) of the solvent is lower than the matrix, the measured value of n for the swollen matrix will

decrease proportionally with the amount of penetrant solvent.[33] The film structure and resistance of the copolymer film to dissolution (due to surface adhesion of the copolymer and intermolecular interactions) can be also inferred from the in-situ measurements. A number of swelling regimes have been observed for glassy copolymers.[52] The traditional understanding of polymer swelling is described by Fickian (diffusion-limited) dynamics (Figure 5.10A). A polymer film swelling according to this regime will experience a change in film thickness, *h*, and refractive index, *n*, where *h* increases proportionally with $t^{0.5}$ and *n* with $-t^{0.5}$. When the polymer film reaches its equilibrium thickness, *h* and *n* level off. However, other swelling behaviours are possible. Case II swelling is not limited by diffusion, but instead by the kinetics of polymer chain rearrangement (Figure 5.10B). This regime is identified by a rapid linear increase of *h* and decrease of *n* when plotted against *t* (as opposed to $t^{0.5}$ for Fickian swelling).

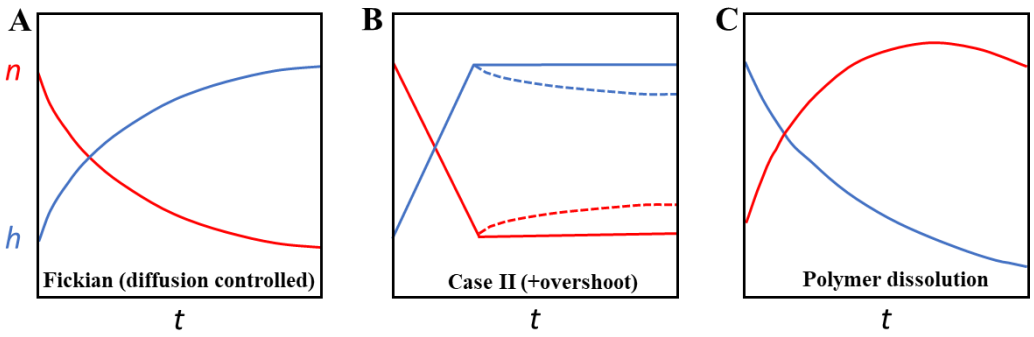

Figure 5.10. Examples of polymer swelling regimes, adapted from reference 52. A) Fickian diffusion B) Case II diffusion (dashed lines represent overshoot dynamics) C) Polymer dissolution.

Negative changes of *h* (after an initial increase) can also be observed in some cases. When accompanied by an increase in *n*, decrease of *h* is usually due to polymer relaxation, where the polymer chains move to their equilibrium conformation after stretching during swelling. This phenomenon is sometimes referred to as "overshoot dynamics".[53] Alternatively, a decrease in *h* accompanied by further decrease in *n*, is associated with polymer dissolution; often a result of strong interaction between solvent and polymer in a non-cross-linked film (Figure 5.10C).

FR-HGD-80/10/10, FR-HD-90/10-(DMF), FR-HG-89/11 and RAFT-HGD-74/13/13 were spin-coated onto silicon wafer (4000 rpm, 75 s, 0.75% copolymer solution in methanol), dried under vacuum, and the dry film thickness was measured using ellipsometry to obtain a baseline for the subsequent swelling measurements. The copolymer films were immersed in buffer solution (0.1 mol dm^{-3} PBS) in a trapezoidal glass cuvette. Film thickness

measurements were obtained at regular intervals using in-situ ellipsometry until the rate of film thickness change had become stable, indicating that the film was close to its equilibrium swelling conformation. At this point, further measurements were taken at 3 different locations on the film, to obtain an average swollen copolymer film thickness.

The four copolymers used in this investigation were comprised of mole fractions of >81% HEMA. Poly(HEMA) is hydrophilic, but considered insoluble in water due to the methacrylate backbone[26] and often chain-coupling caused by traces of ethylene glycol dimethacrylate (EGDMA) (see Chapter 4, section 4.1.1).[26] Significant swelling of the copolymers discussed in this chapter was predicted, and evidence discussed earlier in the chapter supported this; significant hysteresis in the contact angle experiments indicated high chain mobility, often associated with hydrogels, and zeta potential changes at high pH in the electrokinetic measurements indicated swelling.

The swelling dynamics of HEMA-containing copolymers have been reported extensively, usually as cross-linked hydrogel networks.[33, 54, 55] Cross-linked poly(HEMA) hydrogels undergo swelling in water with film thickness increases of up to 55%. An increase in cross-link density results in a decrease in swelling. However, it was reported that in EGDMA-free poly(HEMA) films deposited by chemical vapour deposition, the homopolymer dissolved fully in water after 15 minutes. An increase of EGDMA (crosslinking monomer) composition resulted in light crosslinking, and dissolution was completely prevented only above 25% EGDMA copolymer composition.[56] In the work described here, the copolymer films studied using contact angle and ellipsometry measurements (sections 5.4.2.1 and 5.4.2.2) did not noticeably dissolve or delaminate. This effect could be due to multiple factors including i) the composition of the copolymers, which included water-insoluble GMA and DMA comonomers and ii) potential cross-linking arising from EGDMA, catecholic chain coupling (see Chapter 2) or GMA ring-opening (see section 5.4.1) or iii) effective adhesion to the substrate due to the presence of DMA side chains. In-situ ellipsometry measurements of the copolymers was carried out in an attempt to correlate the copolymer composition with the swelling behaviour.

Figure 5.11 shows the in-situ ellipsometry measurements of the copolymers. Film thickness and normalised refractive index (n_{norm}) are plotted against *t*. n_{norm} was calculated using Equation 5.4:

$$n_{norm} = \frac{n_{swollen} + n_{buffer}}{n_{dry} + n_{buffer}} \qquad 5.4$$

where $n_{swollen}$, n_{dry}, n_{buffer} are the refractive indices for the swollen copolymer, the dry copolymer and the buffer solution respectively (at λ = 633 nm).[52] n_{norm} is used as a comparative measure of the optical properties of the copolymer film. A value of 1 would indicate the refractive index of the film was unchanged upon immersion in solvent (*i.e.* no swelling or dissolution), while a n_{norm} approaching 0 would indicate the refractive index of the immersed film became identical to that of the solvent. A value greater than 1 may occur if the dry copolymer film contains a significant volume of air voids, which are filled with solvent in the swollen film.

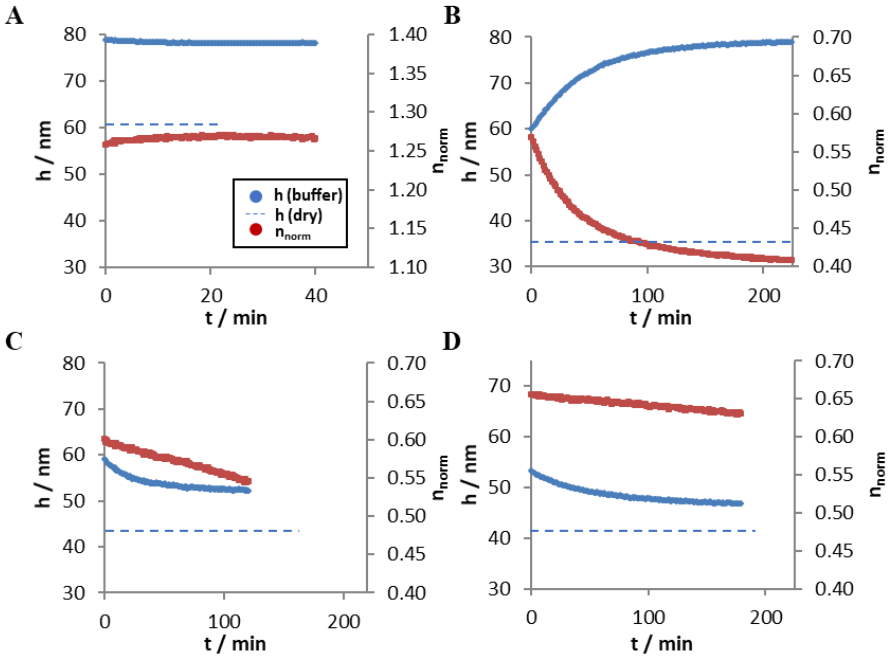

Figure 5.11. Film thickness (h, blue) and normalised refractive index (n_{norm}, red) vs time for in-situ ellipsometry measurements of A) FR-HGD-80/10/10, B) FR-HD-90/10-(DMF), C) FR-HG-89/11 and D) RAFT-HGD-74/13/13. Blue dashed line indicated dry film thickness.

Film thickness and refractive index measurements obtained from the dry film (h_{dry}, n_{dry}) are reported in Table 5.3. The film at t = 0 in the in-situ measurements shown in Figure 5.11 (h_{init}, n_{init}) and the final value for each of the in-situ measurements (h_{final}, n_{final}) are also reported in Table 5.3. The in-situ measurements were obtained at a single location in the centre of the film for consistency. After the in-situ measurements were completed, film thickness measurements were then obtained at various locations on the film to assess the homogeneity of the swelling and the average value is reported (h_{equil}, n_{equil}). A swelling

factor (SF) was also calculated using Equation 5.5 to compare the relative increase in the film thickness.

$$SF = \frac{h_{final}}{h_{dry}} \quad \textbf{5.5}$$

Table 5.3. Film thickness, refractive index and swelling factor data for dry and swollen copolymer samples.

Copolymer	h_{dry} / nm	h_{init} / nm	h_{final} / nm	h_{equil} / nm	n_{dry}	n_{init}	n_{final}	n_{equil}	SF
FR-HGD-80/10/10	61	79	78	79 ± 1	1.42	1.44	1.45	1.45 ± 0.004	1.28
FR-HD-90/10-(DMF)	36	60	79	102 ± 13	1.51	1.44	1.41	1.40 ± 0.006	2.19
FR-HG-89/11	44	59	52	64 ± 17	1.50	1.43	1.42	1.41 ± 0.018	1.34
RAFT-HGD-74/13/13	42	53	47	50 ± 3	1.52	1.46	1.45	1.45 ± 0.004	1.12

Initial swelling of FR-HGD-80/10/10 (Figure 5.11A) took place rapidly (before the first in-situ measurement). In this time the copolymer film had swollen from an initial dry thickness of 60 nm to 79 nm. Rapid swelling, often followed by a slower change in film thickness due to chain relaxation, is commonly observed and is characteristic of the solvent filling free-volume in an amorphous copolymer (*i.e.* rapid entry of solvent into regions not occupied by the copolymer matrix).[52, 53, 57]

Figure 5.11A indicates that after the initial rapid swelling, film thickness decreased very slightly (0.7 nm decrease) over the 40 min measurement period, and n_{norm} increased concomitantly, with a final swelling factor of 1.28. The almost insignificant reduction in film thickness suggested slight relaxation of the copolymer chains to the equilibrium conformation following the rapid swelling.[58] This behaviour is characteristic of so-called Case II swelling with limited overshoot dynamics (Figure 5.10B).[52] The high equilibrium value of n_{norm} indicated the presence of a significant volume of air in the dry copolymer film (n_{norm} = 1.27, note the different scale for n_{norm} and t in comparison with Figure 5.11B, C and D). This is unsurprising and may be rationalised by considering the AFM data presented in Chapter 4; porous films were produced when films of FR-HGD-80/10/10 were spin-coated from methanol using the same spin-coating parameters in this experiment. The porosity of the film may also explain the apparent lack of diffusion-controlled swelling, as the solvent could rapidly reach the entire film through the air voids.

Figure 5.11B shows the in-situ ellipsometry measurements of FR-HD-90/10-(DMF). After the initial rapid swelling from 36 to 60 nm, the copolymer film continued to swell, with a synchronous decrease in n_{norm} suggesting Fickian (diffusion-controlled) swelling dynamics (see Figure 5.10A). The low value of n_{norm} (0.40) shows the swelling of the film is significant, and that the swelling probably arises from solvent diffusion between the copolymer chains rather than the filling of air voids by solvent. The diffusion-controlled swelling dynamics also indicate a less porous film than FR-HGD-80/10/10. Furthermore, the suggestion of a less porous film is supported by the AFM data presented in Chapter 4, which indicated smooth films were produced from FR-HD-90/10-(DMF) when using the spin coating parameters used in this experiment. The increase in film thickness when plotted against t in Figure 5.11B is not perfectly linear, indicating simultaneous solvent diffusion and relaxation processes were occurring.[58] The swelling factor of 2.19 indicated very significant swelling of the film. The degree of swelling is closely linked to the extent of crosslinking in a polymer film.[45] Crosslinking between GMA and HEMA was identified in section 5.4.1 as a probable cause of reduced solubility in the film, so it follows that as FR-HD-90/10-(DMF) contains no GMA and thus experiences very little crosslinking, the swelling factor should be greater than the GMA containing polymers. The absence of GMA was also attributed to the reduction in pH-induced swelling for FR-HD-90/10-(DMF) compared to FR-HGD-80/10/10 implied by the electrokinetic measurements.

Figure 5.11C shows the in-situ ellipsometry measurements of FR-HG-89/11. At the start of the experiment, a rapid film thickness increase from 44 nm to 59 nm was observed, which was similar to the previously described copolymers. The swelling factor was 1.34, which was similar to FR-HGD-80/10/10, supporting the argument that presence of GMA limited swelling. The in-situ ellipsometry profile of FR-HG-89/11, however, was dramatically different from the previously described copolymers. Both film thickness and refractive index decreased with time. This trend is usually indicative of copolymer dissolution (shown in Figure 5.10C).[52] This indicated the lack of DMA reduced the surface adhesion and intermolecular cohesion in the polymer. This finding is consistent with the contact angle analysis (section 5.4.2.1), in which FR-HG-89/11 has the largest hysteresis, assigned to increased surface mobility of the copolymer chains due to the absence of DMA.

Figure 5.11D shows the in-situ ellipsometry measurements of RAFT-HGD-74/13/13 and illustrates behaviour which is similar to that observed for FR-HG-89/11; a rapid increase in film thickness was observed at the start of the measurement, from 41 to 53 nm, followed

by a reduction in h and n_{norm}, indicating dissolution of the copolymer. The swelling factor of 1.12 is the smallest of the four copolymers. The effect of DMA appeared to be diminished in RAFT-HGD-74/13/13, with dissolution of the copolymer indicative of poor surface adhesion. The reason for this is as yet unclear, but the significant difference shown by RAFT-HGD-74/13/13 is consistently observed. In discussions above, the unusual behaviour is attributed to the RAFT end-groups, which can affect the surface and bulk properties of the polymer and could potentially disrupt the stabilising intermolecular hydrogen-bonds. Furthermore, the low molecular weight of RAFT-HGD-74/13/13 could contribute to the reduced adhesion shown by catechol-containing polymers at low molecular weight due to reduced chain entanglement.[59]

The large variation of film thickness in the h_{equil} measurements, particularly for FR-HD-90/10-(DMF) and FR-HG-89/11 are indicative of the swelling of heterogeneous copolymer films. This could be due to roughness in the dry copolymer film arising from the spin-coating process. However, the films of FR-HD-90/10-(DMF) and FR-HG-89/11 had low MSE, indicating few striations, and AFM images of films coated under the same conditions showed smooth films (see Chapter 4). The dry copolymer films may have been in a non-equilibrium conformation, which may result in non-uniform swelling. Polymer films are often annealed to restore the equilibrium conformation,[60] although this was not carried out in this case to protect the epoxide functionality. Ideally, a swollen polymer at equilibrium would be homogenous over the whole coating region, however a real system may take very long time periods (days) to relax to a homogenous conformation.[52] Thus, the copolymers investigated here may not have reached their final equilibrium film structure. Such heterogeneity may decrease the reproducibility of the measurements.

Potential dissolution of the copolymer film was observed, particularly in Figures 5.11 C and D. This indicates a lack of film stability and is undesirable for the polymer films described in this work. As film thickness can be influenced by swelling and dissolution, the relative surface mass density change of the film can be calculated to decouple the two effects. The de Feijter equation (5.6) can be used to calculate the surface mass density of a deposited film, Γ (*i.e.* the amount of material in a film per surface area):

$$\boldsymbol{\Gamma = h\frac{(n - n_{amb})}{dn/dc}} \qquad \textbf{5.6}$$

where h is the film thickness, n and n_{amb} are the refractive indices of the film and the ambient environment (*i.e.* the solvent), and dn/dc refers to the refractive index increment of the deposited species in solution (in this case the copolymer in solution).[61] Film thickness and refractive index are assumed to have a linear relationship in the same medium. The result is that as solvent enters the polymer matrix, if there is no dissolution, the surface mass density will remain the same. Equation 5.7 can be used to define the surface mass density difference between the film at the start and end of the measurements, Γ_{diss}, and thus quantify the dissolution of copolymer:

$$\boldsymbol{\Gamma_{diss} = \Gamma_{init} - \Gamma_{final} = h_{init}\frac{(n_{init}-n_{amb})}{dn/dc} - h_{final}\frac{(n_{final}-n_{amb})}{dn/dc}} \qquad \textbf{5.7}$$

where the subscripts *init* and *final* denote measurements of h, n and calculated values of Γ from the initial and final in-situ ellipsometry measurements respectively. It should be noted that the calculation is only valid if the ambient medium remains constant, so the values h_{init} and n_{init} are taken from the first ellipsometry measurement in the presence of buffer solution.

As the dn/dc is unknown in this case, the absolute surface mass density change cannot be calculated, but Equations 5.8 and 5.9 can be used to calculate a dissolution factor (the percentage surface mass density change between dry and swollen films), Ω, to allow comparison between coatings:

$$\boldsymbol{\Gamma_{diss} \times \frac{dn}{dc} = h_{init}(n_{init} - n_{amb}) - h_{final}(n_{final} - n_{amb}) = \gamma_{init} - \gamma_{final}} \qquad \textbf{5.8}$$

$$\boldsymbol{\Omega = \frac{\gamma_{init} - \gamma_{final}}{\gamma_{init}} \times 100} \qquad \textbf{5.9}$$

where γ_{init} and γ_{final} are parameters describing a representative value for the dissolution and are used to calculate Ω. Ω therefore measures the percentage of copolymer lost *via* dissolution between the initial and final measurements *e.g.* a Ω of 5% indicates that in the period from the first measurement after buffer was added, 5% of the mass was lost to dissolution. Due to the change of ambient environment (change from air to buffer solution), this calculation was not applied to the dry film, so the period between adding the buffer and the first ellipsometry measurement is not considered. Significant swelling occurs in this time, so some dissolution could have also occurred. The average time between filling the cell with buffer and beginning in-situ measurements was around 1 minute.

Table 5.4 shows the calculated dissolution factors for the copolymers used in this study. A value of n_{amb} = 1.3329 was used for the buffer solution (0.01 mol dm^{-1} PBS buffer, measured using a refractometer).

Table 5.4. Dissolution factor Ω for copolymer films at the end of in-situ ellipsometry measurements.

Copolymer	Ω / %
FR-HGD-80/10/10	0.2
FR-HD-90/10-(DMF)	5.6
FR-HG-89/11	19.7
RAFT-HGD-74/13/13	15.7

For FR-HGD-80/10/10, Ω was 0.2%, indicating virtually no copolymer dissolved after the initial swelling period (Table 5.4). The limited dissolution over a period of 40 minutes suggests the remaining copolymer film was strongly adsorbed and stable. Similarly, for FR-HD-90/10-(DMF) the value for Ω was 5.4% indicating limited dissolution after the initial swelling. This result suggested the DMA in FR-HD-90/10-(DMF) was providing strong adhesion to the surface of the substrate and cohesive interactions with other polymers, as indicated by the contact angle measurements. However, adhesion was slightly poorer than for FR-HGD-80/10/10. This could be due to the relatively low molecular weight and lack of crosslinking (as suggested above), which may allow poorly bound chains to dissolve more rapidly. In contrast, Figure 5.11 indicated significant dissolution of FR-HG-89/11. This was attributed to a lack of DMA adhesive and cohesive interactions and is supported by a large Ω of 19.7%. This result suggested that DMA (absent in this case) helps to provide adhesion to the substrate and cohesion in the copolymer film. For RAFT-HGD-74/13/13 the value for Ω was 15.7%, which is consistent with the suggestion of a reasonable degree of copolymer dissolution from the substrate from Figure 5.11, attributed above to low molecular weight and the influence of the RAFT end groups.

In summary, the in-situ ellipsometry results indicate that the bulk swelling of the copolymer was strongly influenced by the presence of GMA, which leads to crosslinking and in turn limits swelling. This is evidenced by generally lower values of the swelling factor (SF) (between 1.12 and 1.34) for GMA containing copolymers whereas FR-HD-90/10-DMF had an SF of 2.19. In contrast, the calculated dissolution of the copolymer films were apparently more strongly influenced by the activity of DMA. This was evidenced by dissolution factors of >6% for FR-HGD-80/10/10 and FR-HD-90/10-(DMF) compared to 19.7% for FR-HG-89/11. The significant dissolution of RAFT-HGD-74/13/13 is unexpected, but reflects the unusual findings from the captive-bubble contact

angle measurements, section 5.4.2.1, and the electrokinetic measurements, section 5.4.2.2 for this copolymer.

5.4.3 Characterisation of the immobilisation of antibodies to a thin copolymer film using in-situ ellipsometry and QCM

It was envisaged that key potential application of the copolymers produced in this study could be the immobilisation of an antibody onto a copolymer film. To explore this possibility, an attempt was made to immobilise antibody for aflatoxin from a buffer solution onto a film of FR-HGD-80/10/10, *via* chemical reaction between the epoxide groups of GMA and primary amine or thiol-containing protein residues. The success of antibody immobilisation was monitored using two complementary methods: in-situ ellipsometry and QCM.[62] The use of these methods allowed evaluation of the suitability of copolymer FR-HGD-80/10/10 for use as a coating in biosensing devices. Due to time constraints, only FR-HGD-80/10/10 was investigated. FR-HGD-80/10/10 was selected as it comprised GMA, which should allow immobilisation of biomolecules,[63] and the DMA had been shown to provide good adhesion to various substrates, evidenced by the very limited dissolution of FR-HGD-80/10/10 and FR-HD-90/10-(DMF) in buffer solution.

Poly(HEMA) has anti-fouling properties, making it suitable for biomedical applications, most notably in contact lenses.[51, 64] A relevant report indicated that human serum albumin protein adsorbed on a crosslinked HEMA hydrogel,[65] however the protein was not strongly bound to the polymer. This was evidenced by removal of the vast majority of protein after washing in PBS solution. A small amount of denatured protein remained on the surface. After washing, only 0.4 mg m^{-2} remained on the surface; much less than a monolayer coating, which is predicted to be 4 – 4.6 mg m^{-2}. The monolayer surface mass density agreed well with another study, which reported that a monolayer coating of 4 mg m^{-2} formed upon the immobilisation of an IgG antibody on poly(styrene-co-acrylamide) latex particles.[66] It has been reported that immobilisation of antibodies on HEMA-containing copolymers was improved in the presence of a monomer with a reactive functional side-chain *e.g. N*-methacryloyl-(L)-histidine methyl ester.[51] These reports gave reasonable target values for the surface density and film thickness of an antibody coating, and justified the necessity of including a reactive functional group (*via* GMA) to immobilise the biomolecules.

Anti-aflatoxin M1, used in this study, is an IgG type antibody. IgG antibodies are Y-shaped proteins with dimensions of around 14.5 x 8.5 x 4 nm,[67] and molecular weight in the region

of 150000 – 160000 g mol^{-1}.[68] The chemical structure of all IgG type antibodies is roughly equivalent; the chemical structure is only specific to each particular antigen at the two "tips" of the Y-shape and joined in the centre by a flexible hinge region containing disulfide bridges (Figure 5.12).[69] The similarity of structure allows the immobilisation of all IgG type antibodies to be reasonably compared. The surface mass density of a layer of immobilised antibody, Γ, can be calculated using the film thickness and refractive index values obtained from ellipsometry measurements.[61]

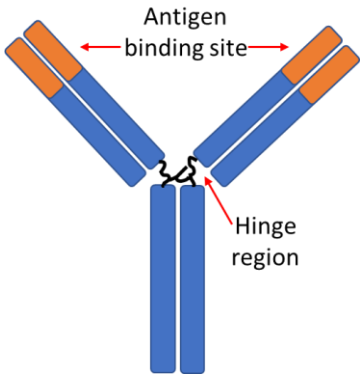

Figure 5.12. Schematic of an IgG antibody.

IgG antibodies have been reported to adsorb more rapidly, and to a greater density at pH values close their IEP, which is generally around pH 6.5.[51, 69] However, the adsorption rate is influenced more strongly by hydrophobic/hydrophilic interactions and protein stability rather than electrostatic interactions. Many proteins may initially bind more strongly to hydrophobic surfaces, so the surface of FR-HGD-80/10/10, which showed the highest θ_r (21°) *i.e.* the least hydrophilic surface in the swollen state, may be the most appropriate choice of the copolymers studied here.

5.4.3.1 Characterisation of antibody immobilisation using in-situ ellipsometry

In-situ ellipsometry was used to monitor the immobilisation of anti-aflatoxin M1 antibody to the surface of a silicon wafer, spin-coated with FR-HGD-80/10/10 (0.75 % w/v from methanol, 4000 rpm, 600 rpm s^{-1}). The 0.01 mol dm^{-3} PBS solution used in the in-situ ellipsometry measurements (section 5.4.2.2) was considered unsuitable for antibody stabilisation due to the high ionic strength, thus 0.001 mol dm^{-3} sodium phosphate buffer (NaPB) was used for the measurements. A 0.08 mg mL^{-1} antibody solution concentration was used for the immobilisation experiments. The refractive index of the NaPB was accurately determined using a refractometer (n = 1.3315).

The spin-coated silicon wafer sample (dry film thickness 34 nm) was immobilised in a trapezoidal cuvette and allowed to swell in NaPB (0.001 mol dm^{-3}). Measurements were obtained at regular time intervals until the values for film thickness and *n* showed no further change; at 46 nm and 1.48 respectively. The swelling factor (1.33) for FR-HGD-80/10/10 was very similar to the value observed in the in-situ ellipsometry measurement for the same copolymer in 0.1 mol dm^{-3} PBS (1.28), suggesting that the change in ionic strength of the buffer had little effect on the copolymer swelling at pH 7.4. The pure buffer solution was then replaced with a solution of antibody (final concentration 0.08 mg mL^{-1}) in NaPB (0.001 mol dm^{-3}). In-situ ellipsometry measurements were obtained periodically until the film thickness had ceased to change (Figure 5.13A). The film thickness increased by 7 nm compared to the pre-swollen film to 52.9 ± 0.1 nm (average for measurements after 35 min). Several previous reports suggest that the thickness of an IgG antibody monolayer is in the region of 4 – 8 nm.[67, 70, 71] Therefore, the observed film thickness corresponded well to a monolayer antibody coating.

The concentration of the antibody solution was subsequently reduced to 0.04 mg mL^{-1} and the film thickness was measured again at regular intervals to determine if the antibody coating would desorb if not irreversibly bound. Figure 5.13B shows the thickness of the antibody coating was reduced to 52.1 ± 0.1 nm for measurements after 30 min, indicating very limited antibody desorption.

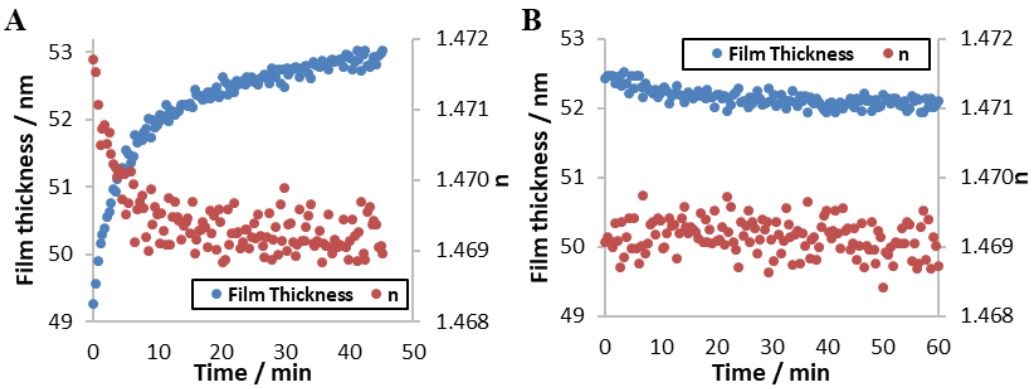

Figure 5.13. In-situ ellipsometry measurements of FR-HGD-80/10/10 for immobilisation of antibody in 0.001 mol dm^{-3} phosphate buffer solution. A) 0.08 mg mL^{-1} antibody concentration B) 0.04 mg mL^{-1} antibody concentration. n = refractive index.

The mass of coated antibody can be calculated using a modified form of the De Feijter equation (see Equation 5.10) to build a two-layer model of the deposition as outlined by Furchner *et al.*[9]:

$$\Gamma_{ab} = d_{swell} \cdot \frac{n_{ab} - n_{swell}}{(dn/dc)_{ab}} + d_{add} \cdot \frac{n_{ab} - n_{amb}}{(dn/dc)_{ab}} \quad \textbf{5.10}$$

where Γ_{ab} is the density of the immobilised layer of antibody, in mg m^{-2}, d_{swell} and d_{add} refer to the thickness of the swollen copolymer and the additional layer, n_{ab}, n_{swell} and n_{amb} are the refractive indices of the film after antibody adhesion, the swollen copolymer and the ambient solution respectively. A *dn/dc* of 0.188 was used for the antibody.[68] Using film thickness and *n* values collected after the antibody concentration had been reduced (52 nm and 0.1469 respectively), a Γ_{ab} value of 3.5 mg m^{-2} was calculated. This was similar to the previously discussed literature values (4 – 4.6 mg m^{-2}), supporting the claim of successful immobilisation of an antibody monolayer.[66]

5.4.3.2 Characterisation of antibody binding using QCM

QCM can be used to monitor the immobilisation of antibodies onto a polymer film immobilised on a quartz crystal.[11, 13, 14, 72] The mass or thickness of a deposited layer can be correlated directly with the change in the frequency of the oscillating crystal using the Sauerbrey equation:

$$\Delta f = -\frac{z}{C} m_f = -\frac{z}{C} \rho_f h_f \quad \textbf{5.11}$$

where Δf is frequency change, m_f is the mass density (per unit area), z is the overtone order, ρ_f and h_f are the density and thickness of the adsorbed film respectively.[72] C is the mass sensitivity constant which is dependent on the resonant frequency of the quartz crystal.

The deposition of anti-aflatoxin antibody on a film of FR-HGD-80/10/10 was investigated and the results compared with the results obtained by in-situ ellipsometry. Frequency and dissipation shift data were obtained and the multiple harmonic overtone frequencies for the measurements are shown, which contributed to the modelling of the data (Figure 5.14A). The film thickness was calculated using the Sauerbrey equation, with an estimated ρ_f value of 1 g cm^{-3} (Figure 5.14B).[14, 72]

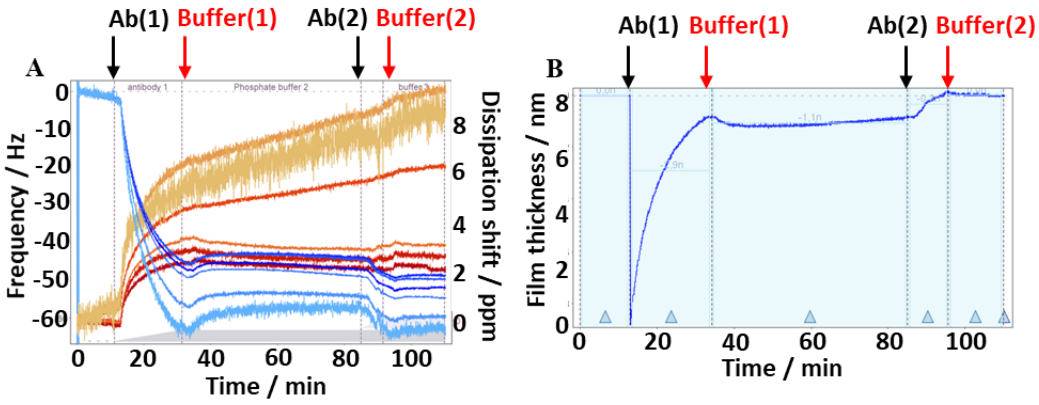

Figure 5.14. QCM data obtained during two immersion/rinse cycles. A) Frequency overtones (blue) and dissipation shift overtones (red/orange) and B) Film thickness calculated using the Sauerbrey equation.

Gold-plated quartz electrodes were spin-coated with FR-HGD-80/10/10 (4000 rpm, 600 rpm s^{-1}, 0.75% in DMF). DMF was used as the spin coating solvent as it was not possible to obtain homogenous coatings from methanol on the electrodes. The coated crystals were mounted in flow cells, through which 0.001 mol dm^{-3} NaPB was flowed for 60 min to allow the copolymer swelling to reach equilibrium. A reduction in the frequency of 2-3 Hz at the start of the measurement period indicated that the film continued to swell slightly. After 10 minutes, a solution of anti-aflatoxin antibody (0.025 mg mL^{-1}) in NaPB was passed continuously through the cell for a further 20 minutes (as indicated by "Ab(1)" on Figure 5.14), which resulted in a sharp decrease in vibrational frequency of at least 45 Hz coupled with an increase in dissipation. A reduction in oscillation frequency occurs upon an increase of mass on the electrode, indicating immobilisation of the antibody on the electrode surface.[73] A concomitant increase in dissipation confirmed the deposition of a film on the electrode.[72] The Sauerbrey model was used to calculate the coating thickness, which is displayed in Figure 5.14B. After the initial period of antibody exposure, a film thickness of 7 nm was estimated.

The flow cell was then flushed with buffer solution for 50 min to determine if the antibody layer could be removed (Buffer(1)), however only a small increase in vibrational frequency was observed (~5 Hz). This corresponded to a slight reduction in antibody film thickness of less than 1 nm. Antibody solution was flowed into the cell again to investigate whether any further immobilisation of antibody would occur (as indicated by Ab(2) in Figure 5.14) and the frequency was reduced to a similar value to that observed after the first antibody flow period, corresponding to a film thickness increase of around 1 nm. Finally, a return to flow of buffer solution (Buffer(2)) yielded no further change in the frequency, indicating

no further removal of antibody. The film thickness change calculated by QCM, 8 nm, correlated well with the results of the in-situ ellipsometry, which had suggested the formation of a 6 nm film.

The combined data from QCM and ellipsometry therefore appeared to provide consistent evidence that a monolayer of anti-aflatoxin antibody was immobilised on the film of FR-HGD-80/10/10. FR-HGD-80/10/10 may therefore be an appropriate candidate for use in biosensing applications. It should be noted that in the absence of a full study of the effects of film swelling and roughness on the binding of antibodies or a more in-depth kinetic study, the measurements should be treated with some caution, as the potential errors may be significant; however, the broad agreement of the two independent methods is encouraging evidence.[10]

5.5 Conclusion

Bulk and surface properties of several spin-coated copolymer films were investigated using various techniques. The aim of the investigation was to correlate the properties of the copolymers to their composition or molecular weight and thus determine which copolymers would be appropriate for use in bio-sensing applications. The immobilisation of antibodies on the films was then monitored using ellipsometry and QCM.

The impact of medium to long-term storage of a selection of copolymers, comprising HEMA as the main component, was investigated. The study revealed that copolymers comprising up to 12% GMA became insoluble in methanol upon storage at 4 °C or above. The presence of DMA did not appear to impact the solubility upon storage up to 35 °C. The insolubility was attributed to slow crosslinking processes caused by nucleophilic attack of the epoxide ring by hydroxyl groups, present in high concentration in the copolymers. These observations have implications for the storage and use of copolymers used as coatings, as they have a limited shelf-life and must be stored in a freezer.

The surface and bulk properties of FR-HGD-80/10/10, FR-HD-90/10-(DMF), FR-HG-89/11 and RAFT-HGD-74/13/13 films were studied by contact angle analysis, streaming current electrokinetic potential measurements and in-situ ellipsometry. Contact angle analysis indicated significant hysteresis for all four copolymers, probably due to their ability to undergo conformational rearrangement to expose hydrophilic or hydrophobic functional groups to the interface. FR-HGD-80/10/10 and FR-HD-90/10-(DMF) exhibited the smallest hysteresis, 44° and 47° respectively, suggesting that DMA inhibited

conformational rearrangement in the film most likely *via* strong intermolecular H-bonding interactions. This was supported by the greater hysteresis observed for the DMA-free film of FR-HG-89/11 (63°), which was assigned to increased surface chain mobility. RAFT-HGD-74/13/13 showed an intermediate value of hysteresis, which was tentatively assigned to the influence of the hydrophobic RAFT end groups.

Electrokinetic measurements showed that all four copolymers had negative zeta potential at neutral pH, as expected for copolymers mainly comprised of HEMA, due to the retention of anions by the film. The IEP of FR-HGD-80/10/10, FR-HD-90/10-(DMF), and RAFT-HGD-74/13/13 was at pH 2.5. The IEP of FR-HG-89/11 was at a higher pH, indicating the presence of DMA significantly contributed to the anionic character of the film surface. The zeta potential of all four copolymers decreased at pH >8 (from >6.5 in the case of RAFT-HGD-74/13/13), which was attributed to pH-induced swelling as the ionisable groups became deprotonated. The pK_a of the ionisable groups appeared to determine the pH of the zeta potential maximum, and the presence of an increasing amount of such groups decreased the zeta potential accordingly at high pH. For RAFT-HGD-74/13/13, the high maximum zeta potential at a relatively low pH was again attributed to the end groups; in this case the low pk_a of the carboxylic acid functional group. In both contact angle and electrokinetic potential measurements, GMA had a negligible effect on the surface properties of the film.

In-situ ellipsometry of the copolymer films resulted in significant swelling in water, as would be expected for copolymers with significant HEMA content. FR-HGD-80/10/10 showed Case II swelling dynamics, consistent with a porous film structure, but (virtually) no dissolution was observed. Likewise, FR-HG-89/11 and RAFT-HGD-74/13/13 also swelled rapidly with Case II dynamics, however some (partial) dissolution of the copolymer was observed. In stark contrast, FR-HD-90/10-(DMF) swelled significantly with diffusion-controlled dynamics and dissolution was very limited. The different swelling regime and markedly reduced degrees of swelling of the three GMA-containing copolymers compared to FR-HD-90/10-(DMF) was attributed to crosslinking involving GMA, which was also proposed as the source of insolubility upon storage. In contrast, dissolution of the films appeared not to correlate with GMA content and was instead tentatively ascribed to the presence of DMA, according to the previously described and well-known adhesive and strong intermolecular H-bonding properties of catechol groups. For RAFT-HGD-74/13/13, the influence of DMA on the adhesion, and hence dissolution,

appeared to be reduced. This was surprising, and the cause not clear, but the behaviour was akin to the unusual behaviour noted in the previous sections. For the dissolution of all four copolymers, good agreement was noted between the contact angle analysis and swelling results, with high hysteresis (assigned to increased local chain rearrangement of functional groups at the polymer surface) correlating with increased copolymer dissolution.

As GMA was considered necessary for antibody binding (*via* the epoxy group) and considering the partial dissolution of FR-HG-89/11 and RAFT-HGD-74/13/13, FR-HGD-80/10/10 was chosen to study the potential immobilisation of anti-aflatoxin antibody. The effectiveness of this copolymer towards antibody immobilisation was investigated using in-situ ellipsometry and QCM. Both techniques suggested that a monolayer of antibodies was immobilised on the film surface which was not removed upon washing with buffer. In combination, the findings suggested FR-HGD-80/10/10 was suitable and effective for the immobilisation of anti-aflatoxin.

Overall, these results successfully demonstrate the potential for the copolymers produced in this study, particularly FR-HGD-80/10/10, to be taken forward for further studies in biosensing applications. However, the investigation also highlighted some practical issues which must be considered, such as the reduction in solubility on storage of the bulk copolymers and potential dissolution of the copolymer films.

5.6 References

1. K. Grundke, K. Poschel, A. Synytska, R. Frenzel, A. Drechsler, M. Nitschke, A. L. Cordeiro, P. Uhlmann and P. B. Welzel, *Adv. Colloid Interface Sci.*, 2015, **222**, 350-376.
2. C. N. C. Lam, R. Wu, D. Li, M. L. Hair and A. W. Neumann, *Adv. Colloid Interface Sci.*, 2002, **96**, 169-191.
3. Y. Rotenberg, L. Boruvka and A. W. Neumann, *J. Colloid Interface Sci.*, 1983, **93**, 169-183.
4. S. M. Saad and A. W. Neumann, *Adv. Colloid Interface Sci.*, 2016, **238**, 62-87.
5. J. F. Oliver, C. Huh and S. G. Mason, *J. Colloid Interface Sci.*, 1977, **59**, 568-581.
6. H. J. Jacobasch, *Prog. Org. Coat.*, 1989, **17**, 115-133.
7. B. J. Kirby and E. F. Hasselbrink, *Electrophoresis*, 2004, **25**, 187-202.
8. J. S. Papanu, D. W. Hess, A. T. Bell and D. S. Soane, *J. Electrochem. Soc.*, 1989, **136**, 1195-1200.
9. E. Bittrich, P. Uhlmann, K.-J. Eichhorn, K. Hinrichs, D. Aulich and A. Furchner, in *Ellipsometry of Functional Organic Surfaces and Films*, Springer, 2014, vol. 52, ch. 8, pp. 79-105.
10. K. A. Marx, *Biomacromolecules*, 2003, **4**, 1099-1120.
11. D. A. Buttry and M. D. Ward, *Chem. Rev. (Washington, DC, U. S.)*, 1992, **92**, 1355-1379.
12. T. Ren, Z. Mao, S. E. Moya and C. Gao, *Chem.--Asian J.*, 2014, **9**, 2132-2139.
13. F. Hook, J. Voros, M. Rodahl, R. Kurrat, P. Boni, J. J. Ramsden, M. Textor, N. D. Spencer, P. Tengvall, J. Gold and B. Kasemo, *Colloids Surf., B*, 2002, **24**, 155-170.
14. S. Adam, M. Koenig, K. B. Rodenhausen, K.-J. Eichhorn, U. Oertel, M. Schubert, M. Stamm and P. Uhlmann, *Appl. Surf. Sci.*, 2017, **421**, 843-851.
15. E. M. Muzammil, A. Khan and M. C. Stuparu, *RSC Advances*, 2017, **7**, 55874-55884.
16. A. V. Reis, A. R. Fajardo, I. T. A. Schuquel, M. R. Guilherme, G. J. Vidotti, A. F. Rubira and E. C. Muniz, *J. Org. Chem.*, 2009, **74**, 3750-3757.
17. H. C. Chitwood and B. T. Freure, *J. Am. Chem. Soc.*, 1946, **68**, 680-683.
18. L. Shechter and J. Wynstra, *Ind. Eng. Chem.*, 1956, **48**, 86-93.
19. J. N. Israelachvili, *Intermolecular and Surface Forces*, Academic press, 2015.
20. H. Yasuda, A. K. Sharma and T. Yasuda, *J. Polym. Sci., Part B: Polym. Phys.*, 1981, **19**, 1287-1291.
21. N. Dhopatkar, E. Anim-Danso, C. Peng, S. Singla, X. H. Liu, A. Joy and A. Dhinojwala, *Macromolecules*, 2018, **51**, 5114-5120.
22. J. A. Crowe and J. Genzer, *J. Am. Chem. Soc.*, 2005, **127**, 17610-17611.
23. D. Wong, C. A. Jalbert, P. A. V. O'Rourke-Muisener and J. T. Koberstein, *Macromolecules*, 2012, **45**, 7973-7984.
24. A. H. Hogt, D. E. Gregonis, J. D. Andrade, S. W. Kim, J. Dankert and J. Feijen, *J. Colloid Interface Sci.*, 1985, **106**.
25. M. Morra, E. Occhiello and F. Garbassi, *J. Colloid Interface Sci.*, 1992, **149**, 84-91.
26. F. J. Holly, *J. Biomed. Mater. Res.*, 1975, **9**, 315-326.
27. A. H. Hogt, J. Dankert and J. Feijen, *J. Biomed. Mater. Res.*, 1986, **20**, 533-545.
28. L. Hermitte, F. Thomas, R. Bougaran and C. Martelet, *J. Colloid Interface Sci.*, 2004, **272**, 82-89.
29. G. Beamson, *J. Electron Spectrosc. Relat. Phenom.*, 2001, **121**, 163-181.

30. H. J. Busscher, A. W. J. Vanpelt, P. Deboer, H. P. Dejong and J. Arends, *Colloids Surf.*, 1984, **9**, 319-331.
31. C. W. Extrand and Y. Kumagai, *J. Colloid Interface Sci.*, 1997, **191**, 378-383.
32. R. Zaleski, P. Krasucka, K. Skrzypiec and J. Goworek, *Macromolecules*, 2017, **50**, 5080-5089.
33. K. Chan and K. K. Gleason, *Langmuir*, 2005, **21**, 8930-8939.
34. J. Saiz-Poseu, J. Mancebo-Aracil, F. Nador, F. Busque and D. Ruiz-Molina, *Angew. Chem., Int. Ed.*, 2019, **58**, 696-714.
35. Y. B. Ma, C. H. Ye, C. Zhang, P. Tangvijitsakul, M. D. Soucek, N. S. Zacharia and B. D. Vogt, *J. Polym. Sci., Part B: Polym. Phys.*, 2017, **55**, 77-84.
36. C. Bellmanna, C. Klingerb, A. Opfermannc, F. Böhmea and H.-J. P. Adlerd, *Prog. Org. Coat.*, 2002, **44**, 93-98.
37. C. Schnitzer and S. Ripperger, *Chem. Eng. Technol.*, 2008, **31**, 1696-1700.
38. J. Lyklema, *Colloids Surf., A*, 2011, **376**, 2-8.
39. R. Zimmermann, U. Freudenberg, R. Schweiss, D. Kuttner and C. Werner, *Curr. Opin. Colloid Interface Sci.*, 2010, **15**, 196-202.
40. H. J. Jacobasch, F. Simon and P. Weidenhammer, *Coll. Polym. Sci.*, 1998, **276**, 434-442.
41. C. Bellmann, C. Klinger, A. Opfermann, F. Bohme and H. J. P. Adler, *Prog. Org. Coat.*, 2002, **44**, 93-98.
42. R. Zimmermann, D. Kuckling, M. Kaufmann, C. Werner and J. F. L. Duval, *Langmuir*, 2010, **26**, 18169-18181.
43. B. Malisova, S. Tosatti, M. Textor, K. Gademann and S. Zurcher, *Langmuir*, 2010, **26**, 4018-4026.
44. D. J. Kim, J. M. Caruthers and N. A. Peppas, *Macromolecules*, 1993, **26**, 1841-1847.
45. Y. Tang, J. R. Lu, A. L. Lewis, T. A. Vick and P. W. Stratford, *Macromolecules*, 2002, **35**, 3955-3964.
46. E. Vasilaki, M. Kaliva, N. Katsarakis and M. Vamvakaki, *Appl. Surf. Sci.*, 2017, **399**, 106-113.
47. T. Yildirim, I. Yildirim, R. Yanez-Macias, S. Stumpf, C. Fritzsche, S. Hoeppener, C. Guerrero-Sanchez, S. Schubert and U. S. Schubert, *Polym. Chem.*, 2017, **8**, 1328-1340.
48. A. G. Vanderput and B. H. Bijsterbosch, *J. Colloid Interface Sci.*, 1983, **92**, 499-507.
49. A. V. Delgado, F. Gonzalez-Caballero, R. J. Hunter, L. K. Koopal and J. Lyklema, *J. Colloid Interface Sci.*, 2007, **309**, 194-224.
50. E. Faure, C. Falentin-Daudré, C. Jérôme, J. Lyskawa, D. Fournier, P. Woisel and C. Detrembleur, *Prog. Polym. Sci.*, 2013, **38**, 236-270.
51. L. Uzun, R. Say and A. Denizli, *React. Funct. Polym.*, 2005, **64**, 93-102.
52. E. J. Kappert, M. J. T. Raaijmakers, K. Tempelman, F. P. Cuperus, W. Ogieglo and N. E. Benes, *J. Membr. Sci.*, 2019, **569**, 177-199.
53. G. Guzman, S. M. Bhaway, T. Nugay, B. D. Vogt and M. Cakmak, *Langmuir*, 2017, **33**, 2900-2910.
54. L. Brannonpeppas and N. A. Peppas, *Biomaterials*, 1990, **11**, 635-644.
55. S. Akgöl, G. Bayramoğlu, Y. Kacar, A. Denizli and M. Y. Arıca, *Polym. Int.*, 2002, **51**, 1316-1322.
56. K. Unger, R. Resel and A. M. Coclite, *Macromol. Chem. Phys.*, 2016, **217**, 2372-2379.
57. D. Turnbull and M. H. Cohen, *J. Chem. Phys.*, 1961, **34**, 120.

58. Y. Tang, J. R. Lu, A. L. Lewis, T. A. Vick and P. W. Stratford, *Macromolecules*, 2001, **34**, 8768-8776.
59. C. L. Jenkins, H. J. Meredith and J. J. Wilker, *ACS Appl. Mater. Interfaces*, 2013, **5**, 5091-5096.
60. J. L. Keddie, R. A. L. Jones and R. A. Cory, *Europhys. Lett.*, 1994, **27**, 59-64.
61. J. A. De Feijter, J. Benjamins and F. A. Veer, *Biopolymers*, 1978, **17**, 1759-1772.
62. R. G. Couston, M. W. Skoda, S. Uddin and C. F. van der Walle, *MAbs*, 2013, **5**, 126-139.
63. G. Bayramoglu, S. Akgol, A. Bulut, A. Denizli and M. Y. Arica, *Biochemical Engineering Journal*, 2003, **14**, 117-126.
64. C. Rodriguez-Emmenegger, O. A. Avramenko, E. Brynda, J. Skvor and A. B. Alles, *Biosens. Bioelectron.*, 2011, **26**, 4545-4551.
65. Q. Garrett and B. K. Milthorpe, *Invest. Ophthalmol. Vis. Sci.*, 1996, **37**, 2594-2602.
66. A. Kondo, S. Uchimura and K. Higashitani, *J. Ferment. Bioeng.*, 1994, **78**, 164-169.
67. K.-B. Lee, S.-J. Park, C. A. Mirkin, J. C. Smith and M. Mrksich, *Science*, 2002, **295**, 1702-1705.
68. C. G. Golander and E. Kiss, *J. Colloid Interface Sci.*, 1988, **121**, 240-253.
69. W. Norde and J. Lyklema, *Adv. Colloid Interface Sci.*, 2012, **179**, 5-13.
70. K. Wadu-Mesthrige, S. Xu, N. A. Amro and G. Y. Liu, *Langmuir*, 1999, **15**, 8580-8583.
71. M. E. BrowningKelley, K. WaduMesthrige, V. Hari and G. Y. Liu, *Langmuir*, 1997, **13**, 343-350.
72. I. Reviakine, D. Johannsmann and R. P. Richter, *Anal. Chem.*, 2011, **83**, 8838-8848.
73. F. Hook, M. Rodahl, P. Brzezinski and B. Kasemo, *Langmuir*, 1998, **14**, 729-734.

Chapter 6 Conclusions and Future Work

6.1 Conclusions

The work described in this thesis has focused on the design of bio-inspired functional adhesive coatings, *via* the synthesis of copolymers containing dopamine methacrylamide (DMA) and its acetonide-protected analogue (ADMA). Several novel copolymers were synthesised by free radical and RAFT polymerisation, comprising DMA or ADMA with methacrylate comonomers. Deposition of a functional copolymer film *via* spin coating allowed the immobilisation of IgG antibodies. The headline conclusions are that i) significant compositional drift was exhibited when ADMA was polymerised with one or more methacrylate comonomers, and ii) the catechol functionality had a significant effect on the free radical and RAFT polymerisations, deposition of coatings and film properties.

DMA was synthesised and subsequently protected as an acetonide. Maximum yields of 67% for DMA synthesis and 81% for ADMA were obtained. Two published workup methods were compared and optimised, and it was established that it was necessary to use column chromatography to obtain sufficiently pure DMA to allow the subsequent synthesis of usable acetonide-protected DMA, as dopamine-containing impurities in ADMA caused inhibition of polymerisations.

Free radical polymerisation of DMA yielded homopolymers which quickly turned brown and became insoluble on exposure to air, ascribed to oxidation of the catechol side chains and subsequent crosslinking. Polymerisation of ADMA exhibited slow reaction kinetics, (20 % after 24 h) which was attributed to trace impurities in the monomer. For the first time, to the best of our knowledge, reactivity ratios were estimated for the free radical copolymerisation of ADMA with i) MMA and ii) GMA. The values obtained by the non-linear least squares regression method for the MMA/ADMA copolymerisation were $r_{MMA} = 2.21 \pm 0.26$ and $r_{ADMA} = 0.17 \pm 0.03$, and for the GMA/ADMA copolymerisation $r_{GMA} = 1.96 \pm 0.49$ and $r_{ADMA} = 0.18 \pm 0.08$. The reactivity ratios demonstrated that, in both cases, the methacrylate monomer has a strong tendency to self-propagate, the ADMA has a strong tendency to cross-propagate and therefore the methacrylate is preferentially incorporated at all monomer feed ratios, giving an important insight into the reactivity of ADMA. A library of co- and terpolymers comprising ADMA were then synthesised using MMA, GMA, HEMA and SMA as comonomers. As predicted by the reactivity ratios, these polymers exhibited significant compositional drift. ADMA-containing copolymers

were successfully deprotected using TFA, although due to acid-catalysed crosslinking, the procedure could not be used for GMA-containing copolymers. Unprotected DMA was polymerised with methacrylate copolymers, using DMA feed mole fractions below 50%, achieving reasonable monomer conversions. Copolymers comprising MMA and DMA showed very low M_n and reasonably narrow dispersity values, suggesting rapid chain transfer due to reaction between the DMA side chain and the propagating radical. In contrast, in copolymers of HEMA and DMA, at monomer feed mole fractions of 30-40% DMA, the copolymers analysed showed M_n values of less than 10000 g mol^{-1} and dispersities >10. This was attributed to chain transfer due to the catechol side chains in DMA, highlighting significant changes to the skeletal structure arising from the use of unprotected DMA.

RAFT polymerisation, using CTP as a RAFT agent, was used to synthesise a homopolymer of ADMA. Poly(ADMA) synthesis using DMF or 1,4-dioxane solvents yielded polymers with relatively poor control over molecular weight and dispersity. In the case of poly(ADMA) synthesised using 1,4-dioxane, the M_n obtained by SEC was significantly higher than the theoretical M_n. This was attributed to incomplete consumption of RAFT agent, leading to the formation of fewer polymer chains (of higher molecular weight) in total. Despite this, after an inhibition period, the polymerisation showed *pseudo*-first order polymerisation kinetics, which implied a reasonably controlled reaction. Homopolymers of SMA, MMA and GMA were also synthesised in 1,4-dioxane, using the same conditions as used to synthesise ADMA homopolymers, yielding reasonably good control over dispersity, but high molecular weight with respect to the theoretical value. The continued poor control of molecular weight was also attributed to the incomplete RAFT agent consumption, inferred during the synthesis of the ADMA homopolymer.

Novel statistical copolymers of ADMA with MMA, GMA, SMA and HEMA and a terpolymer, poly(HEMA-*stat*-GMA-*stat*-ADMA), were also synthesised. In all cases the monomer feed ratio when the polymerisation was quenched contained a significant proportion of ADMA, inferring the formation of gradient copolymers. Due to the nature of RAFT polymerisation, virtually all polymer chains should contain the same proportion of ADMA. Narrow dispersities ($Đ \leq 1.23$) were observed for the copolymers containing MMA, GMA and SMA despite some loss of molecular weight control. In contrast, the HEMA co- and terpolymers were synthesised with excellent molecular weight control, which was attributed to the change in solvent from 1,4-dioxane to DMF. However, a slight

loss of dispersity control ($Đ \leq 1.38$) was observed for the HEMA-containing copolymers. It was also concluded that the slightly larger dispersities were due to side reactions such as bimolecular termination arising from the longer reaction times.

Synthesis of terpolymers comprising HEMA, GMA and DMA resulted in poor control of dispersity, indicating that unprotected DMA negatively affects control in these RAFT polymerisations, probably due to chain coupling *via* aryloxy bond formation between catechol side-chains. Accordingly, the M_{nSEC} was consistently larger than M_{nTheo} and larger than the M_{nSEC} for the equivalent polymers comprising ADMA. Two catechol-containing diblock copolymers were also synthesised. For the synthesis of poly(MMA-*b*-ADMA), poly(MMA) was used as a macro-RAFT agent for the synthesis of the ADMA-block. It was concluded that the block copolymer was a good candidate for a functional adhesive, as it had a narrow dispersity and excellent molecular weight control, although evidence of a small amount of residual poly(MMA) homopolymer was observed. Finally, poly(ADMA-*b*-(HEMA-*stat*-GMA)) was synthesised. Good control of dispersity and reasonable molecular weight control indicated the synthesis of block copolymers of ADMA with HEMA and GMA was a viable approach for potential functional adhesive block copolymers.

Four candidate copolymers, FR-HGD-80/10/10, FR-HD-90/10-(DMF), FR-HG-89/11 and RAFT-HGD-74/13/13, were spin coated from methanol solutions. Film thickness was correlated primarily with solution concentration. Striations, attributed to the Marangoni effect, were observed for films deposited using 2% (w/v) solution concentration. This was ascribed to the increased viscosity of the polymer films with increased concentration. High ellipsometric MSE values, suggesting a strongly light-scattering film, were correlated with the presence of striations. Films of FR-HGD-80/10/10, coated from a 0.75% (w/v) solution in methanol, also exhibited high MSE, which was attributed to an increase in viscosity due to the copolymer composition and high molecular weight; it was suspected that the presence of DMA increased viscosity *via* strong intermolecular H-bonds. In some coatings, porosity was also observed using AFM. The porous structures did not correlate with high ellipsometric MSE and were attributed to a phase separation of polymer and solvent due to poor polymer solubility at increasing concentrations as the methanol evaporated. Thus, rapid evaporation of a volatile solvent resulted in a porous film. In contrast, spin-coating the same polymers using DMF resulted in smooth homogenous films. It was concluded that the lower volatility of DMF compared to methanol and reduced rate of evaporation,

allowed any striations time to level. Furthermore, increased polymer solubility in DMF prevented the formation of phase-separated morphologies.

An alternative coating technique, immersion-coating, was also briefly investigated. It was shown that a 5 nm film of FR-HGD-58/9/33 could be deposited from a 2% solution in DMF with 1% pyridine. It was concluded that film formation was aided by the increased cohesion caused by intermolecular chain coupling from oxidised catechol side chains. Despite this, due to limited data, the full impact of these coating conditions and polymer composition could not be determined.

The surface and bulk properties of spin coated films of FR-HGD-80/10/10, FR-HD-90/10-(DMF), FR-HG-89/11 and RAFT-HGD-74/13/13 were investigated using captive bubble contact angle measurements, electrokinetic potential measurements and in-situ ellipsometry. Captive bubble ADSA-P contact angle measurements indicated significant hysteresis for all four copolymers, possibly due to their ability to undergo local conformational rearrangement due to exposure of hydrophilic or hydrophobic functional groups to the interface. It was concluded that the H-bonding network from DMA catechol side chains inhibited the local chain rearrangement, resulting in reduced contact angle hysteresis, however, RAFT-HGD-74/13/13 showed an intermediate value of hysteresis, potentially due to the influence of the hydrophobic RAFT end group. Electrokinetic potential measurements showed that all four copolymers had negative zeta potential at neutral pH, as expected for copolymers mainly comprised of HEMA. It was concluded that the presence of DMA strongly influenced the zeta potential. For example, DMA-containing polymers exhibited a lower IEP (pH ~2.5) compared to FR-HG-89/11 (pH 5). When pH was increased to above 8, all four copolymers exhibited a reduction in zeta potential, which was attributed to pH induced swelling due to repulsion from deprotonated hydroxyl groups. In-situ ellipsometry demonstrated significant swelling of polymer films at pH 7.4 in an aqueous buffer solution, not induced by pH. The presence of GMA appeared to significantly limit the extent of swelling due to crosslinking, such that the film thickness of FR-HD-90/10-(DMF) increased by a factor of 2.19, compared to <1.34 for the GMA-containing copolymers. FR-HGD-80/10/10, FR-HD-90/10-(DMF) showed good resistance to dissolution, which was attributed to the strong H-bonding interactions, including to the silicon wafer surface, by the catechol side-chains. However, for RAFT-HGD-74/13/13, the influence of DMA appeared to be reduced. This was surprising, and the cause could not be

determined, although it was akin to the unexpected behaviour for RAFT-HGD-74/13/13 in general.

FR-HGD-80/10/10 was chosen to study the potential immobilisation of anti-aflatoxin antibody. The effectiveness of this copolymer towards antibody immobilisation was investigated using in-situ ellipsometry and quartz crystal microbalance. Both techniques suggested that a monolayer of antibodies was covalently immobilised on the film surface. The film thickness was not significantly reduced upon rinsing with buffer solution. In combination, the findings suggested a coating of FR-HGD-80/10/10 was suitable and effective for the immobilisation of antibodies.

6.2 Future work

Several elements of the study could be considered interesting areas for future work. Reactivity ratios were calculated to investigate the kinetics of copolymerisation for ADMA with MMA and GMA in 1,4-dioxane. As DMA is a monomer of increasing interest, it would be useful to perform more extensive kinetic studies, including reactivity ratios of copolymerisation of DMA with further monomers and solvent systems. One of the intriguing questions still to be definitively answered is the effect of catechol protecting group chemistry on the copolymerisation. DMA appears to show similar, but not identical, reactivity in free-radical copolymerisation to its protected monomers, despite probably yielding different polymer structures. A full kinetic study has not yet been carried out. It would be useful to use advanced techniques such as in-situ NMR in combination with integrated computational methods to compare the reactivity ratios of DMA and its protected analogues when polymerised with various comonomers. It would be of further interest to determine the ternary reactivity ratios of the polymerisation of HEMA, GMA and (A)DMA to facilitate more accurate prediction of the terpolymer compositional drift.

RAFT polymerisation using the RAFT agent CTP yielded copolymers with good control over dispersity, but relatively poor molecular weight control. In a future study, the conditions for RAFT polymerisation of ADMA with methacrylate comonomers could be explored further, for example by comparing a selection of RAFT agents. Furthermore, the use of protected DMA could allow the comparison of other forms of RDRP.

The issue of deprotection of acetonide-protected catechol in the presence of an epoxide was not resolved in this work. A full investigation into the conditions necessary for the protection and deprotection of DMA with groups such as silanes would add to the

understanding of the monomer behaviour. Further understanding of the behaviour of protected DMA would allow synthesis of copolymers with HEMA, GMA and subsequently deprotection without loss of epoxide groups. Using RDRP, polymer architectures such as multi-block copolymers (ABC or ABA) could be used to form loops or brushes upon adhesion to a surface, which may alter the efficacy of the adhesive copolymer performance both in terms of adhesion to the surface and ability to conjugate biomolecules. Alternatively, reactive functional groups could be incorporated post-polymerisation using (for example) epoxidation of an alkene side chain after the polymer had been immobilised on a surface using catechol chemistry.

A deeper understanding of the deposition of porous films from methanol could be explored in further studies for potential application as membranes, if the pore size could be controlled reproducibly. The ideal conditions for deposition of these catechol-containing copolymers using immersion-coating also could be investigated further. Widening the scope of this investigation could take advantage of the versatile adhesive properties on a range of metal surfaces, such as metal oxides or polymeric surfaces. This would allow the versatility of the catechol side-chains to be fully considered. Furthermore, the brief investigation into the immersion coating of the catechol-containing copolymers highlighted the potential to use these copolymers directly from solution. A potential application could be coating microfluidic channels with the copolymers, or other surfaces which are difficult to coat by traditional methods. A full investigation of the immersion-coating method would be useful, particularly over a range of pH values and temperatures, to take advantage of the various binding modes of the catechol groups.

Finally, it was demonstrated *via* QCM and in-situ ellipsometry that an antibody could be immobilised on a spin-coated film of FR-HGD-80/10/10. However, due to time constraints, the immobilisation of antibodies was not investigated on the full range of copolymer films. A more in-depth study of the deposition of antibodies on the copolymer coatings would be of interest. QCM would also be useful in a full study of antibody deposition, and x-ray photoelectron spectroscopy (XPS) could be used to confirm the surface chemistry. Following this, the logical step which was not addressed in this study due to a lack of time would be measurement of the activity of the immobilised antibodies. This could be achieved using a number of methods including fluorescence microscopy upon binding of the antigen, or quantitative analysis of the eluent to measure the extent of antigen retention by the antibody.